

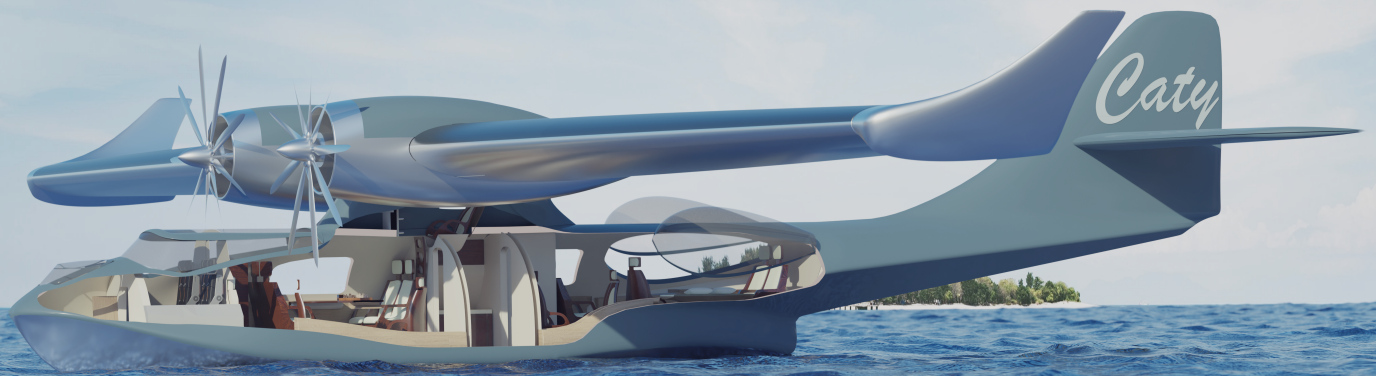
Caty

a Restomod Catalina

Final Report

AE3200: Design Synthesis

Group 4



Delft University of Technology

Caty

a Restomod Catalina

Final Report

by

Group 4

Student Name	Student Number
Jorian van Bemmelen	4790413
Nick Felten	5223679
Ties Harland	4997581
Tim Honing	5040744
Steven van de Kamp	5312809
Maxim Kokorev	5105064
Brian de Vrind	5028426
Jasper Vrolijk	5107202
Adam Wajs	5097789
Twan Wuite	5301769

Instructor: Ronald van Gent
Coaches: Tercio Lima Pereira & Eddy van den Bos
Faculty: Faculty of Aerospace Engineering, Delft
Date: Tuesday 27th June, 2023

Cover: Render by Adam Wajs



Preface

Even though we have worked very hard these last weeks to create this paper, there are some other people who have to be mentioned before reading this report. First of all, we would like to thank our principal tutor Ronald van Gent and our coaches, Eddy van den Bos and Tercio Lima Pereira for their continuous feedback and intensive involvement in our project. We would also like to thank our teaching assistant, Austin Phillips, for his help and involvement in our project. Next to that, there were some specialists who helped us out with some difficult problems. Thanks to Saullo G.P. Castro for his help in the structural design, Abhas Choudary for his expertise in thermoplastic composite materials and Daniel Atherstone for his expertise in Catia. Finally, we would like to thank a special group of volunteers who are restoring an original Catalina in Nieuw-Vennep. A big thanks to Prudent Staal and the rest of the group for all of their knowledge on the Catalina, their enthusiasm and of course all of the data from the original Catalina. This project would not have been possible without all of the contributions from the before mentioned people.

*Group 4
Delft, June 2023*

Contents

Preface	i
Executive Summary	ix
Nomenclature	xv
1 Introduction	1
2 Project Objective	2
3 Market Analysis	4
3.1 Luxury chartering	4
3.2 Scenic Flights	4
3.3 Marine Patrol	5
3.4 Private ownership	5
3.5 Refurbished Catalina	5
3.6 Conclusion Market Analysis	6
4 Mission Analysis	7
4.1 Operations and logistics	7
4.2 FFD & FBD	7
5 Interior Design	10
5.1 Interior Design	10
5.2 Avionics system	13
6 Weight estimations	14
6.1 Class I weight estimation	14
6.2 Class II weight estimation	15
6.2.1 Structure and equipment	15
6.2.2 Propulsion	15
6.2.3 Center of gravity and mass moment of inertia	16
6.3 Further weight estimation	16
6.4 Verification & Validation	16
7 Propulsion Design	17
7.1 Propulsion System Trade-off	17
7.2 Propeller Design	18
7.2.1 Empirical Noise Calculations	18
7.2.2 Blade Element Theory Noise Calculations	19
7.3 Engines and Fuel cells	20
7.4 Aircraft Thermal Management System	21
7.4.1 Cooling relief systems	25
7.4.2 Coolant	26
7.4.3 Radiator Drag	26
7.5 Propulsion Layout	27
7.5.1 Propulsion system Initial design	29
7.5.2 Propulsion system Evolved design	29
7.6 Propulsion Weight	33
8 Aerodynamics	35
8.1 Wing	35
8.1.1 Planform	35

8.1.2	Airfoil	35
8.1.3	Winglets	37
8.2	Drag	40
8.2.1	Rivets	40
8.2.2	Drag of the original aircraft	41
8.2.3	Drag of the Caty	41
9	Structural Internal Loading	43
9.1	Gust load Diagram	43
9.2	Wing	43
9.2.1	Critical cases in z-direction	45
9.2.2	Implementation of a Strut for z-direction	46
9.2.3	Critical cases in x-direction	47
9.2.4	Implementation of a Strut for x-Direction	48
9.2.5	Loading along chord	49
9.3	Fuselage aerodynamic loads	49
9.4	Fuselage water loads	50
9.4.1	Critical loading case	51
10	Structures	53
10.1	Material Trade-off	53
10.1.1	Material properties	53
10.1.2	Fuselage	54
10.1.3	Wing box	55
10.1.4	Leading edge wing box	55
10.1.5	Nacelles engine	56
10.2	Main wing structure	56
10.2.1	Designing of a Strut	56
10.2.2	Bending stiffness	58
10.2.3	Shear stiffness	59
10.2.4	Sheet crippling	61
10.2.5	Final wing box design	63
10.3	Fuselage structure	66
10.3.1	Idealized structure	66
10.3.2	Skin and stringer area sizing	67
10.3.3	Dimension stringers	67
10.3.4	Resulting fuselage structure	67
10.4	Verification & Validation	70
11	Stability & Control	71
11.1	Loading Diagram	71
11.2	Scissor Plot	72
11.3	Wing Stability and Aileron Design	73
11.4	Horizontal Tail Dimensions	74
11.5	Vertical Tail Dimensions	75
11.6	Dynamic Stability	76
11.7	Landing gear	78
11.7.1	Tire sizing	79
11.7.2	Landing gear positioning	79
11.7.3	Landing gear retraction mechanism	80
11.8	Verification and validation	81
12	Performance	83
12.1	General characteristics	83
12.2	Costs	87

12.3	Hydraulic Actuation Systems	89
12.4	Electromechanical Actuation Systems	89
12.5	Block diagrams	90
12.6	Resource Budget Breakdown	94
12.7	Risks	95
12.7.1	Risk Map	95
12.8	RAMS characteristics	97
12.8.1	Reliability	97
12.8.2	Availability	97
12.8.3	Maintainability	98
12.8.4	Safety	98
12.9	Sustainability	98
12.9.1	Sustainable Materials and Production	98
12.9.2	Sustainable Propulsion	98
12.9.3	Sustainable Operation	99
12.10	Compliance matrix	99
12.10.1	Aircraft compliance matrix	99
12.10.2	Propulsion system compliance matrix	103
12.10.3	Wing compliance matrix	105
12.10.4	Empennage compliance matrix	106
12.10.5	Fuselage compliance matrix	107
12.10.6	Landing gear compliance matrix	108
12.11	Feasibility Analysis	108
12.12	Sensitivity analysis	108
13	Future Perspective	111
13.1	Manufacturing, Assembly, Integration Plan	111
13.2	Project design & development logic	113
13.2.1	Finalize detailed aircraft design	113
13.2.2	Manufacturing and certification	114
13.2.3	Distribution of the aircraft	114
13.2.4	Maintenance of the aircraft	115
13.2.5	End-of-life	115
13.3	Gantt chart	115
14	Conclusions & Recommendations	117
14.1	Recommendations	118
14.2	Final Note	118
	References	119

List of Figures

1	Front compartment	ix
2	Back compartment	x
3	Propulsion system layout	xi
4	Translating winglet and floater mechanism concept	xii
5	Wingbox structure of the Caty	xiii
6	Pie chart OEM	xiii
7	Empennage design of the Caty	xiv
8	Landing gear retraction mechanism of the Caty	xiv
4.1	Operations & Logistics Diagram	7
4.2	Fucntional Flow Diagram from the baseline report [2]	8
4.3	Fucntional Breakdown Diagram from the baseline report [2]	9
5.1	Top view of interior	10
5.2	Front compartment	10
5.3	Back compartment	11
5.4	Pylon seat	12
5.5	Side Platform	12
7.1	Cross-section of a stripped-fin radiator [10]	24
7.2	A diffuser-nozzle configuration with an angled radiator as is used in this design [10]	26
7.3	Layout of the hydrogen tank in the wing with the initial nacelle configuration	28
7.4	Layout of the engine nacelle in the initial design	28
7.5	Circular RAM intake and radiator design	30
7.6	RAM intake geometry	31
7.7	Propulsion system assembly. Radiator in light blue, electric motors in red and fuel cell stack in orange.	31
7.8	Propulsion system assembly front view. Radiator in light blue, electric motors in red and fuel cell stack in orange.	32
7.9	Propulsion system assembly side view.	32
7.10	Propulsion system overview, integrated into the aircraft wing.	33
8.1	XFLR5 lift curve from comparing NACA airfoils with various amounts of thickness at 30 m/s.	35
8.2	XFLR5 lift-over-drag curve from comparing NACA airfoils with various amounts of thickness at 56.5 m/s	36
8.3	Winglet and floater integration options from left to right: 1) floater on wingtip, 2) immovable floater, 3) floater under wingtip, 4) winglet on floater	38
8.4	Translating winglet and floater mechanism concept	38
8.5	Stall characteristics of the wing including winglets at $\alpha = 20.5^\circ$	39
8.6	Elliptical lift distribution of the wing at $\alpha = 20.5^\circ$	40
8.7	Lift curve of the original Catalina and the Caty	42
8.8	Lift over drag curve of the original Catalina and the Caty	42
9.1	Loading diagram of the aircraft	43
9.2	Free Body Diagram of the right with containing only forces and loads in Y-Z plane	45
9.3	Discretization example of lift	45
9.4	Internal loading of the strutless right-wing in Y-Z plane	46
9.5	Free body diagram of the right with containing only forces and loads in xy plane	48
9.6	Internal loading of the strutless right-wing in the xy plane.	48

9.7	Internal torsion moment over wingspan	49
9.8	The absolute value of the internal force and moment diagrams of the fuselage	50
9.9	Angle of the step of the hull	51
9.10	Hull weighing factor from CS-23	52
10.1	Internal loading of the right wing containing the strut in the yz plane	56
10.2	Example locations booms	58
10.3	Minimum area material over wing span	58
10.4	Shear flow in the Z-direction on the wing	59
10.5	Minimum side skin thickness	60
10.6	Shear flow in the X-direction in the wing	60
10.7	Minimum top skin thickness	61
10.8	Stringer shape and variables	62
10.9	Crippling stress along the wing span	63
10.10	Wing box skin thicknesses	64
10.11	Material area need vs actual	64
10.12	Deflection of the wing for different cases.	65
10.13	Final wingbox design	66
10.14	Position of the compartment walls of the fuselage	68
10.15	Sensitivity and comparison for the amount of stringers	68
10.16	Skin thickness of the fuselage	69
10.17	Stringer sketch and dimensions	69
11.1	Loading diagram for the Caty. Red dotted lines represent the most forward and aft c.g. positions	72
11.2	Scissor plot for the Caty. Blue dots represent the extreme cg range at cruise conditions	73
11.3	Trim Cruve	75
11.4	Empennage design of the Caty	76
11.5	Tip over and scrape angle of the Caty	80
11.6	Landing gear retraction mechanism of the Caty	80
11.7	Landing gear retraction mechanism of the Caty	81
12.1	Top view Caty	84
12.2	Front view Caty	85
12.3	Side view Caty	86
12.4	Cost Breakdown Structure	88
12.5	Hydraulic actuation system ¹	89
12.6	Electrical block diagram	90
12.7	H/W, S/W block diagram	91
12.8	Communications flow diagram	92
12.9	Data Handling block diagram	93
12.10	Mass Technical Performance Measurement	94
12.11	OEM weight distribution	94
12.12	MTOM weight distribution	94
13.1	MAI plan of the aircraft	112
13.2	Future project & development logic diagram	113
13.3	Gantt chart post DSE activities	116

List of Tables

1	Wing performance characteristics using NACA 1420 for an aircraft mass of 9700 kg	xi
2	Operational costs Cathy	xiv
6.1	List of various aquatic aircraft and aircraft similar to the original PBY Catalina, source from Janes unless otherwise specified ² [1]	14
6.2	Structure weights	15
6.3	Equipment weights	15
6.4	Propulsion	16
7.1	Concept parameters for quantitative criteria	18
7.2	Concept Trade-off	18
7.3	Propeller Airfoils	20
7.4	A-weighted noise estimation at 3000 ft of different propeller configurations.	20
7.5	Geometric and physical parameters of the proposed offset-stripped fin heat exchanger [10]. . .	24
7.6	Propeller Reference Data ³ [14]	34
8.1	Effect of the thickness-to-chord ratio on the aircraft's fuel mass and stall speed	36
8.2	Effect of camber on the lift-over-drag ratio of the aircraft at 56.5 m/s for 11000 kg	37
8.3	Wing performance characteristics using NACA 1420 for an aircraft mass of 9700 kg	37
8.4	Drag reduction due to the removal of rivets.	41
8.5	Breakdown of zero-lift-drag coefficient of the original Catalina ($S = 130.5 \text{ m}^2$)	41
8.6	Breakdown of zero-lift-drag coefficient of the Caty for the old and the new wing surface area. .	42
9.1	Forces acting on the wing in Z-direction, during a 3.9g pull-up manoeuvre.	44
10.1	Material properties	53
10.2	Trade-off fuselage material	55
10.3	Trade-off wing box (part 1) material	55
10.4	Trade-off leading edge wing box material	56
10.5	Stringer flange sizes	62
10.6	Minimum pitch stringers	63
10.7	Minimum pitch stringers	64
10.8	Dimensions stringers per section of the wing box	65
11.1	Stability derivatives	77
11.2	Dynamic stability	78
11.3	Caty tire dimensions and pressures	79
11.4	Landing gear requirements	79
12.1	Operational costs Cathy	87
12.2	Risk Map	95
12.3	Risk Mitigation Map	95
12.4	Risk assessment	96
12.5	Requirements List	99
12.6	Propulsion requirements	103
12.7	Wing requirements	105
12.8	Requirements List Empennage	106
12.9	Fuselage requirements	107
12.10	Landing gear requirements	108

12.11 Sensitivity Analysis 110

Executive Summary

One of the largest challenges of the modern era is the ongoing struggle against global warming. Aviation is a large contributor to this problem and this sector is expected to grow significantly in the future, and with it, its green house emissions. So far, little improvements have been made to drastically reduce aviation emissions and in order to advance technological developments in this area, drastic and innovative concepts are necessary to be refined. These concepts have to appeal to the affluent in order to create incentive for the development of sustainable aircraft. In line with this, producing a modern, state-of-the-art, luxurious traveling experience contained within the classic, romantic, design of the PBY Catalina is the perfect launching platform to propel innovation forwards. Indeed, the Consolidated Model 28, affectionately known by aviators around the globe as the PBY Catalina, possesses a rich history and is celebrated and admired worldwide. We therefore aim to celebrate its legacy by redesigning it such that the next generation is able to enjoy flying it again, while contributing to the transition into a sustainable future. This report therefore covers the preliminary design of a modern, hydrogen-fuelled, electric version of the PBY Catalina, christening this modified aircraft as Caty.

Upon analyzing the present market conditions, it is anticipated that Caty will predominantly be utilized for journeys between tourist destinations, with no real potential present for simple refurbishing of old Catalina aircraft. These trips are likely to span multiple days and involve various activities, with flights serving as transportation between each activity. The design of the Caty is tailored for luxurious cruising with unparalleled views of the outside world. The water landing capability of the Caty, will pioneer a new market where private aviation is merged with adventurous activities. Each coastal town and island becomes accessible with the Caty, resulting in seamless travels between the passengers' destinations, with no need for further transport. With this purpose in mind, the Caty was designed with a range of 500 km and 13 passenger seats.

To ensure the aircraft fits into the luxury market, the comfort of the passengers is of utmost importance. When analysing the original Catalina it was found that 13 passengers could be seated comfortably after some adjustments to the fuselage. Indeed the size of the fuselage was increased in both the width and the height direction with 15 cm and 10 cm respectively, while keeping the iconic low and wide shape of the Catalina. Additionally, to increase comfort of the passengers, insulation was added to create a climate controlled cabin. After the sizing of the fuselage, the pleasant interior could be created as can be seen in Figure 1 and Figure 2.



Figure 1: Front compartment



Figure 2: Back compartment

One of the driving requirements of the design of Caty was the emission free operations. To achieve this, three different concepts were considered: battery, battery hydrogen hybrid, and full hydrogen. All of the propulsion systems use electric engines. For the concepts including hydrogen, two different storing methods were considered: pressurized and liquid hydrogen. For the battery concepts, due to the weight limitation, also a concept was added that only had 230 kilometers range. This meant that in total 6 different concepts were considered. They were all rated on five different criteria: mass, sustainability, risk, cost and volume. The sustainability criteria was split between an emissions and an end of life score. After the trade-off, the full pressurized hydrogen concept was chosen for its low weight and cost, and high sustainability.

The noise requirement set at the beginning of the project was to have a maximum of 65 dB when flying over at 3000 ft. To ensure this was met, an extensive design study was done into the propeller blade number and shape. Two different methods were used for propeller noise estimation, an estimate from empirical data and an estimate from XROTOR. A 9 bladed propeller was deemed most optimal. The noise calculations performed in blade element theory software during climb at 3000 ft is 44.15 dB. It is important to note that the absolute intensity of the noise has a relatively high uncertainty, however a clear decrease in noise intensity can be seen compared to the original. This makes the team confident that the noise requirement can be met. Another important remark is that the propeller has only been designed for aerodynamic performance. In order to ensure structural integrity, the chord of the propellers might have to be enlarged. This might cause some changes to the noise generated, but the noise will likely remain within limits.

A large problem of using hydrogen fuel cells is the cooling, with 50% of produced power being lost in heat. To account for this a liquid cooling system was chosen, mostly due to its technology readiness level and the ease of design. Radiators are used to cool the liquid and a RAM intake is sized to supply this air. An unfortunate side effect is an added drag of 2.5 kN or 140 kW during cruise. Unfortunately however, this was deemed unavoidable. The RAM intake is designed for an incoming airflow of 16 m/s and a variable intake is used to control this speed. In Figure 3, the layout of the propulsion system can be seen. In the figure, the turquoise blocks represent the radiators, the red block represents the electric motor, the orange block represents the fuel cell and the blue blocks represent the fuel cell auxiliary systems. The hydrogen tanks layout can be seen in the figure as well.

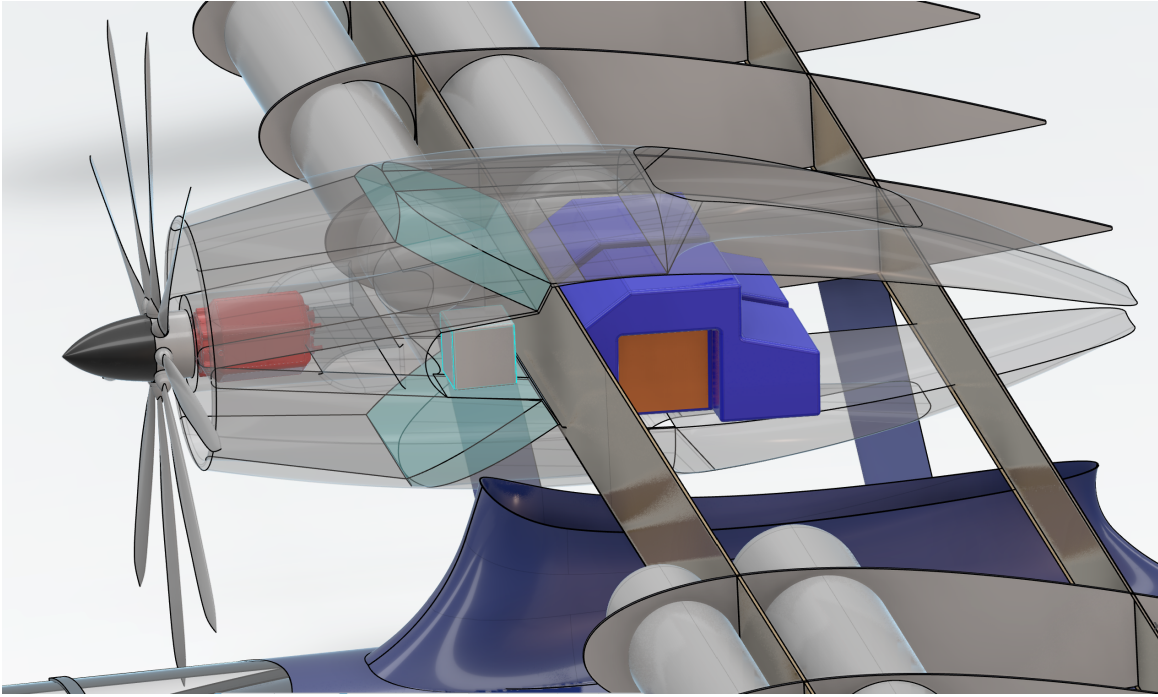


Figure 3: Propulsion system layout

Another characteristic that was identified as a possibility for improvement to the old Catalina, was the aerodynamics. To improve on this, the wing planform was completely redesigned. However, to not lose too much of the iconic feel of the Catalina, a maximum change in dimensions of 10% was set as a requirement.

First, the airfoil shape was chosen from the NACA 4-digit family. This shape mainly affects the stall speed and the fuel mass. When increasing the thickness-to-chord ratio the stall speed increases while the fuel mass decreases. Using the stall speed requirement of 32.4 m/s and a safety factor of 1.1 and an extra margin for other uncertainties a thickness-to-chord ratio of 20% was chosen.

Then the camber was designed. This parameter mainly affects the L/D of the wing. Even though the effect was found to be minimal, still an optimal camber of NACA 1420 was chosen. This all combined results in the following aerodynamic characteristics of the wing, as shown in Table 1.

Table 1: Wing performance characteristics using NACA 1420 for an aircraft mass of 9700 kg

$C_{L_{max}}$	V_{stall} [m/s]	a_{cruise} [°]	$(L/D)_{cruise}$
1.516	28.5	4.4	10.60

An additional improvement to Caty's performance could be by adding winglets. However, the floaters are positioned at the wingtips, so the winglets would have to be integrated with them. The mechanism used for this is shown in Figure 4.

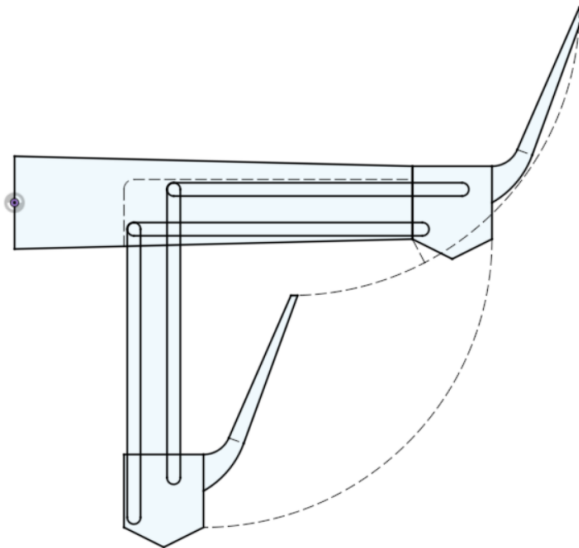


Figure 4: Translating winglet and floater mechanism concept

Then the winglets were sized. Using a trial and error method to find the optimum lift-over-drag ratio, a root chord of 1.5 and a tip chord of 0.5 meters were found to be the smallest effective winglets. This increases the lift-over-drag ratio by 3.5%, increasing it from 10.6 to 11. The addition of the winglets also introduces an additional load on the wingbox, increasing its structural weight. However, this was found to be negligible.

Because of the use of new materials, a rivetless skin is possible. It is expected to reduce the drag and therefore improve the performance of Caty. The expected reduction of the drag coefficient as 8.1. However, due to the increase in fuselage size and wing span, the drag is around 10% larger than the original Catalina.

Then, The structure of the Caty was designed. To be able to do this, first, the correct loads need to be determined and analysed. Using the CS-23 regulations a gust and manoeuvre diagram was created. From this, a maximum load factor of 2.6 g's was found in the positive direction and -1.04 for the negative case. Then, using a 1.5 safety factor, a maximum load factor of 3.9 g and -1.56 g's was used for the loading diagrams. Firstly, the wing loads were analysed. This was done by considering all the different loads on the wing and adding them together to create the internal loading diagram. Using this, an internal shear force and bending moment diagram could be created for the vertical direction (along the z-axis). This was done for multiple scenarios, most notably the case with and without struts, to find the most extreme cases.

Following the load analysis, the structure could be designed. Beforehand, the correct materials had to be chosen. For this, the aircraft was divided into four different main parts: fuselage, wingbox, wing leading edge and engine. The wingbox was then also divided into two different parts, the part until the strut and the part after the strut. This was done mainly to account for the high thermal loads and risks in the first part of the wing due to the fuel cells being there. These trade-offs concluded that the fuselage and the second part of the wing will be made out of thermoplastic composites using PEEK and carbon fibre, and the first part of the wing, the engine and the leading edge of the wing to be made out of aluminium.

Then, the wingbox structure was designed. For this, three different failure modes were identified: bending, buckling and shear. The wingbox was divided into 5 parts where structural sizes could be changed to make manufacturing easier. Then the fuselage structure was designed. For the fuselage structure, the same failure modes are important as for the wingbox. The forces taken into account for the internal loads were simplified to the main contributing forces, namely the forces caused by the main wing, tail wings, and weight. The final structure of the wing is visualised in Figure 5 and Figure 6 shows the weight percentages of the wing and fuselage structures with respect to the OEM.

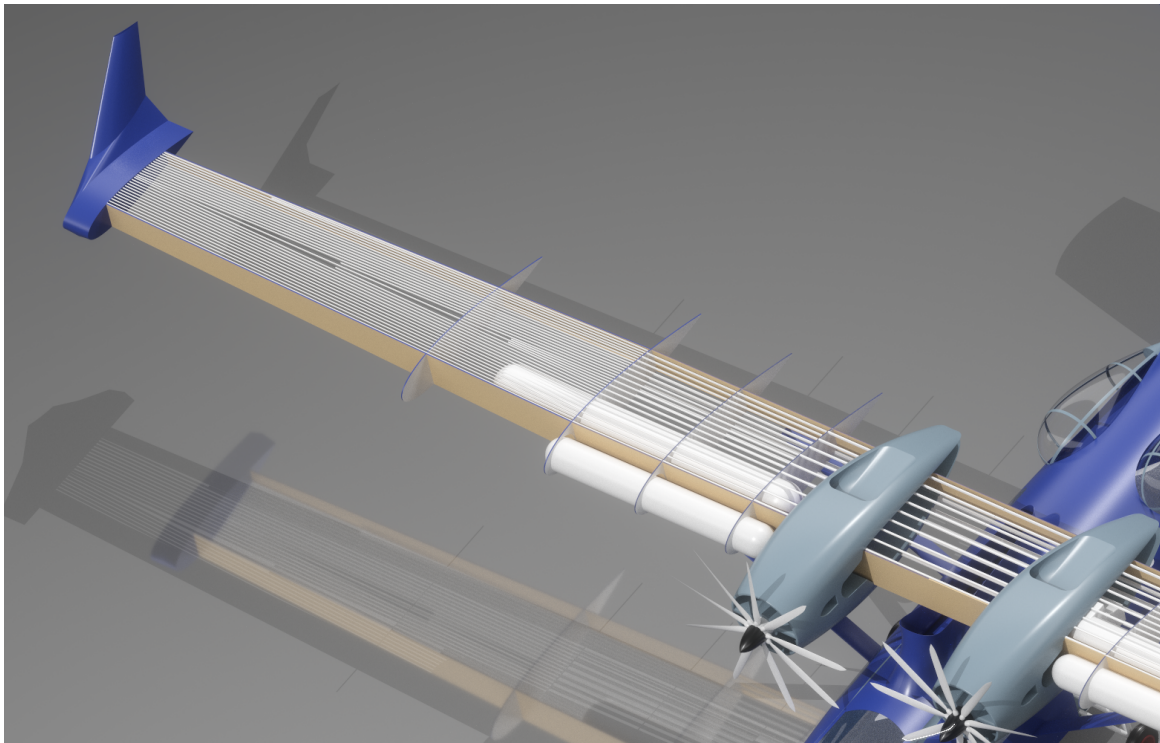


Figure 5: Wingbox structure of the Caty

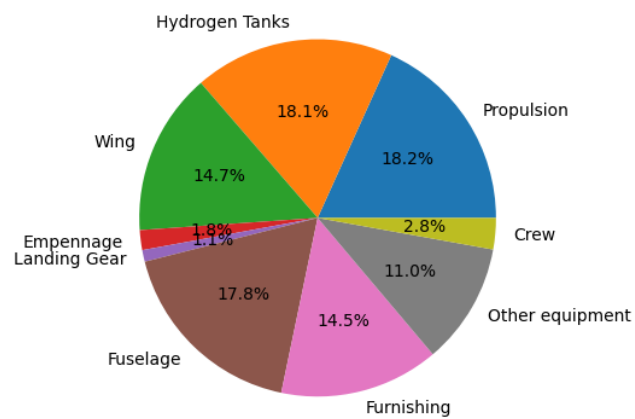


Figure 6: Pie chart OEM

The team also performed a stability and controllability analysis, as the centre of gravity and overall weight changed a lot compared to the original Catalina. To do this, first a loading diagram was created to find the range of the centre of gravity. In doing so, the most extreme loading cases were investigated.

This was then used as an input for the scissor plot. From this scissor plot, the tail could be sized to ensure the stability of the aircraft. In doing so, horizontal and vertical tail designs were obtained, as depicted in Figure 7. In addition to this, the control surfaces were sized, and verified to produce sufficient rotational accelerations.



Figure 7: Empennage design of the Caty

After the sizing of the empennage, the dynamic stability was analysed. All of the eigenmotions were stable except for one, the spiral. However, this is allowed according to CS-23. However, it is important to note that the pilots are aware of it and can react appropriately.

The landing gear was also sized by the team. This was done by doing an analysis of the runway quality of remote islands. It was found that this was a minimum LCN (Load classification number) of 50. This created the landing gear as shown in Figure 8a and Figure 8.

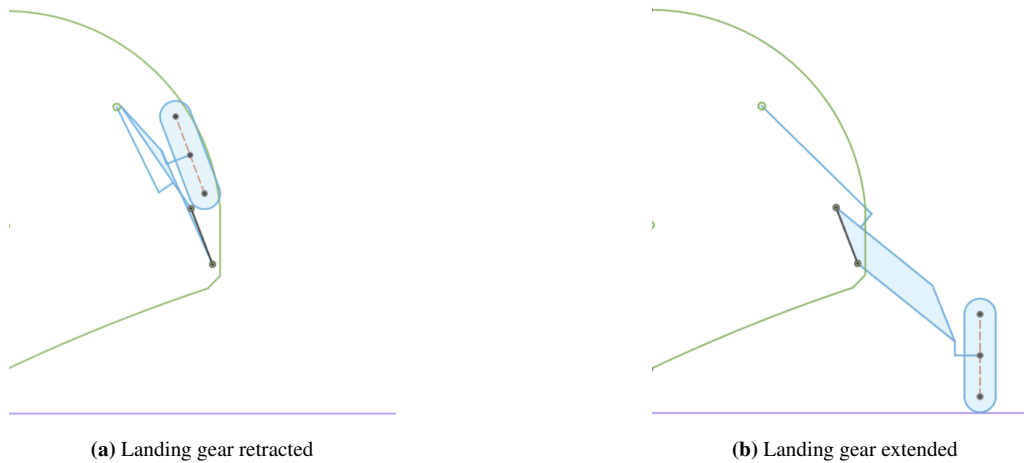


Figure 8: Landing gear retraction mechanism of the Caty

The cost of the aircraft is estimated to be around 25 million dollars, which compares to the upper end of similarly sized private jets. Using this cost, a return on investment of 15 years and the operational costs of around 2050 dollars per flight (Table 2) results in a ticket price per flight per passenger of \$500 - \$800.

Table 2: Operational costs Cathy

	Annually	Per flight
Rent hangar	70 k	
Insurance	100 k	
Unforeseen	100 k	
Crew	250 k	
Propulsion system		800

The new restomodded Catalina, Caty, has improved on the old Catalina in almost all aspects. Mainly in the area of materials, aerodynamics, propulsion, climate impact and user experience. In the next design phase, further investigation is to be done into the cooling of the fuel cells, in order to optimize the design even further. Secondly, the option to add more fuel tanks to increase the range offers another opportunity of increased performance. Finally, the addition of solar panels on the wing surface presents a promising solution for stationary power supply. In conclusion, Caty has succeeded in fulfilling the project objective of becoming a restomod of the original Catalina, using state-of-the-art technology and emission-free operations.

Nomenclature

Abbreviations

Abbreviation	Definition
AoA	Angle of Attack
BMD	Bending Moment Diagram
c.g.	Center of gravity
EOM	Equations of Motion
FBD	Free Body Diagram
LHV	Lower heating value
MAC	Mean Aerodynamic Chord
MMOI	Mass Moment of Inertia
NTU	Number of transfer units
OEW	Operational Empty Weight
RPM	Rotations per minute
SFD	Shear Force Diagram

Symbols

Symbols	Definition
α	Angle of attack
β	Angle of sideslip
δ_a	Aileron deflection
δ_e	Elevator deflection
δ_r	Rudder deflection
θ	Pitch angle
η	Efficiency
μ_b	Lateral non-dimensional mass
μ_c	Longitudinal non-dimensional mass
ρ	(air) density
ϕ	Bank angle
A	Area
A_s	Radiator combined fin area
C	Heat transfer coefficient
$C_{\kappa\lambda}$	Derivative of stability coefficient of parameter κ with respect to parameter λ
c_f	Friction coefficient
D_h	Hydraulic diameter
E	Young's Modulus
g	Gravitational constant
h	Heat transfer coefficient
H_{HX}, W_{HX}, Z_{HX}	Radiator height, width and depth
i_w	Wing incidence angle
i_h	Horizontal tail incidence angle
I	Mass Moment of Inertia
I	Second Moment of Area
K^2	Radius of gyration

Symbols	Definition
L	Lift force
l	Fin length (radiator)
l	Rolling moment
l_h	Distance between aerodynamic centres of wing and horizontal tail
l_v	Distance between aerodynamic centres of wing and vertical tail
l_{str}	Length to strut
L_{str}	Length of the strut
m	Mass
m	Pitching moment
M	Moment
μ	Viscosity of air
\dot{m}	Mass flow rate
N_x	Number of x
n	Yawing moment
P	Power
p	Angular rate of roll
\dot{Q}	Heat
q	Angular rate of pitch
Re	Reynolds number
r	Angular rate of yaw
s	Fin pitch (radiator)
T	Temperature
t	Thickness
u	Difference in airspeed
U	Overall heat transfer coefficient
$v(y)$	Deflection as a function of y
V_r	Airspeed inside radiator
ΔV	Difference in airspeed introduced by the propeller
W	Weight
X	Force in X-direction of the aircraft body axis
Y	Force in Y-direction of the aircraft body axis
Z	Force in Z-direction of the aircraft body axis
$+\uparrow \sum F_z$	Sum of forces in z -direction, with upwards being positive
$\zeta + \sum M_{X,@pylon}$	Sum of moments, with counterclockwise being positive, along the X-axis, calculated at the pylon

1

Introduction

The PBY Catalina is a beloved aircraft that has captured the hearts of aviation enthusiasts worldwide. It earned its fame during World War II for its impressive performance in anti-submarine and maritime warfare. Thanks to its exceptional endurance and amphibious capabilities, the Catalina played a crucial role during that time. Even after the war, its long-lasting capabilities and high payload capacity made it invaluable for firefighting and coast guard operations.

Due to its age, operational Catalinas are rare to find today. Nevertheless, there is a strong desire among admirers to experience the thrill of flying this iconic aircraft, even if it comes with a hefty price tag. This has inspired our group to undertake an exciting project: restoring and modernizing the Catalina, a process known as "restomod". Our goal is to bring a touch of modernity while preserving the nostalgic charm of the Catalina.

The transformed Catalina will be infused with luxury and cutting-edge technologies. We will strive to maintain the original appearance and feel of the aircraft, while upgrading the interior to radiate opulence. By blending classic aesthetics with modern comforts, we aim to create a renewed Catalina experience that captures the best of both worlds. This new aircraft deserves a new name that captures the luxurious and modernized design. Caty will embody both and represent partly the Catalina and partly the luxurious yacht that passengers will experience.

This report is the final report after 9 weeks of hard work of 10 Aerospace Engineering students. A project plan, baseline report and mid-term report have previously been written by this group. The project plan indicated how the group would work together for the coming weeks and how the work would be divided amongst each other. The baseline report mostly focused on the requirements and functional properties that the aircraft should possess. Multiple diagrams were made to ensure that no requirements were missed which Caty should pass. The midterm report explained the preliminary design and concept trade-offs. Mostly the propulsion system concept was handled since this was the biggest decision for Caty. Also, other subsystems were sized and designed such as the wing and empennage.

In chapter 2 the objective of the project will be discussed where the purpose of Caty is discussed and what it will add to the current aviation industry. chapter 3 discusses the market analysis, and how Caty will fit in the market. chapter 4 describes the mission profile and logistics of Caty. It contains the FFD and FBD, together with the requirements that flow out of these. Then the class I & II weight estimations will be performed in chapter 6. chapter 5 shows the interior design of Caty. chapter 7 explains the trade-off performed in the midterm and the recent calculations done on the propulsion system. After that, the aerodynamics of the entire aircraft will be discussed in chapter 8. chapter 9 shows the loads that will act on the aircraft during operations and what the structure should be designed for. Then chapter 10 will design the structures that are able to handle the loads described in the previous chapter. chapter 11 determines the constraints on stability & control and sizes control surfaces and the tail. chapter 12 explains the overall performance of Caty. It contains performance diagrams to explain the technical and project related characteristics. Also, the compliance matrix with sensitivity analysis will be presented. chapter 13 describes the future perspective of Caty. Lastly, the conclusion will be presented in chapter 14.

2

Project Objective

As visionary aircraft designers, our objective is to breathe new life into the iconic PBY Catalina aircraft, transforming it into the epitome of luxury and adventure for private or chartering purposes. We are driven by the desire to combine the luxury and exclusivity of yacht charters with the freedom and mobility of flying, redefining the chartering experience with the redesigned Caty. It opens a world of possibilities, allowing passengers to effortlessly explore remote island groups and coasts in unparalleled style. With its extraordinary views, emissions free propulsion, and impeccable interior, Caty sets a new benchmark for luxury chartering, offering a transformative and unforgettable journey for the affluent and adventurous. To achieve a redesigned PBY Catalina aircraft in this spirit, the following project objectives were established:

Emissions Free Propulsion System

A main driver for this project is the worldwide demand for sustainable aviation. This challenge is yet to be solved and all options must be considered to achieve this goal. The hydrogen-powered Caty concept tests the feasibility of hydrogen aircraft such that passengers can immerse themselves in breathtaking views while enjoying a clear conscience, making it a beacon of sustainable aviation. With zero emissions and a reduced carbon footprint, we aim to pave the way for a greener future and ensure that the pristine beauty of oceans, untouched landscapes, and secluded beaches stay unharmed, all to create an immersive experience that is both luxurious and environmentally responsible.

Increased Aerodynamic Performance

The redesign of the PBY Catalina capitalizes on advancements in aerodynamic knowledge to achieve optimal efficiency. Through the implementation of a new wing profile, planform, and wingtips, as well as the use of new materials and rivetless manufacturing techniques, the aircraft maximizes aerodynamic performance. These improvements play an important role in achieving a range of 500 km and emissions-free propulsion, ensuring the PBY Catalina meets the modern demands for efficiency and sustainability in aviation.

User Experience

The Catalina aircraft's interior will undergo a complete and transformative redesign, aimed at enhancing the ultimate amphibious flying experience for its passengers. The Catalina's interior will feature organic materials that perfectly blend luxury with adventurous utility, making it an ideal choice for coastal explorations and island adventures. The Catalina's redesign will feature a functional galley area, complete with a fully equipped bar. From the galley, the passengers will be served with delicate food and drinks whether the passengers are seated at the tables within the aircraft or out on the expansive wing surface and platform.

Experience the Catalina's redesigned observation decks, both at the front, back and pylon of the aircraft, offering an unrivalled vantage point to behold breathtaking views. Immerse yourself in the beauty of your surroundings from the comfort of beautifully designed spaces, taking your flying experience to a whole new level. Every seat will become a window to breathtaking landscapes, providing a truly remarkable perspective on the world below.

When landing on water, the Catalina's expansive wing surface opens up a vast panorama for you to enjoy the view. Whether you wish to sunbathe or have a drink on the wing, the abundant space afforded by the wing surface invites you to unwind and immerse yourself in the natural beauty that surrounds you. Additionally, the conveniently located platform next to the starboard blister grants effortless access to the water, facilitating

swims or seamless boarding onto boats for further exploration.

The redesigned Catalina interior is destined to redefine the concept of luxury travel, offering an unrivaled combination of elegance, comfort, and functionality. With its spacious interior, wooden accents, luxurious galley, and breathtaking observation decks, the Catalina invites you to embark on a journey where every moment is a once in a lifetime experience. Whether soaring through the skies or floating on the oceans, the Catalina promises a new dimension of luxurious adventure.

3

Market Analysis

With the birth of a new type of luxurious amphibious aircraft chartering, the market analysis will turn to the chartering of mega yachts, tourism flights with amphibious aircraft and marine patrol.

3.1. Luxury chartering

There are some trends in how the super rich wish to spend their free time and mega yacht cruising is high on that list. Excessively large and luxurious yachts are either bought or chartered by wealthy individuals to sail from scenic coastal cities to beautiful islands nearby to visit touristic destinations in a private, luxurious manner. Between destinations, guests have the opportunity to enjoy the water with tenders and other water recreational activities. The yacht is operated by a large crew including cooks to serve fine dinners to the guests. This all comes at a cost depending on the size of the yacht. Typically, a chartering cruise for a 300 ft yacht (150 M\$)¹ costs approximately 1,500,000\$ per week² and a 100 ft motor yacht (10 M\$³) costs 100,000\$ per week⁴.

The journey that the Caty could deliver to the super rich will be of unlimited luxury. Passengers would fly every day to a new island, city or village to spend the day with activities like wine tastings, Michelin dinners, golf courses, etc. The passengers would sleep in luxurious hotels during the night in which the aircraft would be refilled with hydrogen, food and drinks for the upcoming day. Then with a scenic flight they would arrive at a new destination at which a new activity is planned for them. Nothing would have to be arranged by the passengers and all of this would be planned and organized by the company.

3.2. Scenic Flights

The tourism industry is also a potential market for the Caty. Scenic flights were studied in areas along the coast. In Hawaii, approximately 35 companies were found that owned at least one aerial vehicle and offers sightseeing flights. These are fixed-wing aircraft and helicopters. Most companies have between 2 and 6 aircraft available, so they are generally small. This approximation can be extrapolated to the following areas: Caribbean islands, Central America, the Canary Islands, Mediterranean area and European coast, the South- and North American coast, Indian islands, the Oceanic coast, and Pacific islands. It is assumed that the amount of scenic flight companies is equivalent in all aforementioned regions. This would mean that there are as a ballpark number 9 times 35 companies, or 315 companies worldwide which are potential customers [1]. Private jet prices⁵ were studied to get a reference value of purchasing and renting prices of the Caty. For the Caty with 13 passengers and a luxurious interior, a similar aircraft cost 15 million \$ to 30 million \$. Private jet chartering prices⁶ give an indication on the hourly rates of the Caty. The prices range from 2,000 to 11,000 \$ per hour ranging from small turboprop aircraft to large, long range private jets. These prices translate to 336,000 \$ to 1,848,000 \$ per week.

¹<https://www.yachtworld.com/research/the-most-expensive-yachts-in-the-world-5-contenders-in-2021/#:~:text=SUNRAYS%20by%20ceanco%3A%20%24153%2C535%2C800%20USD&text=The%20spectacular%20280%20foot%20superyacht,the%20renowned%20designer%20Terence%20Disdale>. (Accessed on 19-06-2023)

²<https://www.yachtcharterfleet.com/luxury-charter-yacht-22959/sunrays.htm> (Accessed on 19-06-2023)

³https://www.seattleyachts.com/used-yachts-for-sale/108-custom-line-navetta-33-2018-gioia/2788028_1 (Accessed on 19-06-2023)

⁴<https://www.yachtcharterfleet.com/luxury-charter-yacht-59255/our-way.htm> (Accessed on 19-06-2023)

⁵<https://www.bankrate.com/loans/personal-loans/how-much-does-a-private-jet-cost/> (Accessed on 19-06-2023)

⁶<https://www.paramountbusinessjets.com/private-jet-rental-cost> (Accessed on 19-06-2023)

The amount of private aircraft in operation is approximately 21,000⁷. When a average lifetime of 10 to 20 years is expected for private jets⁸, approximately 1000 to 2000 private aircraft are built annually to keep up with demand.

3.3. Marine Patrol

With the use of emissions free propulsion, the range will likely be too short for marine patrol. The US coast guard uses aircraft to perform search and rescue missions with aircraft with long range (8046 km) of which there are 27 in operation. The other aircraft is the C-27J Spartan aircraft with a range of 5056 km. These aircraft could not be replaced by the Caty due to the short range. Helicopters are used for rescue missions from for example sinking boats with a range of 658 to 1300 km. The US coastguard has a total of 144 helicopters. The mission profile of the helicopters could however not be performed by the Caty [1]. The use of the Caty for marine patrol is therefore infeasible.

3.4. Private ownership

For the very wealthy individuals that own a home in some remote place, the Caty can fulfill the purpose of a transportation last mile⁹ solution. Such individuals often live in urban areas¹⁰ far away from earth's paradises where their vacation homes are. This requires them to fly to their vacation destinations with a stopover at a large airport. From there, the Caty can be used for the last mile to their vacation home and from there, they have the Caty always to their disposal for a trip to remote beaches, diving sites, surf spots or beach club within a 250 km range. The interior enables for a week trip with the family or close friends, similar to trips with their yachts. A few days filled with adventure, delicious food and a comfortable bed make it the perfect flying yacht experience that very few get to experience. The expected price of the aircraft is expected to be above the middle of the range given in section 3.2 at 25 M\$.

3.5. Refurbished Catalina

When looking at the market analysis and the project objective, the question arises whether a refurbishing strategy, meaning buying old Catalinas and altering them to our specific needs, might be cheaper. In this section this possibility is analysed and its challenges are highlighted.

When trying to refurbish an old Catalina, it first has to be bought. When scanning the market, a couple of airworthy Catalinas and their prices can be found. Three different aircraft were found with the following prices: \$ 250,000¹¹ \$ 275,000¹² \$ 495,000 airworthy¹³ can last around 10 weeks to refurbish (Caty)¹⁴. These aircraft are quite cheap and also airworthy. However, in total there are, as of today, only 15 airworthy Catalinas left in the world. This is not a large market to pick from which really limits the amount of aircraft that can be sold. This is therefore a limitation for the refurbishing strategy.

Next is the actual refurbishing. As the market case for this aircraft is luxury, a lot of changes need to be made to increase comfort in flight. This means adding insulation, air conditioning, larger, comfortable seats etc. When looking at the Caty, the size of the fuselage was slightly increase to accommodate for these additions, but this is not possible when refurbishing. This means that the size of the fuselage will shrink, decreasing either the comfort of the passengers or the amount of passengers that can be taken aboard. This will then drive up the price of a flight significantly or decrease the user experience.

⁷<https://compareprivateplanes.com/articles/how-many-private-jets-are-there#:~:text=Including%20all%20out%20of%20production,is%20far%20larger%20than%20this.> (Accessed on 19-06-2023)

⁸<https://www.paramountbusinessjets.com/faq/age-of-aircraft-safety-factor#:~:text=Aircraft%20offered%20for%20charter%20by,clients%20want%20more%20luxurious%20interiors.> (Accessed on 19-06-2023)

⁹<https://dictionary.cambridge.org/dictionary/english/last-mile> (Accessed on 19-06-2023)

¹⁰<https://www.theguardian.com/money/2015/nov/15/wealthy-homebuyers-prefer-to-live-in-cities>

¹¹<https://historicalandclassicaircraftsales.com/pbycatalina-0a-10a>(Accessed on 19-06-2023)

¹²<https://aerodynamicmedia.com/pby-5a-n423rs-for-sale/>(Accessed on 19-06-2023)

¹³<https://www.nzcatalina.org/>(Accessed on 19-06-2023)

¹⁴<https://www.key.aero/article/aircraft-refurb-pros-and-cons>(Accessed on 19-06-2023)

One of the main changes that will have to be made is to the propulsion system. As the mission needs to be emission free, the entire propulsion system will have to be changed from combustion based to hydrogen based. This will mean a more concentrated mass of the fuel tanks instead of the distributed load of the original fuel tank, which will also change the centre of gravity, influencing the stability. As the entire engine and nacelle will be changed and the fuel cells and cooling are in there, this does not pose a problem.

Another expected big downside of the refurbishing is the maintenance. As it is not logical to replace all of the structures, as you then might as well build an entirely Caty, the user will probably experience a lot of problems with the maintenance. The aircraft are most likely over 80 years old, they will probably encounter fatigue damage more quickly than a newly built version. The original Catalinas were built to only last 2 years, which means extensive maintenance is necessary to make this lifetime longer, especially if salt water landings are part of the mission. The Caty uses PEEK thermoplastics, which are resistant to salt water¹⁵.

Finally, a big change of the old to the new version is the weight of the aircraft. The old Catalina has a very high OEW because it had to take a lot of fuel, increasing the structural weight. When comparing a refurbished option to a newly designed option, this will also increase operational costs.

3.6. Conclusion Market Analysis

Upon analyzing the present market conditions, it is anticipated that Caty will predominantly be utilized for journeys between tourist destinations. It is expected that Scenic flights and private ownership of the Caty will have a smaller share of the Caty sales. These chartering trips are likely to span multiple days and involve various activities, with flights serving as transportation between each activity. The design of the Caty is tailored for luxurious cruising with unparalleled views of the outside world. The water landing capability of the Caty, will pioneer a new market where private aviation is merged with adventurous activities. Each coastal town and island becomes accessible with the Caty, resulting in seamless travels between the passengers' destinations, with no need for further transport. With this purpose in mind, the Caty was designed with a range of 500 km and 13 passenger seats.

¹⁵Communication with Abhas Choudhary , dd. 26-5-2023

4

Mission Analysis

4.1. Operations and logistics

The operations and logistics diagram shows the main logistical tasks an aircraft has to perform during operation. For the Caty, this consists of the different types of operation types and the production, distribution and fueling of hydrogen. Figure 4.1 shows this diagram. chapter 3 describes the different use cases of Caty. subsection 12.9.3 further elaborates the production and distribution of green hydrogen.

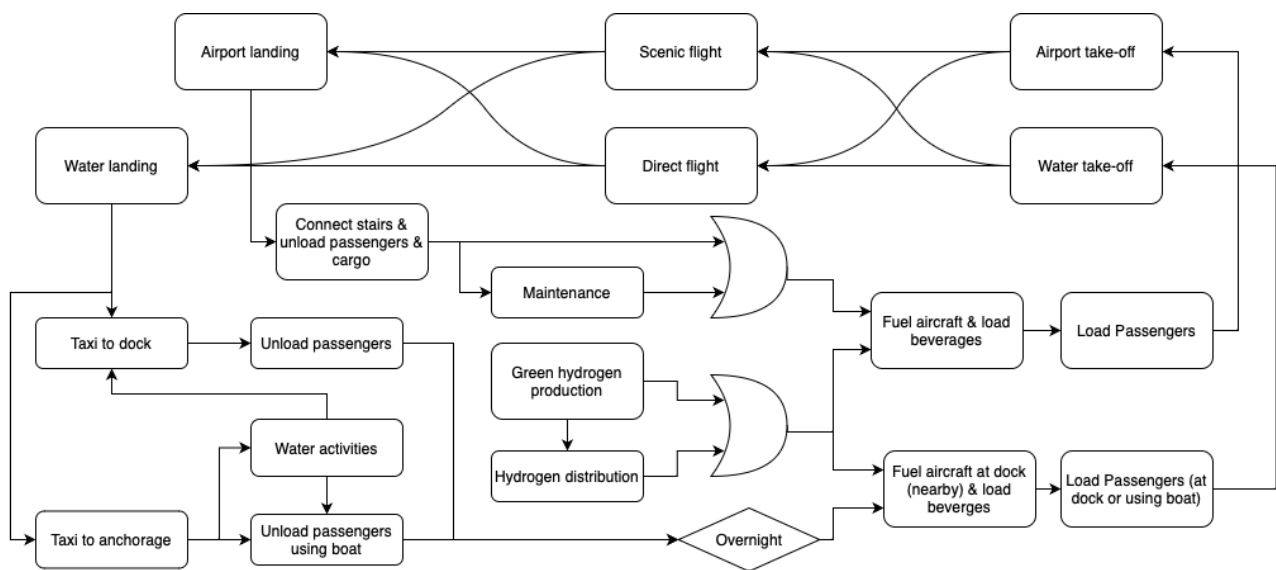
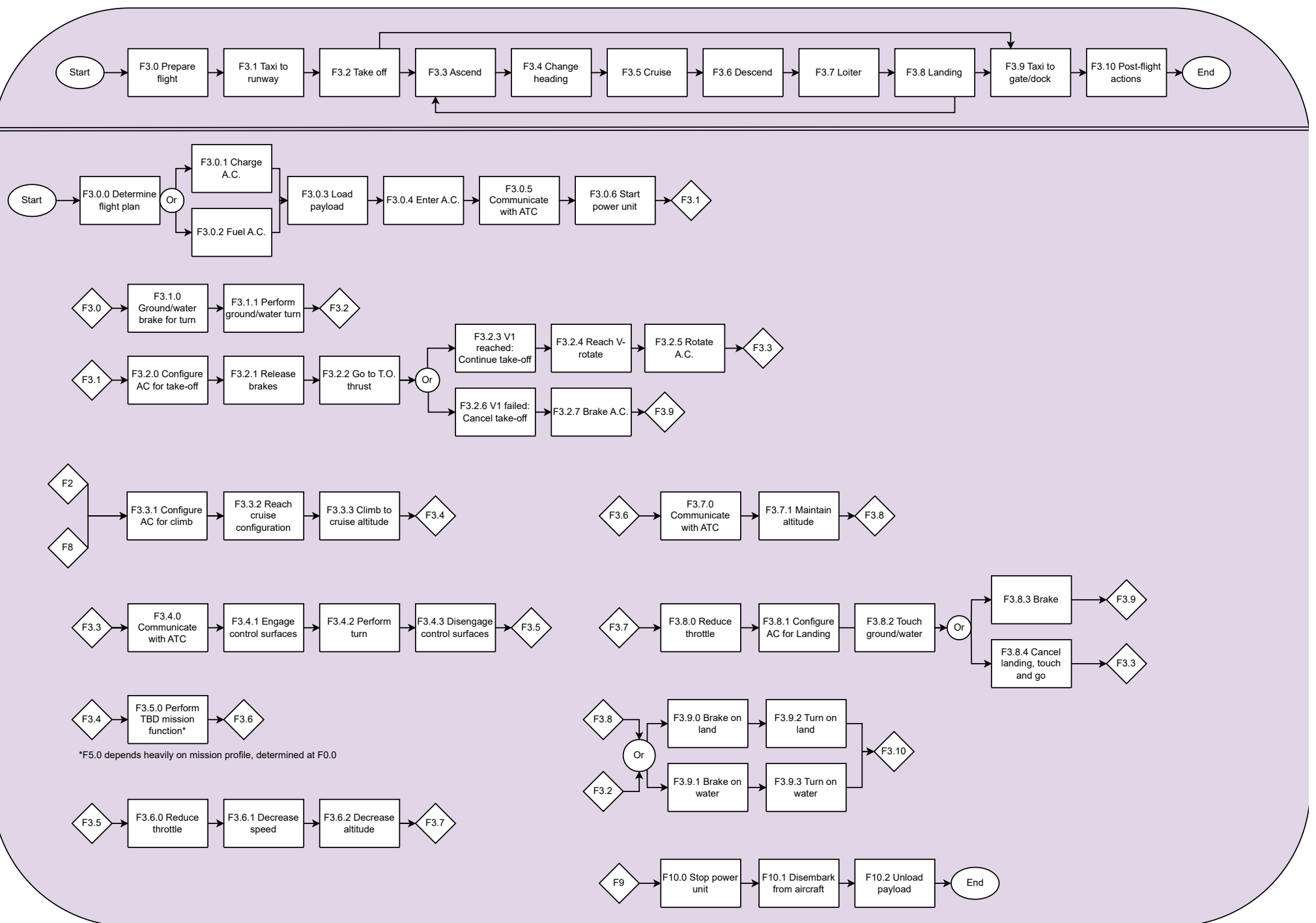
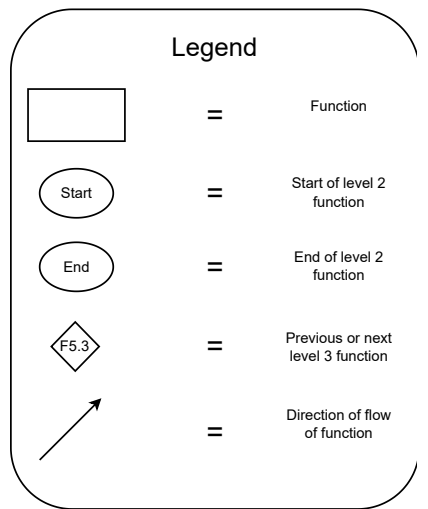
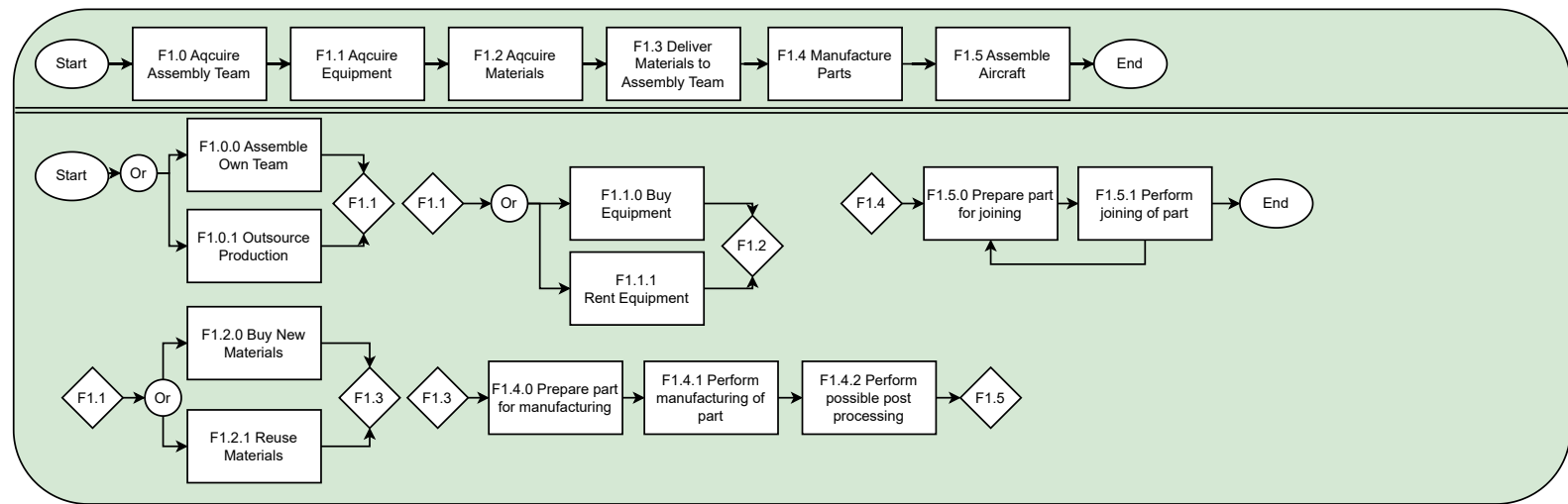
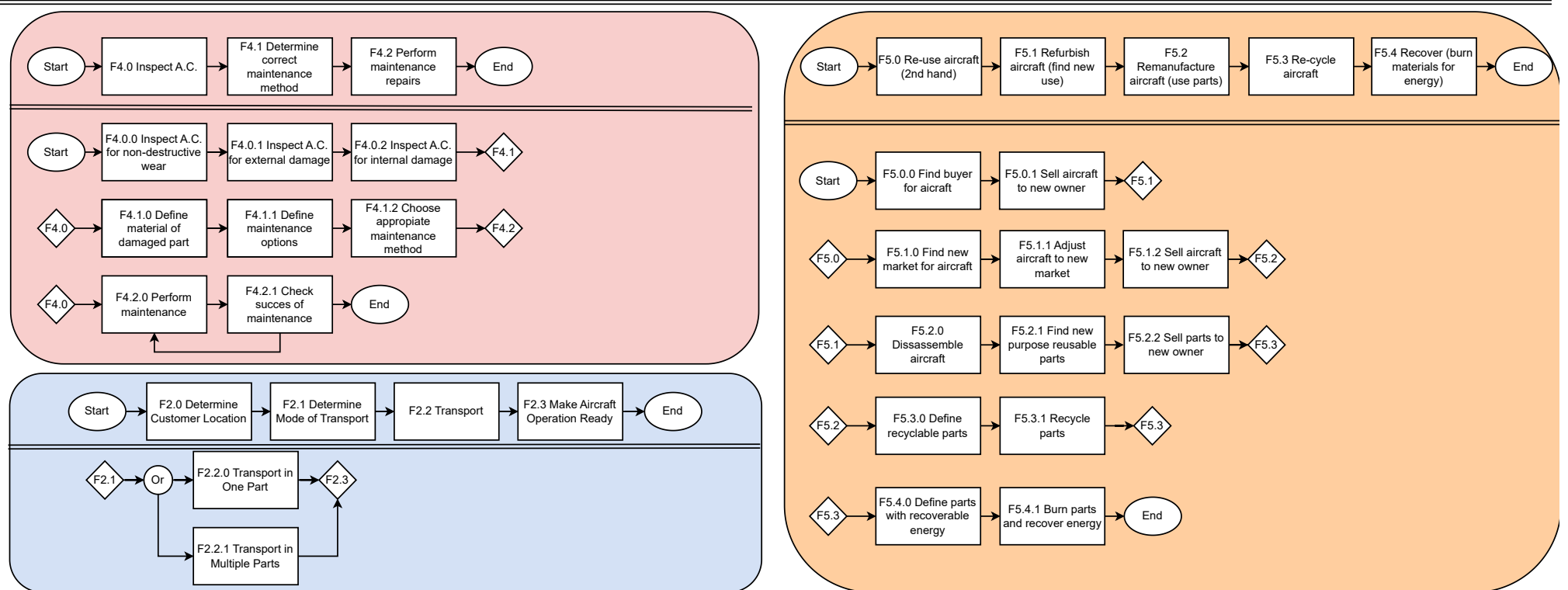
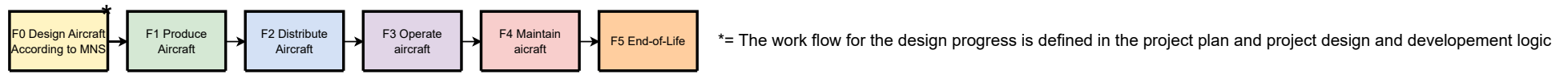
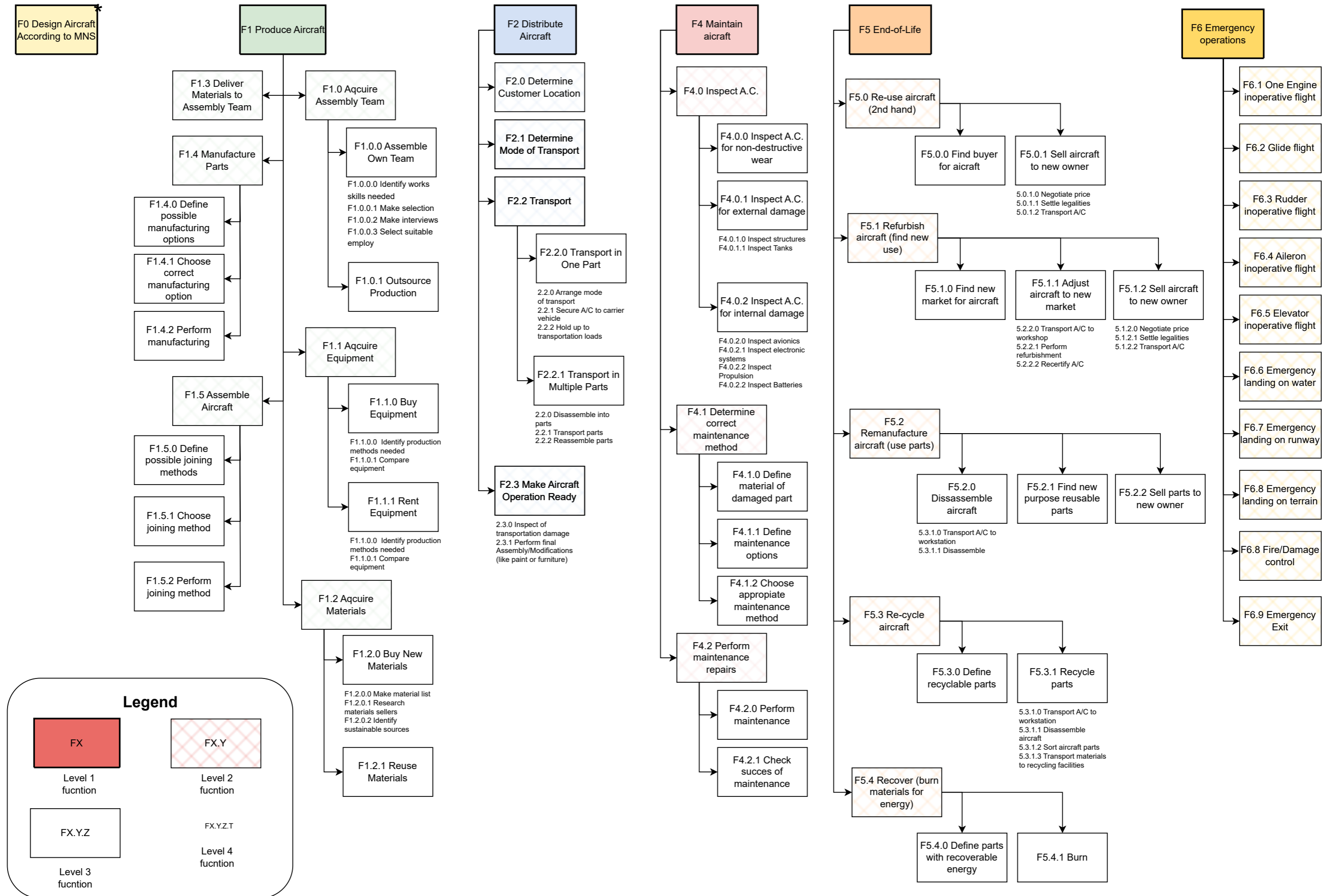


Figure 4.1: Operations & Logistics Diagram

4.2. FFD & FBD

To ensure the aircraft is able to perform the mission correctly, a functional flow diagram and functional breakdown structure was created. This describes the complete lifetime of the aircraft, from design to end of life, and what the aircraft has to be able to do at these stages of its lifetime. It ensures sufficient requirements are set up for the system.





*= The work flow for the design progress is defined in the project plan and project design and development logic

5

Interior Design

The interior design has been designed with the mission profile, use case and regulatory requirements in mind. This chapter covers the design process and the final results, including renders made in Blender.

The main use of the aircraft is luxury chartering where the aircraft is used to fly tourists to their activities on water and on land. During flight, each passenger shall have an easy and good view outside and the observation platforms at the front, engineering station, as well as the blisters at the back, shall be kept. During flight and when landed on water, guests shall be served beverages from the galley.

5.1. Interior Design

In order to accommodate 13 passengers within the aircraft, it became evident that the original Catalina fuselage did not offer sufficient space for comfortable seating. Therefore, the Caty fuselage underwent modifications, incorporating a 10 cm increase in height and a 15 cm expansion in width, while preserving the original Catalina's aesthetic. These adjustments enabled spacious seats, ensuring enough legroom for all passengers. Figure 5.1 shows the aircraft layout in a top view.

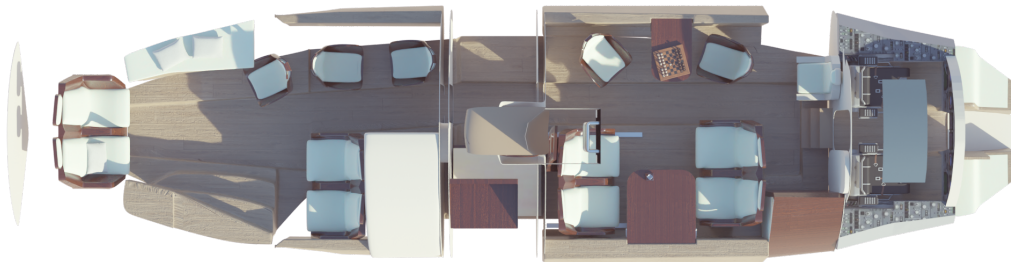


Figure 5.1: Top view of interior



Figure 5.2: Front compartment

To further enhance the seating positions, the aircraft was designed with three seats arranged side by side, accompanied by an off-center pathway within the fuselage. This arrangement gives the aircraft interior a distinctive and unique appearance. In addition, the bulkheads were strategically repositioned to optimize the available space, each equipped with sliding flood doors, serving the purpose of preventing the aircraft from sinking. The engineering station depicted in Figure 5.4 underwent a transformation, resulting in a comfortable observation point situated beneath the wing, affording passengers optimal views of the majestic scenery.

To ensure convenient access to the water, a retractable platform has been installed at the entrance blister. This platform serves the purpose of allowing passengers to dry off before entering the aircraft, preventing a wet interior. During the cruising phase, the stairs leading to the blisters can be converted into a bench, similar to the bench located on the port side. Furthermore, the toilet is positioned behind the two seats illustrated in Figure 5.3. The galley is positioned behind the bulkhead positioned in Figure 5.2.

Throughout the design process, attention was given to incorporating all relevant CS-23 regulations [3]. In this regard, the primary entrance blister and the windows in the front compartment serve a dual purpose as both emergency exits and windows. From analysis, it was determined that, with the closure of all bulkhead doors, the aircraft has the capability to withstand flooding of any two adjacent compartments without the risk of sinking or capsizing.

During the subsequent detailed design phase, emergency exit lights and floor and door markings will be implemented to further enhance safety measures. Moreover, each seat is positioned either forward or backwards during take-off to optimize crash safety considerations.



Figure 5.3: Back compartment

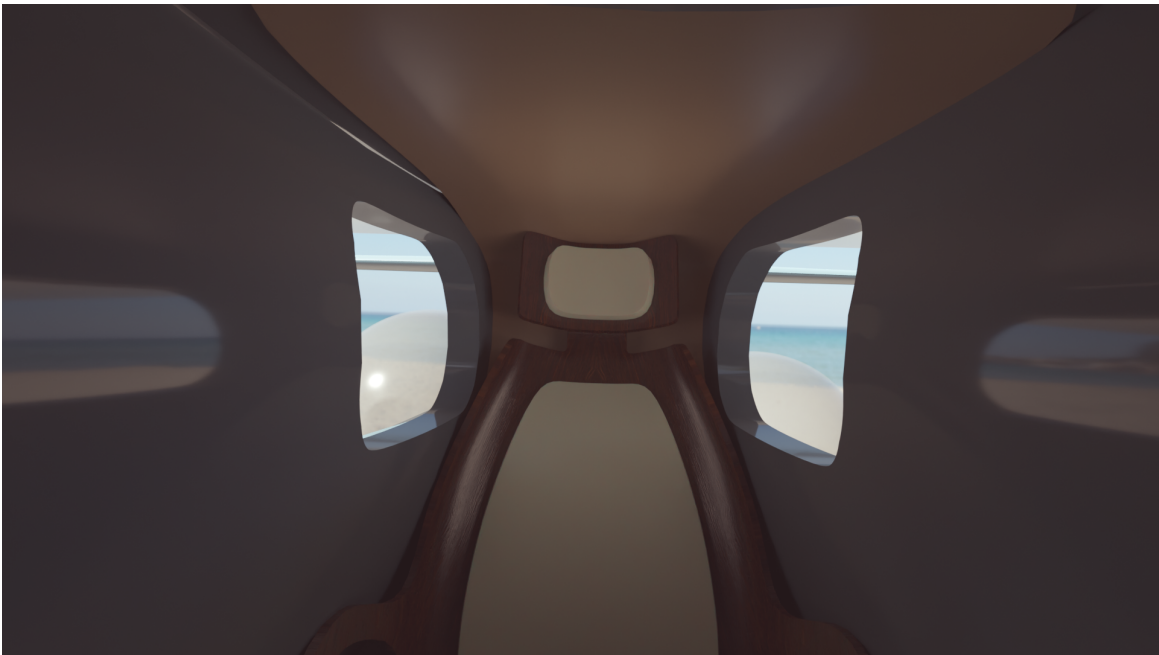


Figure 5.4: Pylon seat

Lastly, Figure 5.5 shows the retractable platform has been added to the exit blister for easy access to the water. This platform can be used when swimming and to board a boat to sail ashore.



Figure 5.5: Side Platform

5.2. Avionics system

With the implementation of hydrogen-electric propulsion, cutting-edge thermoplastic composite structures and a futuristic user experience, the cockpit deserves a modern overhaul with top-of-the-line avionics. Therefore, the Honeywell Anthem is chosen as an avionics system where the following key features made it suit the Caty perfectly. The Caty will become more sophisticated than the original Catalina and an advanced user interface must be implemented to safely and easily control the aircraft. The Anthem system completely redefines the avionics of aircraft by almost exclusively using large touch screens and implementing the flight computers compactly behind the screens. The system is cloud-based which automatically sends all maintenance, flight path and aircraft status data to any authorised user.

6

Weight estimations

The aircraft weight estimation falls into multiple classes. A class I weight estimation looks at the maximum takeoff weight and operational empty weight of aircraft with a similar mission profile in order to extrapolate the maximum take-off mass of the given aircraft. Class II weight estimations use the dimensions and design parameters of the aircraft to estimate the mass of individual components. As these components get designed in more detail, the masses can be calculated from the actual geometry of the parts. All three stages of weight estimation, are described here.

6.1. Class I weight estimation

Table 6.1: List of various aquatic aircraft and aircraft similar to the original PBY Catalina, source from Janes unless otherwise specified¹[1]

	OEW [kg]	MTOW [kg]
FlyNano Nano	70	200
Nordic Omsider	330	600
Svenska Flygfabriken LN-3 Seagull	350	600
Atol Aurora 650	375	650
Lisa akoya	400	650
Vickers Wave ²	421	839
Icon A5	490	685
Dornier S-Ray 007	500	800
EDRA Aeronautica Super Pétrel	500	800
Privateer prototype	1633	2540
Ellison-Mahon Gweduck	1905	2722
Daher Kodiak	2071	3291
Singular SA03	2150	4000
Twin otter 400 [4]	3377	5670
Dornier sea star [5]	3800	5100
Havilland Canada Dash 7 ³	12560	19958
ShinMaywa US-2	25,630	47,700
Canadair CL-415	13,608	19,890

Since the original Catalina was developed in the 1930s, it can be imagined that structural weight improvements can be made. A class I estimation can be done by using similar, more modern aircraft to determine an updated OEW for a certain MTOM since the wing of the Catalina is sized for the MTOW of around 16 tons. A selection of current aquatic aircraft can be found in Table 6.1, of which most are significantly lighter than the Catalina. To also take into account larger weights, some heavier older aircraft are included as well.

Linear regression can be applied to the numbers from Table 6.1 to arrive at $MTOM = 1.76 \cdot OEM + 363$. Assuming this ratio, the OEM of the original PBY with a MTOM of 16000 kg would be 9300 kg, not that far off from the actual OEM of 9485 kg.

¹<https://customer.janes.com/> (accessed on 11/05/2023)

²https://en.wikipedia.org/wiki/Vickers_Aircraft_Wave (Accessed on 23/05/2023)

³https://en.wikipedia.org/wiki/De_Havilland_Canada_Dash_7 (Accessed on 11/05/2023)

6.2. Class II weight estimation

6.2.1. Structure and equipment

For the class II weight estimation, an existing methodology needs to be used. In this case, the USAF methods for small generation airplanes were used. It can be found in Jan Roskams' Aircraft Design Part V [6]. The method applies to "light and utility aircraft with performance up to 300 kts" [6]. This methodology was used for each component of the entire aircraft to make sure all the weights are consistent with each other and nothing is accounted for twice. The class II weight estimations take into account the general dimension of the components and the maximum takeoff weight of the aircraft. For this reason, it needs to be updated constantly as the design proceeds and is therefore implemented as a program. The methodology assumes some of the geometry and does not take into account some of the special design features of Caty such as the strut-brace, the parasol wing and pylon. The furnishing weight is also expected to be much heavier per passenger than for general, utility aircraft, for which the methodology is applicable. To account for this, the furnishing in this weight estimation is doubled.

The weights are divided into three broad categories:

1. Structures
2. Powerplant
3. Fixed Operational equipment

The powerplant weight is only applicable to traditional combustion (turbine or piston engine) aircraft. For this project, this part was replaced with another weight estimation specifically for hydrogen aircraft, presented in subsection 6.2.2. The weights for structures and equipment are presented in tables Table 6.2 and Table 6.3.

Table 6.2: Structure weights

Component	Class II [kg]	Detailed [kg]
Horizontal Tail	92	-
Vertical Tail	42	-
Wing	3040	1200
Gear	85	-
Fuselage	1441	916
Total	4700	2860

Table 6.3: Equipment weights

Component	Class II [kg]
Flight controls	247
Hydraulics	87
Instruments & avionics	95
Electrical systems	87
Air conditioning	310
Furnishing	1168
Paint	48
Total	2052

6.2.2. Propulsion

The propulsion system of a hydrogen-electric aircraft differs enough from combustion-powered aircraft to warrant its own sizing method. Since hydrogen propulsion systems are a pretty new concept and there are barely any flying hydrogen aircraft at this point in time. Also, weight estimations for hydrogen aircraft are still in the early stages and have large uncertainties. For this purpose, a sizing methodology for hydrogen aircraft proposed in a master thesis by George Vonhoff [7] was used. The sizing methodology is designed specifically for aircraft in the CS-23 category, which this aircraft is designed to comply with.

Table 6.4: Propulsion

Component	Class II [kg]	Detailed [kg]
Fuel cell	1157	400
Cooling	203	600
Compressor	2	-
Tanks	1362	-
PMAD	126	-
Motors	306	106
Propellers	208	-
Other	246	-
Total	2491	2843

6.2.3. Center of gravity and mass moment of inertia

Although the center of gravity and mass moment of inertia estimations are part of the weight estimation process, they are presented in chapter 11, since they are uniquely relevant for stability and control. The used mass moment of inertia is still taken from the Class I weight estimation since a more precise value wasn't deemed critical for the purposes it is used. See section 11.6 for the mass moment of inertia estimation or section 11.1 for c.g. estimation.

6.3. Further weight estimation

After the class II weight estimation, the weight estimate of the aircraft keeps being updated as the design of some components matures. For some components like the electric motors or fuel cells, of-the-shelf solutions can be used, for which the actual weight is known. Some other components, like the propeller, wing and cooling have been designed to a stage that a mass estimate can be calculated from the design directly. It can be noted that a lot of these components deviate very strongly from their previous weight estimation. The exact reasons can for this are explained in the chapters respective to the part designs, but mostly the parts that were chosen to be designed more in detail are more special to this specific aircraft and are less presented in generic weight estimation formulas.

6.4. Verification & Validation

Each class of weight estimation can be verified when compared to the previous class of weight estimation. The ratio between the OEM and MTOM was computed from the class II weight estimation and compared with the class I. Similarly, the weight calculated from the actual part designs can be compared with the relevant weight estimations from the class II weight estimation. These comparisons need to be made carefully though, since the previous weight estimation is always a lot more approximate and the weights are expected to deviate. In this case, the OEM increases by 23 % (1282 kg) from Class I to Class II. This increase can be explained by the heavy hydrogen tanks, weighing 1362 kg.

7

Propulsion Design

The propulsion system of the Caty is decisive over multiple aspects of the aircraft. The propulsion system has a major contribution to the overall weight and cost of the aircraft. Additionally, the layout of the interior could be limited by propulsion system components and thus affecting the experience the passengers might have. The noise of the aircraft is also mainly produced by the propulsion system. It is therefore important that a suitable type of propulsion system is chosen, and that it is designed for low noise and mass.

This chapter describes the design process of the propulsion system. First, the trade-off for the type of propulsion system is presented in section 7.1. This trade-off was previously discussed in the mid-term report [1], but has been summarized in this chapter for completeness. Then, in order to determine whether the Caty could retain its original two-engine configuration, an exemplary initial propeller was designed. This was done such that the noise of the aircraft could be determined and for a mass estimation. For the noise estimation, both a calculation based on empirical data and a calculation based on blade element theory are performed in section 7.2. The design method for the propeller is also included in this section. This showcases the feasibility of the two-engine configuration. The engines' and fuel cells' designs are described in section 7.3. Another very critical propulsion system component is the cooling system, the sizing of which has been described in section 7.4. This includes the heat exchanger sizing and intake design.

Once the propulsion type and engine configuration were determined, the layout of the remaining propulsion subsystems were decided. Multiple iterations of this process are described in section 7.5. Finally, the weights of the propulsion system components are estimated in section 7.6.

7.1. Propulsion System Trade-off

For the preliminary propulsion system, multiple design concepts were researched. The five concepts were designed to meet the following criteria: range, climb speed, and payload requirements, and then their preliminary mass, volume, cost, and sustainability were assessed (Table 7.1). The entire trade-off can be seen in Table 7.2, where the trade-off itself is shown as well as the sub-trade-off of the sustainability criteria. The scoring system is also shown with a color scale and meaning of each score. Based on this trade-off, the pressurized hydrogen concept (700 bar) was chosen, whose scores are significantly better than the other options (with the hybrid pressurized as exception). The full battery option was by far the worst option since it couldn't meet all the requirements. The added weight from the hybrid's batteries is not worth the savings in fuel cell weight the aircraft would need to sustain take off thrust for an extended time period. Furthermore, since the range of the aircraft is limited and there is plenty of room in the original aircraft's main wing, the added cost and energy for liquid hydrogen is not worth its potential savings in weight and volume. [1]

Table 7.1: Concept parameters for quantitative criteria

Concept \ Quantitative Criteria	Mass [kg]	Cost [\$/h]	Volume [m^3]	Emission [t/h]
Battery (230 km)	16000	962.6	6.14	0.396
Battery (500 km)	23400	880	14.3	1.065
Hydrogen (700 bar)	14188	447.4	14.38	0.729
Hydrogen (Liquid)	13090	1005.6	10.4	0.778
Hybrid (700 bar)	14072	561.9	12.82	0.824
Hybrid (Liquid)	12901	1157.7	8.72	0.87
"Normal jet"				1.26

Table 7.2: Concept Trade-off

Concept \ Criterion	Mass	Sustainability	Risk	Cost	Volume	Total
Weight [x/4]	1	3	4	3	2	13
Battery (230 km)	3	3	1	2	4	2.3
Battery (500 km)	2	1	1	2	2	1.5
Hydrogen (700 bar)	4	2	3	4	2	2.9
Hydrogen (Liquid)	4	2	2	2	2	2.2
Hybrid (700 bar)	4	2	3	3	2	2.7
Hybrid (Liquid)	4	2	2	2	3	2.3

Concept \ Sustainability	Emissions [t/h]	End-of-life [Qualitative]	Total
Weight [x/4]	4	1	5
Battery (230 km)	3	2	3
Battery (500 km)	1	2	1
Hydrogen (700 bar)	2	3	2
Hydrogen (Liquid)	2	3	2
Hybrid (700 bar)	2	2	2
Hybrid (Liquid)	2	2	2
"Normal jet"	1		

4	Excellent; exceeds requirements
3	Good; meets requirements
2	Correctable deficiencies
1	Unacceptable

7.2. Propeller Design

This section will cover the preliminary propeller design and noise calculations, with the propeller design serving as a means to determine the magnitude of the generated noise. First, empirical noise calculations give a rough estimate of the expected noise values of the aircraft at 3000 ft which comes from empirical data. Blade element theory software is then used to calculate a more accurate estimate for the aircraft noise. The results from both methods partially determine the engine configuration for the aircraft.

7.2.1. Empirical Noise Calculations

A first order noise estimation could be made based on an empirical noise formula as provided by literature, see Equation 7.1 [8, 9]. It bases the noise estimation on the engine shaft power (P_{br}), propeller diameter (D),

rotational tip Mach number (M_t), number of blades per propeller (B), number of propellers (N), and observer distance from propeller (r). A two-engine and four-engine configuration were analysed and the noise was found to be sufficiently low with the two-engine configuration. With aesthetic requirements, power and noise results in mind, the two engine configuration was chosen for the rest of the analysis.

$$\text{PNR}_{\text{weighted}} = 83.4 + 15.3 \log P_{br} - 20 \log D + 38.5 M_t - 3(B - 2) + 10 \log N - 20 \log r - 16 \quad (7.1)$$

The empirical noise formula gives an intuitive sense on what parameters play an important role in the noise generation. With this formula the noise could quickly be estimated, allowing for quick iteration.

Aside from the empirical noise calculations based on literature, noise levels of existing aircraft at different altitudes were compared ¹ where the noise for a standard turboprop aircraft during departure at 3000 ft is found to be 67 dBA. This value can be used to validate the calculation method by using inputs for a conventional turboprop aircraft.

7.2.2. Blade Element Theory Noise Calculations

Next to the empirical noise calculations, blade element software programs are used to estimate the propeller noise of the aircraft. A combination of the programs JavaProp, JavaFoil and XROTOR was used. First, JavaProp was used to design the propeller geometry. JavaProp optimizes a propeller design with the following inputs: Number of blades, revolutions per minute, diameter of propeller, diameter of spinner, aircraft velocity, and propulsive power. It was chosen to design the propeller for an intermediate configuration such that it operates at both max power as well as cruise power. The blade angle can be increased to generate more power but if it is increased too much propulsive efficiency drops significantly. From experimentation, it was chosen to design the propeller for a power of 400 kW and a relatively low RPM of 1200. With this RPM the diameter had to be kept large at 3.5 m similar to the original Catalina. The diameter of the spinner was assumed to be 30 cm from visual inspection of other aircraft. An intermediate velocity was used of 50 m/s between climb and cruise speed and lastly, an intermediate speed of sound and altitude was used between sea level and cruise altitude. The designed propeller was then checked for cruise conditions where the blade angle can be decreased to be more efficient and during climb and take off where the blade angle is increased to generate more thrust.

Furthermore, four airfoils had to be selected along the propeller span, and the angle of attack the different airfoils should operate at could be chosen. These airfoils together with their angle of attack were selected with the help from the user's manual on the website of JavaProp². JavaProp does not take into account the structural strength of the propeller. The propeller is therefore only used as a case study for the noise calculations. More detailed design is needed to arrive at a fully operational design.

Since the aerodynamic performance parameters of the airfoils were already in JavaProp, but couldn't be exported, the airfoils were analysed in JavaFoil. Here the aerodynamic properties of these airfoils were analysed such that they could be exported. For a range of angles of attack, the C_l , C_d , $C_{m_{0.25}}$ and critical Mach number are calculated. These parameters are used in XROTOR where further aerodynamic analysis can be performed. XROTOR is used to estimate the noise at 3000 ft. Further input parameters for XROTOR are altitude, RPM, and engine power.

For the airfoils, the sections chosen in the propeller design are given in Table 7.3. Section 1 is located at the center of the propeller hub and section 4 is at the tip of the propeller. The geometry is extrapolated between the airfoils and the hub is taken into account into the design. Three different propellers were analysed: A propeller similar to the ones mounted on the original Catalina (3 bladed), a six bladed propeller for the Caty, and a nine-bladed propeller for the Caty. The noise estimate for the propeller similar to the original Catalina propeller is based on parameters (e.g. shaft power, RPM) used on the original Catalina, while both other configurations use parameters specific to the Caty.

¹<https://www.nats.aero/environment/noise-and-emissions/measuring-noise/lmax/> (accessed on 08/06/2023)

²<https://www.mh-aerotools.de/airfoils/javaprop.htm> (accessed on 08/06/2023)

Table 7.3: Propeller Airfoils

Section	1	2	3	4
Airfoil	MH 126	MH 112 16.2%	MH 116 9.8%	MH 120 10.03%
Angle of Attack [deg]	3	1	4	3

Noise result

The noise levels found from the analysis can be found in Table 7.4. It is found that the Original Catalina produces a sound level at 3000 ft at climb power of 70 dBA or 65 dBA according to the empirical noise estimate and XROTOR estimate respectively. This is relatively close to the noise figure of a standard turboprop aircraft at 3000 ft as found earlier (67 dBA), but one has to take into account that the noise estimation presented in this report only takes into account the propeller noise.

The difference between the two estimates is 5 dBA. Although 5 dBA might not sound significant, it equals to an increase in intensity by a factor of more than 3. This discrepancy is visible in all analysed configurations, and is most for the the original Catalina at cruise power setting. Here the difference is more than 16 dBA, a intensity factor difference of almost 40. It is therefore evident that these noise estimates should not be taken at face value, as their absolute values might not be valid. However, the noise estimates might still be useful, as they can indicate the trend that the propeller design has on the noise. Hence, the noise estimates will only be used to indicate a relative decrease in sound.

The analysis of the 9-bladed propeller, while flying at a cruising power of 3000 feet, 56.5 m/s, 1200 RPM, and 293.0 kW, indicates a noise estimate ranging between 32 and 42 dBA. Or, more relevant, a decrease in noise of between ~19 and 25 dBA. For the climb power setting a relative noise reduction of between 21 and 24 dBA is estimated compared to the original. When analysing a 6 bladed propeller for the Caty, the relative noise reduction decreases to around 15 dBA to 17 dBA for both cruise and climb power settings.

Next to the intensity changes of the noise, the pitch and timbre of the sound produced by the propulsion system will be different. This will partly be caused by the lack of internal combustion engine noise on the Caty. But the main contributor will likely be the change in pitch of the noise due to the increase in blade number. The base frequency for the original Catalina is estimated to be around 65 Hz, while for the 6 and 9 bladed propeller this will be around 120 and 180 Hz respectively.

Table 7.4: A-weighted noise estimation at 3000 ft of different propeller configurations.

Configuration	Power setting	Empirical noise estimate	XROTOR noise estimate
Original Catalina	Climb	70.41 dBA	64.86 dBA
	Cruise	66.84 dBA	50.45 dBA
Caty 6 bladed	Climb	54.94 dBA	47.89 dBA
	Cruise	51.09 dBA	35.82 dBA
Caty 9 bladed	Climb	45.94 dBA	44.15 dBA
	Cruise	42.09 dBA	32.19 dBA

Overall, by optimizing the propeller to minimize noise production a significant decrease in noise can be expected. This can mostly be done by reducing the mach number of the tip of the blade and increasing the amount of blades. Moreover, by replacing the combustion engine by an electric engine more noise reduction is expected. This, in combination with the lower propulsive power required due to the decrease mass and drag should yield even more noise reduction, such that the requirement of producing less than 65 dBA at an altitude of 3000 ft can be complied with.

7.3. Engines and Fuel cells

The noise calculation showed that a two engine configuration would likely be able to achieve the noise requirement. Together with the desire to keep the two engine configuration for aesthetic reasons, it was chosen to use this configuration.

The electric motor and fuel cells were sized based on the propulsive shaft power needed, which is a total of 708 kW for cruise and 1080 kW for climb power. In the case that one engine were to fail, it was determined that 534 kW would be needed to be produced by the other engine in order to keep operating the aircraft (albeit at reduced performance). Taking into account a small safety margin, it was determined that 600 kW shaft power for each engine would be sufficient.

In order to get a good estimate for the power, size, and efficiency of the engine, existing or in-development engines were examined^{3 4}. The exact engine abiding to all requirements was not found, but with a simple linear regression the parameters for such an engine could still be found. It was estimated that an engine that would be able to produce 600 kW continuous shaft power would weigh around 56 kg (engine and simple gearbox) and can have an overall efficiency of around 95%. It would also be able to provide sufficient torque for a 9 bladed propeller spinning at 1200 rpm if a correct gear ratio would be chosen.

In combination with each engine two 300 kW fuel cells were chosen, totalling the required 600 kW per engine. The two fuel cells per engine configuration was chosen as smaller fuel cells are more readily available. These fuel cells are often modular, allowing straightforward integration of two fuel cells. Additionally, having two fuel cells per engine gives added redundancy. The failure of one fuel cell still leaves 300 kW of available power for the engine connected to that fuel cell. This still leaves the aircraft fully functional, with only a slight decrease in performance, meaning that the design is fail-safe.

One 300 kW fuel cell, without auxiliary subsystems, was estimated to be 100 kg⁵. The fuel cell would have an estimated efficiency between 50% and 55%, depending on the operating power. If less power is required from the fuel cell, it is more efficient.

7.4. Aircraft Thermal Management System

Due to the expected efficiency of the to-be-used hydrogen fuel cell of 50%-55%, a significant amount of heat power needs to be dissipated. The motors need to sustain a max power of around 600 kW each and thus the same amount of power needs to be dissipated by a thermal management system. In addition to this, the motor waste heat of 5% of the input power also needs to be dissipated.

The approach was chosen to use a liquid cooling system, both due to its technology readiness level as well as its relative ease of design. Since the hydrogen cooling solution has not fully been developed yet and due to the only recent interest in the subject since about 2020, limited research is available on the topic. Other cooling methods that in theory could have better performance, but have not been used or built-in practice. This will be done by evaporated cooling by means of evaporating water or using a special coolant similar to what is used in air conditioners [10]. Cooling is a very challenging problem for hydrogen fuel cell aircraft. For example, when it is applied to an Airbus A320 a radiator surface area the size of the fuselage cross-section is required. In addition, the radiators cause additional drag requiring 27% extra power during cruise [11]. Drag can be limited by not letting the airspeed through the radiator increase significantly, since the drag is proportional to the airspeed. A solution for this is a RAM air intake. Normally used for RAM air jets it can also be used to decrease the airspeed of the airflow by expanding it and thus increasing the pressure as can be imagined by applying Bernoulli. The intake or diffuser of the RAM air system will have an expanding geometry as explained in subsection 7.4.3. A straight section follows where the radiator is incorporated at an angle to reduce drag and finally, a nozzle to maximize residual thrust from the radiator [10]. First, a method of calculating the required radiator area that is exposed to air is implemented after which the full radiator geometry can be derived. Finally, the RAM intake system will be designed and integrated into the aircraft.

First, the required cooling power needs to be calculated, the coolant chosen is a water ethylene glycol solution

³<https://www.saluqimotors.com/products/> (accessed on 31/5/2023)

⁴<https://www.h3x.tech/> (accessed on 31/5/2023)

⁵<https://inoce1.com/product/> (accessed on 06/06/2023)

with a 40% mass fraction of ethylene glycol. It is commonly used for liquid cooling purposes [10]. It has a high specific heat of $3752 \frac{J}{kg \cdot K}$ and a density of $1041 \frac{kg}{m^3}$ at an assumed average temperature of $60 C^\circ$ ⁶. Due to the ethylene glycol a freezing temperature of $-25 C^\circ$ is realized which ensures safe operation in even colder climates. Since it is an amphibious aircraft and is not used on ice and its target market is tourism in warmer climates this is not an issue. Due to the low operating ceiling, the temperature is also not an issue there since according to ISA the temperature at 10,000 ft is $-5 C^\circ$.

The target max temperature of the fuel cell is $90 C^\circ$. This is an assumed value since some paper take it to be lower at $70-80 C^\circ$ [10] while others such as [11] take it to be higher at $100 C^\circ$. The considered fuel cells are low-temperature PEM cells which means that they operate at a low temperature, significantly lower than a combustion engine would. This also results in the cooling system size increasing since the obtainable temperature difference after the cooling compared to the intake temperature is very limited.

It is assumed the internal heat exchanger of the fuel cell is designed to reach this temperature of $90 C^\circ$ at the coolant outlet. The fuel cell coolant inlet temperature is an engineering decision and will determine various aspects of the cooling system. For example, a low temperature will result in a low coolant flow but an air heat exchanger increased in size. Various temperatures are evaluated based on the final total cooling system design and in the end, a temperature of $65 C^\circ$ was chosen. With these values, the mass flow rate of the coolant can be calculated with Equation 7.2. \dot{Q} is the heat dissipation required which is based on the power the fuel cells have to produce to deliver the motor power but also to cover the efficiency loss of the motor, and power distribution system. It is increased by 10% as is required by CS-23 [3].

$$\dot{Q} = C_p \cdot \dot{m} \cdot \Delta T \quad (7.2)$$

After the required heat rejection and coolant mass flow is calculated, a preliminary design of a heat exchanger can be done. To start with, the required surface area that is exposed to a certain airflow is calculated. This is done via the Effectiveness-NTU method [12]. The mass-flow of air is calculated by adding the flight velocity and the air velocity generated by the propeller as calculated by Equation 7.3. Since a worse mass flow equals worse cooling performance, the mass flow is calculated with a flight speed of zero.

$$\Delta V = \frac{2 \cdot P_{motor}}{\rho_{air} \cdot A_{propeller_{disk}}} \quad (7.3)$$

A C-coefficient is then calculated by multiplying the C_p and mass-flow of the coolant and air respectively such that a $C_{coolant}$ and C_{air} is obtained. The lowest of these two is then C_{min} and the highest C_{max} . The ratio C_r is then also calculated with C_{min}/C_{max} . Next is where the NTU comes in, a measure of the cooling capacity of the heat exchanger. It is defined by Equation 7.4. A_s in this equation is the surface area of the heat exchanger exposed to air, it is the input of an iteration where the surface area is increased until the heat dissipation requirements are met.

$$NTU = U \cdot A_s / C_{min} \quad (7.4)$$

Following this, the effectiveness of the radiator is calculated. It is based on the C-coefficients and the NTU and acts as the efficiency of practical heat dissipation to the maximum theoretically possible. It is defined by Equation 7.5 and is specifically for a cross-flow heat exchanger as is the most practical for an aircraft such that the coolant can be inserted into the exchanger from the side instead of through in the airflow direction, blocking its own airflow.

$$\eta = 1 - \exp(NTU^{0.22} / C_r \cdot (\exp(-C_r * NTU^{0.78}) - 1)) \quad (7.5)$$

The maximum heat transfer possible is then calculated which is based on the maximum temperature difference possible, or the difference between the coolant and air temperature as if the air is heated up to the coolant temperature. It is calculated with Equation 7.6. The actual heat transfer as follows from the efficiency is then as in Equation 7.7.

⁶https://www.engineeringtoolbox.com/ethylene-glycol-d_146.html (accessed on 14/06/2023)

$$\dot{Q}_{max} = C_{min} \cdot (T_{hot(coolant)} - T_{cold(air)}) \quad (7.6)$$

$$\dot{Q}_{actual} = \eta \cdot \dot{Q}_{max} \quad (7.7)$$

With the actual heat transfer, the outlet temperatures of both the coolant air can be calculated. The outlet temperature of the coolant is in reality already known since it was an input variable so it will result in the same as used for the coolant mass flow calculation. If C_{min} is equal to the air C-coefficient the air outflow temperature and coolant return temperature are determined by Equation 7.8. If C_{min} is equal to the coolant coefficient on the other hand the temperatures are defined by Equation 7.9.

$$\begin{aligned} T_{hot(air)} &= T_{cold(air)} + \dot{Q}_{actual}/C_{min} \\ T_{cold(coolant)} &= T_{hot(coolant)} - \dot{Q}_{actual}/C_{coolant} \end{aligned} \quad (7.8)$$

$$\begin{aligned} T_{cold(coolant)} &= T_{hot(coolant)} - \dot{Q}_{actual}/C_{min} \\ T_{hot(air)} &= T_{cold(air)} + \dot{Q}_{actual}/C_{air} \end{aligned} \quad (7.9)$$

When the actual heat dissipation is higher or equal then the required amount, the area used is sufficient. The required heat dissipation is adjusted by a 10% margin required by CS-23 [3]. In addition, a 10% margin is applied for uncertainties in the heat exchanger layout and efficiency.

Now the required surface area is determined, the physical heat exchanger geometry needs to be designed to size the radiator. The initial goal is to put the radiator inside the nacelle so that the propeller airflow is benefited from. The space that is available is the diameter of the nacelle which was determined to be 1.45 m or about 5 cm wider than the original Catalina. A hole is cut out in the middle for the electric motor and propeller hub assembly with a diameter of 0.5 m. First, a heat sink geometry was used where the heat sink has straight cooling fins perpendicular to plates which contain the coolant tubes. For some estimated fin and plate thicknesses the surface area was calculated which resulted in possible designs. However, a radiator length obtained of more than a meter in length would not only have problems fitting inside the nacelle but also reduces the cooling efficiency significantly since the air is heated up throughout the length thus reducing the heat transfer further down in the heat exchanger.

Another approach was initiated with the recommendation of F. Beltrame, part of the propulsion department of the faculty, to use an offset-stripped fin heat exchanger geometry. It was also recommended to limit the intake velocity to a maximum of 20 m/s. Using Equation 7.3 and assuming a linear increase of energy dissipation to the air along the span as the tip speed is higher, a velocity of around 16 m/s can be obtained in the intake at max-thrust. Afterwards, the airspeed will be enough to meet the 16 m/s requirement. The design consists of a waving loop of fins throughout the radiator where multiple rows are offset from each other to maximise efficiency while limiting the drag. A cross-section of such a radiator is illustrated in Figure 7.1. The radiator consists of a large number of fins offset from each other. All fins will have the same geometry and spacing from each other as is given in Table 7.5 [10]. The same parameters are chosen since it was found small changes would not result in significant differences and the used parameters as given by the source can be assumed to be manufacturable, which might be a challenge if changed due to the delicate nature of the heat exchanger.

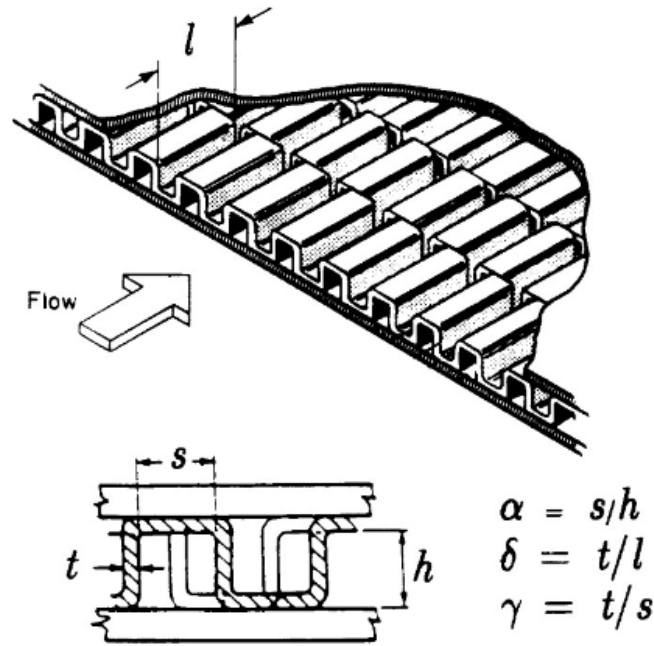


Figure 7.1: Cross-section of a stripped-fin radiator [10]

Table 7.5: Geometric and physical parameters of the proposed offset-stripped fin heat exchanger [10].

Parameter	[mm]
h_{tube}	2.5
t_{tube}	0.1
$t_{channel}$	0.5
h_{fin}	2.3
s	1.16
l	3.1
t_{fin}	0.1

In addition to these parameters, the physical properties of the heat transfer surface and material are required. The heat transfer coefficient of air can be approximated by Equation 7.10 and is dependent on the airspeed⁷. The heat transfer coefficient will then be, following the 16 m/s intake velocity, around $40 \frac{W}{m^2K}$. This matches the 30-60 $\frac{W}{m^2K}$ specified in [12]. For the water-glycol mixture it is approximately $361 \frac{W}{m^2K}$ [13].

$$h_{air} = 12.12 - 1.16 \cdot v + 11.6 \cdot v^2 \quad (7.10)$$

The geometry is then calculated with the step-by-step equations listed in Equation 7.11. The number of fins and fin rows are calculated as well as the surface areas of the inner coolant tubes and exposed outer fins. The inputs to this system of equations are the size of the radiator as a cuboid. These are the width, height, and depth of the heat exchanger, indicated as W_{HX} , H_{HX} , Z_{HX} . In the event of a circular radiator, this can be converted by calculating the equivalent dimensions of a square from the circular available area by setting $\sqrt{area_{circular_radiator}}$. The end result is UA , it is the weighted average heat transfer coefficient times the weighted average surface area. This can be used for the Effectiveness-NTU method to determine if the actual heat dissipation is sufficient. The UA calculated is in this case the $U \cdot A_s$ in Equation 7.4.

⁷https://www.engineeringtoolbox.com/specific-heat-capacity-water-d_660.html (Accessed on 14-06-2023)

$$\begin{aligned}
W_{channel} &= h_{tube} - 2 \cdot t_{tube} \\
N_{tubes} &= \text{round}(H_{HX} / (h_{fin} + h_{tube})) \\
N_{channel_per_tube} &= (Z_{HX} / (W_{channel} + t_{channel})) - 1 \\
N_{channel} &= N_{channel_per_tube} \cdot N_{tubes} \\
A_{hot} &= 2 \cdot W_{channel} \cdot W_{HX} \cdot N_{channel} \\
A_{primary} &= 2 \cdot s \cdot l \\
A_{fin} &= 2 \cdot h_{fin} \cdot l + 2 \cdot h_{fin} \cdot t_{fin} + s \cdot t_{fin} \\
N_{fin_per_width} &= \text{round}(W_{HX} / (s + t_{fin})) - 1 \\
N_{fin_gap_stube} &= N_{tubes} - 1 \\
N_{fin_layers} &= \text{round}(Z_{HX} / l) \\
N_{fin} &= N_{fin_per_width} \cdot N_{fin_gap_stube} \cdot N_{fin_layers} \\
A_{cold} &= N_{fin} \cdot (A_{primary} + A_{fin}) \\
m_l &= \sqrt{(2 \cdot h_{ccold} / (k_{fin} \cdot t_{fin})) \cdot (h_{fin} + t_{fin})} / 2 \\
\eta_{fin} &= \tanh(m_l) / m_l \\
\eta_{surf} &= 1 - ((A_{fin} / A_{cold}) * (1 - \eta_{fin})) \\
UA &= 1 / (1 / (h_{hot} \cdot A_{hot}) + 1 / (h_{ccold} \cdot A_{cold} \cdot \eta_{surf}))
\end{aligned} \tag{7.11}$$

Both the radiator geometry and the Effectiveness-NTU method can be iterated in parallel to determine the optimal and required radiator size. The radiator frontal area is assumed to be fixed in the iteration since it is mainly constrained by aesthetic restrictions and can be defined manually. The length of the radiator is then increased until all the heat can be dissipated.

7.4.1. Cooling relief systems

Two separate factors decrease the amount of heat the thermal management system has to dissipate. One is the heating of hydrogen. Since the hydrogen is pressurized at 700 bars, it will undergo adiabatic expansion while depressurizing to 1 bar before being used in the fuel cell. This means the hydrogen will be at a temperature of 120 K when it depressurizes which can be heated again to normal operating temperatures. This will be assumed to be the same as the coolant intake temperature of 65 °C as the coolant has the same temperature. This means that depending on the power and thus the hydrogen mass flow around 30 kW can be dissipated in this way using Equation 7.2. The hydrogen mass flow is calculated according to Equation 7.12.

$$\dot{M}_{H_2} = P / LHV \cdot \eta_{fuelcell} \tag{7.12}$$

The second way and more useful way to relieve the cooling system is the evaporation of the generated water. The fuel cell can be designed such that a part of the heat will be specifically directed at the exhaust water such that it will evaporate [10]. Since the fuel cell already operates at 90 °C this is not a significant temperature difference until evaporation will occur. The enthalpy of water is very high which relieves the cooling system significantly. Using the mass flow of hydrogen, see Equation 7.12, at the design input power setting and the molar ratio of the fuel cell reaction which turns hydrogen and oxygen into water: $O_2 + 2 \cdot H_2 = H_2O$, the amount of water that is generated can be calculated. Besides the enthalpy, the water also heats up from around 50 °C, as the external air temperature is 36 °C, to the 100 °C required for evaporation. This is assumed since the molar mass of hydrogen is only about 1/8 of the molar mass of water and also only at 65 degrees at the hydrogen intake. This also makes sense since the heating portion of the water is also not very significant compared to the evaporation itself. In the end, around 19.5 kW is dissipated via the heating and 213 kW due to the evaporation. This is about a third of the total heat dissipation of the radiator that can be reduced this way so it is definitely desired to incorporate this system.

7.4.2. Coolant

The coolant mass needs to be estimated for the aircraft mass estimation. A normal coolant flow velocity is roughly 2 m/s ⁸. With the determined coolant mass flow and density the required pipe cross-sectional area can be calculated with Equation 7.13. Straightforwardly the coolant mass can be also calculated by estimating the volume in the total pipe length. For now, this is taken to be 20 m as the total pipe length. Additionally, a coolant tank of 30 L is installed to manage take off power, also satisfying the CS-23 requirement of a minimum coolant tank volume of 3.8 L [3].

$$A = \dot{m} / (\rho \cdot v) \quad (7.13)$$

7.4.3. Radiator Drag

Since the radiator is quite large and has a lot of surface area exposed to the air stream, the drag is sufficiently large to be calculated separately for even the preliminary design. In order to manage drag, the radiator is not exposed to the air stream, but rather within an air duct between a diffuser and a nozzle to slow down the airflow as it flows through the radiator to 16 m/s. The flow velocity of 16 m/s has been deemed a good trade-off between mass flow and drag, as well as the air velocity the propeller can provide at takeoff. A sketch of the geometry can be seen in Figure 7.2.

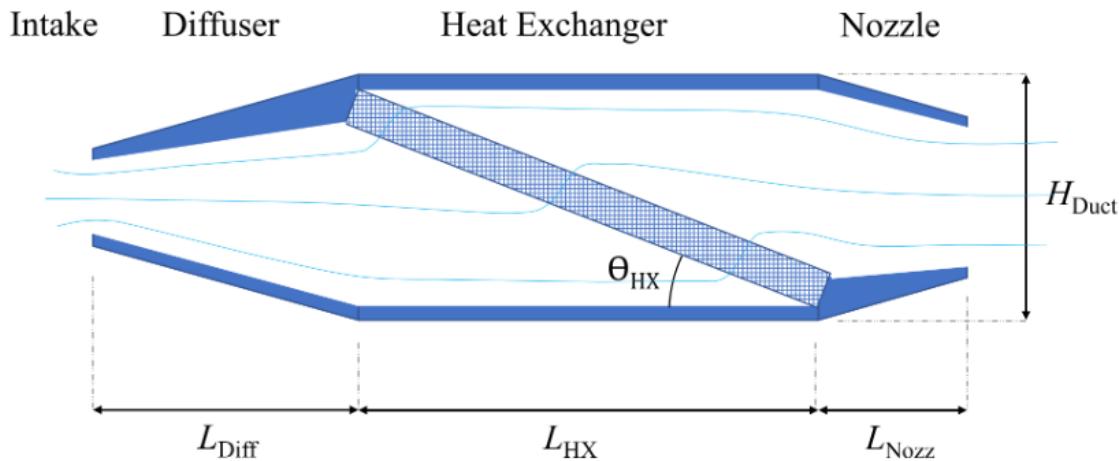


Figure 7.2: A diffuser-nozzle configuration with an angled radiator as is used in this design [10]

In order to provide sufficient airspeed with only the propwash at takeoff without producing unreasonable amounts of drag during cruise, the airspeed within the radiator needs to remain constant. There are multiple solutions for providing that, from ducted fans to different designs of variable geometry air intakes or combinations of both. The version in the final CAD model and seen in Figure 7.6 presents a particular variable geometry solution, but realistically, an in-detail trade-off would need to be performed in order to assess the best solution in terms of space, simplicity, drag and mass.

In order to provide a constant air velocity within the radiator, a variable geometry intake is required. At take off, the air velocity at the intake is just what the propeller can provide, so slowing it down would provide insufficient airflow. In contrast, exposing the radiator to the free airstream would introduce unacceptable amounts of drag during cruise conditions. In fact, the radiator alone would produce more drag than the thrust the aircraft can provide. A variable geometry intake will introduce additional complexity and weight and integration into the already tightly packed nacelle will be major engineering issues. To keep the radiator thickness as small as possible without taking up too much space inside the nacelle and in order to reduce drag, the radiator is placed at an angle of 30° to the airflow direction.

⁸<https://www.enginebasics.com/Engine%20Basics%20Root%20Folder/Engine%20Cooling%20Pg3.html#:~:text=The%20ideal%20coolant%20flow%20rate,per%20second%20should%20be%20avoided.> (Accessed on 15/06/2023)

The area of the radiator has been sized earlier in this section. Since the radiator is angled 30° , the effective area it uses in the nacelle cross-section is half of that. The duct the radiator is in is preceded by a diffuser and succeeded by a nozzle. A diffuser is a diverging duct that serves to decrease the velocity and increase the pressure of the airstream with the nozzle doing the opposite. For simplicity, it is assumed that the flow through both the diffuser and nozzle is isentropic, i.e. no total pressure is lost. This way, the diffuser and nozzle produce no drag. The desired intake area of the diffuser can be sized through the continuity equation, as seen in Equation 7.14, where i is the inlet and r is the radiator.

$$\rho_i A_i V_i = \rho_r A_r V_r \quad (7.14)$$

Since we are well below Mach 0.2 at any point, the airstream can be assumed to be incompressible. Thus $\frac{A_i}{A_r} = \frac{V_r}{V_i}$. With the area and velocity at the radiator known, the area at the intake depends on the velocity at the intake. At takeoff, this area ratio is 1 and it will decrease to 0.22. If it is assumed that the pressure drop at the radiator is the drop in total pressure, the total pressure at the nozzle can be calculated. Knowing the total pressure at the nozzle, the area of the nozzle can be sized such that the static pressure at the nozzle is the ambient pressure at cruising conditions.

The drag caused by the radiator is primarily friction drag, so the Reynolds number inside the radiator is relevant. It is calculated as in Equation 7.15 [11], where V_r is the velocity inside the radiator, μ is the viscosity of air (1.48×10^{-5} m/s²), and D_h is the hydraulic diameter, a geometric parameter calculated as $D_h = 2 \frac{s \cdot h_{fin}}{s + h_{fin}}$ [10].

$$Re = \frac{V_r \rho D_h}{\mu} \quad (7.15)$$

The Reynolds number now around 2100, so the flow can be just be considered laminar and the friction factor c_f can be estimated as $c_f = \frac{16}{Re}$. From this, the drag of the radiator can be calculated by Equation 7.16 [11].

$$\Delta p = 2c_f \rho V_r^2 \frac{Z_{HX}}{D_h} \quad (7.16)$$

The drag area then is the product between the radiator area and the pressure difference. Note that the radiator produces a constant drag independent of airspeed since the airflow inside of the radiator is supposed to be kept at a constant airspeed. The total drag produced by the radiators in both nacelles is 2616 N.

7.5. Propulsion Layout

The layout of the propulsion system in the aircraft is a critical aspect of the feasibility of the propulsion method. If the propulsion system does not fit correctly, a significant redesign might be needed.

First the pressurized hydrogen tanks were implemented into the wing. It was decided to use four hydrogen tanks, such that the available volume would be optimally used. The tanks were placed as far forward as possible, so as to not affect the static stability too much. In total, 7.57 m^3 of tank area would have to be accommodated. These tanks would carry around 150 kg of hydrogen, taking up 3.8 m^3 . The exact tank layout with respect to the engine nacelle can be seen in Figure 7.3. The forward tank has a radius of 0.288 m, while the aft tank has a radius of 0.360 m.

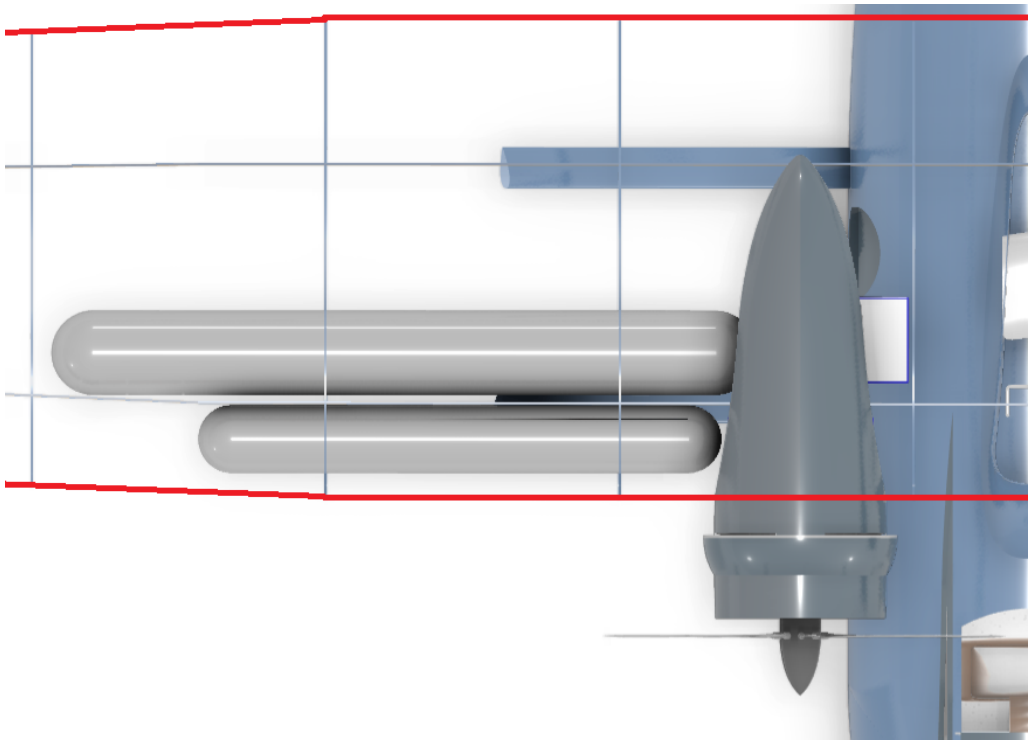


Figure 7.3: Layout of the hydrogen tank in the wing with the initial nacelle configuration

Next to the tank placement, the placement of the fuel cells and electric engine in the nacelle was decided. The electric engine would be as close as possible to the propeller, as to minimize the torsional deflection of the propeller shaft. Around and behind the engine will be space to realize the cooling system of the propulsion system, however, one has to keep in mind that structural components connecting the engine to the wing box will also be present here. Behind the cooling system, the fuel cells and their auxiliary components will be placed. Part of this will likely end up in the wing box. The layout as initially designed can be seen in Figure 7.4. Since the cooling system will still be designed further, the nacelle layout is still subject to change in a detailed design phase.

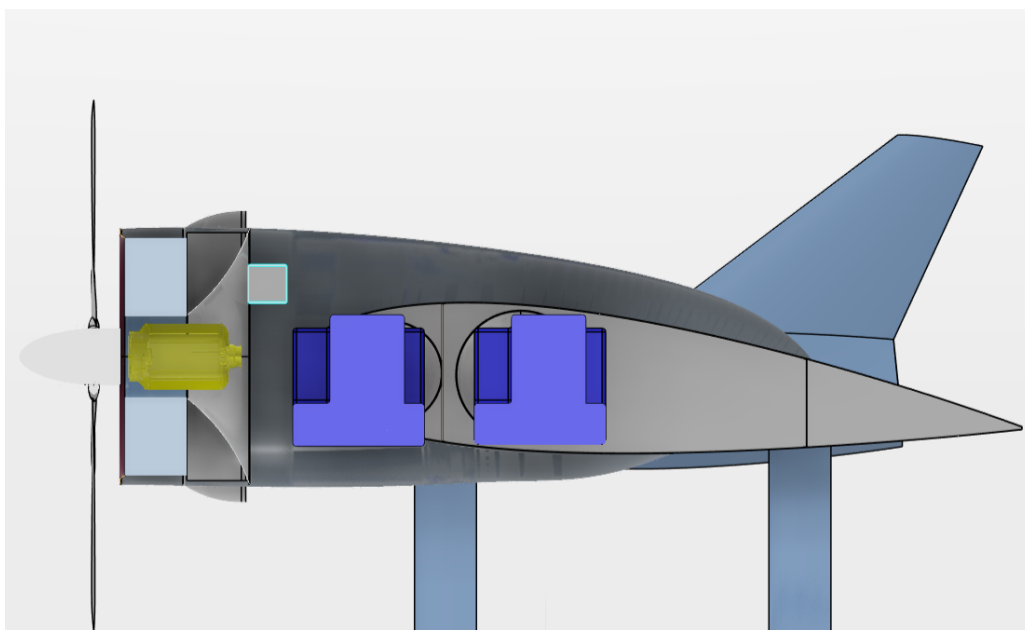


Figure 7.4: Layout of the engine nacelle in the initial design

7.5.1. Propulsion system Initial design

To keep the aesthetics of the original Catalina it was desired to keep the engine nacelles present around the combustion engines. Since electric motors are significantly smaller than the old engines a significant amount of space is available to place the cooling system, since ideally the entire propulsion system except for the hydrogen tanks would be in the two nacelles. If the radiator is placed behind the propellers in the nacelle it should also not cover a significant part of the propeller since that portion of the thrust is largely lost due to drag. The original Catalina nacelle had a diameter of roughly 1.40m, but since a larger frontal area is desired and around the edges of the radiator coolant piping needs to be placed a radiator max diameter of 1.35m was chosen with a gap of 5cm around making it in total a diameter of 1.45m.

The new motor was sized at a diameter of 0.5m, thus a hole of 0.5m is present in the radiator and the entire radiator is circular due to the circular nacelle. The heat exchanger will still be straight plates and fins in parallel to each other, the only difference is that the width of each will vary corresponding to the width of the circular nacelle at each plate location, with the equivalent rectangular dimensions used for the calculations. The radiator was sized to be 35cm long with an exhaust placed behind the radiator. Exhaust holes are present in the nacelle for the airflow as well as an air diverter to reduce drag from the exhaust.

7.5.2. Propulsion system Evolved design

The design in subsection 7.5.1 seemed to work well initially, but adopting the layout presented in Figure 7.2 had a lot of bad consequences. It was also found that longer radiators should be avoided due to the thermal efficiency decreasing rapidly when the length is decreased. The effect of this is difficult to calculate so a hard limit was set for length at 20cm based on other research on radiator sizing [10, 11]. Because of the now angled radiator, the placement inside the RAM intake would also be made more difficult due to the outlet of the radiator increasing the total height since the radiator itself is still a square box section. These changes had a number of effects, first, the nacelle became very large and aesthetically unpleasing as seen in an example in Figure 7.5. The fuel cells were not able to fit into the nacelle even with the enlarged one because of the geometry of a circular ram intake, so they would have to be moved into the wing, which is disadvantageous for stability and integration between propulsion system components. The air duct would have to cut through the wing box, severely compromising the efficiency of the wing structures and severely increasing the weight since the wing box would have to divert around the entire intake. Lastly, the variable geometry of the intake required is way more complex when taking on a circular shape. The radiator length could be reduced however due to this design to 0.16 meters which would increase its cooling capacity significantly compared to the initial design.

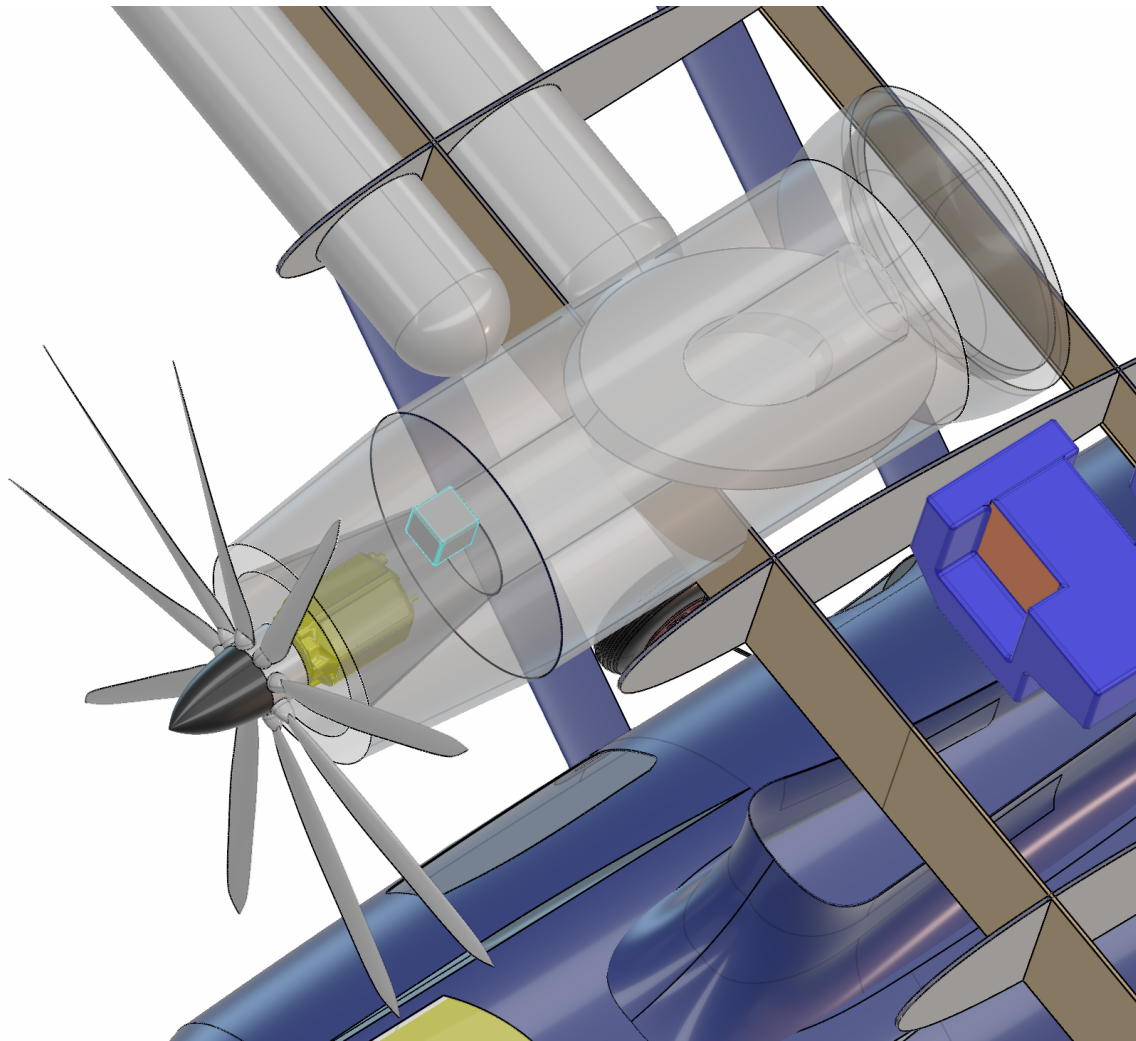


Figure 7.5: Circular RAM intake and radiator design

For all of these reasons, it was decided to place 2 smaller radiators on the top and bottom of the wing. With this configuration, it is possible to place the fuel cells and motors in similar places as the initial design as shown in Figure 7.4. The idea is to put rectangular intakes on the top and bottom of the fuel cells, close to the wing. This way, all the propulsion system components are very efficiently placed volume-wise, the fuel cells are physically close to the cooling and the wing box can stay uncompromised except for a few passages at the top and bottom. Finally, a variable geometry intake is way easier to implement in a rectangular intake as it only requires a singular flap on a hinge per radiator. An example of one of the new radiators can be seen in Figure 7.6. In the figure, the turquoise blocks represent the radiators, the red block represents the electric motor, the orange block represents the fuel cell and the blue blocks represent the fuel cell auxiliary systems. The hydrogen tanks layout can be seen in the figure as well. To minimize the protrusion of the radiators from the wing, the width of the radiators is increased from the old nacelle diameter and the height is limited to 40 cm on both the top and the bottom. The width will be around 1.8 m. Only the radiator and RAM intake shown is developed currently, the motor and fuel cells integration including the nacelle that will cover the whole propulsion system is yet to be developed.

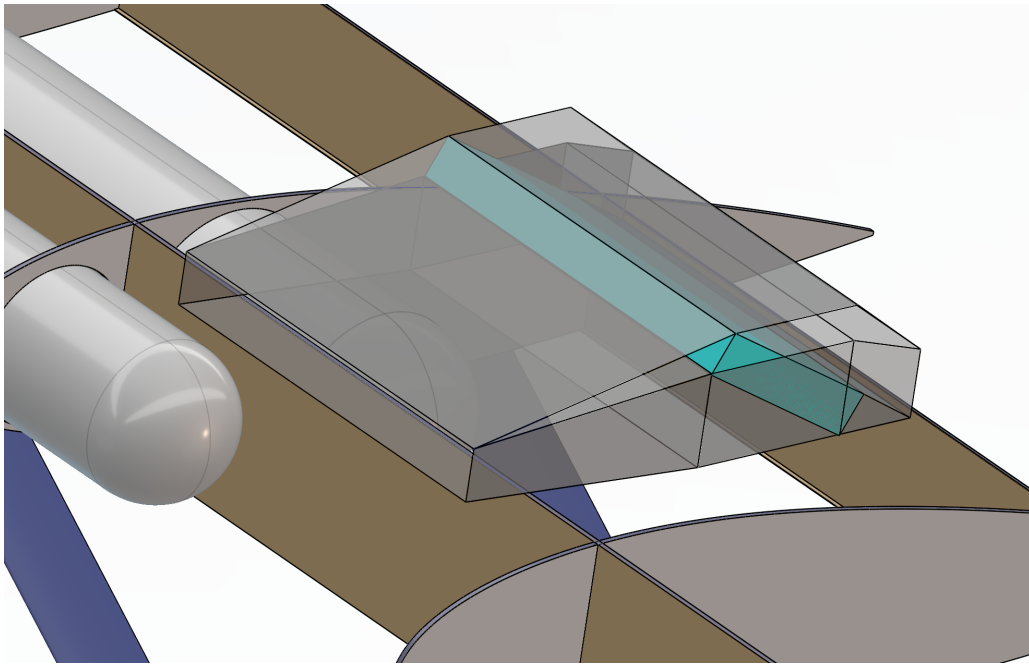


Figure 7.6: RAM intake geometry

A full complete design configuration was not completed yet including the integration of the RAM air variable intake or an additional fan system to input enough air during low speed flight conditions such as take-off and climb. However a nacelle was shaped to integrate the squared radiator design into the aircraft with the fuel cells and motors. This can be seen in Figure 7.7. A possible implementation of the variable intake would be to extend the sloped central surfaces into the airstream, away from the motor. The additional air around the motor can then be directed outwards via an exhaust hole on both sides of the nacelle. This can be seen in Figure 7.8 and in Figure 7.9, additionally an overview of the entire propulsion system including the tanks can be seen in Figure 7.10.

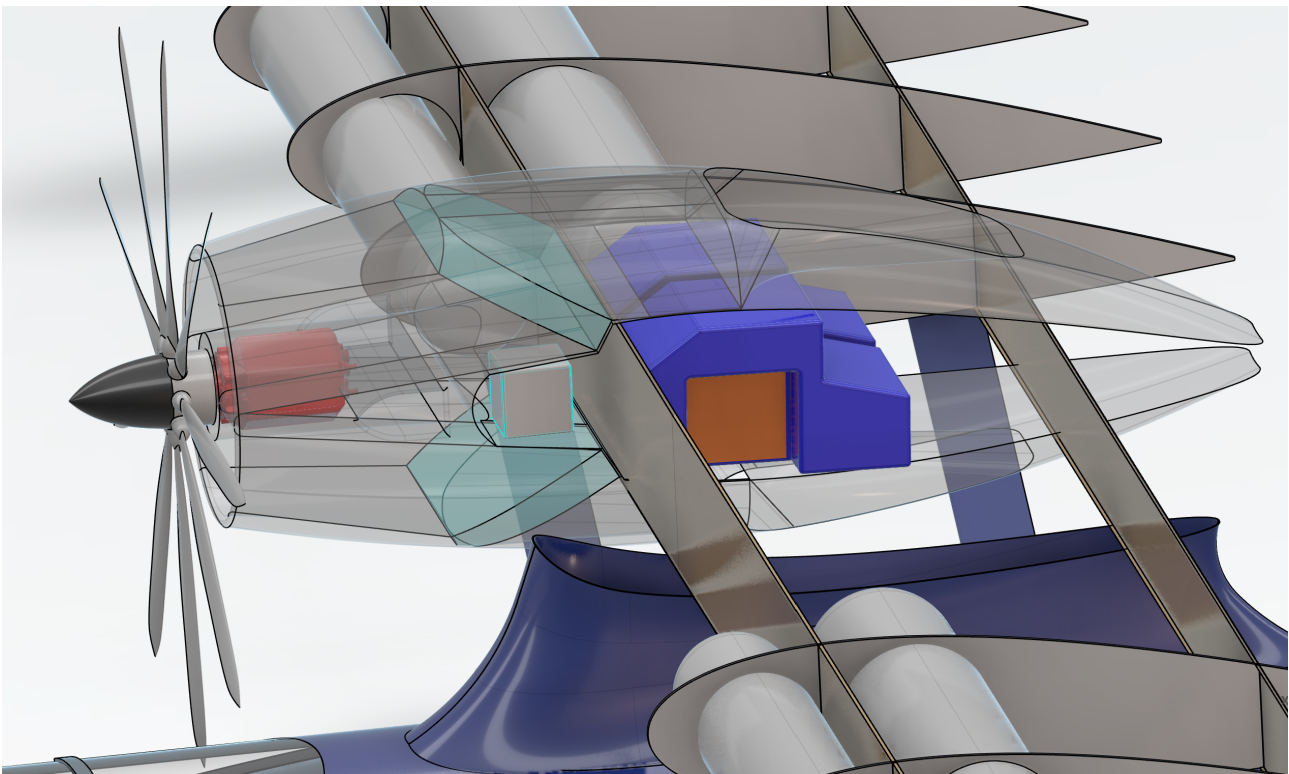


Figure 7.7: Propulsion system assembly. Radiator in light blue, electric motors in red and fuel cell stack in orange.

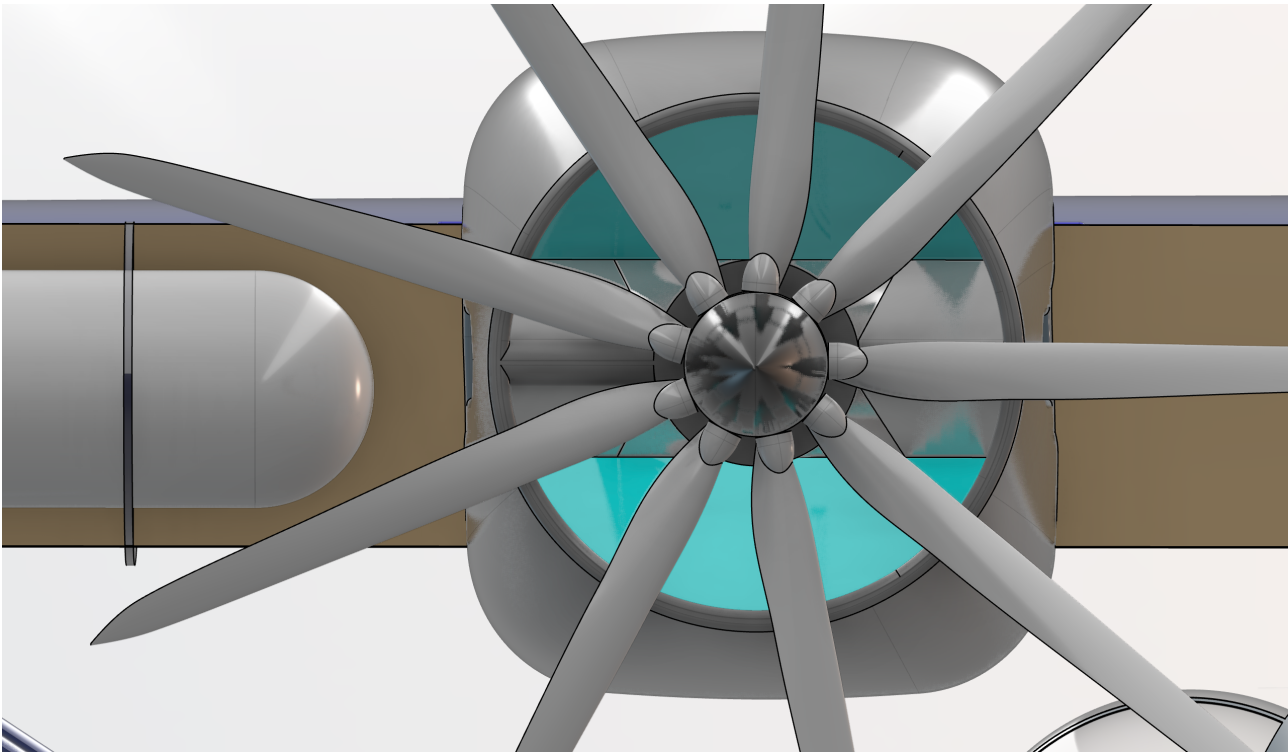


Figure 7.8: Propulsion system assembly front view. Radiator in light blue, electric motors in red and fuel cell stack in orange.

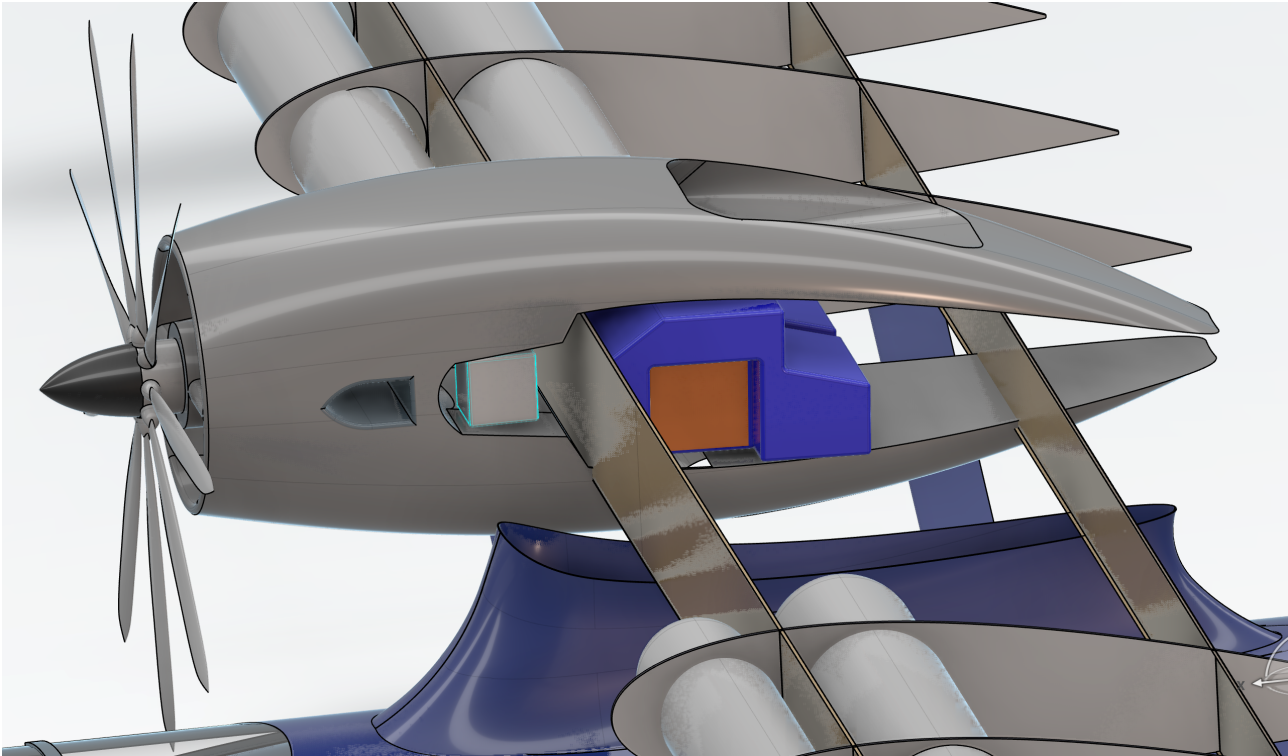


Figure 7.9: Propulsion system assembly side view.

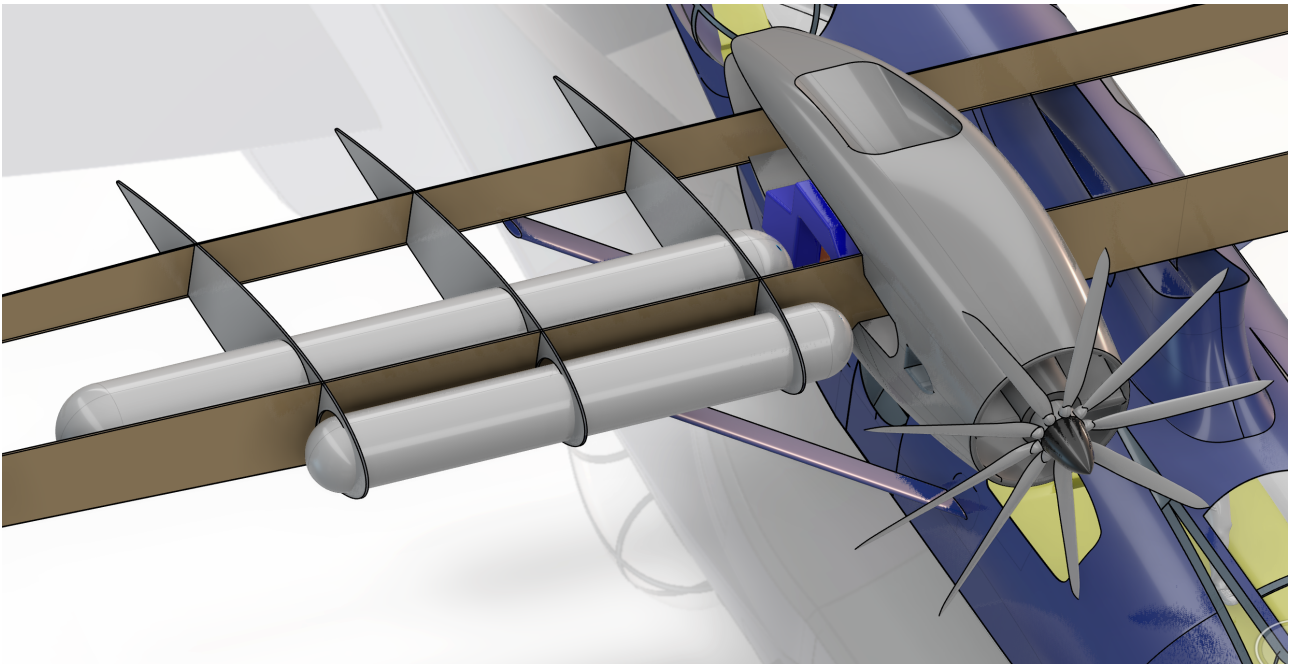


Figure 7.10: Propulsion system overview, integrated into the aircraft wing.

The final heat dissipation requirements for the propulsion system, also taking into account the additional drag due to the radiators are 407 kW for the fuel cells and 32 kW for the electric motor. The limiting factor is the one engine out condition in this case. The propulsion system can be run at max power, after being parked so the coolant is at air temperature, for about 170 seconds before power has to be reduced. This is the time required until all the coolant is heated up until the 65 degrees normal operational temperature. Further design has to be done to improve drag calculations and to implement the variable intake system.

7.6. Propulsion Weight

Understanding the weight distribution and characteristics of the components within the propulsion system is crucial for achieving an optimal aircraft design. The weights for both the class II estimation and detailed estimation can be found summarized in chapter 6 in Table 6.4. In addition to the Class II estimation, for the last version of the propulsion system design, the coolant mass was determined to be 80 kg, the radiator mass was estimated to be 150 kg and a nacelle would weigh in the order of 50-100 kg. The mass of the RAM intake system has not been estimated yet. These masses still correspond to the Class II estimation. The method to obtain the propeller mass has been described here, but the result of it was already included in Table 6.4.

The geometry of the propeller was imported into CATIA and the propeller with the central hub was modelled. The weights were then calculated by CATIA and when the propeller is to be made from carbon fibre, the weight will be 94 kg. For an aluminium propeller, the weight will be 133 kg. A large discrepancy in the weight estimation for the propeller will have a small impact on the stability of the aircraft, making the criticality of the weight estimation not too significant. The material used for the propeller will likely be carbon fibre composite with a wooden core such as the MT propellers [14]. Taking the pure carbon fibre weight of 94 kg and adding 10 % for the added weight of reinforcements near the root of the blades, wooden core and discrepancy into account, the propeller weight is estimated to be 104 kg. This estimation can be further substantiated with Table 7.6. The table shows some reference propeller weights and weight extrapolation for the propeller with 9 blades and 530 kW. The diameter is not taken into account for the extrapolation since the weight of the propeller tip is assumed to be small compared to the root and the hub of the propeller.

Table 7.6: Propeller Reference Data⁹[14]

	Diameter [m]	# Blades	Power [kW]	Weight [kg]	Weight Extrapolation [kg]
Twin Otter	2.4	4	560	66	140.54
MTV 16	2.2	4	950	50	62.76
MTV 5	1.8	5	410	45	104.71
MTV 27	2.2	5	858	74	82.28
MTV 37	2	7	533	76	97.16

⁹<https://www.ips1.aero/mccauley-blackmac/dehavilland/dehavilland-dhc-6-300-twin-otter/> (accessed on 05/06/2023)

This chapter contains the main aerodynamic calculations that were done. The main wing is analysed thoroughly in section 8.1, and its properties and performance are discussed. In subsection 8.1.3 the winglets and their performance are discussed. Lastly, the drag will be discussed in section 8.2.

8.1. Wing

8.1.1. Planform

The aspect ratio of the wing was increased as much as possible, constrained by the requirement to keep the wing within 10% of the dimensions of the original Catalina. However, during the class II weight estimation as performed following *Airplane Design Part V* by Dr. Jan Roskam, it was found that the weight of the wing heavily depends on the aspect ratio [6]. Different aspect ratios were tested, and it was found that achieving a larger (L/D)-ratio by increasing the aspect ratio outweighs the resulting increase in wing weight and consequently fuel used.

8.1.2. Airfoil

An airfoil for the new wing needs to be chosen. For this, the NACA 4-digit airfoil family is considered. Because the thickness-to-chord ratio of the airfoil has a large effect on the structural weight of the wing and thus of the aircraft, this is considered first. After that, the camber is adjusted to alter the maximum lift coefficient and lift-over-drag ratio.

Airfoil thickness

To get a better understanding of the effect of the thickness-to-chord ratio on lift and drag, a range of symmetric airfoils with varying thicknesses are analysed using XFLR5. The newly designed wing planform is used for analysis. The resulting lift curves and drag polars can be seen in Figure 8.1 and 8.2 respectively. As can be seen, both the maximum lift coefficient and the maximum (L/D)-ratio decrease with increasing thickness.

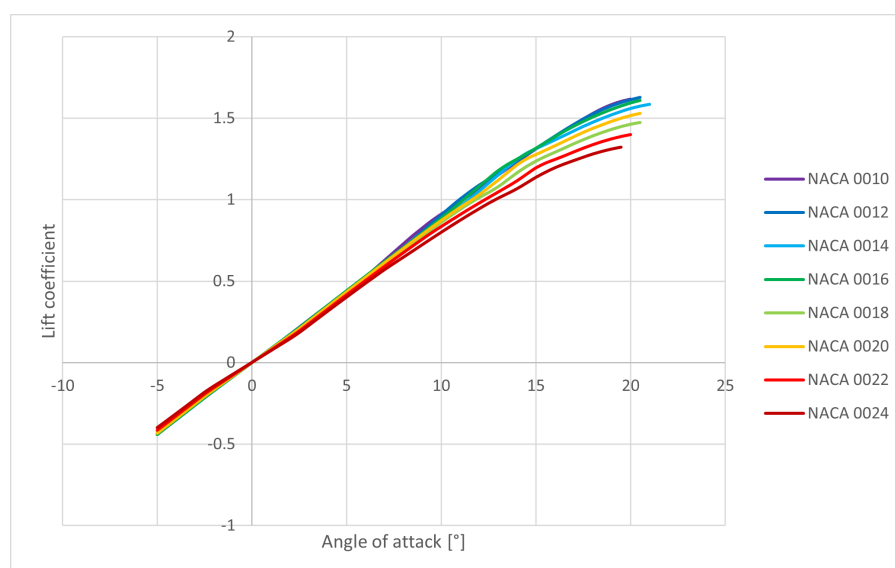


Figure 8.1: XFLR5 lift curve from comparing NACA airfoils with various amounts of thickness at 30 m/s.

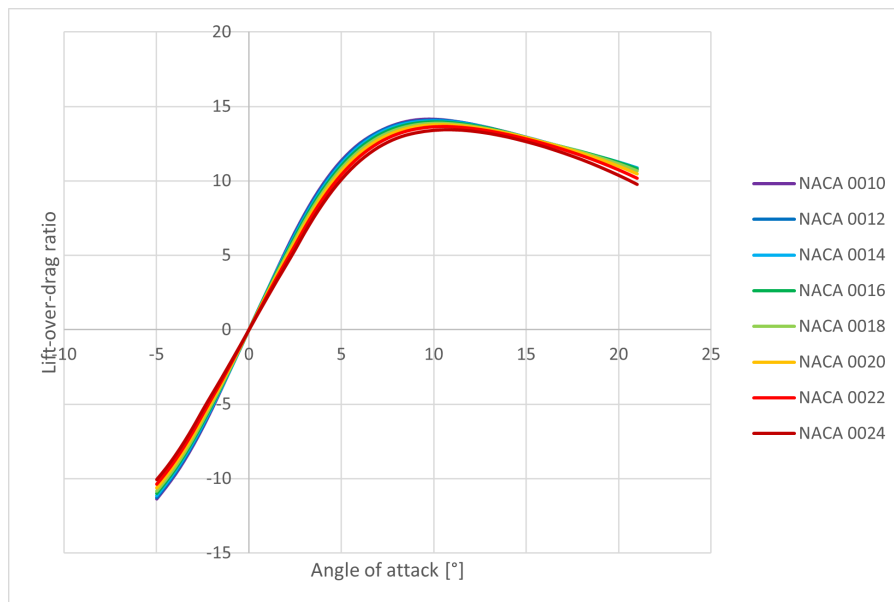


Figure 8.2: XFLR5 lift-over-drag curve from comparing NACA airfoils with various amounts of thickness at 56.5 m/s

Another important effect of changing the (t/c) -ratio is on the structural weight of the wing. Increasing the thickness significantly increases the moment of inertia of the wing spars, improving its resistance to bending. In the end, the most important is the amount of fuel needed for a nominal flight, a function of both the wing weight and the (L/D) -ratio, and the maximum lift coefficient. These results are shown in Table 8.1. Here, the stall speed is calculated at sea level for an aircraft mass of 11000 kg.

Table 8.1: Effect of the thickness-to-chord ratio on the aircraft's fuel mass and stall speed

(t/c) -ratio [%]	M_{fuel} [kg]	V_{stall} [m/s]
10	156.6	29.7
12	152.3	29.5
14	149.2	29.7
16	146.8	29.9
18	144.8	30.5
20	143.3	31.0
22	142.1	31.9
24	140.9	32.8

As can be seen, the fuel mass required decreases with increasing thickness, while the stall speed decreases. The stall speed of the aircraft is required to be a maximum of 70 kts. A further safety factor of 1.1 is applied, thereby arriving at a stall speed of 63 kts, or 32.4 m/s. This safety factor is included in order to accommodate for multiple considerations, the most important of which is to account for inaccuracies within XFLR5. In theory, a thickness-to-chord ratio of 22% would give the required stall speed. However, a couple of factors will reduce the maximum lift, thereby requiring the safety margin, namely:

- Aerodynamic interference between the fuselage and the wing. Although the fuselage is far away from the wing, it will still disturb the flow over it.
- Possible downforce by the vertical tail to keep the aircraft trimmed.
- Higher altitude take-offs and landings. A lower density will either require more lift or higher speeds.
- Wing surface imperfections. Things like rivets and seams will reduce the lift of the wing.
- The propeller wash interfering with the wing. In theory, the lift should increase because of the increased airflow. However, the effect is difficult to estimate [15].

Therefore, a (t/c) -ratio of 20% is chosen. Note that this is higher than was assumed during the preliminary design of the propulsion system, meaning that fitting the system inside the wing should not be an issue.

Because the final aircraft weight was reduced to 9700 kg, in theory, an even thicker airfoil could be used. However, in practice, aircraft rarely have airfoils with a (t/c)-ratio larger than 20%. It is therefore kept at 20%

Airfoil camber

The addition of camber to an airfoil moves both the lift and drag curve to the left, consequently decreasing the angle of attack for the optimal lift-over-drag ratio. The result of adding camber to the wing on the (L/D)-ratio is shown in Table 8.2.

Table 8.2: Effect of camber on the lift-over-drag ratio of the aircraft at 56.5 m/s for 11000 kg

Airfoil	$(L/D)_{cruise}$
0020	12.12
1420	12.14
2420	12.10
3420	12.04
4420	12.10

As can be seen, the camber has a very small effect on the (L/D)-ratio. Nevertheless, the NACA 1420 has the best performance. Furthermore, the camber slightly flattens the bottom side of the wing, making integration of the propulsion system easier. Fuel cells, PMAD housings and radiators are generally rectangular in shape, increasing volumetric efficiency. The final performance characteristics of the wing using the NACA 1420 airfoil can be seen in Table 8.3.

Table 8.3: Wing performance characteristics using NACA 1420 for an aircraft mass of 9700 kg

$C_{L_{max}}$	V_{stall} [m/s]	a_{cruise} [°]	$(L/D)_{cruise}$
1.516	28.5	4.4	10.60

8.1.3. Winglets

Winglets are devices that are located at the wingtip of the aircraft. They decrease the intensity of the vortices that are created by the pressure difference that meets at the wingtip. The winglets act as a wall, but can also be positioned to generate lift in the fuselage and thrust direction. This latter force will counteract the drag that is associated with the vortices. In general, winglets increase the effective aspect ratio of the wing, thus increasing the lift-over-drag ratio. However, they also increase structural weight.

The increase in structural weight of the wingbox due to winglets was analysed. The increase in structural weight was negligible due to the winglets' configuration. They are angled 90° up such that they form no risk of hitting the water in landing configuration. The decision was taken to use winglets since no weight penalty was observed for the wingbox, and their inclusion substantially improves performance.

Floater implementation

The original Catalina had folding wingtip floaters which neatly folded up to become almost flush with the wing and function as wingtips. If winglets are incorporated, this is complicated. The following solutions are considered:

1. Keep the floater and mechanism unchanged and add a winglet to the end of the wing, as can be seen in Figure 8.3. Although the simplest solution, the floater might decrease the effectiveness of the winglet and these effects will be difficult to analyse without using a wind tunnel or CFD model. Furthermore, this solution is aesthetically unpleasing.
2. A simple option would be to remove the folding mechanism, permanently attach the floaters to the wing, and add winglets to the wingtips, as can be seen in Figure 8.3. This solution would be easy to implement and lighter than the original (due to the removal of the mechanism). However, it would make landing on land way more dangerous, as it vastly decreases the allowable roll angle while landing because of the extended floaters. It also increases the drag and looks significantly different compared to the original Catalina.

3. A third option is to fold the floaters up to meet the bottom of the wing, possibly making an indent for it to fit into. A possible configuration is given in Figure 8.3. The winglets could then be mounted normally. As with the first option, the winglets would disrupt the airflow around the wingtips in unpredictable ways. The effectiveness of the winglet would therefore be difficult to estimate.
4. Finally, the winglets could be mounted on the floats themselves and would move as one. Because it is extremely undesirable to have the winglets go into the water, the mechanism for (un)folding the floaters would have to be slightly changed to make it translate in an arc, instead of rotate. A concept can be seen in Figure 8.3. The mechanism would be more complicated and thus heavier, but the integration of the floater is the smoothest of all and is the most aesthetically pleasing.

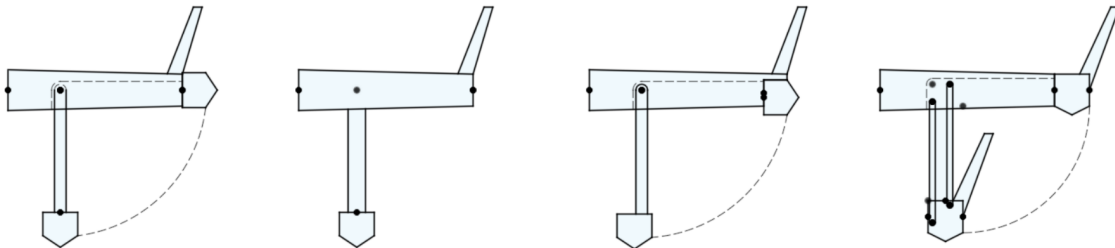


Figure 8.3: Winglet and floater integration options from left to right: 1) floater on wingtip, 2) immovable floater, 3) floater under wingtip, 4) winglet on floater

Of the abovementioned options, the fourth was decided to be the most optimal. Although more complicated, it has the smoothest profile, thus decreasing drag. It also leaves the winglets relatively undisturbed. Finally, with aesthetics being an important aspect of the final design, it was considered the best of the four options.

The concept and mechanism is worked out in more detail in Figure 8.4. The winglet is moved outwards slightly, to allow for clearance between it and the wing while translating. Another concern is the structural rigidity of the part of the wing housing the floater mechanism. The mechanism requires the bottom skin of the wing box to be removed. This would decrease the torsional rigidity of this part of the wing, while also decreasing its resistance to bending. However, the mechanism fits between the main spars, which carry the majority of the bending loads. Furthermore, the torsion the wing is required to carry is very small at the wingtips. Slightly increasing the spar thickness at this position should therefore remedy these problems.

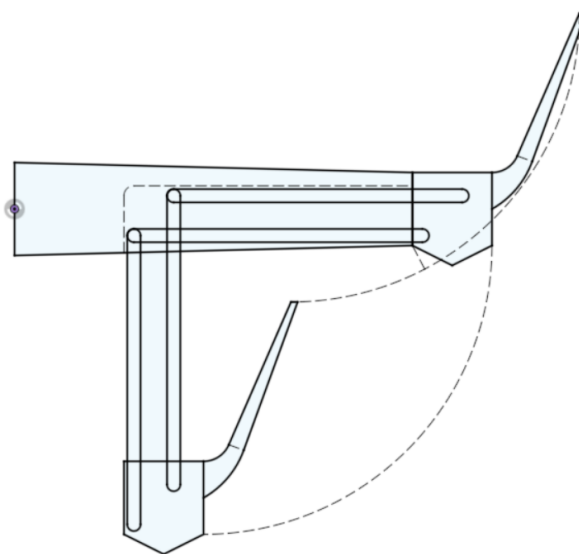


Figure 8.4: Translating winglet and floater mechanism concept

Winglet sizing

Winglets reduce the induced drag at the wingtips. However, exactly analysing this effect is difficult. Usually, winglets are designed using wind tunnel tests or CFD models, as their optimal geometry depends highly on the flow over the wing. Therefore, exactly sizing the winglets is not possible using the time and resources available.

The winglets should not be larger than 5% of the wingspan [16], giving a maximum height of 1.67 m. However, because of clearance issues caused by the selected mechanism, the winglets can only be approximately 1.3 meters tall, assuming a 70° cant angle. Increasing the cant angle would allow for a larger winglet, but this would increase the risk it would enter the water upon take-off, landing or taxiing. The root and tip chords are chosen using trial and error, seeing what values give the most optimal lift-over-drag ratio at cruise ($C_L = 0.55$). It was found that using a root chord of 1.5 meters and a tip chord of 0.5 meters, the smallest effective winglet is obtained. The final winglets increase the (L/D)-ratio by 3.5%, increasing from 10.6 to 11.0. This is in line with expected efficiency increases from literature.

Increasing the size of the winglets would have no significant decrease in total drag, while increasing the loads on the wing and floater mechanism, thus making them heavier.

The winglets should be loaded as much as possible without stalling them. The load can be increased by both increasing the camber of the winglets and by increasing the toe angle. A NACA 6410 airfoil is chosen, together with a toe-out angle of 10 degrees. Adding more camber would decrease the efficiency of the winglet while decreasing the toe angle would risk stalling the winglet before the wing root. This is extremely undesirable, as it would cause a sudden and unpredictable rolling moment. Furthermore, it would make the ailerons less effective, making recovering the roll even more problematic. It is therefore made sure that the centre of the wing stalls well before the winglets and wingtips do. This can be seen in Figure 8.5. The blue line, representing the local lift coefficient, reaches levels much closer to the theoretical stall C_L than the winglets.

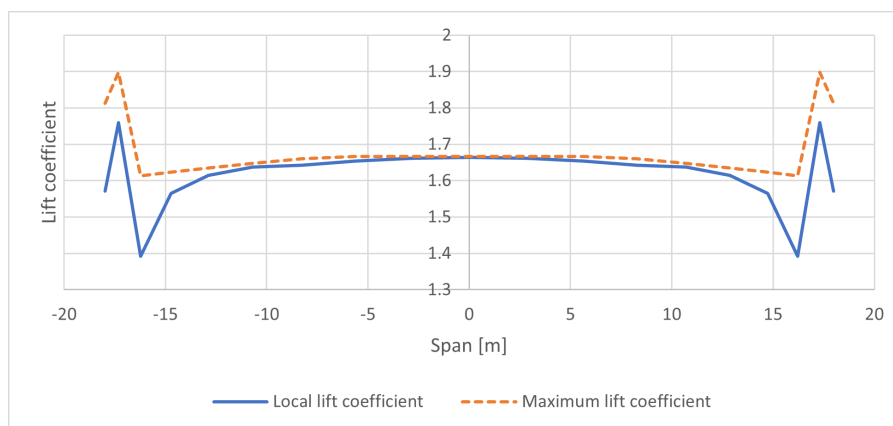


Figure 8.5: Stall characteristics of the wing including winglets at $\alpha = 20.5^\circ$

For the same reason as for the winglets, some wing twist is added to the wingtips. Specifically, the wingtips are given a twist angle of -1° . This increases the likelihood that the wing's centre stalls first, while also getting the lift distribution closer to elliptical (Figure 8.6, slightly increasing its efficiency).

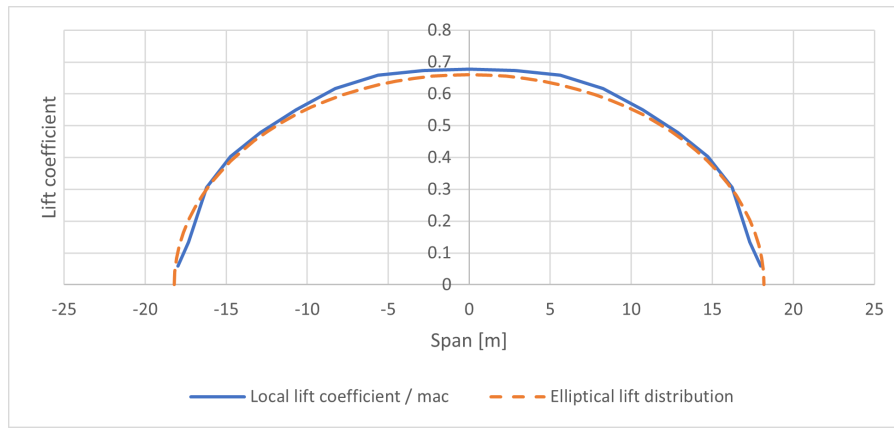


Figure 8.6: Elliptical lift distribution of the wing at $\alpha = 20.5^\circ$

Finally, when the floaters are extended, it is advantageous that they do not generate a large lift force. This would need further strengthening of the mechanism. The combination of the toe angle and camber of the airfoil is therefore also designed such that they generate a very small lift force when extended. Assuming that the floater generates no significant lift, the winglet only has a lift coefficient of -0.2 when extended. This results in a lift force of 132 N (pointed outwards). This is relatively small compared to the forces on the floater expected during manoeuvres in water and can therefore be neglected.

Structural weight

The structural weight of the aircraft will increase if winglets are used. Due to the forces on the winglets, moments will be introduced at the wingtips. Furthermore, the weight of the winglets itself will cause a moment at the wingtips. The moments that the winglets introduce will cause more stresses that need to be accounted for in the wingbox, making the wing heavier. In turn, the entire aircraft becomes heavier, consequently increasing its fuel consumption.

The effect of the winglet is considered as a point moment, the magnitude of which is calculated using the following equation:

$$M_{winglet} = \int_{x_{tip}}^{x_{root}} C_L(x) \cdot c_{winglet}(x) \cdot x dx \cdot \frac{1}{2} \rho V^2 S \quad (8.1)$$

Where x is the distance from the winglet root, $c_{winglet}(x)$ is the winglet chord as a function of x and $C_L(x)$ is the local lift coefficient of the winglet as a function of x , found using XFLR5. In the end, a moment of 2 kNm in the same direction as the wingtip vortices is found. The weight added by the winglets is found to be insignificant. Thus, their addition is beneficial to the design, as it reduces the total drag of the aircraft.

8.2. Drag

8.2.1. Rivets

The original Catalina had a lot of rivets. Since the thermoplastic composite as discussed in section 10.1 requires virtually no rivets, it can be assumed that all rivets can be removed from the aircraft. This would therefore result in a reduction in drag over the entire aircraft.

The drag produced by a surface imperfection is a function of the object's height compared to the boundary layer thickness. The rivets are assumed to be domed and are 8 mm in diameter and 2.5 mm in height. From Hoerner (1965), the drag coefficient per rivet area c_D is found to be 0.025 [17]. Using Equation 8.2, this drag can be adjusted for the local thickness of the boundary layer thickness, which is calculated using Equation 8.3.

$$C_D = c_D \cdot 0.75 \sqrt[3]{h/\delta} \quad (8.2)$$

$$\delta_{99} = 0.37 \frac{x}{Re_x^{1/5}} = 0.37 \left(\frac{x^4 u_\infty}{\nu} \right)^{1/5} \quad (8.3)$$

From reference images and technical drawings, it is assumed that 3% of the total surface area of the original Catalina is covered in rivets. Finally, the total drag caused by the rivets can be calculated using Equation 8.4, where S is the surface area which is covered in rivets.

$$\Delta C_{D_{rivets}} = \frac{F_{rivet}}{S} \iint_S C_D(x) dx dy \quad (8.4)$$

Note that Equation 8.4 calculates the drag coefficient over the area of the section analysed. To be able to directly compare values and calculate the zero-lift drag coefficient of the original Catalina, the value is scaled to the wing surface area of the Caty. The resulting drag reductions can be seen in Table 8.4, expressed in counts, where one count is equal to a factor 10^{-4}

Table 8.4: Drag reduction due to the removal of rivets.

Subsystem	ΔC_{D_0} [counts]
Wing	5.9
Fuselage	1.7
Horizontal stabiliser	0.3
Vertical stabiliser	0.2
Total	8.1

8.2.2. Drag of the original aircraft

The drag coefficient of the empennage and struts can be estimated using XFLR5. For the empennage and struts, a NACA 0020 and 0036 airfoil are assumed, according to maintenance manuals. The horizontal and vertical tails have a zero-lift-drag coefficient of 63.8 and 62.7 counts, respectively. The struts have a relatively high drag coefficient of 213 counts. However, this is relative to their own surface area. Since C_{D_0} of the entire aircraft is only known with respect to the wing area, the values need to be scaled accordingly, the results of which can be seen in Table 8.5.

Table 8.5: Breakdown of zero-lift-drag coefficient of the original Catalina ($S = 130.5 \text{ m}^2$)

Subsystem	C_D [counts]
Main wing	54.5
Horizontal tail	12.2
Vertical tail	4.2
Struts (x4)	5.2
Rivets	8.1
Fuselage + residual	224.8
Total	309

Because of the complexity of the shape of the fuselage, it is not possible to calculate the drag of the fuselage using the available tools and time. It is therefore assumed that the fuselage's drag is equal to the total drag minus the drag of the wing and stabilisers. As can be seen from Table 8.5, the majority of the drag is caused by the fuselage. This includes drag directly caused by the shape of the fuselage, but also residual drag like interference drag or that of the engine nacelles. Because the shape of the fuselage is not going to change significantly, it is assumed that the change in fuselage drag of the fuselage scales linearly with the change in the fuselage's surface area.

8.2.3. Drag of the Caty

The drag of the Caty can be mostly found by using analysis in XFLR5. The zero-lift-drag coefficient of the wing, struts and empennage can all be found this way. For the fuselage, it is assumed that the shape is basically the same as the old one and has the same C_{D_0} . The only difference is the increase in fuselage surface area and

the decrease in the wing's surface area, which results in a higher C_{D_0} for the new fuselage. This is detailed in Table 8.6

Table 8.6: Breakdown of zero-lift-drag coefficient of the Caty for the old and the new wing surface area.

Subsystem	$C_{D_{130.5m^2}}$ [counts]	$C_{D_{124.6m^2}}$ [counts]
Main wing	66.0	69.1
Horizontal tail	10.4	10.9
Vertical tail	4.2	4.4
Struts (x4)	5.2	5.4
Fuselage + residual	238.3	249.6
Total	324.1	339.4

The lift curve of the Caty versus the original can be seen in Figure 8.7. As can be seen, the wing has a higher $C_{L_{max}}$. Despite the smaller wing area, this results in a lower theoretical stall speed of 59.5 kts (calculated at 11000 kg and with floaters extended), versus 63 kts for the old plane (at 27000 lbs).

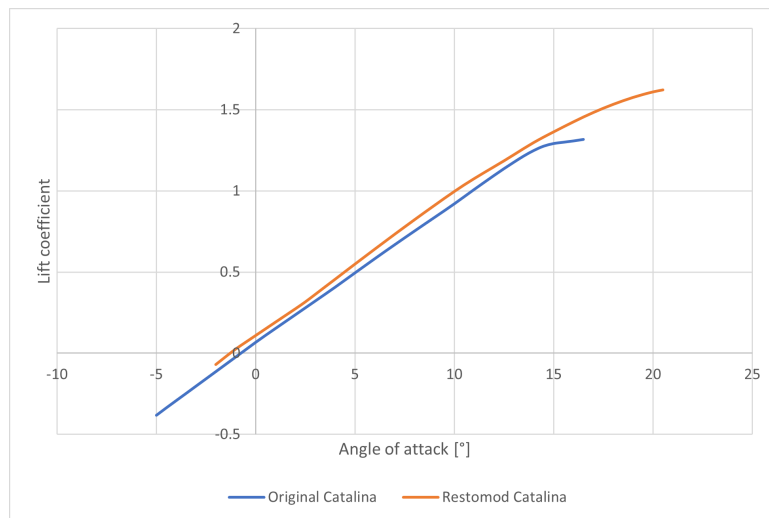


Figure 8.7: Lift curve of the original Catalina and the Caty

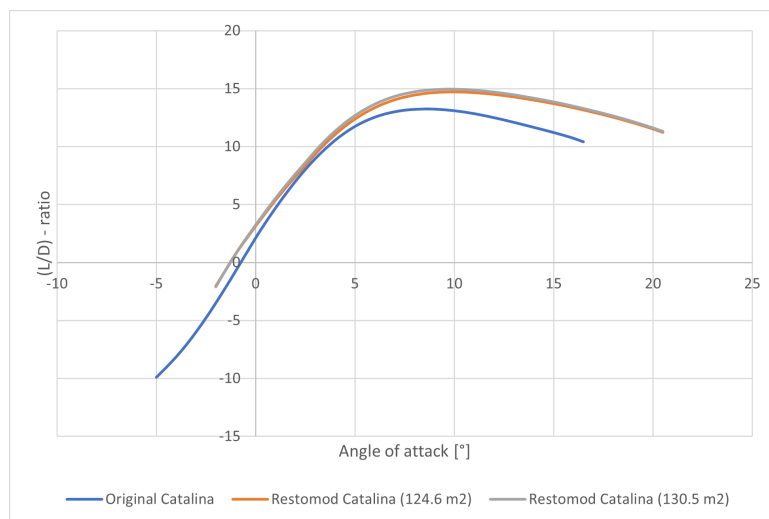


Figure 8.8: Lift over drag curve of the original Catalina and the Caty

Structural Internal Loading

In the following chapter, the loading for the wing and the fuselage will be explained and calculated. This chapter follows on the findings from Section 11.4 of the midterm report[1]. All of the loads will be analysed and modelled for the critical load cases using a Free Body Diagram (FBD), Shear Force Diagram (SFD) and Bending Moment Diagram (BMD). This will be used to design the physical structure for the wing.

9.1. Gust load Diagram

During the design phase of an aircraft, the most critical loads must be determined and designed for. This is firstly done by creating a gust load diagram, which contains what loads the aircraft must withstand. Based on the requirements as well as CS-23 [3], the following loading diagram can be made for the Caty.

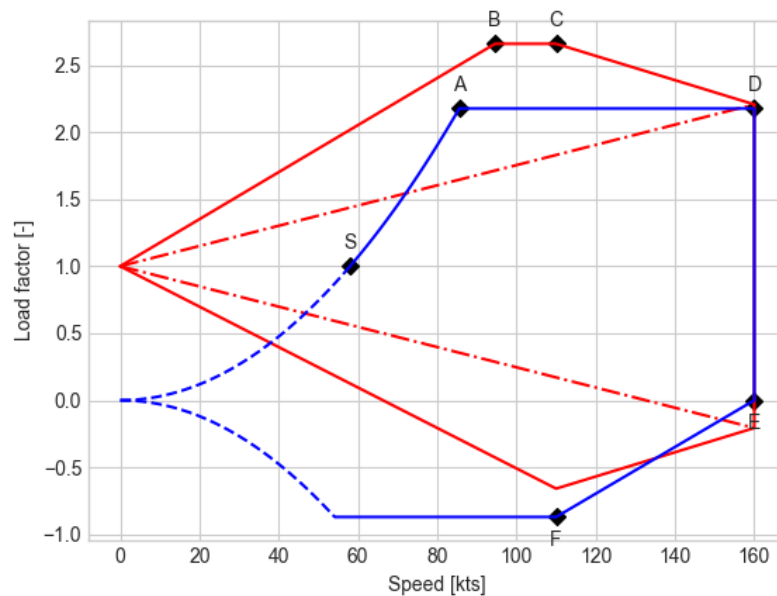


Figure 9.1: Loading diagram of the aircraft

Based on the gust diagram (see Figure 9.1) it can be seen that the greatest load which the plane must withstand is 2.6g in positive direction, and -1.04 in the negative. Furthermore, it has been chosen to add an additional safety factor of 1.5. This leads to a total load factor of +3.9 and -1.56 respectively which has to be designed for.

9.2. Wing

The required nominal lift has been calculated for the MTOM, which is **9700 kg**, and a speed of 56.5 m/s. This speed has been chosen arbitrarily, as the total lift produced remains the same, namely the weight, at every speed for equilibrium. It should be noted that the lift distribution is dependent on the speed. The wingtips are relatively more loaded at lower speeds. This also justifies the use of the cruise speed instead of the top speed as more bending will be produced and thus this is more critical. At a lower speed, the aircraft is not able to pull +3.9 g's, since the wing would stall. All of this creates a situation where the aircraft performs, at approximately

cruise speed, a sharp pull-up manoeuvre to achieve +3.9 g. While for the negative case, this can be achieved by pitching down.

In this case, only the right wing will be looked at, as the wings are symmetric and so are the loads on them. Furthermore, each wing will contain fuel tanks, as well as nacelle weight (engine, fuel cells, compressor, cooling ...) and more. These will always be present during flight and thus alleviate the wing partially both in shear as well as in bending.

When considering the loads acting on the wing, the following free body diagram, Figure 9.2, and summarizing table, Table 9.1, can be created. Note that the wing strut, which goes from the fuselage to the wing, is not yet included in this table. The reason is that its effectiveness will be assessed, in subsection 10.2.1, as it will add mass to the aircraft, though also reduce mass by decreasing the loads on the wing and thus the wing box may be sized smaller.

Finally, it should be mentioned that a point moment will be added caused by the winglets as well as the rotation from the engine. These values have been added to Table 9.1 and the BMD, but not Figure 9.2, in order to keep a better overview. Furthermore, in the SFD and BMD diagrams, the wing will be looked at from the back, such that Y points to the right and Z downwards.

Table 9.1: Forces acting on the wing in Z-direction, during a 3.9g pull-up manoeuvre.

Force Index	Load	Type of Force	Direction along Z-axis	Colour in graph
L	$MTOM * g * n * 0.5$	Distributed, quasi-elliptical, lift force	+	Blue
R_p	reaction force	Point force, due to the reaction force of the pylon	+	Green
W_{TLE}	$m_{TLE} * g * 0.5$	Distributed, constant, due to leading edge tank	-	Red
W_{TWB}	$m_{TWB} * g * 0.5$	Distributed, constant, due to wing box tank	-	Red
$W_{nacelle}$	$(m_{FC} + m_{cool} + m_{compr} + m_{eng} + m_{PMAD} + m_{other}) * g * 0.5$	Distributed, constant, weight due to fuel cells, engines and other components	-	Red
W_{Fl}	$m_{Fl} * g * 0.5$	Point force, Floater	-	Red
W_{str}	$m_{str} * g * 0.5$	Distributed, complex, due to wing structure	-	Green
$M_{R,pylon}$	reaction moment	Point moment, due to reaction moment of the pylon	Clockwise	Not included
M_{nac}	M_{engine}	Point moment, due to engine	Clockwise	Not included
M_{WL}	$M_{winglet}$	Point moment, due to winglet	Counterclockwise	Not included

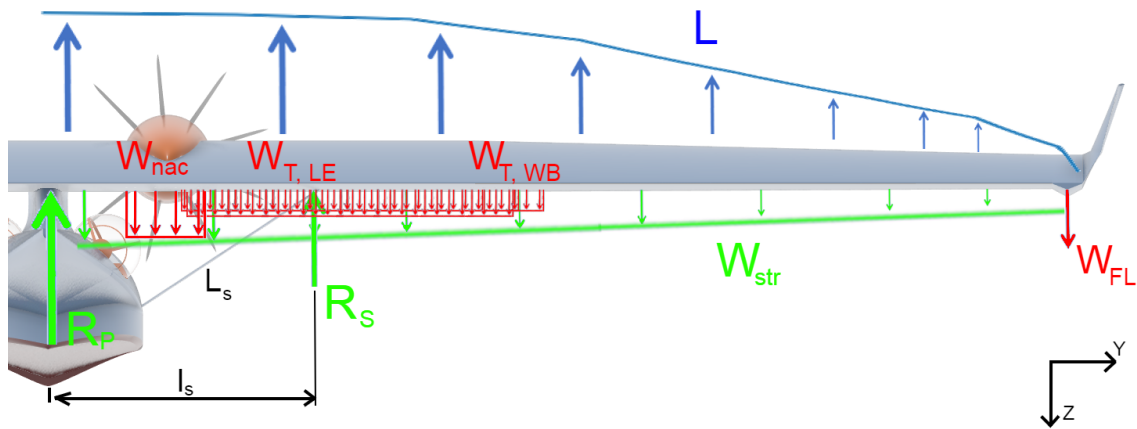


Figure 9.2: Free Body Diagram of the right with containing only forces and loads in Y-Z plane

In Table 9.1, g is the gravitational constant, n is the total load factor and the factor of one half is because half of the total force (i.e. lift, nacelle, tanks ...) is being carried by 1 wing. MTOM is the Maximum Take Off Mass, m is the mass of the component(s) and M is the moment of each respective component.

Lastly, it should be noted that for the calculations all the distributions have been divided into points with a certain resolution, a certain constant step. These values are then iteratively used such that the value is multiplied by the step and then summed to acquire the total force, while for moments each value is respectively multiplied by the step and its moment arm. This is called discretizing a continuous function, and does mean that an error is present, though this is relatively small and can be decreased by decreasing the step size. A crude example of a lift distribution discretization can be seen in Figure 9.3. During the actual calculations, this step is constant and small. For the other weight distributions, like the tank weights, past the actual structure, the weight is set to 0. This means that the weight of the leading edge tank is, in reality, an array along the whole wingspan, where a value is present at the location of the tank, but 0 at all other locations. This simplifies the moment calculations in and programming.

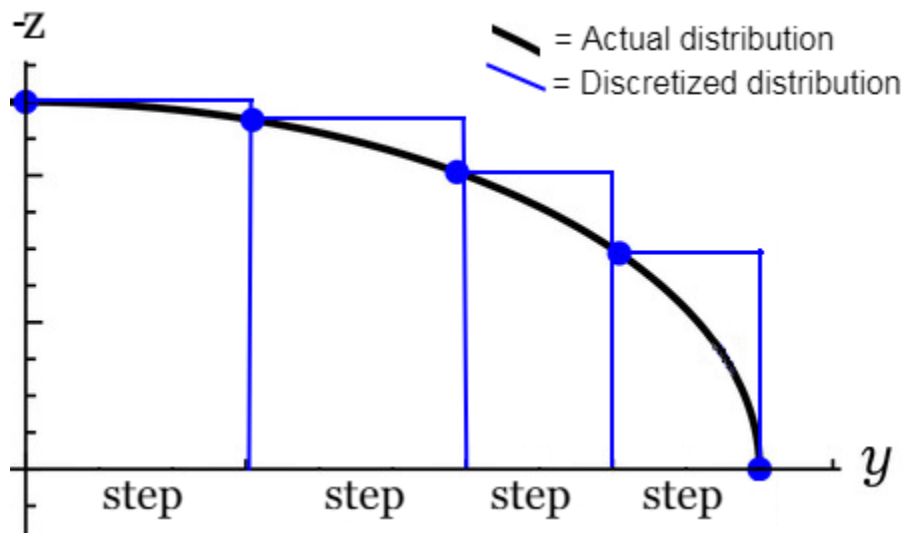


Figure 9.3: Discretization example of lift

9.2.1. Critical cases in z-direction

In addition to the total load factors, the critical cases with the greatest loads, which will lead to the greatest stresses, must be determined and designed for. In order to do this the forces must be looked at and assessed in what scenario which ones will act.

For the most upwards case, during the pull-up manoeuvre, the forces will be acting as displayed on Figure 9.2. The only exception is that the loads arriving from the tanks will be lighter as the fuel will be less than the

maximum. For simplicity, it will be assumed that these are empty. This leads to the following reaction forces and moments:

$$\begin{aligned}
 +\uparrow \sum F_z : \quad 0 &= R_p + L - W_{nac} - W_{TLE} - W_{TWB} - W_{Fl} - W_{Str} \\
 \therefore -R_p &= L - W_{nac} - W_{TLE} - W_{TWB} - W_{Fl} - W_{Str} \\
 \zeta + \sum M_{X,@pylon} : \quad 0 &= -M_p + l_L L - l_{W_{str}} W_{str} - l_{W_{eng}} W_{eng} - l_{W_{T,WB}} W_{T,WB} - l_{W_{T,LE}} W_{T,LE} \\
 &\quad - l_{W_{fl}} W_{fl} - M_{eng} + M_{WL} \\
 \therefore M_p &= l_L L - l_{W_{str}} W_{str} - l_{W_{eng}} W_{eng} - l_{W_{T,WB}} W_{T,WB} - l_{W_{T,LE}} W_{T,LE} - l_{W_{fl}} W_{fl} \\
 &\quad - M_{eng} + M_{WL}
 \end{aligned} \tag{9.1}$$

For the negative loading case, the same equations can be used, as only the lift will change direction, but this is accounted for using the load factor, n , which is included in L from Table 9.1.

After solving Equations 9.1, an internal shear force and bending moment diagram can be made, or SFD and BMD, as can be seen in Figure 9.4a and Figure 9.4b. This will be used to compare the original loading cases to the case where the strut included.

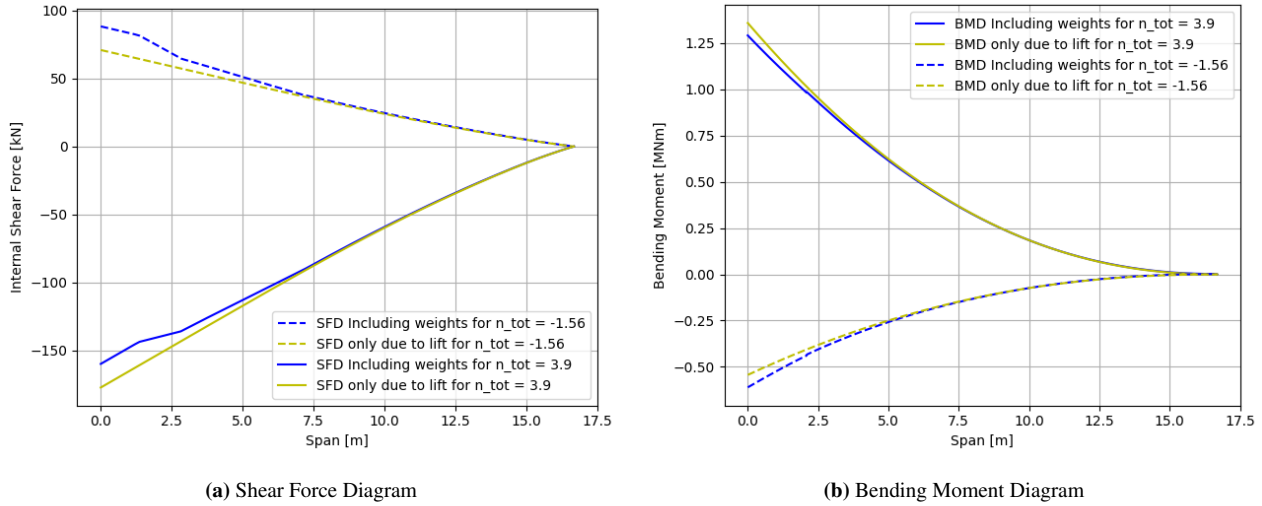


Figure 9.4: Internal loading of the strutless right-wing in Y-Z plane

Based on the plots above, it can be seen that the highest bending moment for a wing without a strut is 1.29 and -0.65 MNm for the positive and negative load factors respectively. Here, a positive value indicates a clockwise reaction moment and a negative a counterclockwise. For the internal shear force, the minimum and maximum loads are -162 and 85 kN, meaning for the positive loading case, a downward reaction force is present and vice versa. This is because an upwards lift force points in the negative z direction. Note that the distribution of the wing without any weights in it has been added too, to show how much the maximum shear force and bending moment change due to the weights in the wing. The acquired plots are as expected since a downwards pointing force, will alleviate the wing from its shear and bending for the positive load factor, and thus decrease the total magnitudes of the internal loading diagrams. However, it can also be seen that the stress relief is relatively minor.

9.2.2. Implementation of a Strut for z-direction

The airplane has 2 struts on each side which connect the wing to the fuselage. These struts will be located at a distance l_s from the pylon (in the y -direction). Furthermore, these struts, which will usually be in tension, are pin supported to the fuselage, meaning they can carry loads in x,y,z and moments around y and z , though not around x . Each strut will add mass, though also alleviate the wing in bending and shear, and thus decrease the mass of the wing box. The loads and their masses will be calculated and assessed for $l_s = 3.5m$

When adding the strut to the FBD, a statically indeterminate problem occurs as there are 3 unknowns, R_p, R_s and M_p , while only 2 equations are present (see Equation 9.1). This means an additional equation is required to

account for R_s and relate the unknowns to each other. For this, the moment-displacement equations can be used. This equation relates the moment equation of a beam, $M(y)$, to the second derivative of its deflection, $v(y)$, thus also taking into account structural characteristics such as the Young's modulus, E , and Second Moment of Area, I [18]. This equation can be seen in Equation 9.2. Furthermore, a compatibility equation relating the deflection of the wing to the elongation of the strut must be implemented as well in order to complete the system.

$$\frac{d^2v}{dy^2} = -\frac{M(y)}{EI} = v''(y)$$

$$v(y) = \frac{My^2}{2EI} + c_1y + C_2 \quad (9.2)$$

$$\text{For the strut: } v(L_s) = \frac{R_s \cos(\theta) L_{str}}{E_{str} A_{str}}$$

If this is integrated twice, two integration constants appear. However, both these constants are 0 due to the boundary conditions as both the deflection and angle at the root are 0: $v(0) = 0$ and $v'(0) = 0$. These equations, for the case with the strut, can be seen in Equation 9.3. It should be noted that according to [18], loads and moments behind the point the deflection is being calculated at, are not accounted for and are 'turned off' which can be seen in the last 2 lines of Equation 9.3 where the M_{WL} is not included. Though, they are accounted for as the reaction bending moment is calculated assuming the moment M_{WL} is present, see the second dot. This should also be taken into account for the values of distributed loads that are located past the point for which the deflection is being calculated. Lastly, for the compatibility equation, the deflection of the strut must be vertical, and not along the length of the strut, that is the reason why an additional $\cos(\theta)$ appears on the left-hand side of the third dot.

$$\begin{aligned} & \bullet + \uparrow \sum F_z : 0 = R_p + R_s + L - W_{nac} - W_{TLE} - W_{TWB} - W_{Fl} - W_{Str} \\ & \quad \therefore -R_p - R_s = L - W_{nac} - W_{TLE} - W_{TWB} - W_{Fl} - W_{Str} \\ & \bullet \zeta + \sum M_{X,@pylon} : 0 = -M_p + R_s l_s + l_L L - l_{W_{str}} W_{str} - l_{W_{nac}} W_{nac} - l_{W_{T,WB}} W_{T,WB} - l_{W_{T,LE}} W_{T,LE} - l_{W_{fl}} W_{fl} \\ & \quad - M_{eng} + M_{WL} \\ & \quad \therefore -R_s l_s + M_p = l_L L - l_{W_{str}} W_{str} - l_{W_{nac}} W_{nac} - l_{W_{T,WB}} W_{T,WB} - l_{W_{T,LE}} W_{T,LE} - l_{W_{fl}} W_{fl} - M_{eng} + M_{WL} \\ & \bullet -EIv(l_s) = \zeta + \iint M_{X,@l_s} : -EI \frac{R_s \cos(\theta) L_{str}}{E_{str} A_{str}} \frac{1}{\cos(\theta)} = \frac{M_p l_s^2}{2} + \frac{R_p l_s^3}{6} + \frac{L l_s^3}{6} - \frac{W_{T,WB} l_s^3}{6} - \frac{W_{T,LE} l_s^3}{6} \\ & \quad - \frac{W_{nac} l_s^3}{6} - \frac{W_{str} l_s^3}{6} + \frac{M_{eng} l_s^2}{2} \\ \therefore \frac{-R_p l_s^3}{6} - EI \frac{R_s L_{str}}{E_{str} A_{str}} - \frac{M_p l_s^2}{2} = \frac{L l_s^3}{6} - \frac{W_{T,WB} l_s^3}{6} - \frac{W_{T,LE} l_s^3}{6} - \frac{W_{nac} l_s^3}{6} - \frac{W_{str} l_s^3}{6} + \frac{M_{eng} l_s^2}{2} \end{aligned} \quad (9.3)$$

Using these equations, the 3 unknowns can be solved. Furthermore, the deflection of the strut, and thus wing, can be influenced by changing the struts' parameters (E_{str} , A_{str} and L_{str}). For example, assuming a shorter strut, meaning less total deflection, or decreasing A_{str} , thinning the rod, allowing more wing deflection, and thus R_{str} is relatively smaller.

9.2.3. Critical cases in x-direction

For the direction in the length of the fuselage (x-direction), only 2 main forces act, namely the drag and thrust, as can be seen in Figure 9.5. The most critical case, where the most loads act in the negative X direction, is when the engines are not providing any thrust, yet the aircraft is flying and produces drag, this corresponds to a situation where a 3.9g pull-up manoeuvre is taking place, while the engines are turned off. The case with the most loads in the positive x-direction corresponds to a situation where there is only thrust. This happens when the plane is standing still and applying full thrust, like during take-off. The magnitudes of these forces are a lot smaller than those in z-direction. This means the wing box can be designed to withstand fewer loads in x-direction.

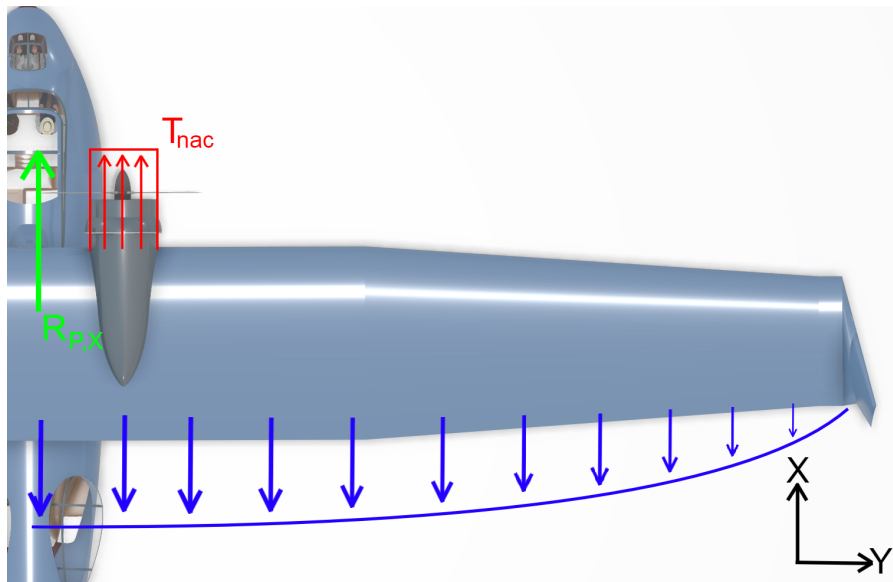


Figure 9.5: Free body diagram of the right wing containing only forces and loads in xy plane

$$\begin{aligned}
 +\uparrow \sum F_x : \quad 0 &= R_{p,x} + T_{nac} - D \\
 R_{p,x} &= D - T_{nac} \\
 \zeta + \sum M_{z,@pylon} : \quad 0 &= -M_{p,z} + Dl_D - T_{nac}l_{nac} \\
 M_{p,z} &= Dl_D - T_{nac}l_{nac}
 \end{aligned}
 \tag{9.4}$$

After solving these equations, the internal shear force and bending moment diagrams can be made.

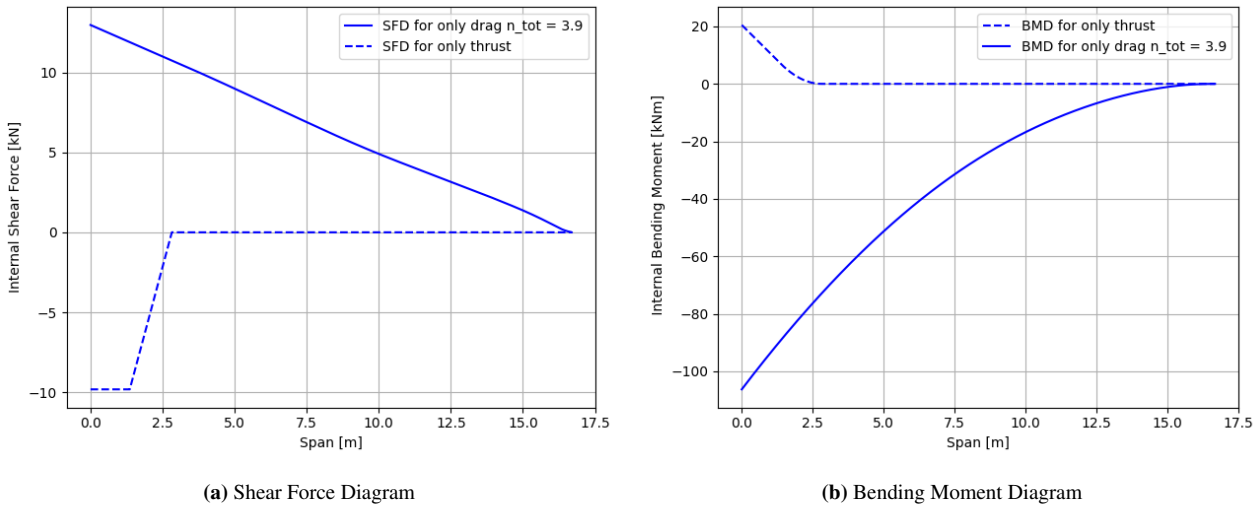


Figure 9.6: Internal loading of the strutless right-wing in the xy plane.

Based on the plots, it can be seen that the greatest stresses that the pylon has to withstand in the x-direction are 13.3 and -9.7 kN, with the sign convention according to Figure 9.5. While for bending along z, these are -106,6 and 21 kNm where a positive value means that the reaction moment is clockwise from the viewpoint of Figure 9.5.

9.2.4. Implementation of a Strut for x-Direction

It can be seen that the horizontal loads which the pylon has to withstand are a lot smaller than the loads in the vertical z-direction. Namely, approximately 12 times smaller. This means that if a strut were to be included, it would have to carry a lot more loads in the vertical direction than in the horizontal, and would fail easier vertically. Due to time constraints, as well as the reason mentioned before, it has been chosen to omit these calculations as the vertical direction is way more critical. Nevertheless, the method would be similar to

subsection 9.2.2, where the compatibility equation would once again relate the deflection of the wing to the deflection of the strut. It should be noted that instead of an axial deformation, the strut will bend.

9.2.5. Loading along chord

Due to the distance between the centre of pressure of the lift force and the centre of gravity of the wing, a torsional force will be created. For this, the distance of the centre of pressure and the centre of gravity needs to be estimated. Following from the aerodynamics and the centre of gravity calculations, this distance is 17% of the chord. This is then multiplied with the chord length to find the moment arm. Then this is filled into Equation 9.5 to find the internal torsion force.

$$T = V * l \quad (9.5)$$

Using this, the following the internal torsional moment can be found as shown in Figure 9.7.

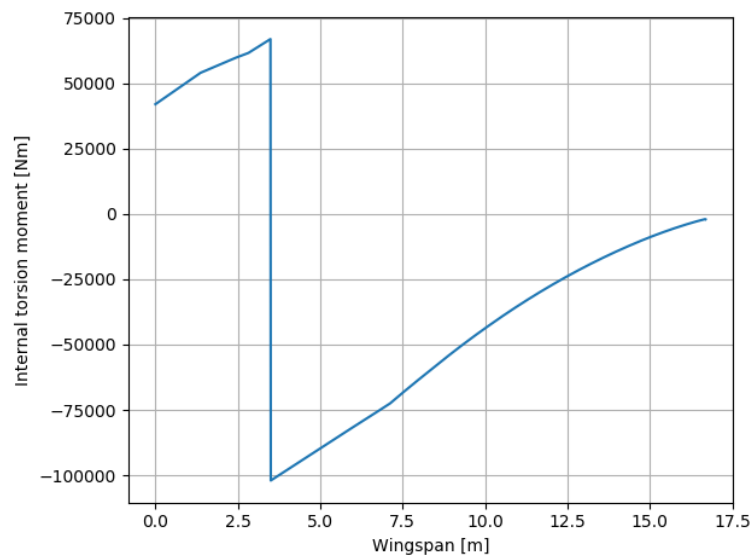


Figure 9.7: Internal torsion moment over wingspan

9.3. Fuselage aerodynamic loads

This section deals with the quantitation of the loads in the fuselage caused by aerodynamic forces. Several loading cases to the fuselage are considered. The fuselage should be able to withstand these loads during all operations. The loads that will be discussed are deemed to be the critical cases that have to be accounted for.

For the calculations, the conventional aircraft axis system has been used, where the x-axis points towards the nose, the y-axis points towards the right wing, and the z-axis downwards. The loads are divided into three categories: the loads which can be seen from the side, which consists of forces parallel to the z-axis and moments around the y-axis, the loads which can be seen from the top, which consists of y-axis forces and z-axis moments and finally, the torsion in the fuselage, which is the moment around the x-axis.

Side view

The first loading case that will be analysed is one caused by the main wing and tail lift forces. The wing is attached to the fuselage with the pylon and thus will be considered as a point force with a moment around the quarter chord point. The lift of the horizontal tail will be considered as a point force located at the centre of gravity of the horizontal tail, and no moment will be considered since this would be negligible compared to the main wing moment. The force of the tail will be calculated with the ratio of the wing lift to the horizontal tail lift, which was calculated for stability & control in chapter 11. Together, these forces will counteract the weight of the fuselage and will give the fuselage zero resulting moments.

Top view

The second loading case that will be analysed is a one-engine inoperative loading. This loading will be added to the first loading case. Due to a one-engine inoperative scenario, a moment will be created around the z-axis

of the aircraft. This moment must be countered by a force of the vertical tail. When the aircraft is flying in this configuration it still needs to be able to produce more yawing forces with the rudder in order to be controllable, thus the yaw force will be multiplied by a factor of 2 to account for this. The force that will counteract the aircraft from moving in the direction of the vertical tail force is the aerodynamic loads on the fuselage. This force will have the same magnitude as the vertical tail load but opposite direction, ensuring equilibrium in forces.

Torsion

From the top view and side view, it is visible that the vertical tail force is not acting in the centroid of the fuselage and thus a torsion load is present. This torsion load will be counteracted by a roll force due to the main wing. This means that a constant torsion will be present between the main wing and the vertical tail.

Loading diagrams

The internal loading diagrams for the nominal loads are reported in Figure 9.8. Keep in mind that these diagrams display a simplified reflection of reality. In reality, the internal forces will not be zero in the nose of the aircraft, but because the weight was assumed to be acting in the centre of gravity the forces are zero in the diagrams. Similarly, the diagrams show no forces after the aerodynamic centre of either the horizontal or vertical tail. Again, in reality, these internal forces will be present. The method to still design for these forces is described in the subsection 10.3.4.

Next to the nominal loads, Figure 9.8 includes the loads with an extra factor applied. This factor was chosen to be 3. This includes doubling of the loading to take into account peak loads (as compared to nominal continuous loading). For these peak loads, one might think of hard runway/water landings, or extra loads due to the presence of cut-outs in the fuselage (windows, doors, etc.). These extra loads are hard to quantify and therefore modelled using an extra margin. Adding this extra margin will also make the fuselage more resistant to fatigue of the material. Furthermore, a 1.5 design safety margin has been added. This safety margin is needed since some structure sizing methods are based on empirical formulas, and additional small loads in the fuselage are neglected.

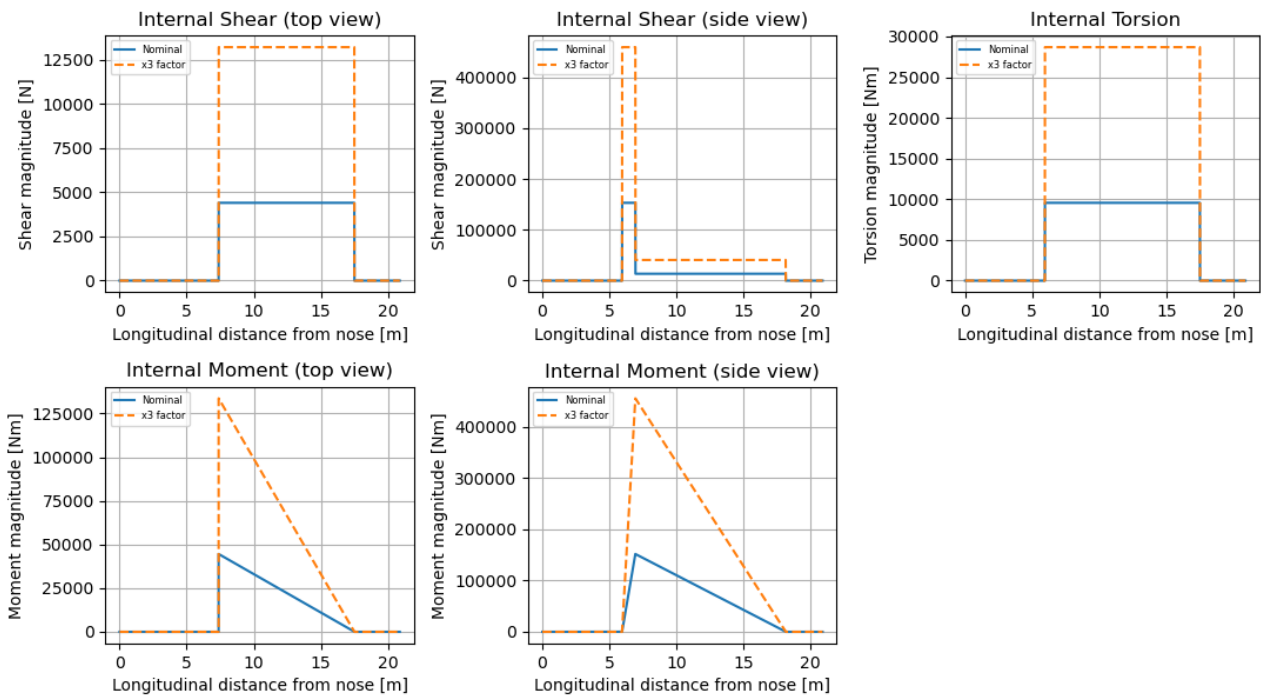


Figure 9.8: The absolute value of the internal force and moment diagrams of the fuselage

9.4. Fuselage water loads

To make sure the aircraft also maintains structural integrity whilst performing water operations, the hull structure needs to be designed. But this can not be done without the loading cases that are present at the hull. Within

the CS-23 regulations, there are rules on how large the loads are that need to be designed for. In this section, these load cases will be considered and applied to the Caty. Note that due to lack of time and resources, water loads are not considered when designing the the fuselage's structure.

9.4.1. Critical loading case

As the Caty has a single step, the formulas for single-step flying boats need to be used from CS-23. The first load case considered is for landing on water. The impact will be at the step in the keel. To calculate the load factor here Equation 9.6 is used.

$$n_w = \frac{C_l * V_{so}^2}{\tan(\beta)^{\frac{2}{3}} * W^{\frac{1}{3}}} \quad (9.6)$$

Where C_l is a constant (0.012 for landing), V_{so} is the stall speed at landing conditions, β is the angle of the hull to a horizontal line, as shown in Figure 9.9 and W is the weight during the manoeuvre. When calculating the load factors for the take-off the load factor comes to 3.2. This means the keel has to be designed for a load factor of 3.2, as this is the most critical case. It states in CS-23 that this load can be distributed over the hull to avoid excessive local shear and bending moments. The pressures can not be smaller than the pressures that are calculated in Equation 9.8 and Equation 9.7.

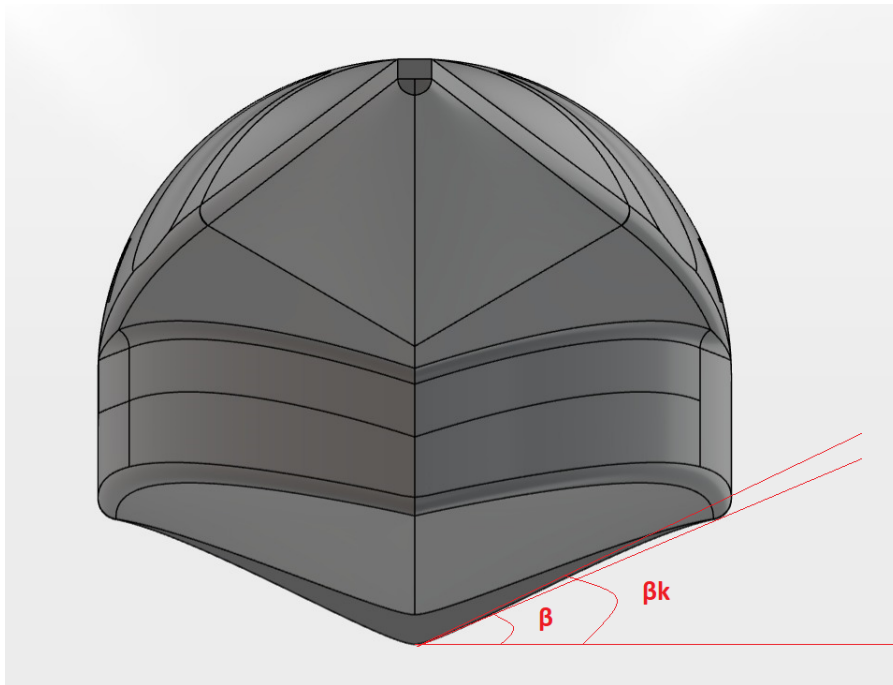


Figure 9.9: Angle of the step of the hull

Next, the pressure loads on the hull need to be calculated due to the movement through the water. For this, it has to be defined whether the fuselage has a flared or an unflared bottom. For an unflared bottom, the pressure decreases linearly from the keel to the chine. The pressure at the keel is calculated from CS-23 as shown in Equation 9.7.

$$p_k = \frac{C_2 * K_2 * V_{S1}^2}{\tan\beta_k} \quad (9.7)$$

In this formula, a couple of new parameters are shown. C_2 is a constant, K_2 is the hull station weighing factor and depends on the position of the fuselage as shown in Figure 9.10. β_k is the angle as shown in Figure 9.9.

10

Structures

All of the modifications made to the original Catalina will also have an effect on the internal structure. Additionally, modern materials could give large reductions in the structural weight of the Caty. In this chapter, the structure will be redesigned by inputting all of the modifications made and deciding on the best materials for each structure. Firstly, the materials are chosen in section 10.1. The wing box structure will be designed in section 10.2. Then the fuselage structure will be designed in section 10.3.

10.1. Material Trade-off

Before the structures for all of the sub-systems can be designed, the proper materials need to be chosen. For this, the following main sub-systems are defined:

- Fuselage
- Wing box
- Wing leading edge
- Engine

Then, the potential materials that might be used are defined. For this, the following materials were chosen:

- aluminium
- Thermoplastic composites (carbon fibre - PEEK)

In earlier analyses, thermoset composites were also considered. However, due to their poor recyclability, they are taken out of the analysis as the team considers this unacceptable [1].

10.1.1. Material properties

Before the correct materials can be chosen for each part of the aircraft, their properties need to be quantified to make a correct comparison. These are shown in Table 10.1 [1]^{1 2 3}.

Table 10.1: Material properties

Material	σ_{ult} [MPa]	τ_{shear} [MPa]	E [GPa]	Poisson ratio	ρ [kg/m ³]
aluminium	400	120	70	0.3	2810
TPC (Quasi-isotropic)	775	195	54	0.3	1700
TPC (Uni-directional)	2350	-	138	0.3	1700

A couple of remarks need to be made regarding these values. First of all, the Poisson ratio for TPCs was a difficult parameter to find and differed between 0.25 and 0.35, therefore the average was taken. Additionally, the shear strength for quasi-isotropic TPC was hard to find. Therefore, the assumption was made that, due to the nature of quasi-isotropic composites, the material can carry 1/4th of its ultimate stress in shear. Finally, the ultimate stress in aluminium is defined as the yield stress, where this is ultimate stress for the composite case. This is because composites are brittle and do not yield.

¹https://www.researchgate.net/publication/356588363_High_Performance_Thermoplastic_Polymers_And_Composites (accessed on 05/06/2023)

²<https://pubs.aip.org/aip/acp/article/2051/1/020278/887903/Evaluation-of-the-mechanical-properties-for-a> (accessed on 05/06/2023)

³https://www.victrex.com/-/media/downloads/literature/en/victrex-aerospace-brochure_final2014_lowres.pdf (accessed on 05/06/2023)

10.1.2. Fuselage

For the fuselage the following trade-off criteria are chosen, as these properties are considered the most important:

- Recyclability
- Weight
- Cost
- Technology readiness level
- Aerodynamics (Rivets)

For the thermoplastic composites, it is important to note that the values are for quasi-isotropic, as in the fuselage there are not only forces in one direction but in all directions.

The criteria are weighed from 1/4 to 4/4 to what is most important to the fuselage. The weight, recyclability, cost and technology readiness level are all valued the same for all structures. The aerodynamics, however, are taken into account as well, due to the large amount of rivets in the fuselage and the removal of them with thermoplastic composites.

Firstly, the recyclability is analysed. For the thermoplastic composites an expert⁴ from SAM XL⁵ was contacted to specify the recyclability of TPC. He mentioned that the material can be recycled for multiple heat cycles, but not infinite. Therefore the score was 3 out of 4. Aluminium however is completely recyclable⁶ and therefore gets a 4 out of 4.

Next is the weight. For this the specific Young's modulus and specific ultimate stresses are important. These have to be maximised to get the best performance for the least mass added to the structure. These are for TPC (quasi-isotropic) $0.032 \text{ GPa} \cdot \text{m}^3/\text{kg}$ and $0.46 \text{ MPa} \cdot \text{m}^3/\text{kg}$ respectively[1]. For aluminium, these are $0.025 \text{ GPa} \cdot \text{m}^3/\text{kg}$ and $0.14 \text{ MPa} \cdot \text{m}^3/\text{kg}$ [1].

Next is the cost of the material. It is very difficult to find a cost for the thermoplastic composites. Therefore, this analysis is done qualitatively. It can safely be said, due to the more difficult manufacturing in comparison to aluminium, that the TPC will be more expensive than aluminium.

Next is the technology readiness level (TRL). This is also done qualitatively. As aluminium is readily available and has been for many years, this gets the maximum score. TPCs have been used for specific parts already in aerospace, but for large structural parts, this is very new. However, when talking to the expert⁷ it became clear that this will be ready for the next generation of aircraft.

Then finally the aerodynamic improvement. When manufacturing with TPC it is possible to mend parts together by using the material's properties to become liquid when heated. Therefore, no rivets need to be used which is very useful for the aerodynamic performance of the fuselage. For aluminium, however, a lot of rivets need to be used, which is unfavourable for the drag.

Finally, the trade-off table is shown in Table 10.2. From this, the conclusion can be drawn that thermoplastic composites are the best choice for the fuselage structure.

⁴Communication with Abhas Choudhary , dd. 26-5-2023

⁵<https://www.samxl.com/> (accessed on 06-06-2023)

⁶https://circulareconomy.europa.eu/platform/sites/default/files/euric_metal_recycling_factsheet.pdf(accessed on 06-06-2023)

⁷Communication with Abhas Choudhary , dd. 26-5-2023

Table 10.2: Trade-off fuselage material

	Recyclability	Weight	Cost	TRL	Aerodynamics	Final score
Trade-off weight	4/4	4/4	2/4	2/4	2/4	
aluminium	4	2	3	4	2	38
TPC	3	4	2	3	4	42

10.1.3. Wing box

For the wing box, the trade-off is similar to the fuselage. However, there are some things to take into account that differ from the fuselage. The main issue is thermal management. As one of the fuel cells is located in the wing box in each wing, there is a chance of high temperatures in this area of the wing. As this fuel cell is placed in the first part of the wing, between the strut and the fuselage, there needs to be a separate trade-off which includes thermal resistance for this part of the wing. This creates the following trade-off criteria:

- Recyclability
- Weight
- Cost
- Technology readiness level
- Aerodynamics (Rivets)
- Thermal resistance

For thermal resistance, it is important that the thermoplastic material has a glass transition temperature of around 130 degrees Celsius according to the expert. This is deemed too critical for this part of the wing. The maximum temperature of the fuel cells will be around 90 degrees, which is beneath this value. However, when any type of failure happens with the cooling, this temperature might increase and this is a big risk for the structural integrity of the wing. Aluminium on the other hand will lose some of its strength but can handle significantly higher temperatures than thermoplastic composites. From this, the trade-off is shown in Table 10.3.

Table 10.3: Trade-off wing box (part 1) material

	Recyclability	Weight	Cost	TRL	Aerodynamics	Thermal resistance	Final score
Trade-off weight	4/4	4/4	2/4	2/4	2/4	4/4	
aluminium	4	2	3	4	2	3	50
TPC	3	4	2	3	4	1	46

As mentioned before, for the part of the wing after the strut, the trade-off is the same as for the fuselage. So for that part, TPCs are also chosen.

10.1.4. Leading edge wing box

The trade-off for the leading edge of the wing box is slightly different. As this part is assumed to be non-load bearing, the structural performance, or weight, is deemed less important. Additionally, as de-icing is important at the leading edge and the team wants to do this by using the excess heat from the fuel cells, the thermal resistance is again important. This gives the following trade-off criteria:

- Recyclability
- Weight
- Cost
- Technology readiness level
- Aerodynamics (Rivets)
- Thermal resistance

Using the same scores as for the previous trade-offs, but with new weights, the trade-off as shown in Table 10.4

Table 10.4: Trade-off leading edge wing box material

	Recyclability	Weight	Cost	TRL	Aerodynamics	Thermal resistance	Final score
Trade-off weight	4/4	2/4	2/4	2/4	2/4	4/4	
aluminium	4	2	3	4	2	3	46
TPC	3	4	2	3	4	1	38

10.1.5. Nacelles engine

Finally, the material for the nacelles of the engine is chosen. For this trade-off, the same criteria are used for the leading edge of the wing box, as there are also fuel cells in the nacelle and the nacelle only carries aerodynamic loads. So naturally, the conclusion is also the same, meaning the nacelles will be made out of aluminium.

10.2. Main wing structure

For the Caty, a lot of modifications have been made to the wing structure. The main change is for the propulsion system. In the original Catalina, there was a large amount of weight added to the wing by the heavy engines and the large amount of fuel weight. Both of these have a large effect on the structure as the wing will experience less lift relief in the wing. However, there is also a large decrease in weight, in the order of magnitude of 6000 kg. This will of course also affect the necessary structural mass in the wing.

To design the wing box, 3 main structural elements are defined: the skin, the stringers and the ribs. Additionally, there are 3 different loading cases following from chapter 9: torsion, shear and bending. When designing all of the different structural elements, different types of loading are important. When designing for bending, the moment of inertia is the design variable. For torsion, the skin thickness is the most important. For the shear force, it is also the skin thickness, but mainly the thickness of the spars. Then lastly, for the compression in the top plate, the stringer spacing is the most important to account for buckling. All of these loading cases are discussed in the following sections. First, the bending stiffness is analysed in subsection 10.2.2. Then the skin thickness necessary for shear flow is calculated in subsection 10.2.3. Lastly, the stringer pitch is calculated subsection 10.2.4.

10.2.1. Designing of a Strut

As has been mentioned in subsection 9.2.2, implementing a strut to the wing would reduce the loads the pylon experiences. When solving Equation 9.3, and assuming the strut is made of unidirectional TPC, with $E = 138$ GPa and $\sigma_{ult} = 2350$ MPa, while the area is assumed to be 2 cm^2 . The following diagrams and reaction forces can be acquired.

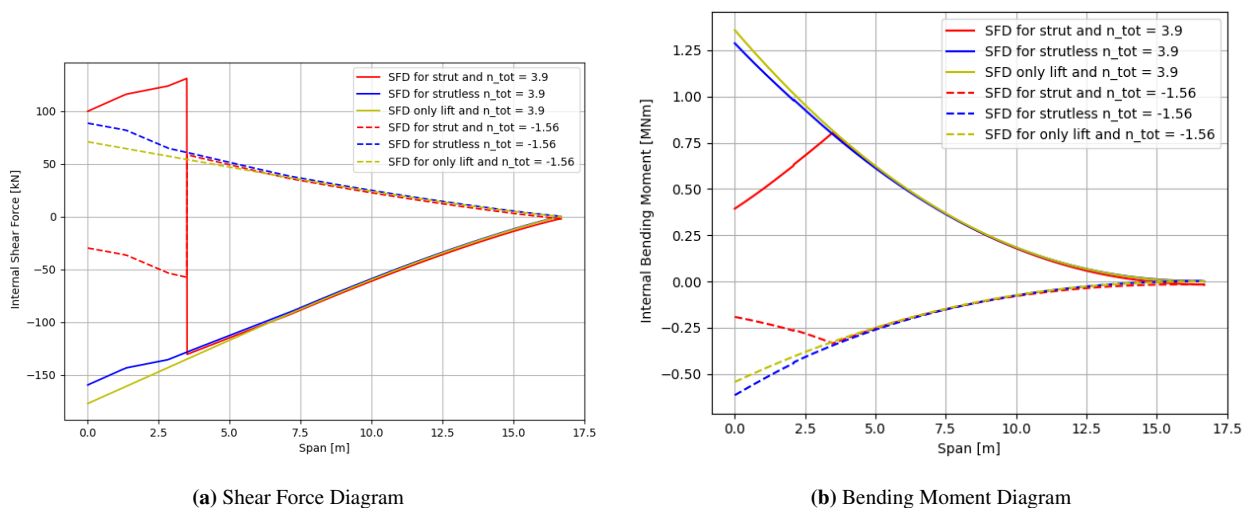


Figure 10.1: Internal loading of the right wing containing the strut in the yz plane

It can be seen that the internal shear force switches signs at the strut. The following reaction forces are calculated for the vertical reaction force in the pylon, the strut and the moment in the pylon respectively: 100kN, -266 kN, 0,39 MNm. Though it should be noted that the greatest magnitudes that occur are 136 kN and 0.80 MNm. The direction of the forces is according to Figure 9.2 and the reaction moment is assumed to be clockwise.

It should be checked whether the strut can actually carry this load. This can be done by calculating $\sigma = F/A$ where F is $R_s \cos(\theta)$ and A the cross-sectional area of 2 cm^2 , see Figure 9.2. This yields a stress of 730 MPa which is below the σ_{ult} of 2350 MPa, meaning the struts can withstand the most critical loads. It should be noted that assuming the strut is made of pure uni-directional TPC is possibly a wrong assumption. However, the stress in the rod is also smaller than the σ_{ult} of quasi-isotropic TPC. This means that the strut will be strong enough to withstand the loads the wing will experience, with the set parameters.

The mass of the strut can be calculated by multiplying its volume by the density. This is done in Equation 10.1, which yields a total mass of 1.424 kg, meaning each strut must be 0.712 kg as there is 2 on each side, which is very low.

$$m = \rho V = \rho A L_{str} \quad (10.1)$$

An additional load that should be designed for is when the strut experiences compression. The maximal compression load, based on Figure 9.6a, is 116 kN. This is divided by 2 struts meaning each strut has to carry 58 kN. In terms of compression strength, it is strong enough, based on the σ_{ult} . However, it could buckle which must be avoided. Based on [19], the critical load a beam can withstand in compression before it buckles is determined by Equation 10.2:

$$P_{cr} = \frac{\pi^2 I_{xx} E}{\left(\frac{L_{str}}{2}\right)^2} \quad (10.2)$$

Filling in the 58 kN for P_{cr} and solving for I_{xx} yields a Mass Moment Of Inertia (MMOI) of $1.87 * 10^{-7}$. This means the minimum MMOI should be more than this to withstand the critical buckling load. It has been chosen to design the strut in the shape of a NACA 0030 airfoil, since it has low drag but is relatively thick, meaning it has higher bending resistance. However, it will be assumed that the airfoil is purely present for aerodynamic reasons, while a hollow cylindrical rod inside the airfoil shape will be load-carrying.

$$I_{xx} = \frac{\pi D_{outer}^4}{64} - \frac{\pi D_{inner}^4}{64} \quad (10.3)$$

If the outer radius is taken as 2.5 cm and the inner as 2 cm, this yields an I_{xx} of $1.81 * 10^{-7} m^4$, according to Equation 10.3. This rod has a respective P_{cr} of 56.3 kN. This will be slightly below the required load of 58 kN it should carry. The reasoning for this is that the strut will break before the wing/pylon does during compression loads, this acts as a fail-safe and ensures the pylon does not pierce through the aircraft damaging the payload inside. This means that during failure, first the strut will break, after which the wing box follows, at the strut connection, as suddenly the loads, during the negative loading case, become too much for the wing box to withstand. Nevertheless, the strut will help during hard landings to transfer compression loads from the landing gear and fuselage to the wing.

Using Equation 10.1 the new mass can be calculated. The total surface area of the rod will be 7 cm^2 , which yields a mass per strut of 5.03 kg. It will be assumed this only acts during compression, as else the reaction force of the strut will increase drastically due to a stiffer strut, increasing the load it will carry, which again leads to an increase in the size of the strut. The weight of the aerodynamic fairing around the strut is neglected.

The decrease in stress leads to a lighter MTOM, lighter lift, etc. A snowball effect takes place and thus a fair comparison is difficult to make between the aircraft with and without the strut. Nevertheless, it can be seen that the diagrams for the strut case have smaller magnitudes of forces/moments and thus it can be concluded that the wing box will be lighter. Furthermore, as the total mass of the struts is only 20.13 kg, while the stresses decrease substantially, it can be concluded that the case for the strut is beneficial in terms of weight, compared to the strutless situation, this will be used throughout the rest of the report.

It should be noted that this process is very iterative as changing the wing box mass, will decrease the loading relieving of the wing, meaning the strut has to carry more loads again and change the reaction forces, which once again affects the wing box. The Second Moment of Area, which has been used in Equation 9.3 for the calculations of the strut, will be calculated and designed in the following sections. This MMOI will be used for the strut calculations and iterated.

10.2.2. Bending stiffness

During flight, there is a very large bending moment present in the wing of the aircraft. To ensure the loads are transferred to the middle of the wing correctly and without failure, the structure needs to be designed to withstand the maximum load case as stated in chapter 9. To perform this analysis, a few assumptions are made to simplify calculations. The first assumption is the simplification of the structure by using "booms". Booms are theoretical point areas of the structure. They are used to estimate the shape of the airfoil and get rid of the assumption of a completely rectangular wing box. Their effect on the second moment of area can be easily calculated by using Equation 10.4, where A is the total area of booms necessary and d is the distance from the booms to the centre of gravity of the wing box.

$$I_{xx} = A_{boom} * d^2 \quad (10.4)$$

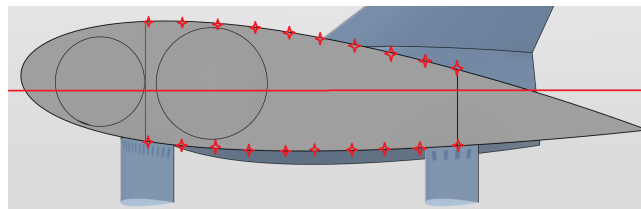


Figure 10.2: Example locations booms

To find the total MMOI necessary to ensure bending stiffness over the entire wing, Equation 10.5 is used. However, there are a couple of parameters that need to be assumed here. Firstly, the stress that will be designed for is the yield stress, as that can never be exceeded. The yield stress is however different along the wingspan, as the material is also different. Then the wing box will be designed for the most critical point on the airfoil, which is the point with the most distance. Finally, the thickness of the top skin and the area of the stringers are assumed constant along the cross-section, and therefore all the booms must have the same area. Then with the safety factor of 1.5 as assumed in chapter 9 the equations are combined to find the minimum area of material at the top and bottom part of the wing box as shown in Figure 10.3

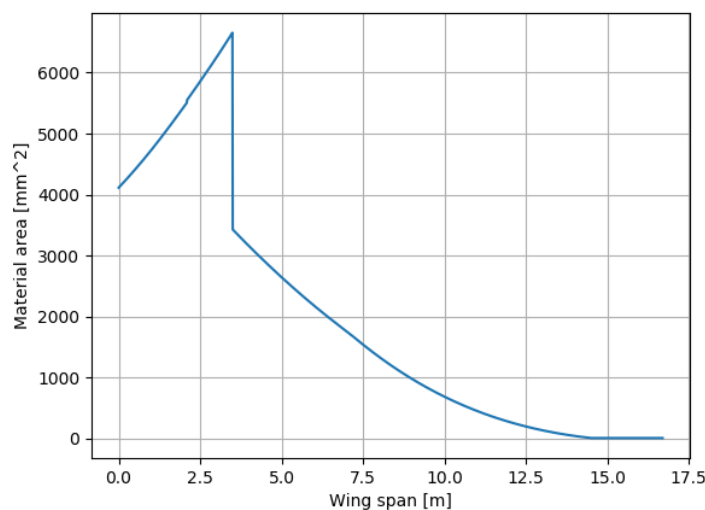


Figure 10.3: Minimum area material over wing span

When this requirement of minimum area on the top and bottom plate is met, the wing will not yield at its maximum load.

$$I_{xx} = \frac{M_y * h}{\sigma_y} \quad (10.5)$$

10.2.3. Shear stiffness

To design the structure for shear stiffness, three different loading diagrams have to be combined. These are the torsion diagram, the vertical shear force diagram and the horizontal shear force diagram. These can then be superimposed to find the skin thickness necessary for the shear flow along the entire wing box.

First, torsion is considered. The shear flow following from the torsion diagram is constant along the entire wing box. The torsional diagram as shown in chapter 9 is converted to a shear flow in Equation 10.6. Here T is the torsion force and A is the enclosed area by the wing box.

$$q_t = \frac{T}{2 * A} \quad (10.6)$$

Using this formula, the shear flow due to the torsion can be calculated. This shear flow is constant along the entirety of the wing box, but differs over the wing span. The results are shown in Figure 10.4a.

Next up is the vertical shear flow. This is slightly less elementary to calculate. It is important that the most critical case is considered for this, which is the shear flow at the neutral axis. Additionally, to simplify the calculations, the thickness at the side panels are considered constant at a cross-section. They are however different from the thickness at the top and bottom panels, as other loading cases are critical there.

To calculate the shear flow at these critical points on the neutral axis Equation 10.7 is used. There are a couple inputs to this formula. First of all is the vertical shear force diagram as calculated in chapter 9. Next up is the Q parameter. This parameter is the first moment of inertia and determines where the shear flow is the highest. This is the point, above and below which is the same area. The total area is gotten from the bending analysis in subsection 10.2.2. Last is I_{xx} , which is also gotten from the bending analysis in subsection 10.2.2.

$$q_{V_y} = \frac{Q * V}{I_{xx}} \quad (10.7)$$

Following from this, the shear flow due to the lift and weight forces can be calculated. The results are shown in Figure 10.4b.

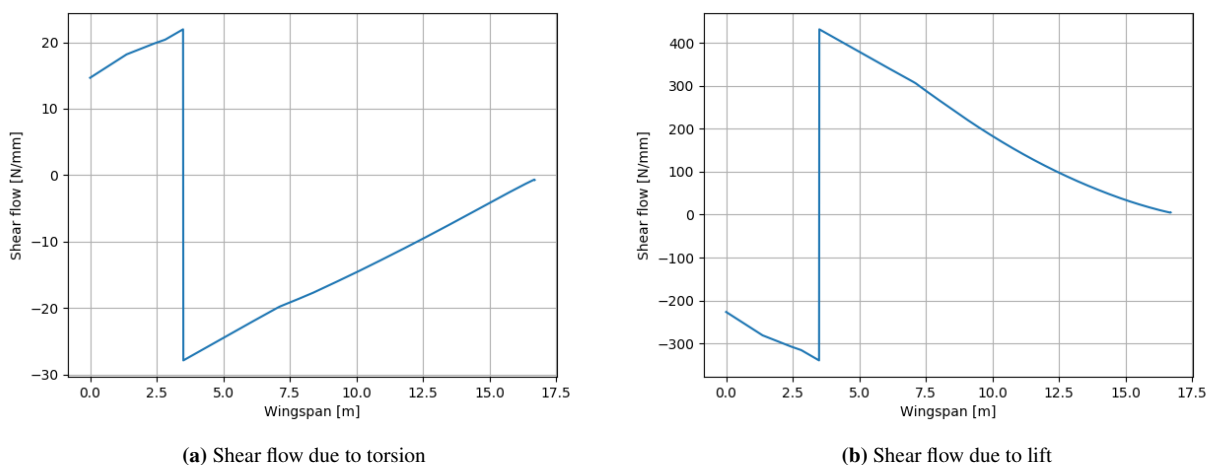


Figure 10.4: Shear flow in the Z-direction on the wing

This can then be used to calculate the minimum thickness of the side panels. It is important to note that even though the sign is different in these figures, the absolute values need to be added because the wing box has two

sides and the shear flow due to torsion is up on one side and down on the other, so the critical case is always the absolute value added together. This is done via Equation 10.8.

$$t = \frac{q}{\tau_{shear}} \tag{10.8}$$

This then creates the following minimal thickness of the side skins, better known as spars, as shown in Figure 10.5.

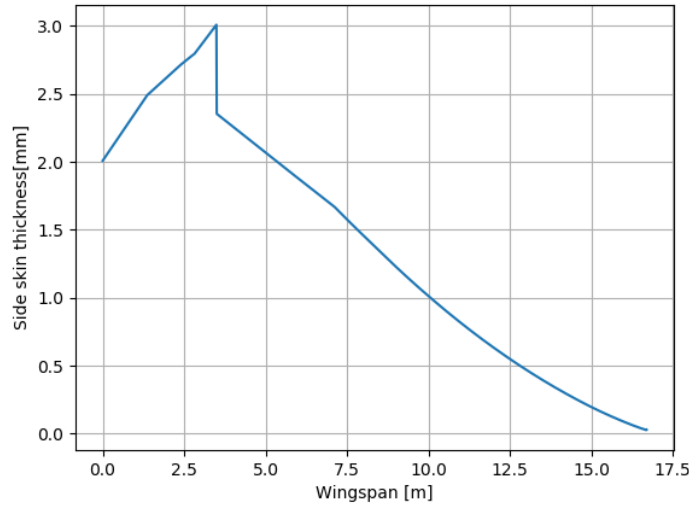
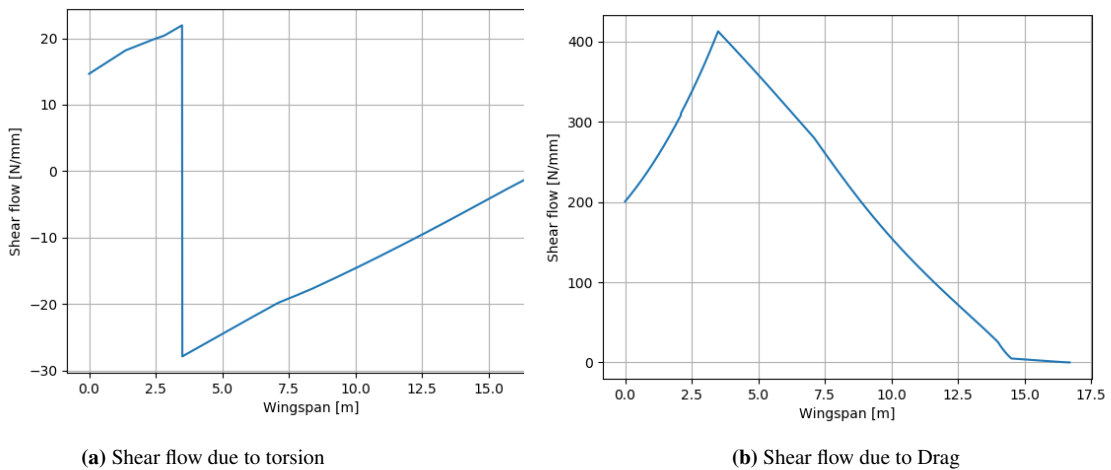


Figure 10.5: Minimum side skin thickness

Next is the horizontal shear flow. This is calculated similarly to the vertical shear, but then using the horizontal forces, which are the drag and the engine thrust. The critical loading case for this is on the top and bottom plate, as the neutral axis runs from the top to the bottom for this case. Firstly, the relevant shear flows are shown Figure 10.6.



centring

(a) Shear flow due to torsion

(b) Shear flow due to Drag

Figure 10.6: Shear flow in the X-direction in the wing

This results in the following minimum thickness over the wingspan.

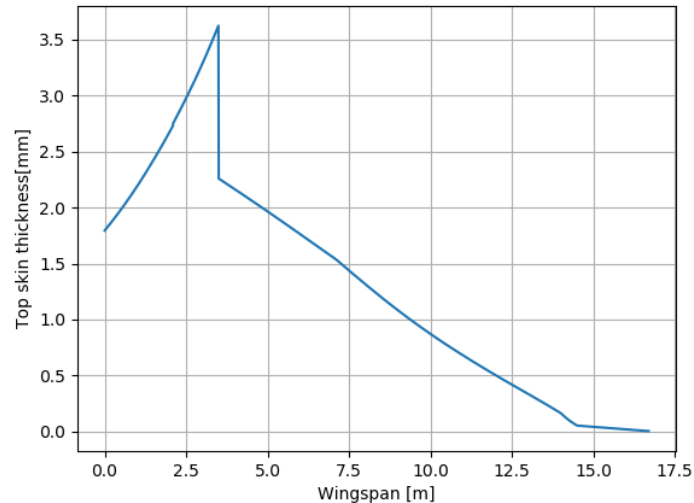


Figure 10.7: Minimum top skin thickness

10.2.4. Sheet crippling

Another important failure mode for the wing box is crippling. This will happen when a plate is in compression. It is important to note that it is not necessary to design for crippling at the maximum load, as it does not mean instant failure. However, it is important that the skin does not cripple regularly.

In principle, there are three different aspects to this design problem: buckling of the stringer, buckling of the skin and crippling of the sheet (stringers and skin combined).

First, the buckling of the stringers is analysed. This is done via Equation 10.9.

$$\frac{\sigma_{cc}}{\sigma_y} = \alpha * \left(\frac{C * \pi^2 * E}{\sigma_y * 12 * (1 - \nu^2)} * \left(\frac{t}{w} \right)^2 \right)^{1-n} \quad (10.9)$$

As it is unfavourable for the stringers to buckle before they yield, the left side of the equation is set to 1, so the stringers theoretically buckle and yield at the same time. α and n in this formula are correction factors that came from empirical data. The C is the clamping condition, which differs per flange of the stringer. The stringers chosen for this are Z-stringers, as shown in Figure 10.8. These stringers are chosen due to their ease of assembly, inspection and maintenance.

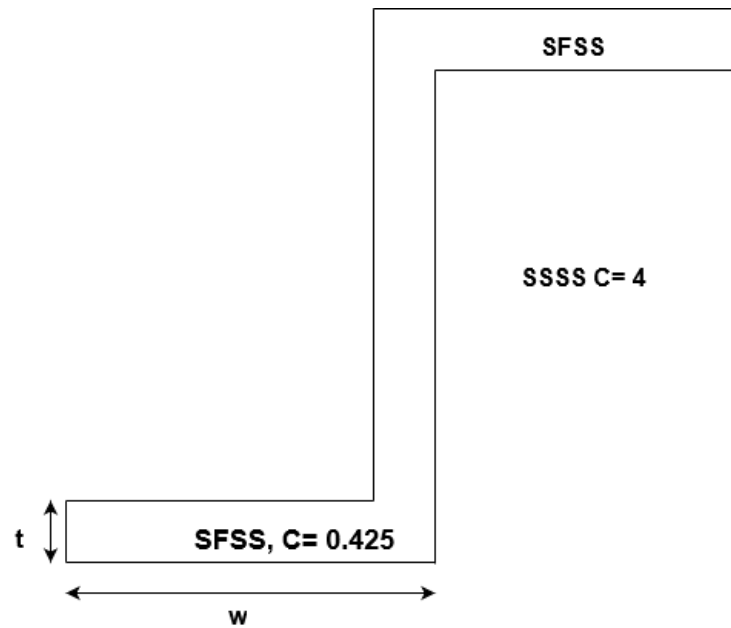


Figure 10.8: Stringer shape and variables

The main parameter that needs to be gained from this is the ratio of the thicknesses of the flanges to their width. In a later stage, when the number of stringers and their minimal areas are found, they can be sized.

The values coming from this are shown in Table 10.5.

Table 10.5: Stringer flange sizes

Position on span	Material	Clamping	t/w
0-3.5 m	aluminium	SFSS	0.161
-	-	SSSS	0.053
3.5-16.7 m	TPC	SFSS	0.255
-	-	SSSS	0.083

Next is the buckling of the skin. The skin without stringers is allowed to buckle, as that is what stringers are added for. To be able to approximate this buckling mode, a new parameter needs to be introduced: the effective width. When a thin plate is in compression, the width of skin that can carry the load gets smaller the larger the stress is. This is approximated by creating this variable. It is calculated as follows:

$$2we = t * \sqrt{\frac{C * \pi^2}{12 * (1 - \nu^2)}} \sqrt{\frac{E}{\sigma_{cc}}} \quad (10.10)$$

From this formula, the crippling stress of the sheet can be found. The width of the sheet is decreased by subtracting the effective width of the pitch of the stringers as shown in Equation 10.11.

$$\sigma_{cr} = \frac{C * \pi^2 * E}{12 * (1 - \nu^2)} \left(\frac{t}{b - 2we} \right)^2 \quad (10.11)$$

The b in this equation is the pitch of the stringers. Now that the critical stresses for both the stringers and the skin are defined, they can be combined to find the crippling stress of the sheet. This is a combination of three things: the stringer area with its buckling stress as calculated in Figure 10.8, the effective sheet with the stringer buckling stress as calculated in Equation 10.10 and the sheet minus the effective width and their buckling stress as calculated in Equation 10.11. These are multiplied and added to each other to then be divided by the total area as follows:

$$(\sigma_{cc})_{panel} = \frac{\sum \sigma_{cc}^i A_i}{\sum A_i} \quad (10.12)$$

Then, using an iterative process for the area of the stringers and the pitch of the stringers, a minimum pitch for the stringers along the span was found. The stringer pitch was allowed to change at a number of points to ensure ease of manufacturing. This is shown by the bumps in the graph in Equation 10.11

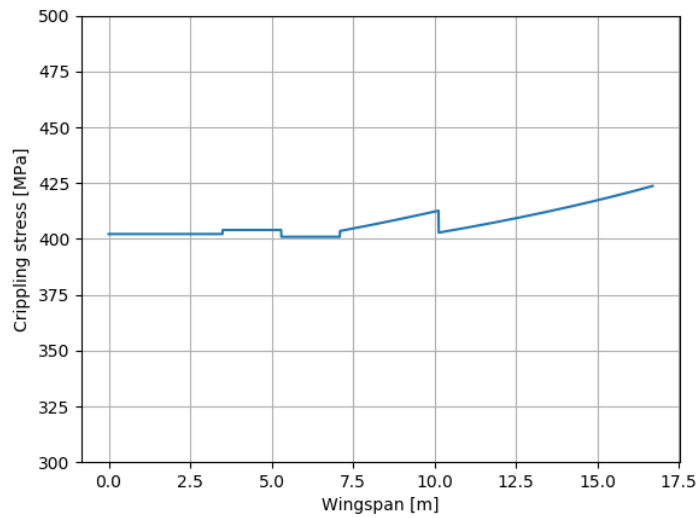


Figure 10.9: Crippling stress along the wing span

These sections are also used to change the other parameters, which will be explained in subsection 10.2.5. The minimum pitch for the stringers for each section is shown in Table 10.6.

Table 10.6: Minimum pitch stringers

Section	Minimum pitch (mm)
0 - 3.5 m	240
3.5 - 5.3 m	185
5.3 - 7.1 m	150
7.1 - 10.1 m	115
10.1 - 16.7 m	60

10.2.5. Final wing box design

It is now important to bring all of these failure modes together to converge to a final design. Firstly, the manufacturability needs to be taken into account. It is very difficult to have a variable thickness over the entire wing, a number of points will be chosen where this will be changed. The first point is the position of the strut, which is at 3.5 m. As the material changes here as well as loadings change a lot, this was chosen as a natural point. Next is the wing break, so where the taper starts. One point was put halfway between these points to reduce the mass of the structure there. The final point was at the quarter length point between the wing break and the tip, also to reduce the structural weight.

Firstly, the skin thicknesses are analysed. For this, it was found that the shear forces in combination with the torsional shear flow are the critical loading case. Then for each section, the maximum value was taken to determine the thickness in that part, resulting in the thicknesses as shown in

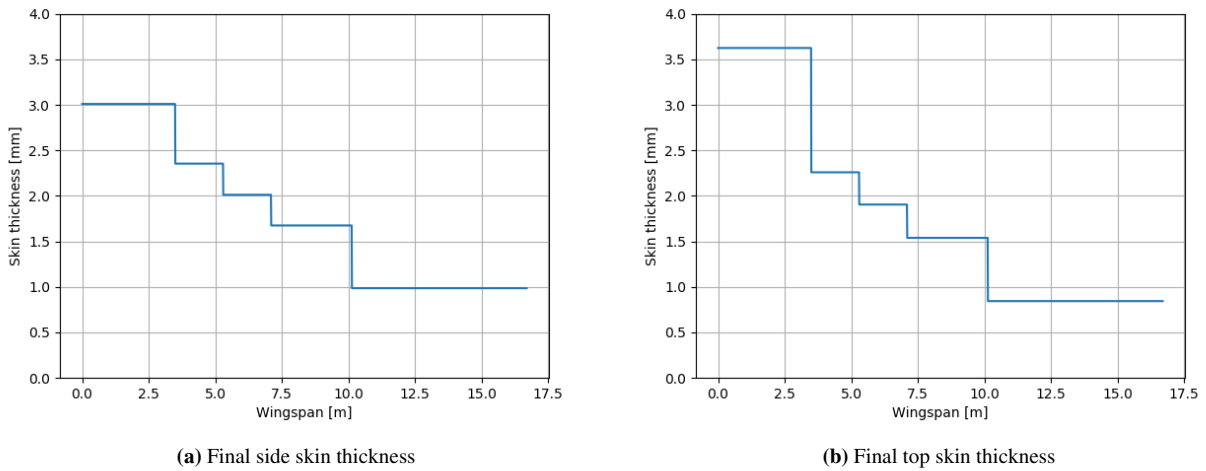


Figure 10.10: Wing box skin thicknesses

Next up is the stringer sizing and spacing. For this it is important to first know whether the area requirement needed for bending stiffness is met with the skin thickness. To check for this, the total material area of the top and bottom skin is compared with the minimal area needed on the top and bottom skin.

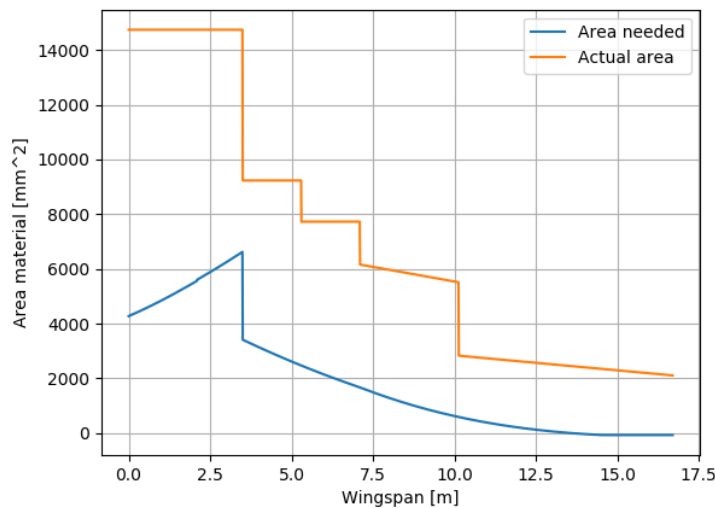


Figure 10.11: Material area need vs actual

Therefore it can be concluded that the stringers are not necessary for the bending stiffness. However, for the buckling of the skin stringers are still necessary. The minimum stringer pitch as shown in subsection 10.2.4 is used for this. However, there are also dimensional constraints, which means that not every pitch will fit. Therefore the higher estimate is taken, giving the following stringer numbers for each section.

Table 10.7: Minimum pitch stringers

Section	Stringer number
0 - 3.5 m	10
3.5 - 5.3 m	13
5.3 - 7.1 m	15
7.1 - 10.1 m	19
10.1 - 16.7 m	32

Using the ratios for the dimensions of the stringers found in subsection 10.2.4, the dimensions can be found in

Table 10.8:

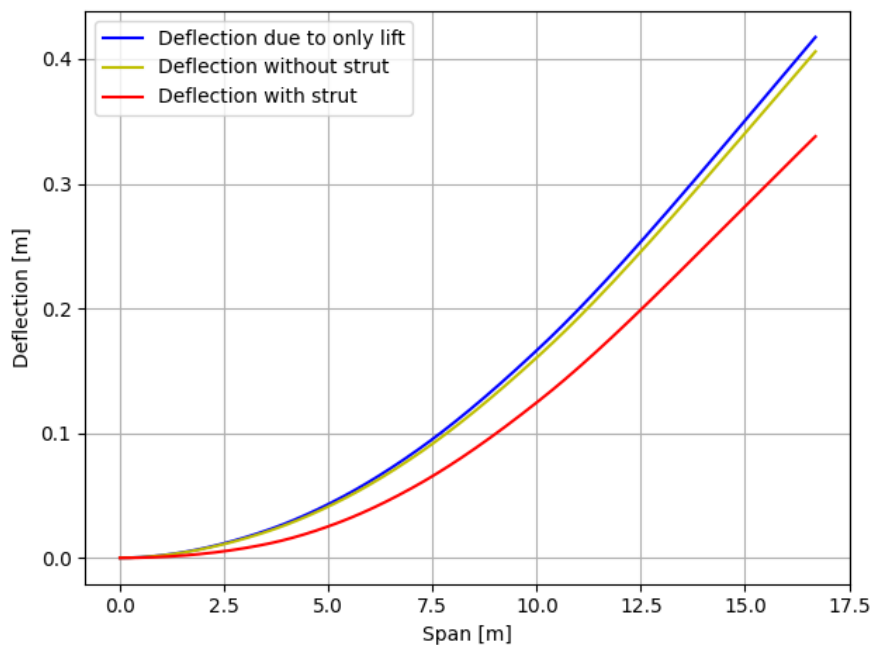
Table 10.8: Dimensions stringers per section of the wing box

Part	bottom and top flange t/b [mm]	middle flange t/b [mm]
0 - 3.5 m	3.55/22	1.7/33
3.5 - 5.3 m	3.50/13.7	1.7/20.6
5.3 - 7.1 m	2.77/10.9	1.36/16.3
7.1 - 10.1 m	2.03/7.94	0.99/11.9
10.1 - 16.7 m	0.93/3.63	0.45/5.44

When looking at these results for buckling, a couple of counterintuitive results stand out. The main one is the increase in the number of stringers when getting closer to the tip. The reason for this is the way the wing is designed. The wing is designed in such a way that the stresses are the same in each part of the wing. This means a decreasing skin thickness and therefore a decrease in flexural stability. This means more stringers are necessary to account for this. However, as the skin is thinner, so can the stringers. As a result, the cross-sectional area of stringers is smaller but there are more of them

Finally, when adding all the masses together, the minimal mass of the wing box is 1065 kg. This is quite low compared to the class II weight estimation. However, a number of reasons can be given for this. Firstly, the class II weight estimation is not made for a wing with struts. This massively reduces the weight of the wing. Secondly, the new materials reduce the weight a lot as well due to their high strength and low density. Lastly, the new materials are completely rivetless, which reduces the weight as well.

After iterating the masses and loads, a final Mass Moment of Inertia can be acquired, which can be solved and plotted using Equation 9.3. This yields a deflection of the wing, which can be seen in Figure 10.12. Finally, Figure 10.13 shows the final wing structure.

**Figure 10.12:** Deflection of the wing for different cases.

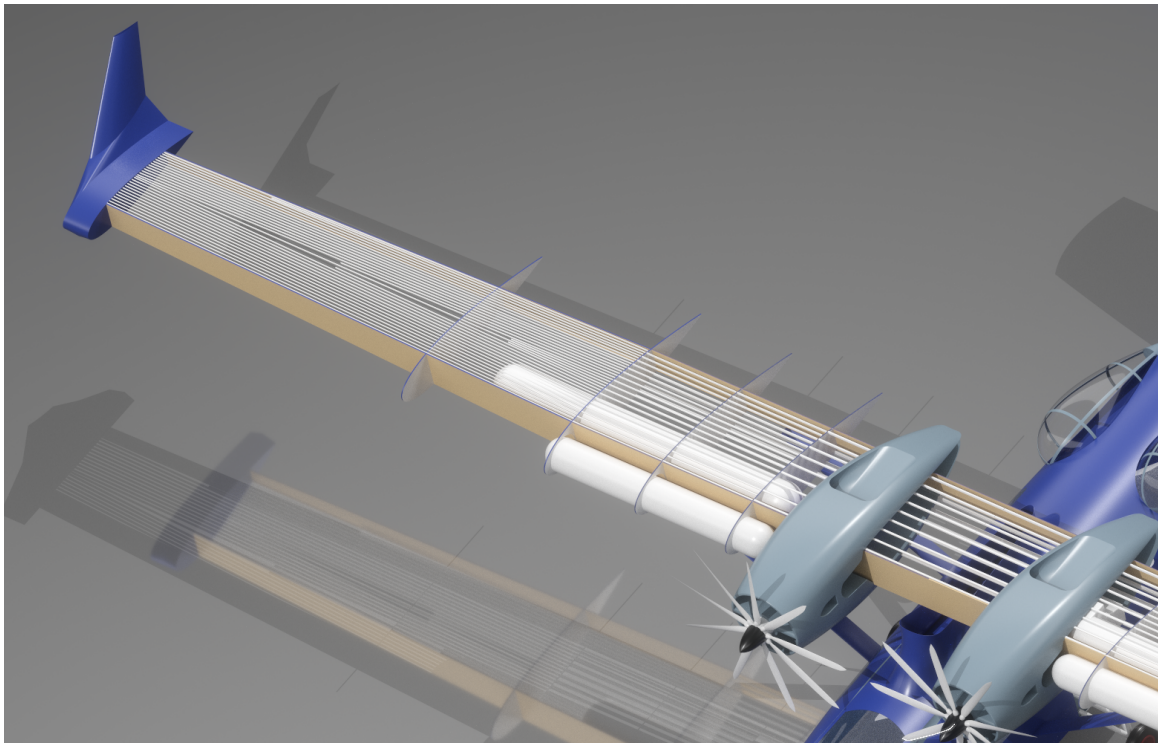


Figure 10.13: Final wingbox design

10.3. Fuselage structure

In this section, a preliminary fuselage structure is presented. The fuselage structure is solely designed for the aerodynamic loads as described in section 9.3. The design of the bottom half of the fuselage structure (the hull), which would normally also be designed for the water loads as described in section 9.4, has not reached a mature state yet. Due to limited time and resources, the design of the hull structure was excluded from the scope of this report. However, since hull structures are already present in existing aircraft, their design is not deemed critical for the feasibility of the aircraft.

10.3.1. Idealized structure

The structure of the fuselage will be considered as an idealised structure. The skin and stringers will be replaced by multiple booms which will be located at the skin of the fuselage. The booms will manage the normal and bending stress, and the skin will manage the shear stresses. The skin thickness contribution will be included in the booms such that the results are more accurate.

Multiple assumptions were made to simplify the analysis of the fuselage. The cross-section of the fuselage will be assumed to be a perfect circle. This will make the calculation for the moment of inertia less complex. Also I_{yz} will be 0 since there is at least 1 symmetry axis (2 symmetry axes are present) for the fuselage. This will further decrease calculations for the shear and bending stresses.

Also, no cutouts or discontinuities are considered for the structure of the fuselage. Frames will have to be locally applied to compensate for the loss of structural strength at the cut-out. The size of stringers and the skin will be increased to compensate partly for the cut-outs to ensure that the general strength of the fuselage suffices. Lastly, a linear taper will be applied to the radius for the nose and tail cone. This will be used to simplify the radius of the fuselage along the fuselage.

The idealized structure can be analysed in normal, shear and bending stresses. Normal stresses will only be caused by bending stresses since no axial forces are applied to the fuselage. The method and results of this will be shown in the following subsections.

10.3.2. Skin and stringer area sizing

The first step of the process is choosing the amount and position of the booms. These booms were placed such that the fuselage cross-section remained symmetric around two axes.

An initial total boom area (skin + stringers) could then be calculated by considering the normal stresses into booms. The boom areas were set to all be equal, as the loads experienced by the fuselage are fairly omnidirectional. Since the normal stresses should remain below the yield stress of the material, the area can be obtained with Equation 10.13.

$$B_i = \frac{M_x \cdot y_i \cdot \sum_{r=1}^n x_n^2 + M_y \cdot x_i \cdot \sum_{r=1}^n y_n^2}{\sum_{r=1}^n x_n^2 \cdot \sum_{r=1}^n y_n^2 \cdot \sigma_y} \quad (10.13)$$

With the amount of booms and their areas known, together with the locations of the booms, the shear flows between the booms can be calculated with Equation 10.14.

$$q_s = q_b + q_{s0} = -\frac{V_y I_{yy}}{I_{xx} I_{yy}} \left[\sum_{r=1}^n B_r y \right] - \frac{V_x I_{xx}}{I_{xx} I_{yy}} \left[\sum_{r=1}^n B_r x \right] + q_{s0} \quad (10.14)$$

When the shear flows between the booms are calculated, the skin thickness can be obtained by Equation 10.15, thus sizing it that the shear strength of the material is never exceeded. The magnitude of the shear flow differs around the cross-section of the fuselage. The skin thickness was chosen to be constant in the cross-section. Therefore, the maximum shear flow found in the fuselage cross-section will be used to size the thickness of the entire fuselage perimeter.

$$\tau = \frac{q}{t} \quad (10.15)$$

Using Equation 10.16, the contribution of the skin to the booms of the idealized structure can be calculated.

$$B_n = \frac{t_{skin} b}{6} \left(2 + \frac{\sigma_{n+1}}{\sigma_n} \right) + \frac{t_{skin} b}{6} \left(2 + \frac{\sigma_{n-1}}{\sigma_n} \right) \quad (10.16)$$

This contribution of the skin is then subtracted from the boom areas, such that the area of the stringers is left. The skin thickness and the stringer areas are used in the analysis of the crippling of the fuselage.

The crippling analysis of the fuselage has been performed similarly as in subsection 10.2.4, using Equation 10.11, 10.10 and 10.12. This crippling analysis yields the strength that the panels of the fuselage can resist. Since this strength is likely lower than what is applied, the boom areas have to be iterated upon. The skin buckling in shear has not been taken into account in the design, as the skin is allowed to elastically buckle in this mode. This is therefore not leading in the design.

In each iteration, the total boom area was slightly increased by a certain percentage. From this follows a new moment of inertia and thus new internal stresses. Moreover, the buckling strength will increase due to the boom area increase. If the buckling strength becomes larger than the stress, indicating the structure is sufficiently strong, the iteration loop is stopped. Otherwise, another iteration is started.

10.3.3. Dimension stringers

Now that the areas of the stringers are known, the dimensions can be calculated with Equation 10.17. These dimensions are calculated with a $\frac{\sigma_{cc}}{\sigma_y} = 1$ such that the stringers will fail due to buckling and yield strength at the same time. The design of the structure is optimal and the most performance is extracted from the material at this point.

$$\frac{\sigma_{cc}^{(i)}}{\sigma_y} = \alpha \left[\frac{C}{\sigma_y} \frac{\pi^2 E}{12(1-\nu^2)} \left(\frac{t}{b} \right)^2 \right]^{1-n} \quad (10.17)$$

10.3.4. Resulting fuselage structure

First, based on the interior design, the compartment walls were placed as in Figure 10.14. The rationale behind the placement can be found in chapter 5 about the interior design.

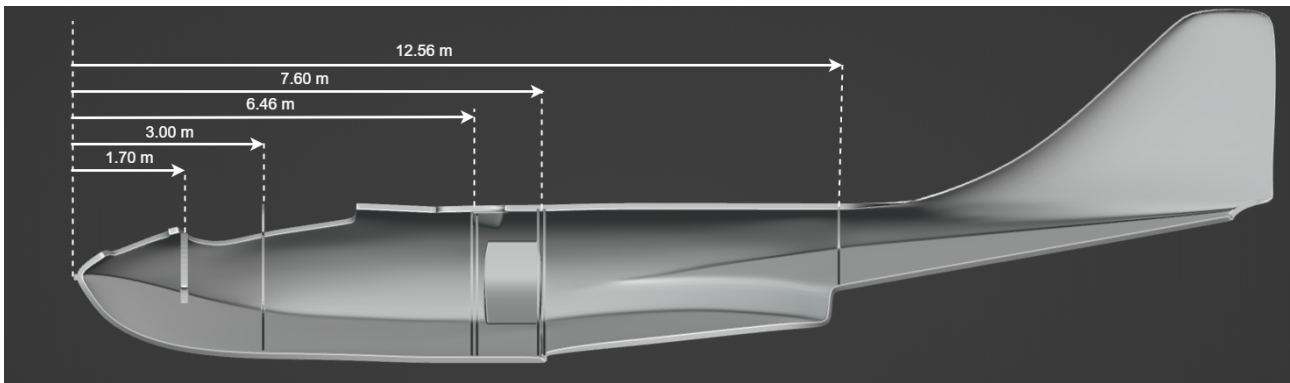
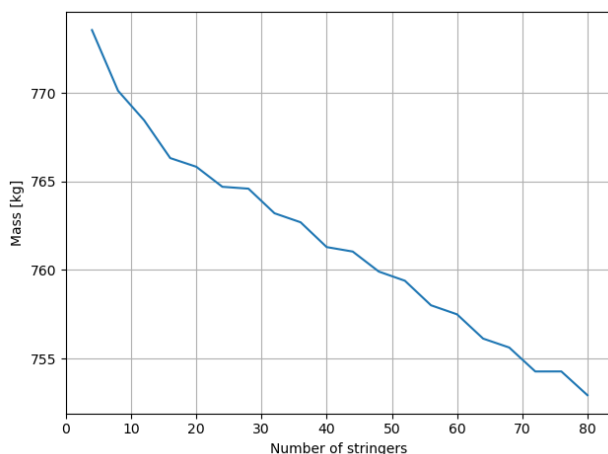


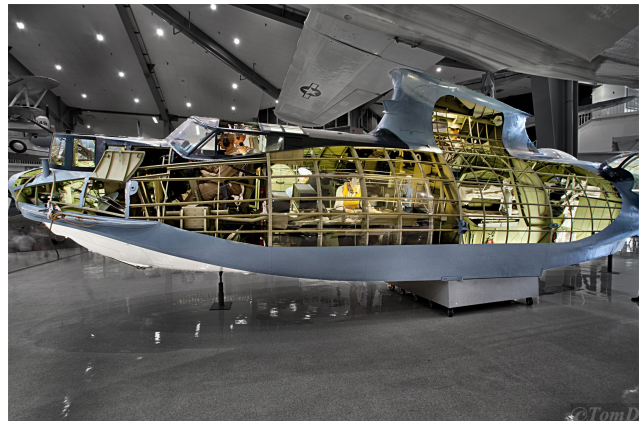
Figure 10.14: Position of the compartment walls of the fuselage

In order to choose how many stringers would be used on the fuselage, its effect on the mass was analysed. This can be seen in Figure 10.15a. As one can see, the mass of the fuselage decreases with an increasing number of stringers. Especially at a low number of stringers an increase in stringer number leads to a great amount of mass savings. However, what is not taken into account is the decrease in manufacturability with an increasing number of stringers. Therefore, it will not be beneficial to choose a very high number of stringers.

Analysing the original Catalina aircraft, see Figure 10.15b, yields a stringer count of approximately 7 stringers per quarter fuselage. To stay realistic, while still realizing extra weight savings, a configuration of 9 stringers per quarter fuselage was chosen. This totals 36 stringers divided over the whole fuselage cross-section.



(a) Effect of the number of stringers on the mass of the fuselage



(b) Cutaway of the original Catalina ⁸

Figure 10.15: Sensitivity and comparison for the amount of stringers

The skin thickness over the fuselage is depicted in Figure 10.16. It contains both the thickness required and the thickness chosen. The thickness required at points where there are no internal loads is zero and is therefore not plotted. Furthermore, the thicknesses are rounded-up to a precision of 0.5 mm, to ease in manufacturing.

The skin thicknesses were then chosen as follows. The thickness was set to remain constant in certain sections of the fuselage. First, the maximum required thickness in the middle section (1.70 m til 12.56 m) is calculated. This thickness is chosen to be used in the whole middle section. Similarly, the maximum required thickness in the rest of the aircraft was calculated, which was used for both the nose and tail of the aircraft. Using this method, one can still come to a design at places where no loads are found due to the simplifications, while remaining realistic and manufacturable.

⁸<https://www.flickr.com/photos/tomd77/7668673506> (accessed on 19/06/2023)

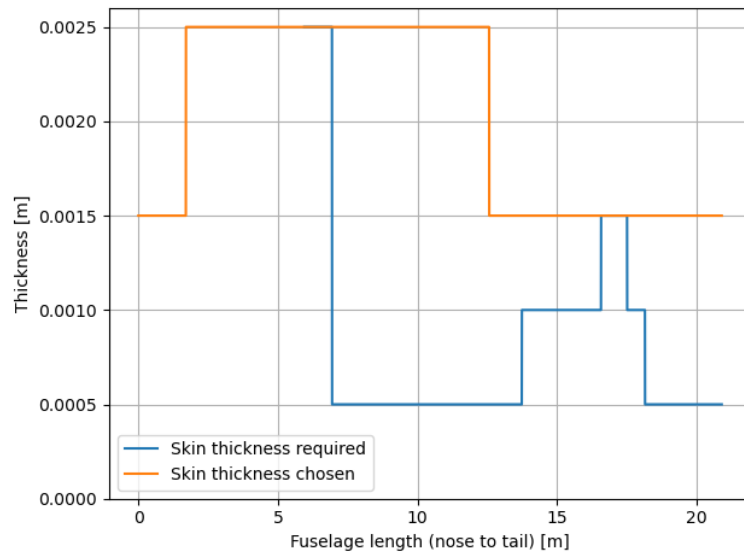
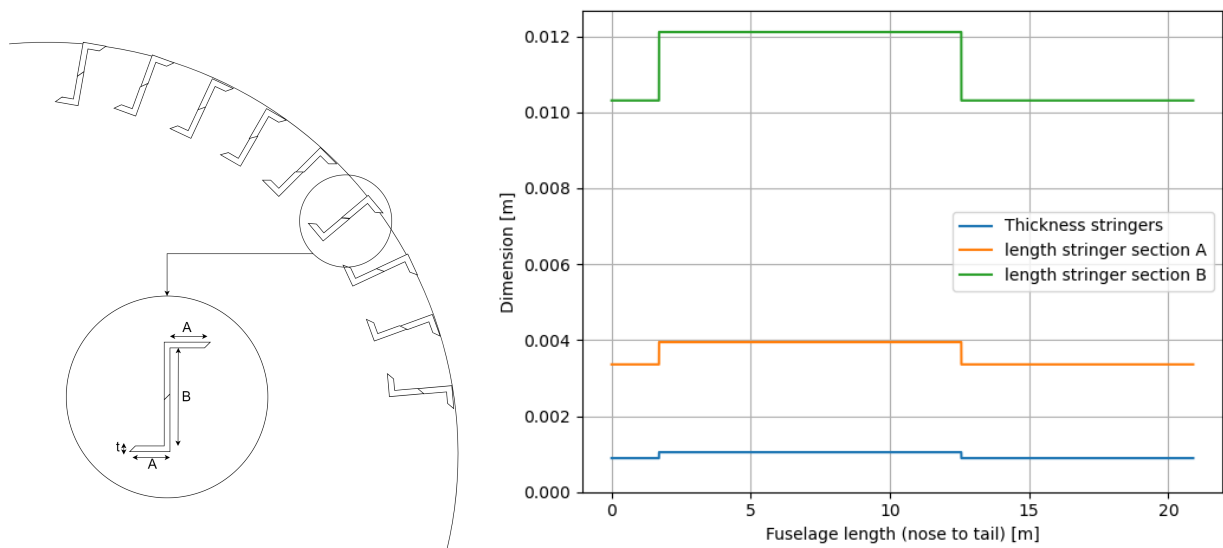


Figure 10.16: Skin thickness of the fuselage

A simple sketch of a fuselage cross-section can be seen in Figure 10.17a. As can be seen, the stringers of the fuselage have a z-shape. This has been chosen for similar reasons as for the wing box, namely easy manufacturing, attaching and inspection of the stringers. This figure also shows the definition of the stringer dimensions. The dimensions required for the stringers throughout the fuselage can also be found in Figure 10.17b. The same constraints as those for the skin thickness have been applied, where there is a middle section with constant stringer dimensions and a front and rear section with a constant length.



(a) Quarter of the simplified fuselage (not to scale)

(b) Stringer dimensions needed at different places over the fuselage

Figure 10.17: Stringer sketch and dimensions

Concluding, the fuselage, made out of thermoplastic composite, will consist of 36 stringers equally divided over the fuselage cross-section. At the nose and tail, the skin of the fuselage will be 1.5 mm thick. The stringers attached here will have a thickness of 0.9 mm. Section A of the stringer will have a length of 3.4 mm, whereas section B will have a length of 10.3 mm.

In the middle section, the skin will have a thickness of 2.5 mm and the stringers a thickness of 1.1 mm. Section A and B of the stringers measure 4 mm and 12.1 mm respectively.

Although it is realised that these values show a significant decrease in the size of the stringers compared to the

original, one has to recognise that the thermoplastic composite material used is notably stronger than the aluminium used on the original. Furthermore, the aircraft has seen a great overall weight reduction. This reduced loads on the fuselage, leading to a less stringent design.

The frames of the fuselage (similar to the compartment walls, but just the perimeter) have not been quantitatively designed. Based on the original Catalina, together with a qualitative analysis, an average of four frames per compartment was considered for the mass calculation.

The total mass of the fuselage structure was computed to be 763 kg with the presented configuration. This is however with a relatively high uncertainty as the hull structure is not included. Taking into account a contingency of 20% for this leads to 916 kg. The exact mass figure for this should be evaluated in a more detailed design phase.

10.4. Verification & Validation

The designing of the structures has mostly been performed in Python. In order to confirm that no calculation mistakes were made the Python tool was verified. Furthermore, to ensure that the results are realistic, the computations are validated.

The code was continuously verified while it was being written. This was done by so-called unit testing, where sections of the code are isolated and ran with example inputs. First, these inputs were chosen realistically, such that could be checked whether the result was also realistic. Following this, inputs became unrealistic. These inputs were chosen such that the limits of the program could be tested. In limit-cases, certain outputs of the program are expected, which can easily be checked for correctness. For example, letting the internal forces go towards zero should also yield a structure size and mass that goes towards zero. Similarly, changing the material properties to a very stiff material should yield negligible deformations of the structure. If the code passed all unit tests it was integrated with the rest of the code.

Next to unit testing, results were often plotted. These plots do not only demonstrate that the results are realistic, and show the data visually, but they can also show outliers or discontinuities that might not be expected. This was especially useful for the deflection verification. The deflection of the wing box is always expected to be continuous, however, this was not the case at first instance. It was therefore evident that a mistake had to be fixed in the code.

The validity of the calculations was ensured in multiple ways. First of all, all the formulas that were used were from well-established sources. These formulas are therefore well-tested, guaranteeing realistic results. Alongside this, critical calculations were performed by two methods if available. Agreement between the results of these two methods confirms the correctness. Finally, results were compared to the original Catalina. The original Catalina is a flight-proven aircraft, and is a great baseline to compare against.

11

Stability & Control

An important consideration in the modification of the design of the original Catalina is the control and stability of the aircraft. Indeed with a drastically different propulsion system, the integration of modern materials, and a luxuriously tailored internal layout, the stability characteristics are bound to vary from their antecedent values. To that end, an analysis of these behaviours is to be carried out, and changes to the aircraft design are to be made in order to ensure its stability. Particularly, the empennage sizing will be affected and is to be sized in order to maintain as minimal modifications as possible to the aircraft design and resulting aesthetics. Naturally, the design of the entire aircraft will affect this as well, and those considerations are to be taken into account as well.

In commencing this analysis, an initial decision was made on the empennage configuration, resulting in the selection of a crucifix design. This was done to prevent deep stall as well as the horizontal tail getting caught by the water during nautical operations.

11.1. Loading Diagram

To examine the stability of the design, a complete investigation of the weight and the center of gravity (c.g.) of each different aircraft component is to be carried out. In particular, the masses of these components were obtained resulting from the class II weight estimation, such that only their c.g.'s remain to be estimated. Making use of the internal layout from chapter 5 as detailed from the investigations into user experience, passenger seating positions were identified, as well as the locations of any additional furnishings or cargo holds.

With these parameters identified, an estimation into the c.g. range of the design was made. Considering the intended touristic use of the aircraft, free movement of the passengers along the aircraft was considered, arriving at a worst-case c.g. range. Particularly, the most forward c.g. was estimated to be attained upon the concentration of passengers in the most forward cabin, with four passengers standing in the aisle in addition to filling all six seats, as well as filling the front observation deck and all seats in the center cabin. For the most aft c.g. the most aft cabin was filled, with three persons seated on each bench as well as three persons standing in the aisle, four persons filling the center cabin seats in addition to one in the aisle, and one on the lavatory. In this way, extreme loading cases were considered, although in practice these may not be attained. This therefore also introduced some safety margins. In these estimations, one cabin steward was also considered, while the pilots were considered to remain stationary in their seats. Then, estimating 77 kg per passenger and 120 kg of cargo, a loading diagram was obtained as depicted in Figure 11.1. Some uncertainty was present in the estimation of the c.g. at OEW, the lower and upper bounds of which are represented in the diagram by dotted blue lines.

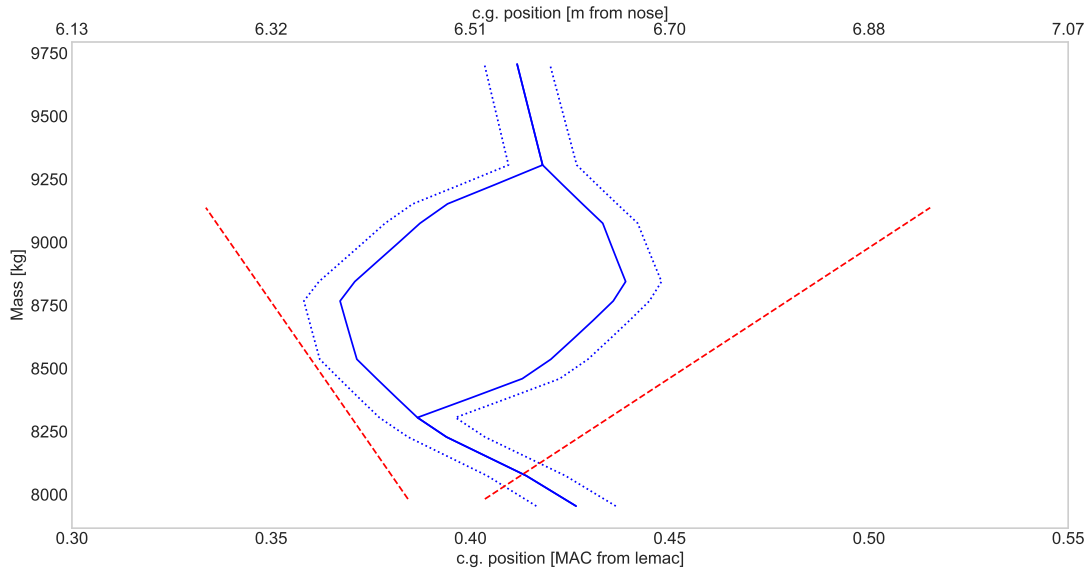


Figure 11.1: Loading diagram for the Caty. Red dotted lines represent the most forward and aft c.g. positions

As is quickly seen, the c.g. range is centered quite aft on the wing, with the worst case even reaching 52% of MAC. With this far aft position, the neutral point is quickly approached, and stability can rapidly be identified as the limiting factor in the design, with controllability not posing as much of an issue.

11.2. Scissor Plot

The scissor plot as can be seen in Figure 11.2 combines the requirements for aircraft stability and controllability. The stability curve (green) plots the required tail size for a certain c.g. position. The tail size as a function of c.g. to ensure stability can be found in Equation 11.2 with $C_{L\alpha_h}$ being the lift slope of the tail and $C_{L\alpha_{A-h}}$ the lift slope of the aircraft without the tail [20]. Furthermore, l_h denotes the distance between the respective aerodynamic centres of the wing and the horizontal tail, and $\frac{V_h}{V}$ is the ratio of respective airspeed incident on the horizontal and the wing, obtained from Roskam's *Airplane Design Part VI* [21].

$$\frac{S_h}{S} = \frac{\bar{x}_{cg} - \bar{x}_{ac}}{\frac{C_{L\alpha_h}}{C_{L\alpha_{A-h}}} \left(1 - \frac{d\varepsilon}{d\alpha}\right) \frac{l_h}{\bar{c}} \left(\frac{V_h}{V}\right)^2} \quad (11.1)$$

The controllability curve (red) plots the tail size as a function of the c.g. to ensure controllability. Its equation can be found in Equation 11.2, where $C_{L_{A-h}}$ and C_{L_h} denote the contributions to the lift coefficient at take off angle of attack due to the tail-less aircraft and the horizontal tail, respectively.

$$\frac{S_h}{S} = \frac{\bar{x}_{cg} + \frac{C_{mac}}{C_{L_{A-h}}} - \bar{x}_{ac}}{\frac{C_{L_h}}{C_{L_{A-h}}} \frac{l_h}{\bar{c}} \left(\frac{V_h}{V}\right)^2} \quad (11.2)$$

To be aerodynamically stable, the aircraft must be to the left of the stability curve and to the right of the controllability curve for all c.g.s that may occur in flight. To account for various deviations, a safety factor is included for the stability curve. Because the c.g. range already accounts for exceptional cases as described in section 11.1, a relatively low safety margin of 1.5 % MAC was chosen. The y-axis of the scissor plot represents the tail surface area as a function of the main wing surface area. The larger the tail is, the larger the c.g. range can be for the aircraft to be both stable and controllable. The initial scissor plot is shown in Figure 11.2.

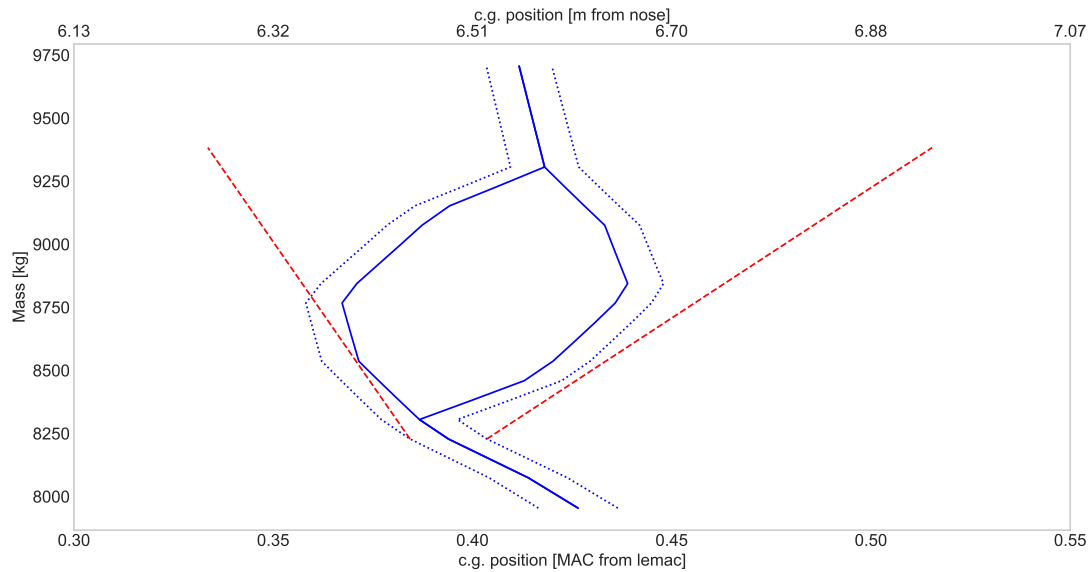


Figure 11.2: Scissor plot for the Caty. Blue dots represent the extreme cg range at cruise conditions

In generating this, all design results as explained in previous chapters are integrated, with the c.g.'s and masses of all subsystems obtained from their design and sizing. Then, assuming the same general dimensions of the original PBY-5A, in terms of wing position and any other design adjustments to the airfoil and wing planform, the plot is obtained. Two things can be observed: the aircraft is very far from being uncontrollable, and it just achieves stability across the entire c.g. range for a horizontal tail surface of 19% of the wing surface area. The main reason for this critical stability performance is the removal of the old heavy engines hanging in front of the wing in the original aircraft which is exacerbated by the added weight of luxury furnishings across the cabins. With this achieved stability, no major design changes are required to be made to the position of the wing, and for design simplicity and in order to preserve aesthetics, it is hence decided to maintain the original wing position. The main longitudinal stability design parameter is then the horizontal tail surface area, the value of which amounted to 15% of the wing area, as obtained from the United States Navy maintenance handbook of the PBY-5A original Catalina [22]. Furthermore, a detailed design of the control surfaces of the wing and horizontal and vertical tails is then carried out. In these analyses, use is frequently made of numerous stability and control derivatives, which have all been estimated following the methods detailed in *Airplane Design Part VI* by Dr. Jan Roskam, and all have been presented in Table 11.1 [21].

11.3. Wing Stability and Aileron Design

As was seen in section 11.2, the centre of gravity of the design is quite aft on the wing, but not to such an extent that modifications to the wing position are warranted. Nevertheless, some design is required such that sufficient stability and control are maintained. Particularly, the incidence angle of the wing i_w is determined, and the ailerons are sized in order to accommodate sufficient roll control.

Indeed, with only some limited amount of space in the wing to incorporate ailerons, due to the presence of the rear spar, the main design parameter to vary for this sizing was the span of the aileron. Taking a similar aileron span as the original Catalina, from existing measurements and technical drawings, the ailerons were determined to span from the wingtip to a point 60% along the half wingspan, or 6.7 m from the wingtip, with a maximum deflection taken at 20° [22]. Using this size, an estimate for the roll-moment-due-to-aileron derivative $C_{l_{\delta a}}$ is obtained following the methods detailed in Chapter 10 of Dr. Jan Roskam's *Airplane Design Part VI* [21]. Using this derivative and at the maximum deflection, a roll rate of $49.5^\circ/s^2$ is achieved. While this is large, the value can be explained by the substantial wingspan, which contributes to the large rolling moment provided. With a requirement on roll rate of accelerating to 60° in 7 seconds as specified from CS 23.157, resulting in a roll acceleration of $4.90^\circ/s^2$, this performance is comfortably achieved [3]. Indeed, this corresponds to rolling

from a 30° bank angle to a 30° bank angle in the opposite direction in 2.2 s.

Finally, the wing incidence angle can be found such that the angle of attack of the fuselage with respect to airspeed is zero during cruise conditions. This has been decided in order to facilitate passenger comfort during cruise, by maintaining a level cabin floor. To that end, the required angle of attack to reach cruise lift coefficient $C_{L_{cruise}}$ can be calculated, and set as the wing incidence angle. Resulting from this method, a value of $i_w = 5.7^\circ$ was found.

11.4. Horizontal Tail Dimensions

As detailed in section 11.2, the minimum horizontal tail surface area for stability and control of the aircraft is 19% of the main wing surface area. With this requirement, the horizontal tail dimensions can be determined. In order to preserve the aesthetic characteristics of the original Catalina, the same taper and aspect ratio were utilised, such that in effect the planform proportions are scaled up or down with surface area. For a horizontal tail surface of 19% of the wing area, this results in a span of 9.70 m and a mean chord of 2.43 m. However, this does not constitute the only parameter in sizing the horizontal tail. Indeed, apart from providing stability, it should be large enough so as to be able to fit the required elevator size based on pitch angular acceleration requirements, and it should be mounted at an angle of incidence such that elevator deflection at cruise is zero.

Firstly, a certain pitch angular acceleration can be designed for. In particular, general aviation aircraft achieve take-off pitch angular accelerations between $8^\circ/s^2$ and $10^\circ/s^2$ at 80% of the take-off velocity [23]. Taking an average required roll angular acceleration of $9^\circ/s^2$, the subsequent elevator deflection can be found depending on the fraction of elevator chord to horizontal tail MAC. Using a value of 0.5 for this ratio, equal to the original Catalina, and letting the elevator span along the entire horizontal tail, an estimate for the pitching-moment-due-to-elevator derivative $C_{m_{\delta_e}}$ is obtained following Chapter 10 of *Airplane Design Part VI* by Dr. Jan Roskam [21]. With this value, considering maximum take-off mass, a required elevator deflection of 9.3° up is obtained. This is well within acceptable deflection ranges such that flow separation is not encountered, of which the onset is considered to be around 20° to 25° [23].

In addition, the horizontal tail should be mounted at an angle of incidence with respect to the longitudinal body axis such that the elevator deflection for trim during cruise conditions is zero. To aid with this, a trim curve is constructed, depicting the required elevator deflection for a given aircraft angle of attack such that a net moment coefficient of zero is attained. For a cruise angle of attack of 0° , the moment coefficient at cruise conditions can be calculated from Equation 11.3. With a given wing angle of incidence i_w , the angle of incidence i_h can then be varied such that C_m at cruise is zero.

$$C_m = C_{m_{ac}} + (C_{m_\alpha})_w (\alpha + i_w) + (C_{m_\alpha})_h \left(\alpha + i_h - \frac{d\varepsilon}{d\alpha} \alpha \right) \quad (11.3)$$

Subsequently, taking a range of angle of attacks from -15° to 15° , the elevator effectiveness $C_{m_{\delta_e}}$ can be used to generate the trim elevator deflection for each angle of attack, as shown in Figure 11.3. In plotting this curve, the minimum and maximum c.g.'s for cruise as detailed in section 11.1 are averaged, with this average being used to find a horizontal tail incidence angle. As can be seen, with the given incidence of $i_h = 0.75^\circ$, the required elevator deflection for trim in cruise conditions is zero.

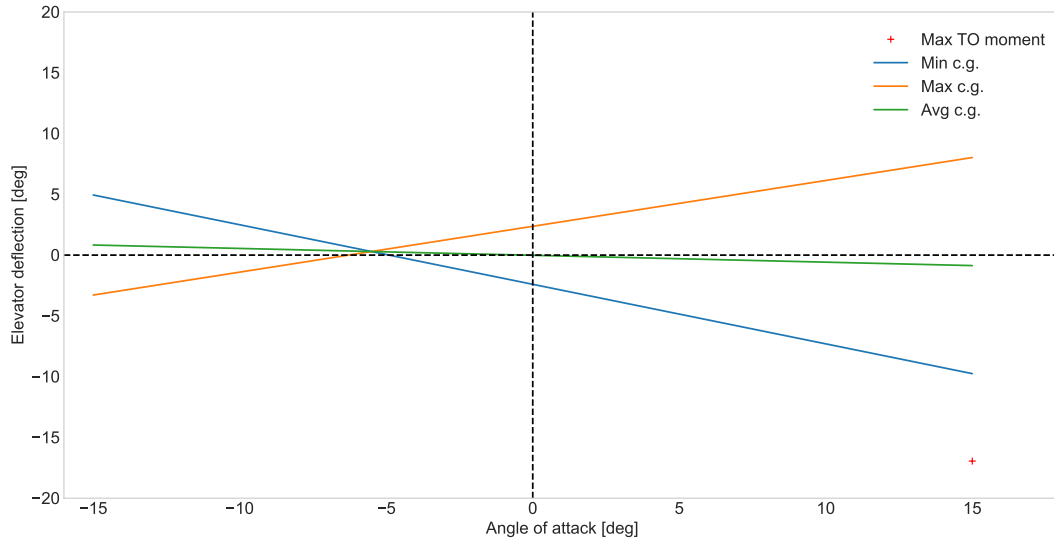


Figure 11.3: Trim Curve

11.5. Vertical Tail Dimensions

Until now this chapter was only concerned with longitudinal stability and control and the design of the horizontal tail. The vertical tail has to be designed on its own for lateral stability and control. For this, two situations were considered: passive stability of the aircraft and rudder deflection for 1 inoperative engine. For both methods, the steps 11.8 – 11.16 from *Airplane Design Part II* by Dr. Jan Roskam were followed exactly [24]. These steps are summarized below.

For the aircraft to be inherently stable, according to Roskam, $C_{n\beta} \geq 0.001 \frac{1}{\text{deg}}$. Since the fuselage has a destabilizing effect on $C_{n\beta}$, whereas the tail is intended to have a stabilizing effect, the requirement on the target $C_{n\beta}$ gives a minimum value for the tail height. Furthermore, the tail is to provide enough control to counter the yaw moment experienced by the aircraft in the event of failure of one of the engines. The critical condition in this situation is at V1 (no-return speed). This is the lowest dynamic pressure the aircraft can experience while operating at maximum power. The required rudder deflection for this condition is shown in Equation 11.4, where T_{T0} is the thrust at take-off, y_{engine} is the distance from the engine to the fuselage. The created moment is multiplied by 1.1 to account for the additional drag from the inoperative engine. This deflection shall not exceed 20° .

$$\delta_{r,\text{inop}} = \frac{T_{TO} \cdot y_{\text{engine}} \cdot 1.1}{\bar{q} S b C_{n\delta_r}} \tag{11.4}$$

With a rudder spanning along the entire vertical tail, taking up 50% of its chord, a minimum rudder effectiveness of $C_{n\delta_r} = -0.02$ is obtained for cruise conditions at most aft centre of gravity. This in turn results in $C_{n\beta} = 0.0005/^\circ$ and a $\delta_{r,\text{inop}} = 14.8^\circ$, both parameters comfortably satisfying static stability requirements.

Since for low aspect ratios, the lift coefficient is roughly proportional to the aspect ratio, the tail chord and the rest of the vertical tail planform has little effect on the aerodynamics and is sized for aesthetic, structural and weight considerations.

Finally, the horizontal and vertical tail are depicted in Figure 11.4.



Figure 11.4: Empennage design of the Caty

11.6. Dynamic Stability

All the stability analyzed to this point is static stability, which describes the initial response of the aircraft to return towards its neutral position. Achieving static stability is necessary, but not sufficient for a well-handling aircraft. Dynamic stability investigates the long-term behaviour of the response of an aircraft to certain inputs instead of just focusing on the instantaneous response.

In order to commence the analysis into dynamic stability, first an estimate of the mass moments of inertia (MMOI) of the design is necessary. At this stage of the design, these are obtained through a Class I investigation as detailed in Chapter 3 of Dr. Jan Roskam's *Airplane Design Part V* [6]. In particular, the MMOI around the x-axis, I_{xx} , around the y-axis, I_{yy} , and around the z-axis, I_{zz} are estimated, with I_{xy} , I_{xz} , and I_{yz} assumed zero at this stage of the design. Assuming non-dimensional radii of gyration based on data from Dr. Roskam of $\bar{R}_x = 0.258$, $\bar{R}_y = 0.341$, and $\bar{R}_z = 0.399$, the MMOI can be estimated as detailed in Equation 11.5 with b and L representing the wingspan and aircraft length respectively [6].

$$I_{xx} = b^2 \frac{\bar{R}_x^2}{4} \frac{W}{g} \quad I_{yy} = L^2 \frac{\bar{R}_y^2}{4} \frac{W}{g} \quad I_{zz} = \left(\frac{b+L}{2} \right)^2 \frac{\bar{R}_z^2}{4} \frac{W}{g} \quad (11.5)$$

With this obtained, estimates of various stability and control derivatives can be made, after which the dynamic equations of motions can be solved. To investigate the dynamic stability properly, the equations of motion (EOM) of the aircraft are needed. The EOM can be decoupled into two so-called symmetric and asymmetric EOM, describing motion in longitudinal and lateral directions respectively, since both are generally independent of each other. When linearized, the non-dimensional EOM can be written as presented in Equation 11.7 and Equation 11.6. Solving these EOM can be done for different flight conditions, in order to analyse the behaviour of the aircraft during different parts of the mission, some of which are more critical than others. In particular, two flight conditions are investigated: behaviour during cruise, and during take-off and landing conditions. For cruise conditions, further separate considerations are made, analyzing the situations with maximum aft and maximum forward c.g. respectively, thus resulting in three separate conditions.

$$\begin{bmatrix} C_{X_u} - 2\mu_c D_c & C_{X_\alpha} & C_{Z_0} & C_{X_q} \\ C_{Z_u} & C_{Z_\alpha} + (C_{Z_{\dot{\alpha}}} - 2\mu_c) D_c & -C_{X_0} & C_{Z_q} + 2\mu_c \\ 0 & 0 & -D_c & 1 \\ C_{m_u} & C_{m_\alpha} + C_{m_\alpha} D_c & 0 & C_{m_q} - 2\mu_c K_{yy}^2 D_c \end{bmatrix} \begin{bmatrix} \frac{u}{V} \\ \alpha \\ \theta \\ \frac{q\bar{c}}{V} \end{bmatrix} = \begin{bmatrix} -C_{X_\delta} \\ -C_{Z_\delta} \\ 0 \\ -C_{m_\delta} \end{bmatrix} \delta_e \quad (11.6)$$

$$\begin{bmatrix} C_{Y_\beta} + (C_{Y_{\dot{\beta}}} - 2\mu_b) D_b & C_L & C_{Y_p} & C_{Y_r} - 4\mu_b \\ 0 & -\frac{1}{2} D_b & 1 & 0 \\ C_{l_\beta} & 0 & C_{l_p} - 4\mu_b K_{xx}^2 D_b & C_{l_r} + 4\mu_b K_{xz} D_b \\ C_{n_\beta} + C_{n_\beta} D_b & 0 & C_{n_p} + 4\mu_b K_{xz} D_b & C_{n_r} - 4\mu_b K_{zz}^2 D_b \end{bmatrix} \begin{bmatrix} \beta \\ \phi \\ \frac{pb}{2V} \\ \frac{rb}{2V} \end{bmatrix} = \begin{bmatrix} -C_{Y_{\delta_a}} \\ 0 \\ -C_{l_{\delta_a}} \\ -C_{n_{\delta_a}} \end{bmatrix} \delta_a + \begin{bmatrix} -C_{Y_{\delta_r}} \\ 0 \\ -C_{l_{\delta_r}} \\ -C_{n_{\delta_r}} \end{bmatrix} \delta_r \quad (11.7)$$

The symbols used in these matrices, aside from the non-dimensional stability derivatives, are:

1. The non-dimensional masses $\mu_c = \frac{m}{\rho S \bar{c}}$ and $\mu_b = \frac{m}{\rho S b}$

2. The non-dimensional principal moments of inertia $K_{xx/zz}^2 = \frac{I_{xx/zz}}{mb^2}$ and $K_{yy}^2 = \frac{I_{yy}}{m\bar{c}^2}$
3. The non-dimensional moment of inertia K_{xz} which is assumed 0 at this stage of design
4. The non-dimensional differential operators $D_c = \frac{\bar{c}}{V} \frac{\partial}{\partial x}$ and $D_b = \frac{b}{V} \frac{\partial}{\partial x}$ are differential operators included to make the notation of the state-space system more compact.
5. The non-dimensional states of the system, in particular the angles of attack and sideslip, α and β respectively, pitch angle θ , bank angle ϕ , absolute deviation u from airspeed V , and angular rates of roll, pitch, and yaw p , q , and r
6. The control inputs from the aileron, elevator, and rudder δ_a , δ_e , and δ_r respectively

Furthermore, non-dimensional stability and control derivatives are prominently used across the EOM. The values of all these derivatives were obtained according to the methodology laid out in Chapter 10 of Jan Roskam's *Airplane Design Part VI* [21]. Note that some of the stability derivatives, like $C_{n\beta}$ or $C_{m\alpha}$ were discussed earlier in the chapter. The values of these derivatives change depending on the c.g. position and the flight conditions, and are presented in Table 11.1.

Table 11.1: Stability derivatives

(a) Cruise, most forward c.g.				(b) Cruise, most aft c.g.				(c) Take-off and Landing			
		$C_{Y\beta}$	-0.14			$C_{Y\beta}$	-0.14			$C_{Y\beta}$	-0.14
$C_{Z\alpha}$	-6.26	$C_{Y\beta}$	0.02	$C_{Z\alpha}$	-6.26	$C_{Y\beta}$	0.02	$C_{Z\alpha}$	-6.03	$C_{Y\beta}$	0.02
$C_{Z\dot{\alpha}}$	3.59	C_{Yp}	-0.00	$C_{Z\dot{\alpha}}$	3.40	C_{Yp}	-0.00	$C_{Z\dot{\alpha}}$	2.78	C_{Yp}	0.02
C_{Zq}	4.93	C_{Yr}	0.09	C_{Zq}	2.67	C_{Yr}	0.09	C_{Zq}	3.96	C_{Yr}	0.09
C_{Zu}	0.98	$C_{l\beta}$	-0.02	C_{Zu}	0.98	$C_{l\beta}$	-0.02	C_{Zu}	2.74	$C_{l\beta}$	-0.06
$C_{X\alpha}$	-1.01	C_{lp}	-0.44	$C_{X\alpha}$	-1.01	C_{lp}	-0.44	$C_{X\alpha}$	-3.04	C_{lp}	-0.46
C_{Xq}	0.00	C_{lr}	0.12	C_{Xq}	0.00	C_{lr}	0.12	C_{Xq}	0.00	C_{lr}	0.35
C_{Xu}	-0.00	$C_{n\beta}$	0.03	C_{Xu}	-0.00	$C_{n\beta}$	0.03	C_{Xu}	0.54	$C_{n\beta}$	0.03
$C_{m\alpha}$	-1.34	$C_{n\beta}$	0.02	$C_{m\alpha}$	-0.19	$C_{n\beta}$	0.02	$C_{m\alpha}$	-0.78	$C_{n\beta}$	0.02
$C_{m\dot{\alpha}}$	-12.35	C_{np}	-0.06	$C_{m\dot{\alpha}}$	-11.07	C_{np}	-0.06	$C_{m\dot{\alpha}}$	-9.47	C_{np}	-0.17
C_{mq}	-32.05	C_{nr}	-0.03	C_{mq}	-28.67	C_{nr}	-0.03	C_{mq}	-24.65	C_{nr}	-0.03
C_{mu}	0.00	$C_{Y\delta_r}$	0.08	C_{mu}	0.00	$C_{Y\delta_r}$	0.08	C_{mu}	0.00	$C_{Y\delta_r}$	0.08
C_{Z_0}	0.48	$C_{l\delta_r}$	0.01	C_{Z_0}	0.48	$C_{l\delta_r}$	0.01	C_{Z_0}	1.36	$C_{l\delta_r}$	0.00
Z_{X_0}	-0.04	$C_{n\delta_r}$	-0.03	Z_{X_0}	-0.04	$C_{n\delta_r}$	-0.02	Z_{X_0}	-0.37	$C_{n\delta_r}$	-0.03
$C_{m\delta_e}$	-1.28	$C_{Y\delta_a}$	0.00	$C_{m\delta_e}$	-1.21	$C_{Y\delta_a}$	0.00	$C_{m\delta_e}$	-0.99	$C_{Y\delta_a}$	0.00
$C_{L\delta_e}$	0.37	$C_{l\delta_a}$	0.27	$C_{L\delta_e}$	0.37	$C_{l\delta_a}$	0.27	$C_{L\delta_e}$	0.29	$C_{l\delta_a}$	0.27
		$C_{n\delta_a}$	-0.01			$C_{n\delta_a}$	-0.01			$C_{n\delta_a}$	-0.04

In particular, the two conditions at cruise consider the aircraft flying at a cruise speed of 110 kts and a cruise altitude of 7000 ft, in ISA conditions, with the only difference between the two being their respective c.g. positions. As part of the definition of cruise conditions, a cruise angle of attack of 0° is considered, as discussed in section 11.3. By contrast, the third flight condition examines flight at stall speed and sea level conditions, at an angle of attack of 11.0° . In this situation, due to this large AoA, the horizontal tail is assumed to fall outside of the slipstream of the propellers, the so-called propwash, the effect of which is an increased stabilizer effect inside the slipstream due to an accelerated airflow. These conditions are considered to represent take-off and landing situations.

For each of these flight conditions, solving the equations of motion produce solutions corresponding to five different characteristic modes of motion, the so-called eigenmotions. Particularly, two symmetric solutions are obtained, the short period and phugoid motions, in addition to the asymmetric Dutch roll, spiral, and aperiodic roll motions. Of these modes, the short period, phugoid, and Dutch roll are periodic modes, therefore given by complex eigenvalues, while the spiral and aperiodic roll are not oscillatory in nature. In line with this, the period and damping are presented in Table 11.2 for oscillatory modes, along with the time to half amplitude for the aperiodic solutions.

With these characteristics known, dynamic stability can be investigated. Making use of CS 23.181, the short period is required to "be heavily damped", the Dutch roll "must be damped to 1/10 amplitude in 7 cycles", and

Table 11.2: Dynamic stability

(a) Cruise, most forward c.g.				(b) Cruise, most aft c.g.			
Mode	λ	Period	Damping	Mode	λ	Period	Damping
Short period	$-0.711 \pm -0.568i$	0.7 s	0.782	Short period	$-0.635 \pm -0.523i$	0.8 s	0.772
Phugoid	$-0.001 \pm -0.008i$	55.5 s	0.194	Phugoid	$-0.002 \pm -0.003i$	146.7 s	0.537
Dutch Roll	$-0.081 \pm 0.498i$	7.5 s	0.160	Dutch Roll	$-0.073 \pm 0.475i$	7.8 s	0.153
Mode	λ	$T_{1/2}$		Mode	λ	$T_{1/2}$	
Spiral	0.021	-19.4 s		Spiral	0.021	-19.4 s	
Aperiodic Roll	-2.827	0.1 s		Aperiodic Roll	-2.827	0.1 s	

(c) Take-off and Landing			
Mode	λ	Period	Damping
Short period	$-0.692 \pm -0.540i$	1.5 s	0.789
Phugoid	$-0.009 \pm -0.020i$	39.4 s	0.419
Dutch Roll	$-0.102 \pm 0.523i$	13.5 s	0.192
Mode	λ	$T_{1/2}$	
Spiral	0.114	-6.8 s	
Aperiodic Roll	-3.613	0.2 s	

the phugoid "must not be so unstable as to cause an unacceptable increase in pilot workload or otherwise endanger the aeroplane" [3]. These requirements do not specify certain flight conditions, and are applicable to any situation. As mentioned, the presented flight conditions are considered the most critical, and as such the worst stability performance among all three conditions is compared with the requirements in order to examine compliance with CS 23.181. At cruise with most aft c.g., the damping ratio is least with a value of 0.772. However, this is still quite strongly damped, and with the longest time to half amplitude at take-off and landing conditions still only at $T_{\frac{1}{2}} = 0.13$ s, the short period oscillation can be said to be strongly damped and thereby fulfil the requirement. Furthermore, even with the smallest amount of damping on the Dutch roll at 0.153 during cruise with most aft c.g., the number of cycles to one-tenth amplitude is $C_{\frac{1}{10}} = 2.4$, which also comfortably meets CS 23.181. Finally, with the longest phugoid time to half amplitude at $T_{\frac{1}{2}} = 31$ s during take-off and landing conditions, this can also be deemed to be damped quite strongly such that no substantial efforts are required from the pilot.

In addition to these oscillatory modes, which all display sufficient dynamic stability as defined by CS 23.181, the aperiodic eigenmotions can be investigated. Although no requirements on their dynamic stability are offered in CS 23, the roll motion is mentioned to usually be strongly damped and "almost always be satisfactory as judged by the ability to precisely control bank angle", and the spiral "may be stable, but is often neutrally stable or even mildly divergent in roll and yaw" [3]. With the aperiodic roll having the longest time to half amplitude of $T_{\frac{1}{2}} = 0.2$ s, this convergence can also be said to be present in the Caty. By contrast, the spiral mode time to half amplitude is negative for all three flight conditions, meaning that this eigenmotion actually diverges, and this time $T_{\frac{1}{2}}$ represents a doubling in amplitude. This time is shortest for take-off and landing conditions, with the spiral amplitude doubling every $T_2 = 6.8$ s, which is quite short. However, pilot controls are very involved during take-off and landing phases of the mission, and this time double amplitude extends to minimally $T_2 = 19.4$ s during cruise, offering a substantial amount of response time to the pilots.

It is important to note that these aircraft motions are dynamic responses to certain unit, step, or pulse inputs, after which the controls are left free. Therefore, pilot control inputs to recover static aircraft stability are an effective manner to exit unstable motions such as the spiral. With all other eigenmotions sufficiently damped, the aircraft can be deemed as offering adequate dynamic stability.

11.7. Landing gear

Because of the changes in the aircraft's cg, weight and requirements, the landing gear needs to be redesigned. First, the tire dimensions are determined in subsection 11.7.1, followed by the landing gear positioning in

subsection 11.7.2 and the design of the retraction mechanism in subsection 11.7.3.

11.7.1. Tire sizing

The original aircraft's landing gear was installed as a retrofit since the preceding version was purely a seaplane. Hence, the landing gear was off the shelf and not fully optimized for the aircraft ¹. The landing gear was oversized, which did give the aircraft the capability to land on grass runways. The Caty does not need this capability, and it was found that the lowest-rated runway the plane is expected to land on has a load classification number (LCN) of 50. This gives an approximate maximum tire pressure of 1000 kPa [25].

For stability and controllability during ground manoeuvres, it is assumed that between 8 and 15% of the total aircraft's weight rests on the nose gear, the remaining weight resting on the main gear. The most critical for the nose gear is when $0.15 \cdot 10500 = 1575$ kg is resting on it. For the main gear, this is $0.92 \cdot 10500 \cdot 1/2 = 4830$ kg, assuming the plane has 2 main gear wheels, the same as the original. Dual wheels on each main gear would be wider and would take up too much room inside the fuselage, hence the original configuration is kept. Using the calculated loads, the following tire dimensions are selected [25], as can be seen in Table 11.3.

Table 11.3: Caty tire dimensions and pressures

Parameters	Main gear	Nose gear
Load (per wheel) [kg]	4830	1575
Tire diameter [mm]	762	444
Rim diameter [mm]	381	191
Tire width [mm]	229	140
Tire pressure [kPa]	785	670
Tire name	30 x 9 - 15	17.5 x 5.5 - 7.5

As can be seen from Table 11.3, the pressures are below the 1000 kPa required for landing on a runway with an LCN of 50.

11.7.2. Landing gear positioning

The landing gear position is constrained by the following requirements:

Table 11.4: Landing gear requirements

Requirement ID	Requirement
Geometric Requirements (GEO)	
Landing Gear (LDG)	
GEO-LDG-1	The nose gear shall bear more than or equal to 8% of the MTOM at the most aft c.g.
GEO-LDG-2	The nose gear shall bear less than or equal to 15% of the MTOM at the most forward c.g.
GEO-LDG-3	The scrape angle shall allow take-off and landing at kts.
GEO-LDG-4	The tip-back angle shall be smaller than the scrape angle.
GEO-LDG-5	The overturn angle shall be larger than 55 degrees.

When taking off at 70 kts, a lift coefficient of 1.00 is required. This corresponds to an angle of attack of the wing 10.4° . Since the wing is angled at 4.8° with respect to the fuselage, the fuselage only needs to rotate by $10.4 - 4.8 = 5.6$ degrees. Hence, the scrape angle needs to be larger than 5.6° .

The overturn angle constrains the main landing gear track. It is calculated using Equation 11.8. Here, l_n and l_m are the distances from the c.g. to the nose and main gears respectively, z is the height of the c.g. from the ground and ψ is the overturn angle.

¹Communication with Prudent Staal, dd. 10-5-2023

$$y_{MLG} > (l_n + l_m) \left(\frac{l_n^2 \tan^2 \psi}{z^2} - 1 \right)^{-\frac{1}{2}} = 2.37m \quad (11.8)$$

The main landing gear thus needs to be at least 2.37 meters from the aircraft's centerline. The nose gear is placed on the centerline, as it was for the original. Space for this has been allocated. The longitudinal position of the landing gear is determined using Figure 11.5.

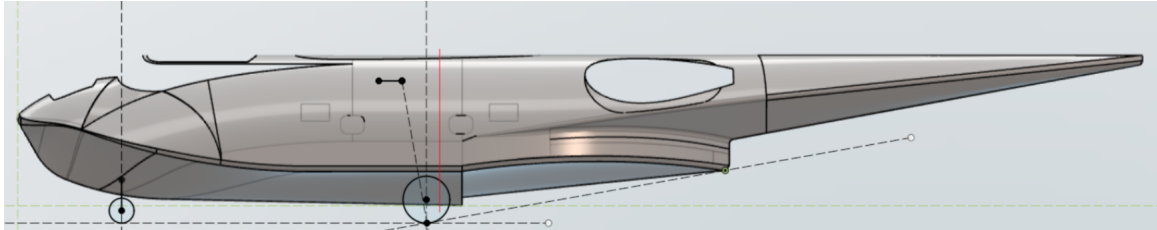
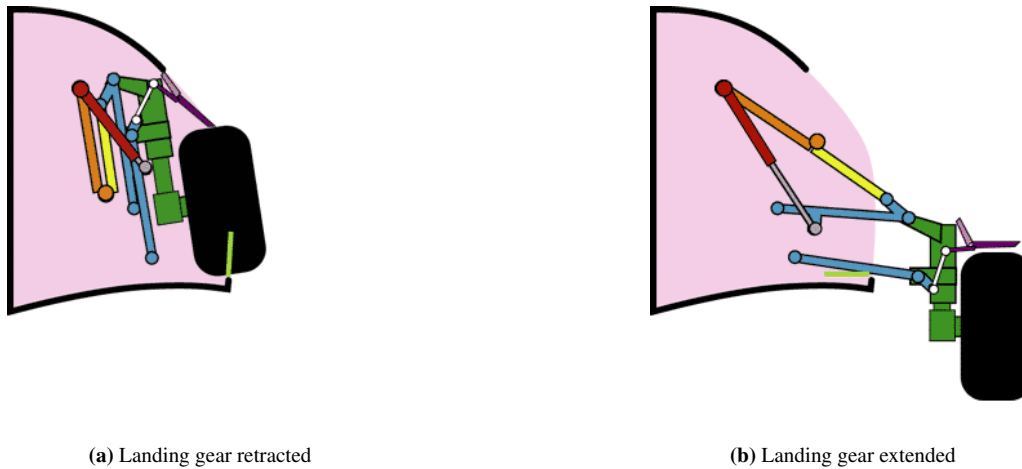


Figure 11.5: Tip over and scrape angle of the Caty

From this, the main landing gear is positioned 7.12 m from the aircraft's nose, or 0.425 m behind the most aft c.g. When fully compressed, it extends 0.30 m below the bottom of the aircraft, resulting in a scrape and tip-back angle of 10.0 degrees. The nose gear is placed at the same height as the main gear, and 1.81 m behind the nose of the aircraft.

11.7.3. Landing gear retraction mechanism

The original aircraft used a retraction mechanism very similar to double wishbone suspension used in cars. A diagram showing the landing gear mechanism of the PBY Catalina is shown in Figure 11.6.



(a) Landing gear retracted

(b) Landing gear extended

Figure 11.6: Landing gear retraction mechanism of the Caty

The new mechanism will be based on this same idea, but the geometry will need to be changed. Since the new landing gear has smaller tires, it needs to extend down more to reach the required height. This leads to longer linkages with longer travel. The result can be seen in Figure 11.7.

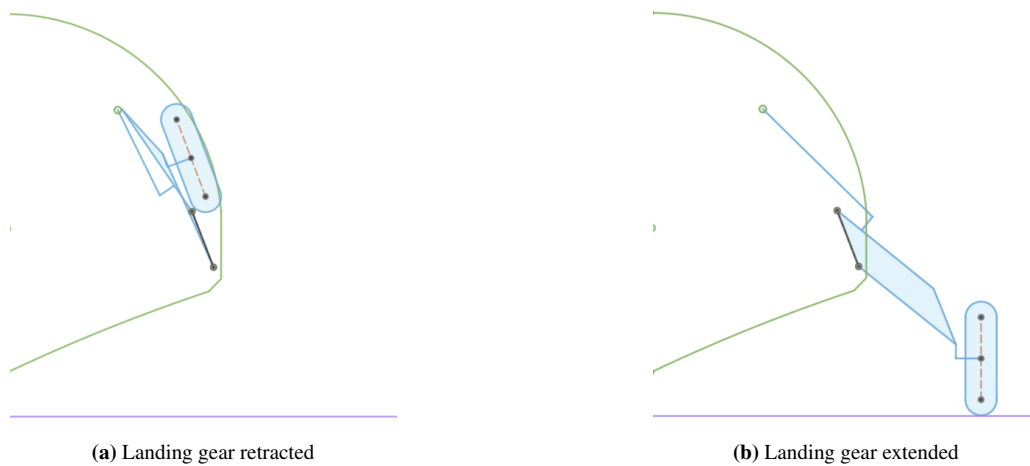


Figure 11.7: Landing gear retraction mechanism of the Caty

As can be seen, the linkages are longer, causing the gear to be stored higher up on the aircraft's fuselage. However, the space taken up by the mechanism is smaller than that of the original.

11.8. Verification and validation

Verification and validation of the stability and control analysis is to be done in two aspects. For one, the python code calculating the different plots and dynamic stability solutions can be checked for errors. Since certain shapes are expected, any deviation from this shape can be retraced and verified such that potential mistakes can be rectified.

For example, the initial stability curve slope was very minimal, to such an extent that a c.g. range with the most aft point at almost 50% of the MAC would only necessitate a minimum horizontal tail surface area of 7% of the wing surface area. This was deemed much too optimistic, and by investigating the parameters affecting the slope, it was eventually found that the lift coefficient gradients of the tailless aircraft and the horizontal tail respectively were switched when calling the function that gave the estimation of these parameters. Upon correcting this mistake, a much more realistic curve was found, and the limiting stability performance was as such obtained.

Furthermore, during the investigation into dynamic stability, it was found that the phugoid eigenmotion was unstable for some conditions, and quickly diverged. Through following which values in the calculation of the solutions to the EoM rendered the real part of the eigenvalue to be positive, the stability derivatives in X direction, meaning the body axis going aft from nose to tail, had the opposite sign, since the derivatives act together with the drag. Upon rectifying this, the phugoid was then stable. Another example of such a method of verification was when the solutions for the short-period motion were found not to have an imaginary part, which clashed with the theory of this motion being a heavily damped oscillatory motion. Investigation into the values of the solution calculation which would be responsible for imaginary components yielded another such sign error, owing to differences in conventions between two different sources, the correction of which resulted in short-period eigenvalues that were more realistic.

Another aspect in which verification was done is the estimation of the various derivatives and coefficients, which can be verified through comparison with their respective values for existing aircraft, obtained from Dr. Jan Roskam's *Airplane Design Part VI* [21]. Since the specific data will differ, this verification consists of comparing orders of magnitude and signs, as well as the relations and patterns between different parameters. If the calculated value for a certain derivative is decisively outside the order of magnitude or has an opposite sign as compared to its value given for different real aircraft, analysis is done into where in the estimation process an error might have been made to warrant this discrepancy, in addition to which an attempt is made at reasoning the value. For example, with the very large wingspan of the Caty, it would be expected to have quite a large magnitude of roll resistance C_{l_p} . Moreover, different relations between derivatives can be used for verification. For example, it is expected that the yaw-moment-due-to-rudder deflection derivative $C_{n_{\delta_r}}$ is proportional to the

sideforce-due-to-rudder deflection $C_{Y_{\delta_r}}$, exactly by the moment arm of this force. These two derivatives should therefore have opposite sign, since their respective positive orientations are in opposite coordinate directions.

12

Performance

12.1. General characteristics

The Caty has undergone multiple characteristic changes. This is done to improve the performance and also to give the passengers a more luxurious experience. To see the new Caty and some general size characteristics see figures 12.1 to 12.3 (The scaling of the figures are about 5% or 10% smaller than they should be). All the shown measurements are given in millimeters.

The first big change is to increase the wingspan of the aircraft compared to the original PBY Catalina. This is due to aerodynamic performances. Another component that is added to improved aerodynamic characteristics are the winglets. These are also connected to the floaters such that the floaters can still extend for water landings.

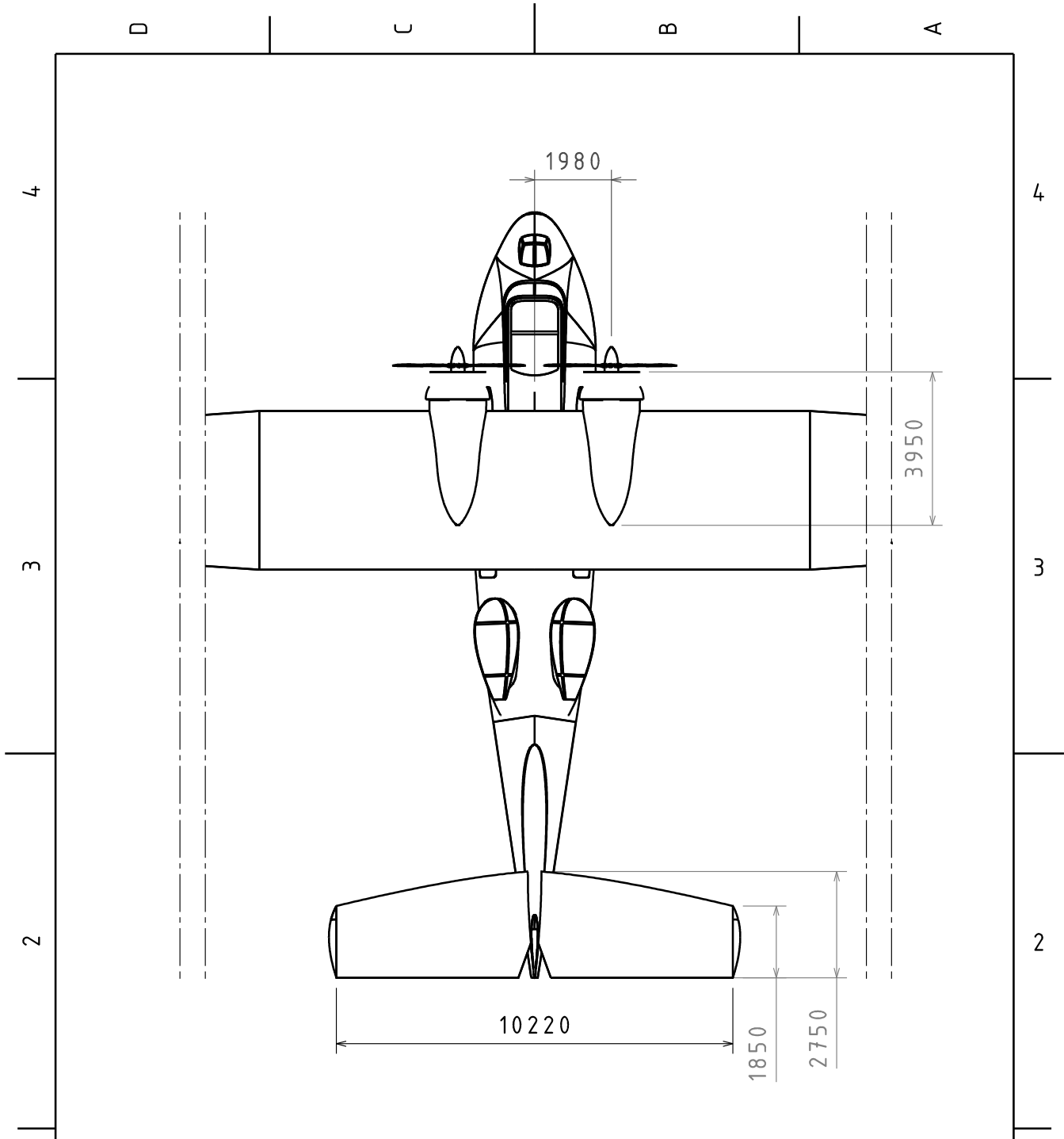
For the Caty to become stable, the empennage size had to be changed too. To make the Caty stable the vertical and horizontal tail size slightly increased such that a greater counterforce can be produced.

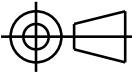
To improve the passenger experience and comfort, the aircraft's fuselage was increased. This was done by lowering the fuselage floor by 10cm and widening the fuselage by 15cm such that passengers can fit more comfortably. This gives more space for the passengers and keeps the shape similar to the view of the original Catalina.

The aircraft engines have also undergone modifications. The engines are electrical and their position has slightly changed. Furthermore, the propeller diameter has decreased while the amount of propeller blades has increased to 9. This is done to reduce the sound produced by the engine and adhere to the sound requirements of staying below 65 dB at 3000ft.

One of the biggest modifications compared to the original Catalina is changing the front blister. Originally it was a gunner and bomber seat. Now it has a more aerodynamic shape and a passenger can sit in there and enjoy the view during flight.

The last mayor modification is the positioning and size of the landing gear. The change in position has been performed to improve and cope with the new center of gravity of the aircraft. Whereas the wheel size has been decreased due to the decrease in MTOW, as well as to improve the aerodynamics due to the wheels sticking out of fuselage when stored.

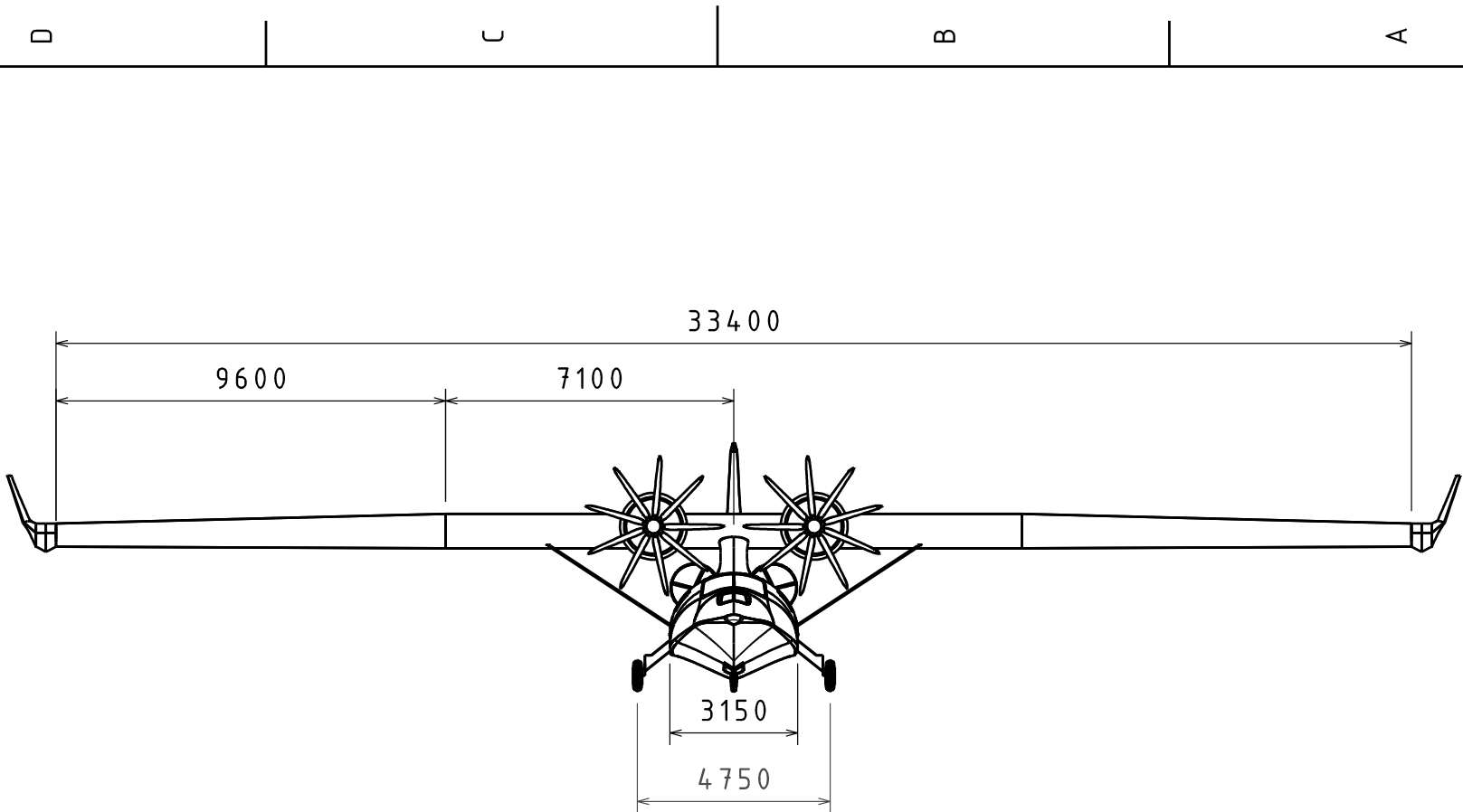


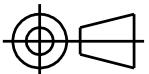
DESIGNED BY: School		<h1>Final aircraft</h1>		I	-
DATE: 21/06/2023				H	-
CHECKED BY: XXX		<h2>DASSAULT SYSTEMES</h2>		G	-
DATE: XXX				F	-
SIZE A4		<h3>DRAWING NUMBER</h3> XXX		E	-
SCALE 1:130	WEIGHT (kg) XXX			D	-
		<h3>SHEET</h3> 2/3		C	-
				B	-
				A	-

This drawing is our property; it can't be reproduced or communicated without our written agreement.

D A

Figure 12.2: Front view Caty

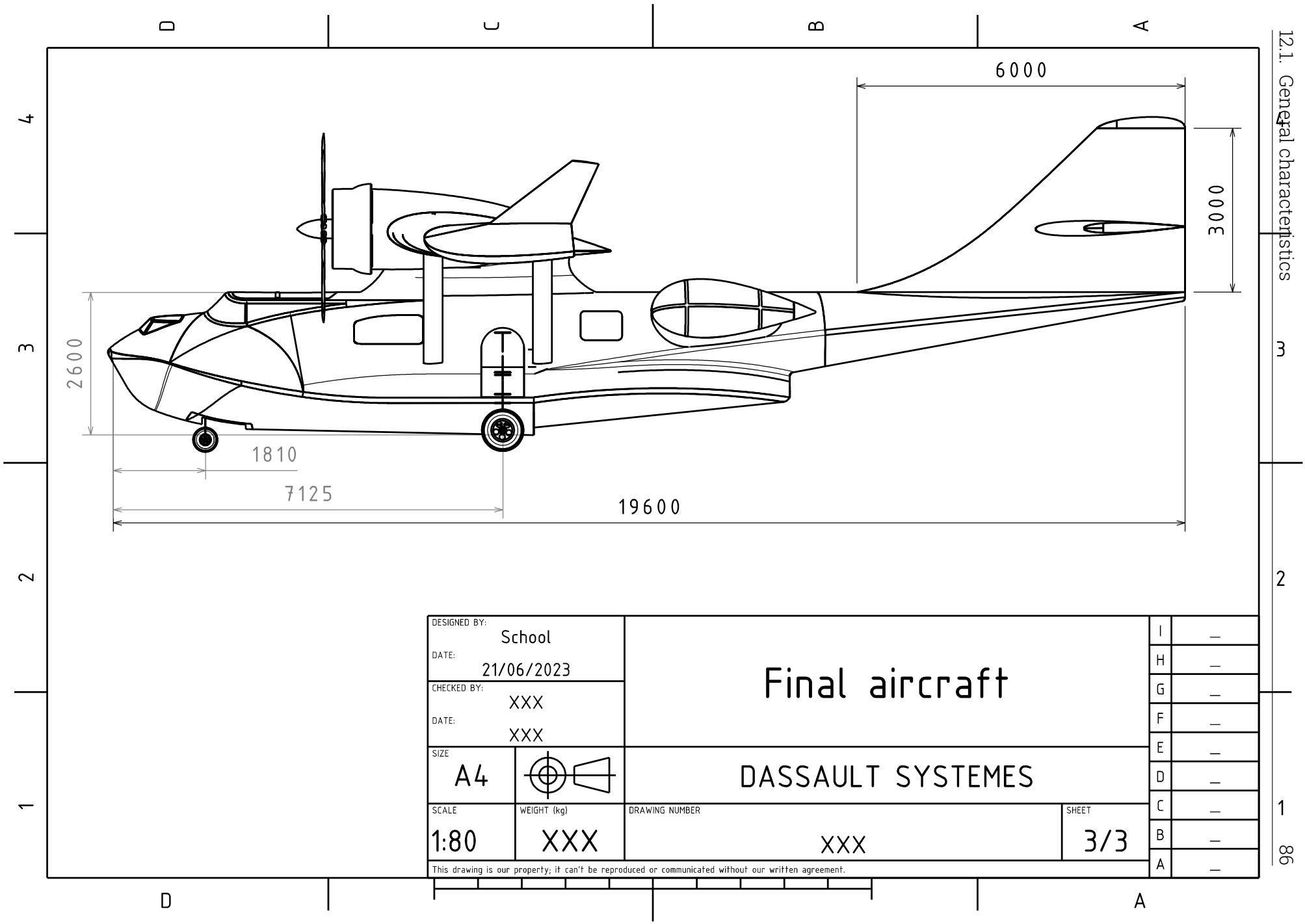


DESIGNED BY: School		<h1>Final aircraft</h1>		I	—
DATE: 21/06/2023				H	—
CHECKED BY: XXX		<h2>DASSAULT SYSTEMES</h2>		G	—
DATE: XXX				F	—
SIZE A4		<h3>DRAWING NUMBER</h3> XXX		E	—
SCALE 1:150	WEIGHT (kg) XXX			<h3>SHEET</h3> 1/3	
		<h3>DRAWING NUMBER</h3> XXX			
				<h3>DRAWING NUMBER</h3> XXX	
		<h3>DRAWING NUMBER</h3> XXX			

This drawing is our property; it can't be reproduced or communicated without our written agreement.

12.1. General characteristics 85

Figure 12.3: Side view Caty



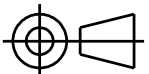
12.1. General characteristics

3

2

1

86

DESIGNED BY: School		<h1>Final aircraft</h1>		I	—
DATE: 21/06/2023				H	—
CHECKED BY: XXX		<h1>DASSAULT SYSTEMES</h1>		G	—
DATE: XXX				F	—
SIZE A4		<h1>DASSAULT SYSTEMES</h1>		E	—
SCALE 1:80	WEIGHT (kg) XXX			D	—
DRAWING NUMBER XXX		<h1>DASSAULT SYSTEMES</h1>		C	—
SHEET 3/3				B	—
This drawing is our property; it can't be reproduced or communicated without our written agreement.				A	—

D

A

12.2. Costs

The initial acquisition cost of the aircraft is estimated at \$25,000,000. A range of \$15 million - \$30 million is given for private jets. The Caty was estimated to lie in the upper region of this range, due to the high luxury of the Caty. After the initial investment, multiple long-term costs arise, that need to be accounted for during the lifetime of the Caty. The rental cost for the hangar is expected to be \$70,000 per year¹.

Operational costs

The insurance costs will be estimated at \$100,000 a year². This will include costs that are made due to accidents happening with the aircraft or the people inside of it. Other annual unforeseen costs will be estimated at \$100,000 a year. This could also be assigned to an increase in budget for other employees, marketing or downtime during maintenance. Other costs that have to be included are crew salaries, as well as maintenance and replacement of the propulsion system together with fuel costs. The crew consist of 2 pilots together with a cabin attendant. The propulsion system costs have been calculated in the midterm[1], this yields \$320 per hour of flight [1].

Table 12.1: Operational costs Cathy

	Annually	Per flight
Rent hangar	70 k	
Insurance	100 k	
Unforeseen	100 k	
Crew	250 k	
Propulsion system		800

Table 12.1 shows costs of Cathy and how they are accounted for. These costs are only the operational costs and the initial capital costs will be calculated in Table 12.2. The total operating costs are \$1800 - \$2800 per flight. This calculation uses 2.5 hours per flight and 5 to 10 flights a week. This would have to be divided by the number of passengers per flight which would be \$140 - \$215 per flight per passenger.

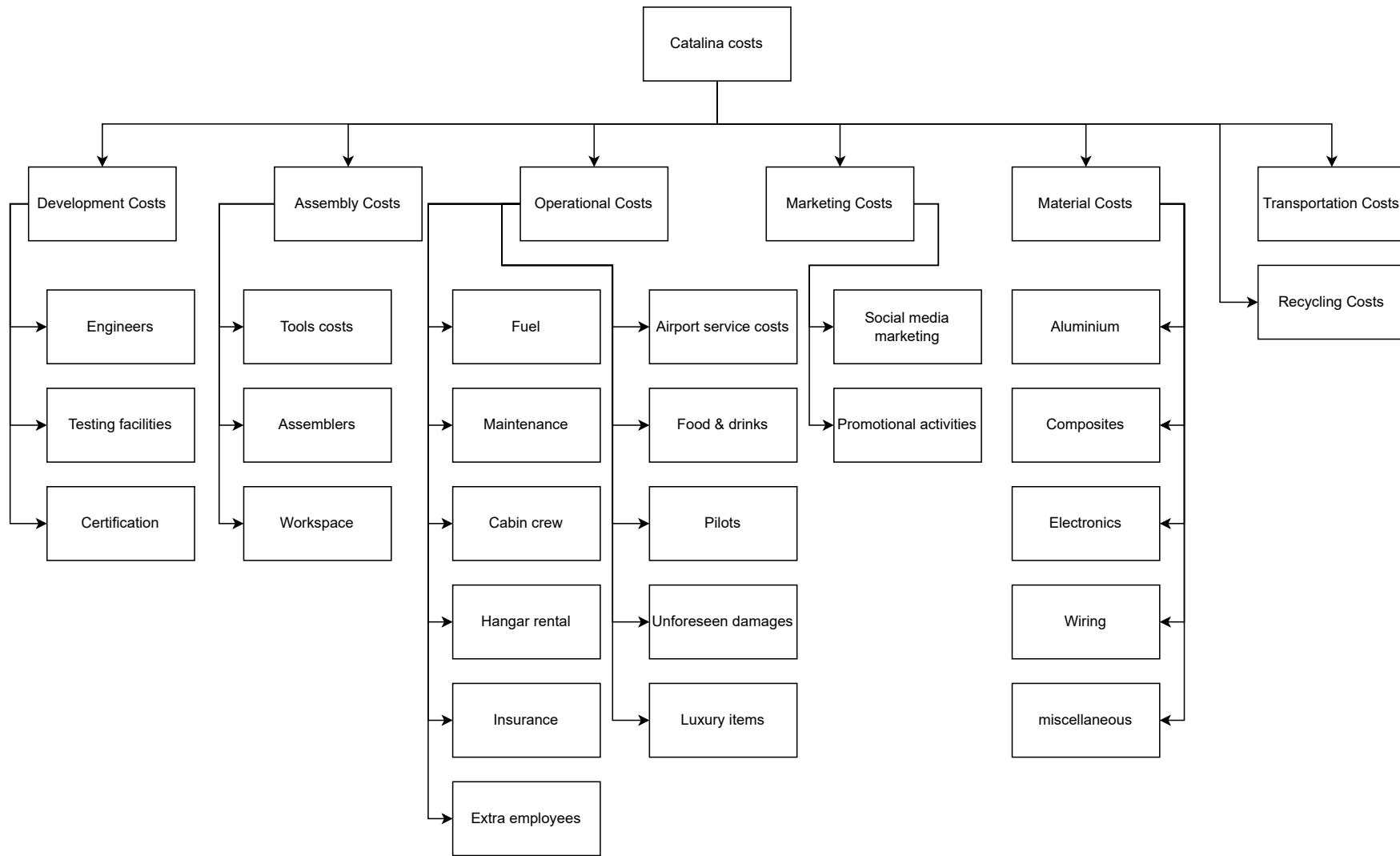
Capital costs

The initial capital of the aircraft is \$25,000,000. Calculating what the company has to charge the passengers to make a profit after 15 years is calculated with Equation 12.1. DR is the discount rate and will be estimated at 3%, this is the average inflation globally. n is the number of years after which the capital costs will be paid and the break-even point is reached, this will be set at 15 years. The costs that arise due to this are \$4000 - \$8000 per flight. Add this to the \$1800 - \$2800 of section 12.2, and a total of \$6000 - \$11000 has to be charged for every flight. Which will be between \$500 - \$850 per passenger per flight.

$$CFR = \frac{DR}{1 - (1 + DR)^{-n}} \quad (12.1)$$

¹<https://republicjetcenter.com/hangar-space-for-rent-everything-you-need-to-know/> (Accessed on: 17/06/2023)

²<https://bwifly.com/private-jet-insurance/> (15/06/2023)



12.3. Hydraulic Actuation Systems

Most existing aircraft use hydraulic actuators to move the control surfaces, retract/extend landing gear, brake, steer and pitch their propellers. This is a proven concept which can deliver high torque and precise control over the steering angle. It is resistant to temperature and vibration effects and simple to troubleshoot. There are however drawbacks to hydraulics. The systems are relatively heavy compared to other systems, complex plumbing is required and it is prone to leakage and contamination. Hydraulics require regular inspection and servicing to ensure proper operation and safety. For safety, the system must be redundant to failure of any part of the system and therefore systems consist of three separate systems as can be seen in Figure 12.5. In total, 9 pumps are required to sustain pressure in case of any system failure indicated by EDP's, ACM's, ACMP's, ADP's and RAT. Plumbing is required to connect all systems to the actuators³.

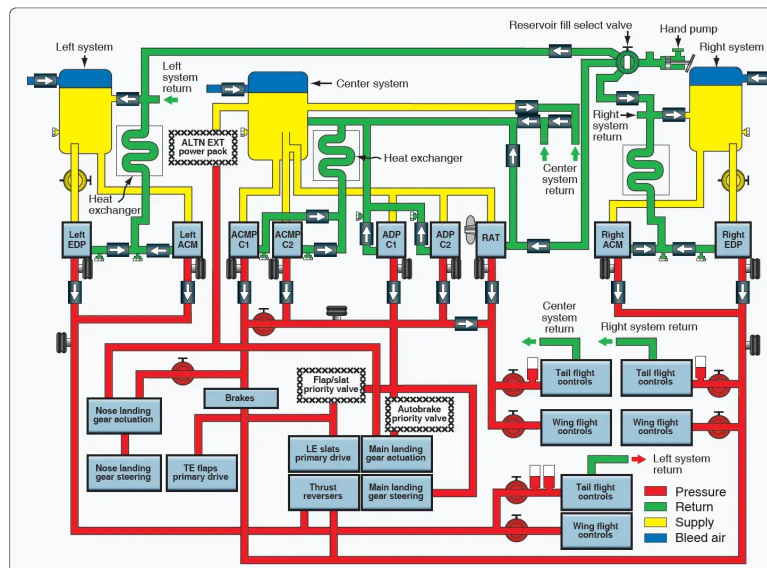


Figure 12.5: Hydraulic actuation system⁴

12.4. Electromechanical Actuation Systems

The use of electromechanical actuators (EMA) has promising benefits over hydraulic actuator systems especially for electric powered aircraft. The technology is relatively new but is already implemented in the rudder actuation of the Boeing 787³. The weight reduction and simplicity and compact design are the major advantages to implement such a system into the Caty. Other advantages to EMAs are low noise, lower maintenance costs than hydraulic actuators, they are easier to integrate with digital control systems and sensors, ease of power management, as well as reductions of environmental pollution and fuel burn. Some disadvantages to EMAs are lower torque and speed than hydraulic actuators, they may be affected by electromagnetic interference and they are time consuming to troubleshoot⁴.

The engines are powered by 4 fuel cells which results in redundant power supply to the actuator system. Every engine has one transformer and inverter and every inverter is powered by one of two available fuel cells, the power supply has therefore sufficient redundancy. The amount of components are significantly lower for EMA systems and are therefore also less complex than traditional hydraulic systems⁵. For all reasons mentioned above, the EMA system is chosen as actuation system.

³<https://www.linkedin.com/advice/1/what-trade-offs-between-hydraulic-electric-steering>(Accessed on: 07/06/2023)

²<https://www.aircraftsystemstech.com/p/hydraulic-system-components> (accessed on 07/06/2023)

³<https://www.moog.com/products/actuation-systems/aircraft/primary-flight-control-actuation-system-for-787.html>(Accessed on: 07/06/2023)

⁴<https://www.linkedin.com/advice/1/what-trade-offs-between-hydraulic-electric-steering>(Accessed on: 07/06/2023)

⁵<https://www.linkedin.com/advice/1/what-trade-offs-between-hydraulic-electric-steering>(Accessed on: 07/06/2023)

12.5. Block diagrams

Several aircraft system diagrams have been developed to illustrate the way the aircraft will communicate between people, hardware and software. First, an electrical diagram in Figure 12.6 shows the electrical systems in the aircraft and the connections between all systems. Secondly, a H/W and S/W diagram was made to show the interaction between hardware such as the propulsion system with its hydrogen systems and the software control systems starting from the cockpit, see Figure 12.7. Figure 12.8 shows the flow of communication in the aircraft such as between the pilot and Air Traffic Control. Finally, Figure 12.9 shows how data is handled between systems utilizing data buses.

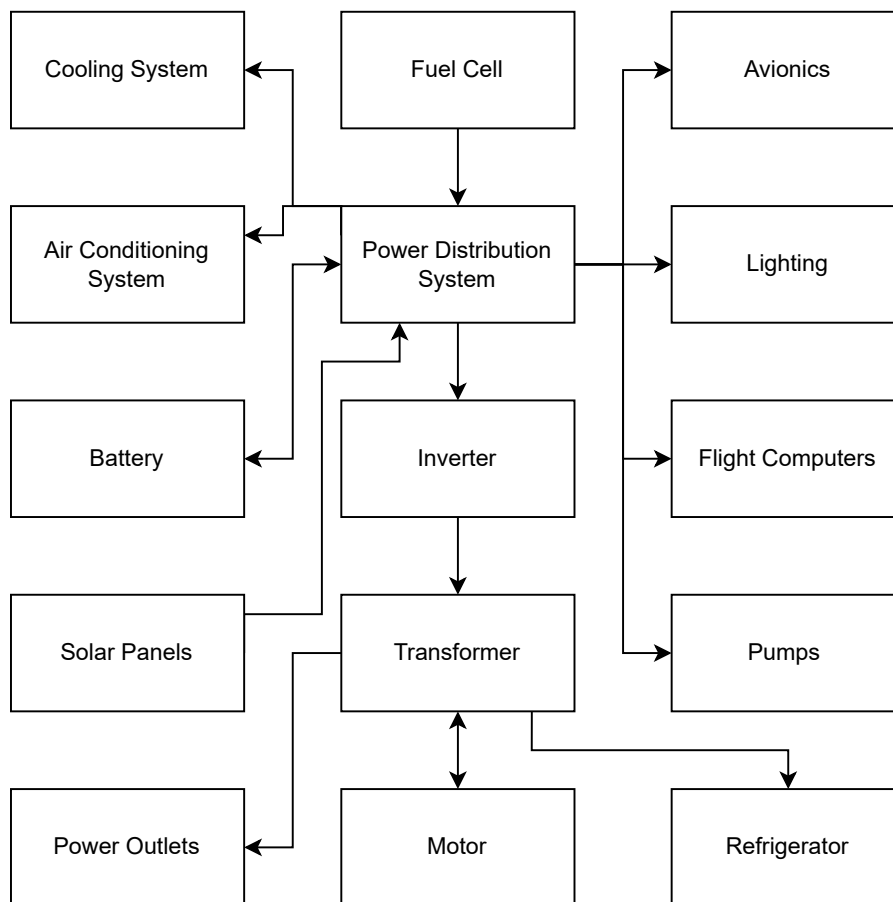
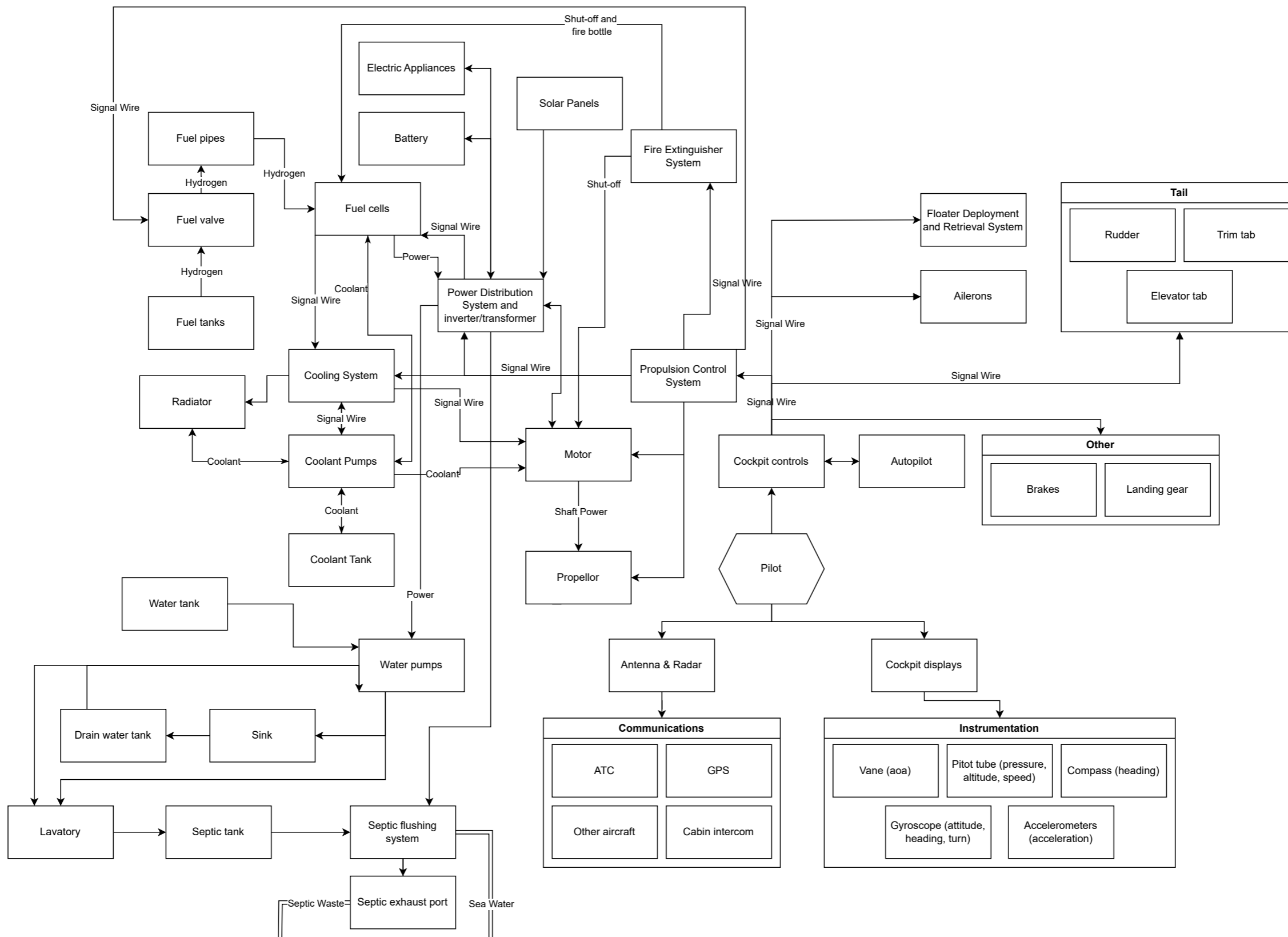
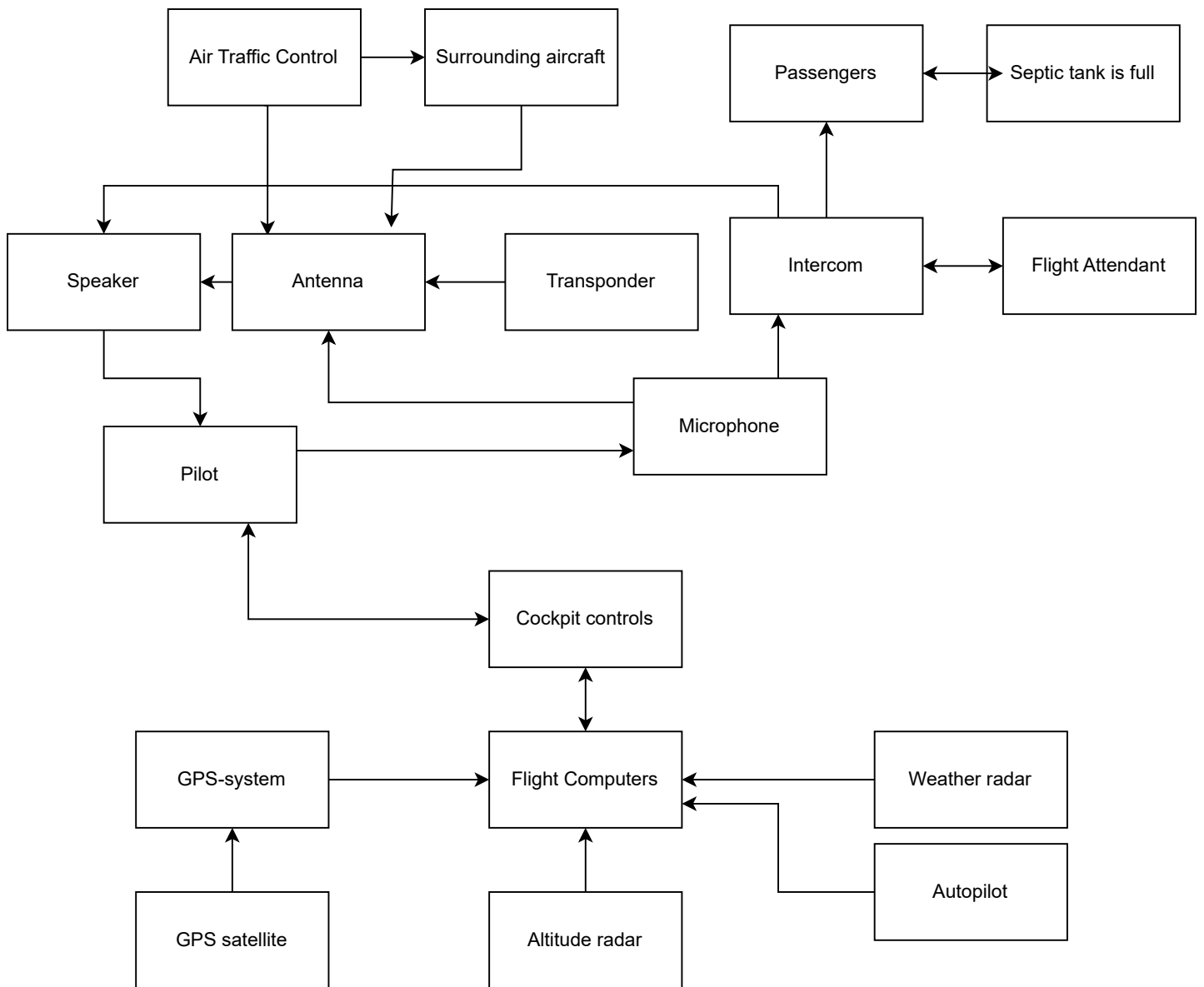
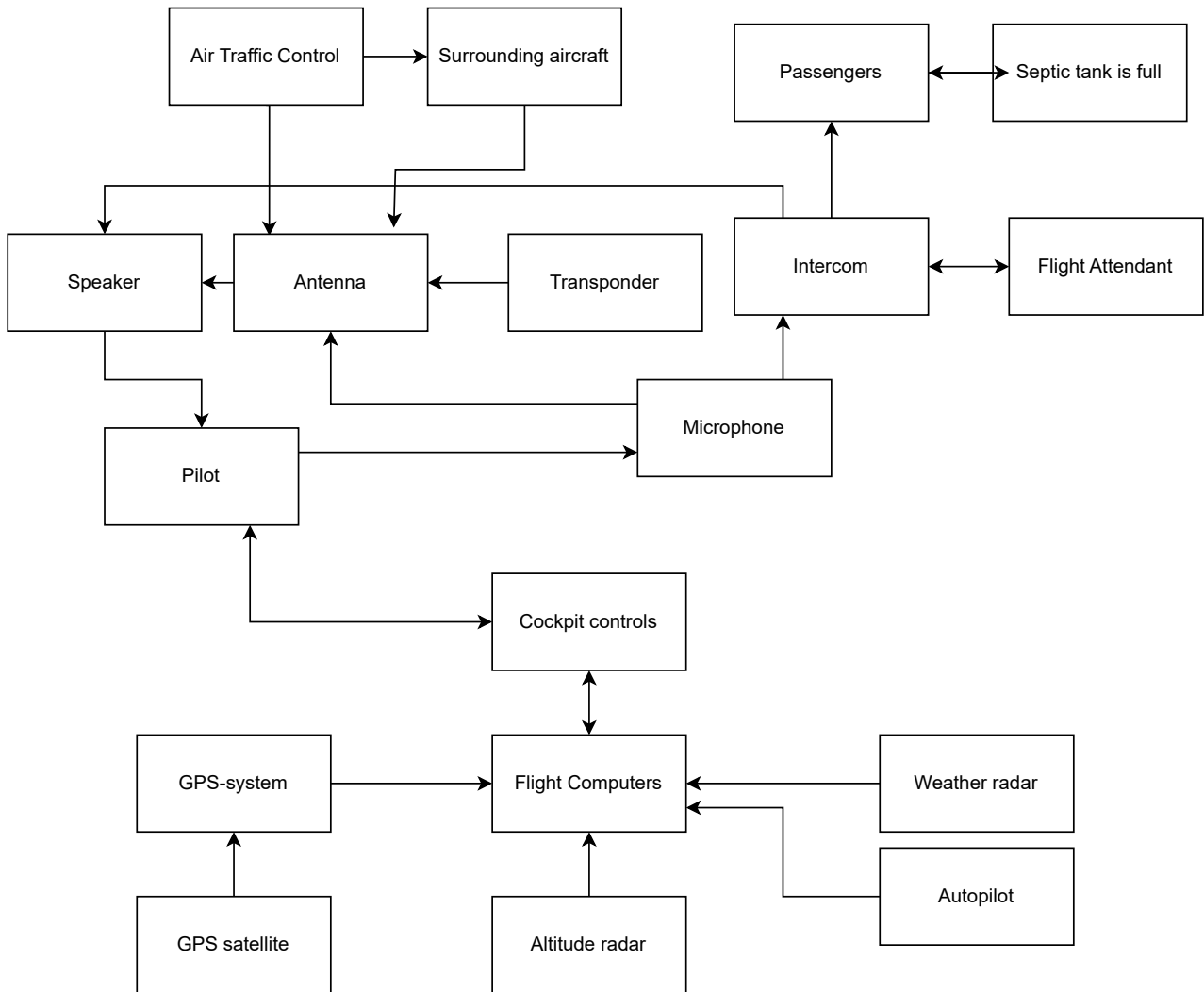


Figure 12.6: Electrical block diagram







12.6. Resource Budget Breakdown

The mass of the aircraft is the parameter that greatly influences the overall performance of the aircraft and therefore, the mass was monitored closely during the project. The progress of the mass estimation is visualised in Figure 12.10 as the target curve where the weight estimations of the hydrogen concept from the previous concepts were assumed. The specification curve represents the estimation including a contingency of 50%, 20% and 10% respectively for the baseline, midterm and final report. In the baseline report [2], one method for initial weight estimations was through comparison and regression with similar aircraft. It was however found that this method would be unreliable since there is not an existing aircraft with similar combinations of range, weights and propulsion. The method chosen was therefore the weight estimation based on range estimations equations of battery powered aircraft since the fuel consumption weight can be neglected. This resulted in a very accurate estimation since a 20% reduction in OEM was assumed with respect to the original Catalina. With a payload mass of 2,000 kg, and 111 kg of fuel weight, the value of 8,931 kg was obtained. In the midterm report, the weight of the hydrogen concept was 14,188 kg. Class I weight estimation was performed where a conservative reduction in structural weight was assumed, resulting in a relatively heavy aircraft. After the midterm report, structural analysis was performed which resulted in more accurate structural weight estimation. The critical load cases were identified and after multiple iterations, the weight reduced to an OEM of 7,606 kg and a MTOM of 9,067 kg.

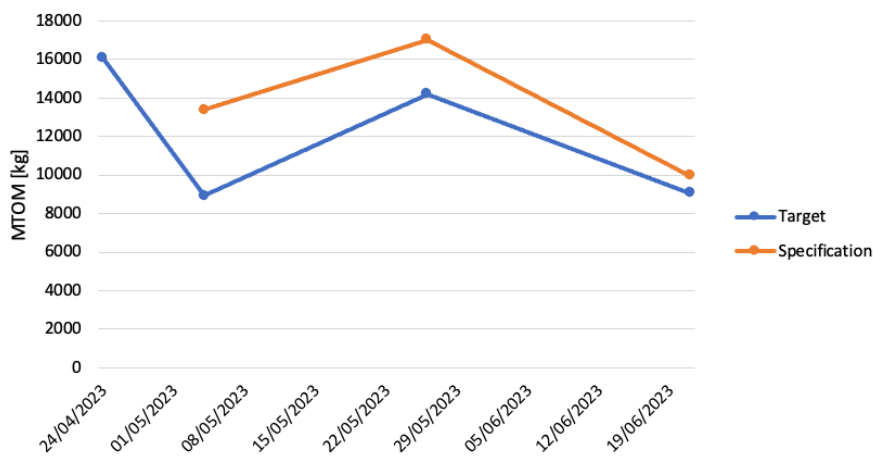


Figure 12.10: Mass Technical Performance Measurement

The final weight distribution of the different assemblies, payload and fuel are given in Figure 12.11 and Figure 12.12. The propulsion part consists of the motor, fuel cells, radiators, propellers and auxiliary systems. The components in "Other" are flight controls, actuators, instruments and avionics, electrical systems, air conditioning and paint.

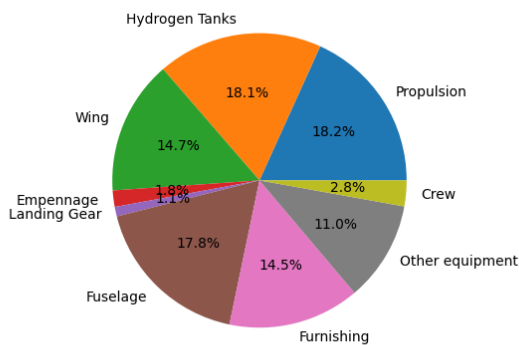


Figure 12.11: OEM weight distribution

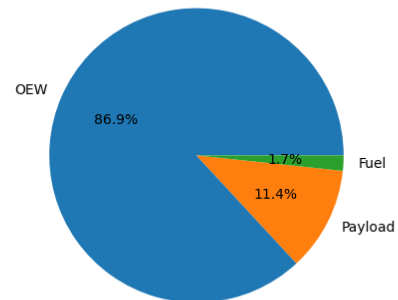


Figure 12.12: MTOM weight distribution

12.7. Risks

Throughout the Design Synthesis Exercise, risks were identified and handled using a risk management procedure. These risks were monitored, avoided or mitigated to avoid the failure of the aircraft design. Every risk was rated on probability (P) and consequence (C) where the probability ranged from Very Unlikely (1) to Very Likely (5) and the consequence ranged from Negligible (1) to Catastrophic (4).

The first major risks were identified at the preliminary design phase where the trade-off between propulsion systems was performed. The risks attached to every system were identified and taken into account at the trade-off. Caty Propulsion Risks CPR-10 and CPR-11 were identified as the most critical risks. For the initial design of the aircraft, the Caty Design Risks (CDR) were identified. Table 12.4 shows the risk map where the risks, probability, consequence, impact and handling procedure are stated.

12.7.1. Risk Map

Table 12.2 gives the risk map which visualises the most important risks which need to be mitigated or avoided. For CTR-10 and CTR-11, a mitigation or avoidance action has to be taken to reduce the risks. In Table 12.2 it can be seen that all risk are outside the mitigate/avoid region and therefore only CTR-10 and CTR-11 need extensive T&C and most other risks need T&C. [1]

Table 12.2: Risk Map

Very Likely		CDR-8		
Likely	CDR-5	CDR-1&2	CPR-10&11	
Even Chance		CDR-3&4	CDR-11	
Unlikely		CDR-10	CDR-12	
Very Unlikely		CDR-6,7&9		
	Negligible	Marginal	Critical	Catastrophic

Table 12.3: Risk Mitigation Map

Very Likely				
Likely	CDR-2,5			
Even Chance	CDR-3&4	CDR-1&8		
Unlikely		CDR-10	CDR-1,11,12	
Very Unlikely		CDR-6,7&9	CPR-10&11	
	Negligible	Marginal	Critical	Catastrophic
	Accept	T&C	T&C/Mitigation	Mitigate/Avoid

Table 12.4: Risk assessment

Risk		P	C	Impact	Handling
CPR-10	The battery concept battery energy density of 350 W/kg is unavailable at the start of production	4	3	The aircraft range will be less than estimated in the design process	<i>Avoiding:</i> To avoid this risk it can be done by selecting another concept.
CPR-11	Hydrogen is not available at the customers airports	4	3	The aircraft cannot reach the desired location deteriorating it's use case	<i>Avoiding:</i> Avoid this risk by selecting another concept. Else, mitigate by installing hydrogen fueling at landing sight or ship hydrogen to desired airport.
CDR-1	The weight of the aircraft moves too far aft resulting in an unstable design	4	2	The aircraft becomes unstable	<i>Mitigation:</i> Move the wing more aft or concentrate payload further forward.
CDR-2	The aircraft hull is under designed	4	2	More structural weight is required in the detailed design	<i>Mitigation:</i> Slightly overestimate the hull thickness
CDR-3	Unrealistically oversimplified assumptions for structures	3	2	The wing structure requires more material in the detailed design phase resulting in heavier wing weight	<i>Mitigate:</i> Consult experts to check assumptions for realistic design
CDR-4	Missing failure modes or load cases for structures	3	2	Redesign required at detailed design phase, requiring more structural weight	<i>Mitigate:</i> Consult experts to check assumptions for realistic design
CDR-5	Windows make fuselage structure unfeasible	4	1	Redesign required at detailed design phase, requiring more structural weight	<i>Accept:</i> The weight of the aircraft is not critical and the small weight penalty to implement windows can therefore be accepted.
CDR-6	Too little space for fuel cell auxiliary systems	1	2	The nacelle becomes too large for propeller longitudinal clearance	<i>Mitigate:</i> Position auxiliary systems inside the wing
CDR-7	Tested propeller noise larger than requirement	1	2	Noise inside the cabin is too loud	<i>Mitigate:</i> Redesign of propellers is required or more sound insulation inside the aircraft is required
CDR-8	The initial propeller design is structurally unfeasible	5	2	The replacement or adjusted design does not meet the noise requirements	<i>Mitigate:</i> Redesign of propellers is required or more sound insulation inside the aircraft is required
CDR-9	Unfeasible floater & wingtip design	1	2	Redesigned wingtip results in unattractive aircraft design	<i>Mitigate:</i> Remove wingtip or further design an elegant wingtip design
CDR-10	Insufficient space in cockpit to climb into front observation deck due to regulations	2	2	Front observation deck becomes unusable	<i>Mitigate:</i> Repurpose observation deck to hydrogen tank, radar or other auxiliary systems
CDR-11	The aircraft interior is not luxurious enough for intended market	3	3	The aircraft sales are too low to reach the break even point	<i>Avoid:</i> Perform extensive market analysis to ensure convincing design at aircraft launch
CDR-12	The aircraft has too little range for the intended market	2	3	The aircraft sales are too low to reach the break even point	<i>Mitigate:</i> Increase hydrogen tank size for a longer range

12.8. RAMS characteristics

12.8.1. Reliability

Propulsion system

To determine the hydrogen propulsion system is hard to determine. It is rarely used at the moment. Thus it will be assumed that it has a bad reliability, because it is very rarely used and not at all in aircraft's.

The most reliable part of the engine will be the electric motors. This is due that there are not a lot moving parts in the system, thus this reduces the change of failure of the motor.

Materials

The use of the new PEEK material will decrease the reliability of the aircraft. This new composite material has not been used in aircraft in load-bearing structures yet. Since there is not much experience with this material, the reliability of the overall aircraft will decrease. Extensive testing will have to be done to certify the material which will thus increase information known about the material and its characteristics. Once certification is done, enough information should be known to say with certainty that the material will operate as intended.

Water landings

Water landings place a heavier burden on the aircraft structure than normal landings. The impact causes high loads on the structure and thus this structure should be able to handle these multiple times. The structure will be different from standard fuselage structures and will be specially designed for this. However, multiple amphibious aircraft have been built along the years⁶, so the design of this structure is achievable.

12.8.2. Availability

Hydrogen

Green hydrogen production can be integrated into the sustainable energy infrastructure of an island group. As renewable energy sources continue to expand, the disparity between energy supply and demand becomes more pronounced. To address this issue, surplus energy needs to be stored or injected into a larger electricity grid. While batteries have limitations in terms of cost and capacity, electrolysis-based hydrogen production offers a viable solution. By constructing large storage tanks, hydrogen can serve as a sizable and efficient alternative to chemical batteries. The stored hydrogen can then power hydrogen vehicles, including cars, trucks, and aircraft. Several island groups have already implemented such systems, and as the prospect of hydrogen-powered transportation, such as cars and aircraft, gains traction, more financial incentives are expected to drive the adoption of these systems. Pairing a hydrogen fuel cell-powered aircraft with green hydrogen production ensures a sustainable operation for the Caty.

Propulsion system technology

The propulsion technology for hydrogen is relatively new. All aerospace applications with hydrogen are conceptual. Besides the entire sub systems are mostly proven concepts. This is the case for the electric motors and pressurised gas vessels.

Electric motors are already used in day to day tasks like cars and other applications. The only improvements that have to come in this area are power per performance and efficiency in order to get higher performance gains. In the end the availability of the engines will not be an issue. The hydrogen tanks are basic pressure vessels. These are very commonly used in the world. The only difference with stored hydrogen is that it can not be stored in metal tanks, because the hydrogen can cause embrittlement within the tank. Thus a composite tank is needed. Beside that it is most likely that the tanks only need some extra certification and some extra safety procedures have to developed. The main limitations of hydrogen use in the aircraft are the volumes at which the hydrogen has to be stored to have an effective gravimetric hydrogen storage density.

A component that is not as readily available in the propulsion system are the fuel cells. The use of this is relatively new in cars and airplanes. These also have to be certified to be flight ready as well. They can be a leading cause of issues in the airplanes.

⁶<https://encyclopedia.pub/entry/33161> (Accessed on: 16/06/2023)

12.8.3. Maintainability

Propulsion system

The maintainability of the propulsion system can be tricky. This is because the hydrogen tanks are composites that are in the wing. Due to that the tanks are high pressured it needs a lot of maintenance. The issue is that the tanks are made out of composites and it is difficult to find defects in those tanks.

For the maintainability of the electric motors is most likely to be simpler than a regular combustion engine. Thus the maintainability will most likely be low

For the fuel cell it is difficult to say how the maintainability should look like, because they are not used in aviation applications.

Water hull

The water hull should be maintained regularly to ensure the structural integrity. The structure of the water hull could be damaged by the multiple water landings which act more stresses on the structure than normal landings. By implementing more regular maintenance checks, material defects can be detected in the early stage. This will minimize down-time in the long run and decrease the costs of bigger material defects such that large structures won't have to be replaced but only small structures.

12.8.4. Safety

Hydrogen propulsion system

If maintained correctly it should be safe and low risks. It is difficult to determine the dangers of the systems except for the hydrogen tank. If maintained badly or is over pressurized it can explode or cause fire. The motor will most likely also be safe and most likely not cause issues. This is because it is electric and does not have a lot of moving parts and thus a high reliability. The propeller is also a component that is safe if used correctly. The only dangers that can happen if people go too close of the propeller and if a bird strikes it.

12.9. Sustainability

Sustainability approach has multiple facets and the first can be best described by the sustainability considerations taken in the design phase to make the production of the aircraft as sustainable as possible. The sustainability approach looks at the emissions produced of the aircraft from the start of production to the end of life when the aircraft is recycled. Aside from a sustainable product, the design process itself also has to be sustainable which means the efficient use of time and other resources during design [1].

12.9.1. Sustainable Materials and Production

The use of thermoplastics in composites enables the full recyclability of composites. Recently, aircraft parts have been made from carbon fibre thermoplastic composites by the company SAM XL⁷. This concept has been studied in section 10.1. Other materials used in the Caty must also be sourced as locally as possible and recyclable and/or previously recycled. For sustainable production of the Caty, lean production⁸ must be implemented in every aspect of production [1].

12.9.2. Sustainable Propulsion

Implementing hydrogen fuel cell propulsion results in the largest decrease relative to current turbine powered aircraft. Hydrogen is a promising propulsion method for aircraft and in section 7.1, the hydrogen concept is chosen as propulsion system [1]. The hydrogen must be produced with renewable energy to make the hydrogen propulsion system sustainable.

Green hydrogen production can be implemented in the sustainable grid of an island group. With upcoming renewable energy sources, the mismatch between supply and demand increases as well. This excess energy has to be stored or injected in a larger electricity grid. Since batteries are still expensive and have limited capacities, the production of hydrogen via electrolysis can be a solution since large storage tanks can be built. It acts as a large battery and outperforms capacity and cost limitations of chemical batteries. The stored hydrogen can be used to power hydrogen cars, trucks and aircraft. Some island groups have already implemented such

⁷<https://www.samxl.com> (Accessed on: 12/06/2023)

⁸<https://www.leanproduction.com>(Accessed on: 12/06/2023)

systems⁹ and with the anticipation of hydrogen cars and aircraft, more financial incentive will implement such systems. The combination of a hydrogen fuel cell powered aircraft with green production of hydrogen ensures a sustainable operation of the Caty [1].

12.9.3. Sustainable Operation

To stimulate the use of green hydrogen, a collaboration with a sustainable hydrogen production and distribution company will enable a complete package for the customer. The hydrogen company shall have tailored hydrogen tanking solutions for the different use cases. For scenic flights, hydrogen can be tanked at the airport or hangar where the aircraft is stored. The hydrogen can either be shipped to the hangar or a hydrogen production plant can be installed when there is a abundance of renewable energy. For chartering, a network of hydrogen pump stations must be available to fuel the aircraft at the different landing locations. The chartering company has some standardised trips available where they can ship the hydrogen to beforehand, if a hydrogen station is not nearby. For private owned aircraft, the owner can install green hydrogen at their hangar or can choose to have the hydrogen shipped to their hangar or destination. The operational logistics of hydrogen fueling is further elaborated in section 4.1.

12.10. Compliance matrix

In the compliance matrix, each requirement is stated and checked off using a checkmark (✓) if the requirement is met. If the requirement was not yet defined, it is left blank, and the attained value for the aircraft is included if the relevant analysis was performed. If a requirement is not met it is marked with an X and the actual value is included. These are discussed further in section 12.11.

12.10.1. Aircraft compliance matrix

Table 12.5: Requirements List

Requirement ID	Type	Requirement	Check	Value
Operational Requirements (OPE)				
General (GEN)				
Communication (COM)				
OPE-GEN-COM-1	☹	The aircraft shall be able to communicate with ATC.	✓	
OPE-GEN-COM-2	☹	The aircraft shall be able to communicate with surrounding aerial vehicles.	✓	
Accessibility (ACC)				
OPE-GEN-ACC-1	☹	The aircraft shall have a door with minimal dimensions compliant with CS23.	✓	
OPE-GEN-ACC-2	☹	The aircraft door shall be water sealable.	✓	
OPE-GEN-ACC-3	☹	The aircraft shall have an alleyway in compliance with CS23.	✓	
OPE-GEN-ACC-4	☹	The aircraft shall be able to be disembarked in 90 seconds in compliance with CS23.	✓	
OPE-GEN-ACC-4	☹	The aircraft entrance shall be accessible for passengers.	✓	
OPE-GEN-ACC-5	☹	The aircraft shall be accessible for maintenance.	✓	
OPE-GEN-ACC-6		The aircraft shall have a cleaning time not longer than TBD.	✓	
Cargo (CAR)				
OPE-GEN-CAR-1		The aircraft shall have a space for cargo payload.	✓	

⁹<https://assets.siemens-energy.com/siemens/assets/api/uuid:79d192b9-031c-40ca-a3c4-3b120b30fae3/20130-preparing-the-way-for-hydrogen-final.pdf> (Accessed on: 12/06/2023)

OPE-GEN-CAR-2		The cargo space shall be accessible by airport personnel.	✓	
OPE-GEN-CAR-3		The cargo space shall have a minimum volume of TBD m ³ .		0.64 m ³
OPE-GEN-CAR-4		The cargo space shall have minimum dimensions TBD.		1.6 x 0.8 x 0.8 m ³
OPE-GEN-CAR-5		The cargo space shall be able to hold a minimum mass of TBD kg.		120 kg
OPE-GEN-CAR-6		The cargo space shall be waterproof.	✓	
OPE-GEN-CAR-7		The cargo shall be fixable in the cargo space.	✓	
OPE-GEN-CAR-8		The cargo loading time shall be lower than TBD.		
OPE-GEN-CAR-9		The cargo unloading time shall be lower than TBD.		
Fuel ¹⁰ (FUE)				
OPE-GEN-FUE-1		The fuel shall contain a minimal TBD J/kg.		120 MJ/kg
OPE-GEN-FUE-2	☹	The aircraft shall be refuelable.	✓	
OPE-GEN-FUE-3	☹	The aircraft fuel inlet shall be accessible.	✓	
OPE-GEN-FUE-4	☹	The fuel system should be waterproof	✓	
OPE-GEN-FUE-5		The fuel time from empty to full shall be lower than TBD.		
OPE-GEN-FUE-6		The fuel shall be useable in the temperature range TBD.		min -25 °C, max 38 °C
OPE-GEN-FUE-7	☹	The fueling safety shall be compliant with CS23 regulation.	✓	
OPE-GEN-FUE-8		The fuel shall be removable from the aircraft.	✓	
Propulsion System (PRS)				
OPE-GEN-PRS-1	☹	The propulsion system shall be able to be turned on and off.	✓	
OPE-GEN-PRS-2	☹	The aircraft shall be operable inside the aircraft.	✓	
OPE-GEN-PRS-4		The thrust sensitivity shall be better than TBD.		
OPE-GEN-PRS-5	☹	The propulsion system shall be electrical	✓	
Taxi (TAX)				
Movement (MVM)				
OPE-TAX-MVM-1		The aircraft shall be steerable on the ground during taxi.	✓	
OPE-TAX-MVM-2		The steering mechanism shall be dynamically stable.		
OPE-TAX-MVM-3		The steering mechanism shall have a damping higher than the critical damping.		
OPE-TAX-MVM-4		The aircraft shall be able to actively brake.	✓	
OPE-TAX-MVM-5		The aircraft shall be able to move on the ground with 1 engine operable.	✓	
OPE-TAX-MVM-6		The aircraft shall be able to move backwards.	✓	
OPE-TAX-MVM-7		The pilot shall be able to look outside of the aircraft when located inside the aircraft.	✓	
OPE-TAX-MVM-8		The steering accuracy shall be better than TBD.		
Take off (TAO)				
Ground Movement (GMV)				

¹⁰Fuel should be interpreted in the widest interpretation as possible, e.g. sustainable aircraft fuel, electricity, hydrogen, etc.

OPE-TAO-GMV-1		The aircraft shall have a minimal acceleration on the ground of TBD m/s ² .		
OPE-TAO-GMV-2		The aircraft shall be steerable during take off.	✓	
OPE-TAO-GMV-3		The aircraft acceleration shall be controllable.	✓	
Performance (PFM)				
OPE-TAO-PMV-1		The aircraft shall have a take-off speed lower than TBD m/s.		30.4 m/s
OPE-TAO-PMV-2	⊙	The aircraft shall need a take-off distance less than TBD m.		
OPE-TAO-PMV-3		The aircraft shall have a V ₁ higher than TBD m/s.		
OPE-TAO-PMV-4		The aircraft shall have a V _r lower than TBD m/s.		30.4 m/s
Clearance (CLE)				
OPE-TAO-CLE-1		The aircraft shall be able to have a positive vertical rate.	✓	
OPE-TAO-CLE-	☹	The aircraft shall have a fuselage to-ground clearance in compliance with CS23.	✓	
OPE-TAO-CLE-	☹	The aircraft shall have an engine-to-ground clearance in compliance with CS23.	✓	
OPE-TAO-CLE-	☹	The aircraft shall have a wing-to-ground clearance in compliance with CS23.	✓	
Climb (CLI)				
OPE-CLI-1		The aircraft shall be able to have a climb angle of TBD.		8.2°
OPE-CLI-2		The aircraft shall be able to reach an altitude of TBD m.		3 km
OPE-CLI-3		The aircraft shall be able to have a climb rate of TBD.		6 m/s
OPE-CLI-4		The aircraft shall be able to have a pitch rate of TBD.		12.9 °/s
Change Heading (CHE)				
Motions (MOI)				
OPE-CHE-MOI-1		The aircraft should be dynamically stable.	X	Unstable spiral
OPE-CHE-MOI-2	☹	The eigenmotions of the aircraft should be in compliance with CS23.	✓	
OPE-CHE-MOI-3		The aircraft should be controllable in 6 degrees of freedom.	✓	
Control Surfaces (CSF)				
OPE-CHE-CSF-1		The aircraft shall be able to produce a roll rate of TBD.		40.9 °/s
OPE-CHE-CSF-2		The aircraft shall be able to produce a roll angle of TBD.		
OPE-CHE-CSF-3		The aircraft shall be able to produce a yaw rate of TBD.		57.0 °/s
OPE-CHE-CSF-4		The aircraft shall be able to produce a yaw angle of TBD.		
Cruise (CRU)				
OPE-CRU-1	☹ ⊙	The aircraft shall have a cruise speed higher than 110 kts.	✓	
OPE-CRU-2	☹ ⊙	The aircraft shall have a max speed higher than 180 kts.	X	139.7 kts
OPE-CRU-3	☹ ⊙	The aircraft shall have a stall speed lower than 70 kts.	✓	
OPE-CRU-4		The aircraft shall be compliant with the CS23 loading diagram.	✓	
OPE-CRU-5		Aircraft shall be trimmable in cruise condition.	✓	
Descend (DSC)				

OPE-DSC-1		The aircraft shall be able to have a glide ratio higher than TBD.		14.5
Loiter (LOI)				
OPE-LOI-1	🔑	The aircraft shall have an endurance longer than 2.5 hrs.	✓	
OPE-LOI-2	🔑	The aircraft shall have a range larger than 500 km at MTOW.	✓	
Landings (LAN)				
Ground (GRN)				
OPE-LAN-GRN-1		The aircraft shall have a maximum vertical deceleration of TBD.		
OPE-LAN-GRN-2		The aircraft shall have a maximum brake force higher than TBD.		
OPE-LAN-GRN-3		The aircraft shall have a landing distance on runways shorter than 1200 m.		
OPE-LAN-GRN-4		The aircraft shall have a take-off distance on runways shorter than 1200 m.	✓	
OPE-LAN-5	☠	The Aircraft shall be able to operate in aquatic conditions with waves of at least 0.6 m.	✓	
Touch & Go Around (TGA)				
OPE-LAN-TGA-1	☠	The aircraft shall comply with CS23 touch & go around regulations.	✓	
Non-operational Requirements (NOP)				
Legal requirements (LEG)				
NOP-LEG-1	☠	The A.C. shall comply with CS-23 regulations.	✓	
Cost requirements (COS)				
NOP-COS-1	🔑	The aircraft operational costs shall be comparable to the twin otter for amphibious purposes, 2000\$/hour.	✓	
Stakeholder requirements (STA)				
Airport (ARP)				
NOP-STA-ARP-1	☠	The aircraft shall be able to communicate with the airport control tower.	✓	
NOP-STA-ARP-2	☠	The aircraft shall adhere to (small) airport rules fitting to mission profile (TBD).	✓	
Airline (ARL)				
NOP-STA-ARL-1		The aircraft shall be able to create a profit of TBD\$ per trip.		\$3500 per flight
NOP-STA-ARL-2		Flying the aircraft shall be similar to similar aircraft.	✓	
NOP-STA-ARL-3	☠	The aircraft shall be maintainable.	✓	
NOP-STA-ARL-4	☠	Damaged parts shall be replaceable.	✓	
NOP-STA-ARL-5		The aircraft shall have a fuel efficiency of TBD.		30.9 kg/h
NOP-STA-ARL-6	☠	The aircraft shall be compatible with TBD level airport from CS-23.		
NOP-STA-ARL-7		The aircraft can be refuelled at all compatible airports.		
NOP-STA-ARL-8		The aircraft shall be transportable in a TBD volume.		
NOP-STA-ARL-9		The aircraft shall carry at least 15 passengers.	X	13
Passenger (PAS)				

NOP-STA-PAS-1		The aircraft shall have a climate control system.	✓	
NOP-STA-PAS-2		The aircraft shall have a baggage capacity of 100 kg per person.	X	
NOP-STA-PAS-3	☠	The passengers shall be able to look outside.	✓	
NOP-STA-PAS-4		The passengers shall be able to enter the aircraft comfortably.	✓	
Residents (RES)				
NOP-STA-RES-1	🔑	The aircraft shall have a noise level lower than 65dB at a flyover of 3000 ft.	✓	
NOP-STA-RES-2		The aircraft shall improve tourism at remote locations.	✓	
Historic feel (HIS)				
NOP-HIS-1	🔑 🌐	The span of of the wing shall be within 10% of the original Catalina.	✓	
NOP-HIS-2	🔑 🌐	The aircraft shall have observation platforms in the back and front, similar to the original Catalina.	✓	
NOP-HIS-3	🔑 🌐	The aircraft shall have a maximum of 4 engines.	✓	
NOP-HIS-4	🔑 🌐	The aircraft's fuselage dimensions shall be within 10% of the original Catalina.	✓	
NOP-HIS-5		The pitch of the sound produced by the aircraft shall be similar to the original Catalina sound pitch.	X	Frequency 3 times higher.
NOP-HIS-6	🌐	The aircraft shall have a parasol wing.	✓	
NOP-HIS-7	🌐	The aircraft shall have a high engine configuration.	✓	
Resources (RSC)				
NOP-RSC-1	🔑 🌐	The aircraft shall have less than 10% waste at end-of-life.	✓	
NOP-RSC-2		The lifetime of the aircraft shall be at least TBD.		30 years.
NOP-RSC-3		The aircraft shall be made of readily available materials.	✓	
NOP-RSC-4		The aircraft materials shall have detectability for cracks.	✓	
NOP-RSC-5		The materials shall allow fixing of cracks.	✓	
NOP-RSC-6		The aircraft shall be refurbishable.	✓	
NOP-RSC-7		The aircraft shall be able to be produced using readily available production methods.	✓	
NOP-RSC-8		The aircraft can be disassembled	✓	
NOP-RSC-9	🌐 ☠	The materials on the exterior shall be fresh water resistant.	✓	
NOP-RSC-10	🌐 ☠	The materials on the exterior shall be salt water resistant.	✓	
Schedule (SCH)				
NOP-SCH-1		The aircraft shall be designed within 10 weeks.	✓	
NOP-SCH-2		The aircraft shall be designed by 10 students.	✓	

12.10.2. Propulsion system compliance matrix

Table 12.6: Propulsion requirements

Requirement ID	Requirement	Check	Value
Propulsion Requirements (PROP)			
System Requirements (SYS)			
PROP-SYS-1	The propulsion system shall have an electric motor.	✓	

PROP-SYS-2	The propulsion system shall have no in-flight CO ₂ emissions.	✓	
PROP-SYS-3	The propulsion system shall have no in-flight NO _x emissions.	✓	
PROP-SYS-4	The propulsion system shall have a noise level lower than 65dB at a distance of 3000 ft.	✓	
PROP-SYS-5	The propulsion system shall have a maximum thrust of at least TBD N.		1200 kW
PROP-SYS-6	The propulsion system shall have a continuous thrust of at least TBD N.		
PROP-SYS-7	The energy storage capacity of the propulsion system shall be greater than the energy required for an effective aircraft range of 500 km.	✓	
PROP-SYS-8	The propulsion system shall have an endurance of 2.5 hours at a continuous thrust level of TBD.	✓	
PROP-SYS-9	The energy storage shall be refilled in TBD minutes.		
PROP-SYS-10	The propulsion system shall be placed such that it can be made entirely accessible for maintenance.	✓	
PROP-SYS-11	The propulsion system energy storage input apparatus shall be accessible.		
PROP-SYS-12	The propulsion system propulsive devices shall be waterproof.	✓	
PROP-SYS-13	The available propulsion system thrust settings shall have a minimum resolution of TBD %.		electric: virtually infinite resolution
PROP-SYS-14	The propulsion system shall be able to be feathered in case of a one-engine-out scenario.	✓	
PROP-SYS-15	The propulsion system shall have an operating cost of TBD \$.		\$2000 per flight
PROP-SYS-16	The propulsion system shall have less than TBD% EOL waste.		
PROP-SYS-17	The propulsion system shall not generate a yaw moment that is unable to be compensated by the nose-wheel steering system.	✓	
PROP-SYS-18	The propulsion system shall not generate a yaw moment that is unable to be compensated by the rudder.	✓	
PROP-SYS-19	Propulsion system parts should be replaceable in the event of failure.	✓	
PROP-SYS-20	Non-replaceable parts of the propulsion system shall have a minimum lifespan of at least 30 years after the commissioning of the aircraft.	✓	
Subsystem Compatibility Requirements (COMP)			
PROP-COMP-1	The mass of the propulsion system shall not result in an aircraft c.g. position that would make the aircraft unstable.	✓	
PROP-COMP-2	The volume of the propulsion system shall not be larger than TBD.		18.1 m ³
PROP-COMP-3	The propulsion system weight shall not result in an aircraft c.g. position that is unstable at all times.	✓	
PROP-COMP-4	The propulsion system shall be supported by an attachment integrated into the wing	✓	

Regulatory Requirements (REG)			
PROP-REG-1	The energy storage capacity of the propulsion system shall be greater than the energy required to divert the aircraft 225 km, in addition to the effective aircraft range.	✓	
PROP-REG-2	The propulsion system shall not interfere with the entrance and exit door.	✓	
PROP-REG-3	The propulsion system shall have no external rotating parts TBD seconds after shutdown in an emergency.		
PROP-REG-4	The propulsion system shall have a ground clearance according to CS-23.	✓	
PROP-REG-5	External rotating parts of the propulsion system shall not fail due to cracks before faults can be detected by non-destructive testing.		
PROP-REG-6	If part of the propulsion system fails it shall not affect the rest of the propulsion system.	X	Tank failure is critical, if improbable.
PROP-REG-7	The propulsion system shall be restartable in flight.	✓	
PROP-REG-8	The propulsion systems shall have the possibility to stop all rotating elements in flight.	✓	
PROP-REG-9	The propulsion systems shall have the possibility to turn off and isolate power-generating elements in flight.	✓	
PROP-REG-10	The propulsion system shall be able to operate for at least 0.5 hours at maximum power setting.	X	85 s
PROP-REG-11	The energy storage system shall be able to withstand maximum acceleration without damage.	✓	
PROP-REG-12	The energy storage system shall be able to regulate pressure in the case of gaseous or liquid fuels.	✓	
PROP-REG-13	The propulsion system emergency stop shall remain functioning in case of an engine fire.	✓	
PROP-REG-14	The energy storage system shall be able to detect when it's filled up.	✓	
Auxiliary Propulsion System Requirements (AUX)			
PROP-AUX-1	The energy storage system temperature shall remain below TBD °C		
PROP-AUX-2	The propulsion system temperature shall remain below TBD °C		85°C
PROP-AUX-3	The propulsion system shall be able to provide thermal energy for the cabin and aircraft system heating.	✓	
PROP-AUX-4	The propulsion system shall be able to provide a continuous power of TBD kW to power the air conditioning system.		
PROP-AUX-5	The propulsion system shall be able to provide a continuous power of TBD kW to power the avionics systems.		

12.10.3. Wing compliance matrix

Table 12.7: Wing requirements

Requirement ID	Requirement	Check	Value
----------------	-------------	-------	-------

Geometric Requirements (GEO)			
Wing (WNG)			
GEO-WNG-1	The span of the wing b shall be within 10% of the original Catalina (30.48m).	✓	
GEO-WNG-2	The wing root chord c_r shall be within 10% of 4.57m.	✓	
GEO-WNG-3	The wing tip chord c_t shall be within 10% of 3.05m.	✓	
GEO-WNG-4	The mean aerodynamic chord c_{MAC} shall be within 10% of 4.18m.	✓	
GEO-WNG-5	The quarter chord sweep $\Lambda_{c/4}$ shall be within 10° range of 0.	✓	
GEO-WNG-6	The taper ratio λ shall be within 10% of 0.667.	✓	
GEO-WNG-7	The wing shall have a minimum internal volume of 14.4 m ³ .	✓	
Performance Requirements (PFM)			
Wing (WNG)			
PFM-WNG-1	The wing shall generate lift higher than the MTOW of the aircraft.	✓	
PFM-WNG-2	The aircraft angle of attack α_b during take-off and landing shall be below 10°.	✓	
PFM-WNG-3	The aircraft shall have a cruise speed higher than 110kts.	✓	
PFM-WNG-4	The aircraft shall have a max speed higher than 180kts.	X	139.7 kts
PFM-WNG-5	The aircraft shall have a stall speed lower than 70kts.	✓	

12.10.4. Empennage compliance matrix

Table 12.8: Requirements List Empennage

Requirement ID	Requirement	Check	Value
Operational Requirements (OPE)			
Empennage (EMP)			
OPE-EMP-1	The horizontal tail when landing shall not hit the water.	✓	
OPE-EMP-2	The rudder shall not be in the water when it is stationary in the water.	✓	
OPE-EMP-3	The vertical tail shall have a rudder.	✓	
OPE-EMP-4	The horizontal and vertical tale shall have a trim tab.	✓	
OPE-EMP-5	The horizontal tail shall be a fixed tail.	✓	
OPE-EMP-6	The horizontal tail shall be able to pitch the aircraft.	✓	
OPE-EMP-7	The vertical tail shall be able to yaw the aircraft.	✓	
OPE-EMP-8	The empennage shall not be moved more than 1.9 meters compared to the position of the empennage on the original Catalina.	✓	
OPE-EMP-9	The empennage shall create a $\frac{dC_m}{D\alpha} < 0$ for the aircraft.	✓	
OPE-EMP-10	The tail shall not be in the wake of the wing during landing avoid deep stall.	✓	
OPE-EMP-11	The tail shall not be in the wake of the wing during take-off to avoid deep stall.	✓	
OPE-EMP-12	The tail shall not hinder the propulsion system during cruise.	✓	
OPE-EMP-13	The tail shall not hinder the propulsion system during landing.	✓	

OPE-EMP-14	The tail shall not hinder the propulsion system during take-off.	✓	
------------	--	---	--

12.10.5. Fuselage compliance matrix

Table 12.9: Fuselage requirements

Requirement ID	Requirement	Check	Value
Fuselage Requirements (FUS)			
Subsystem Compatibility Requirements (SCR)			
FUS-SCR-1	The fuselage shall fit the landing gear when retracted.	✓	
FUS-SCR-2	The fuselage shall have a centre of mass at TBD \pm TBD from the nose .		8.15 m \pm 0.21 m
FUS-SCR-3	The fuselage shall be designed to carry landing gear loads as described in CS 23.729.	✓	
FUS-SCR-4	The fuselage shall be designed to carry wing loads through the wing pylon and wing struts.	✓	
FUS-SCR-5	The fuselage shall be designed to carry tailplane loads.	✓	
Regulatory Requirements (REG)			
FUS-REG-1	Water spray may not impair vision according to CS 23.239.	✓	
FUS-REG-2	There shall be no vibrations able to damage the aircraft under any conditions CS 23.251.		
FUS-REG-4	The fuselage shall be designed according to water loads as calculated in accordance with CS 23.527.		
FUS-REG-5	The fuselage shall be designed according to the ambient pressure loads as calculated in accordance with CS 23.533.	✓	
FUS-REG-6	The fuselage shall be designed such that the aircraft can be landed in accordance with CS 23.529.		
FUS-REG-7	The fuselage shall be designed such that the aircraft can take-off in accordance with CS 23.531.		
FUS-REG-8	The aircraft shall comply with CS 23.535 and CS 23.757 related to auxiliary floats.		
FUS-REG-9	The maximum loads on passengers during emergency landings shall not exceed loads as specified in CS 23.561.		
FUS-REG-10	Seats shall comply with CS 23.562 and CS 23.785.		
FUS-REG-11	The fuselage shall have watertight compartments in accordance with CS 23.755.		
FUS-REG-12	The cockpit shall be designed in accordance with CS 23.771.	✓	
FUS-REG-13	The windows have to comply with CS 23.775.	✓	
FUS-REG-14	Doors have to comply with CS 23.783.		
FUS-REG-15	Doors shall not be located under the propeller.	✓	
FUS-REG-16	Door dimensions shall be at least: 61 x 122 cm.		
FUS-REG-17	The cargo compartments shall be compliant with CS 23.787.		
FUS-REG-18	There shall be at least one emergency exit in compliance with CS 23.807 of 48 x 66 cm.	✓	

12.10.6. Landing gear compliance matrix

Table 12.10: Landing gear requirements

Requirement ID	Type	Requirement	
Geometric Requirements (GEO)			
Landing Gear (LDG)			
GEO-LDG-1	The nose gear shall bear more than or equal to 8% of the MTOM at the most aft c.g.	✓	
GEO-LDG-2	The nose gear shall bear less than or equal to 15% of the MTOM at the most forward c.g.	✓	
GEO-LDG-3	The scrape angle shall allow take-off and landing at kts.	✓	
GEO-LDG-4	The tip-back angle shall be smaller than the scrape angle.	✓	
GEO-LDG-5	The overturn angle shall be larger than 55 degrees.	✓	

12.11. Feasibility Analysis

With the compliance of requirements as detailed in Table 12.5, four kinds of requirement compliances are presented. A requirement is either met, not met, not investigated, or the requirement is not quantified. Since the most critical performance is the failure to meet a requirement, these will be discussed first.

1. OPE-CHE-MOI-1: Of all eigenmotions, only the aperiodic spiral is unstable. However, as discussed in chapter 11, this is not critical and is deemed acceptable by CS 23.181.
2. OPE-CRU-2: During sizing of the propulsion system, it was found that the top speed was sizing the entire system, requiring over 2 MW of power to fly at 180 kts, compared to 1.2 MW for take-off and climb. From market research, it was found that the top speed is not essential, and it was therefore reduced.
3. NOP-STA-ARL-9: With further investigation into market analysis, a number of 13 passengers was deemed acceptable for tourism use cases, although 16 persons including two pilots and one flight attendant.
4. NOP-STA-PAS-2: In the touristic use case with a capacity of 13 passengers in addition to the crew, a cargo space of 120 kg is available, resulting in 9.2 kg per passenger. From the market analysis, this is deemed acceptable for the scenic flight use case.
5. NOP-HIS-5: The frequency of the sound produced by the propellers is 3 times higher than for the original Catalina, due to the increased number of propellers. This was however deemed to not be as relevant as the requirement on noise levels, which was instrumental in deciding the propeller configuration.
6. PROP-REG-6: Should the fuel tank fail, combustion and explosions could critically damage the propulsion system as well as other subsystems. However, this is quite improbable, with the tank being designed to withstand an enormous amount of loads, since it is already designed to resist 700 bar of pressure.
7. PROP-REG-10: Because cooling is a critical problem with hydrogen-powered planes, the radiators are sized such that they can cool the propulsion system at continuous climb power. Higher power settings are only required during take-offs and go-arounds. These are shorter than 85 seconds.
8. PFM-WNG-4: See OPE-CRU-2.

12.12. Sensitivity analysis

In order to further investigate the feasibility of the design, a sensitivity analysis is carried out, such that the critical parameters on which the design depends are identified. This is done by selecting several baseline design parameters, and varying them in the adverse direction until criticality in some metric of performance is encountered. For example, the volumetric fuel cell power density is a value that was set based on existing values and a reasonable expected future value, but if this fuel cell performance is in fact found not to be achieved, some criticality in necessary volume might be found. In line with this, all parameters that were investigated as part of this analysis are explained below, for each detailing the value of the current design, as well as the limiting value and the factor which poses this limit.

Volumetric fuel cell power density measures the amount of power a cubic meter of fuel cell can output. Because of the tight packaging of the power and accompanying cooling systems, a reduction in density would limit the volume of fuel cells able to fit inside the nacelles. Since cooling is already close to the limit, it is possible to fit an extra fuel cell and radiator module inside the pylon. This would reduce the passenger capacity of the airplane by one. However, this is deemed an acceptable sacrifice to keep the aircraft flying. In total, the power density could decrease from 350 to 280 kW/m³. The increased fuel cell volume would move one of the fuel cells and accompanying radiators to the pylon, leaving 2 600 kg fuel cells inside the nacelles.

Fuel cell efficiency is currently assumed to be 50% at maximum power. However, the performance numbers of the high-power fuel cells required for the aircraft are not yet proven. If the efficiency were to drop, both more fuel and more cooling would be required. If an additional radiator would be placed inside the pylon, 1500 kW of heat can be dissipated. Using this, the minimum fuel cell efficiency is calculated to be 44.4%. In this case, the design would thus be limited by cooling. The fuel tank weight would only increase by 12.5%.

Maximum lift coefficient of the aircraft dictates the stall speed of the design, which is required to be below 70 kn. Including a safety factor of 10%, to account for factors such as the fuselage-wing interaction or that may have been neglected by XFLR5, the limiting value of this stall speed is set at 63 kn. With a current value at $C_{L_{max}} = 1.54$, the maximum lift coefficient should have a value of 1.18 at minimum.

True range is determined starting from an effective range of 500 km, which is increased by 45% to account for contingency, alternate, reserve and minimum additional fuel. If the effective range is required to be higher, more fuel would be required. The maximum true range would be 1480 km which equates to an effective range of 1150 km. Limiting is the stall speed, required to be 70 kts. However, a safety factor of 1.1 is chosen, decreasing it to 63 kts. The maximum weight is then given to be 12390 kg. Because the hydrogen tanks are very heavy, this is the first limit. If the wing were to be modified to increase its lift, the true range could be increased to 1560 kg. In this case, the available volume for fuel tanks inside the wings is the limiting factor.

Maximum power required could come from either the climb, cruise, or maximum speed requirements. With a maximum speed as detailed from section 12.11, the current maximum power required of 1192 kW comes from the climbing performance. As detailed in the discussion of the volumetric fuel cell power density parameter, there is a volumetric limit on the number of fuel cell and radiator modules that can be carried in the design. With a current count of 4 such modules, providing a total of 1200 kW, increasing this number to this limit of 5 would provide 1490 kW of power. With this power, different performance characteristics could also be increased, as detailed in the next two parameters explained.

Climb rate affects, together with the cruise speed, the power required for climb. Since the cruise speed is a requirement set in conjunction with the market analysis, and increasing this speed is not in fact desirable, then by the limit on the maximum power required a limit is defined on the maximum climb rate. Indeed, with a current value of 5.1 m/s, the maximum climb rate is limited to 7.1 m/s.

Maximum speed also is limited by the maximum power. With the requirement dropped as was explained in section 12.11, a current maximum speed of 140 kts is determined by the current maximum power. Taking the limit on the maximum power, a new maximum speed of 153 kts is obtained.

Table 12.11: Sensitivity Analysis

Parameter	Old value	Limit	Limiting factor
Volumetric fuel cell power density	350 kW/m ³	280 kW/m ³	Volume for the fuel cells and radiators (placed inside the pylon).
Fuel cell efficiency	50%	44%	Volume for the fuel cell radiators. (placed inside the pylon).
Maximum lift coefficient	1.54	1.18	Stall speed limited.
True range	725 km	1480 km	Stall speed limited because of the increased weight.
Maximum power required	1192 kW	1490 kW	Volume for the fuel cells and radiators (placed inside the pylon).

To conclude, the plane is mainly limited by its ability to dissipate the fuel cell's heat. The current radiators snugly fit inside the nacelles. Increasing the fuel cell power or decreasing the fuel cell efficiency would require an extra fuel cell and radiator combination to be placed inside the pylon, reducing the passenger capacity to 12. The fuel cell and radiator volume can be increased by a maximum of 25% from either increased power requirements, less efficient fuel cells or less compact fuel cells. The most sensitive of these is the efficiency. However, fuel cells with an efficiency of 50% have already been proven, so the risk of the design becoming unfeasible because of it is low.

The second limiting factor is the required stall speed. However, there is a lot margin left for either the lift coefficient to decrease from possible overestimates or inaccurate simulation or the range requirement to increase.

13

Future Perspective

13.1. Manufacturing, Assembly, Integration Plan

In order to get an overview of how to produce the aircraft a MAI plan has to be created. The MAI plan stands for Manufacturing, Assembly and Integration plan. This will give a chronological timeline of the production steps that the aircraft has to take in order to be produced.

Figure 13.1 shows the order in which the production will take place. It shows an overview of the parts and systems in which section of the production they are created. It is also shown that some parts will be bought from other companies.

To give a short description of what the MAI plan looks like. The first two steps are at the same time, producing and buying parts together with subsystems from external suppliers. This is then followed by the sub-sub-assemblies of the aircraft. Then the sub-assemblies are made with the created/bought parts and sub-sub-assemblies. This is all put together in the final assembly. Before the aircraft is finished it needs a paint job. Customers can choose the paint scheme of the aircraft in which way they see fit. Before the aircraft is flight-ready tests have to be done. Tests are also done during the manufacturing of the parts and assembly processes. If the aircraft passes all the tests, the plane is certified and delivered to the customers.

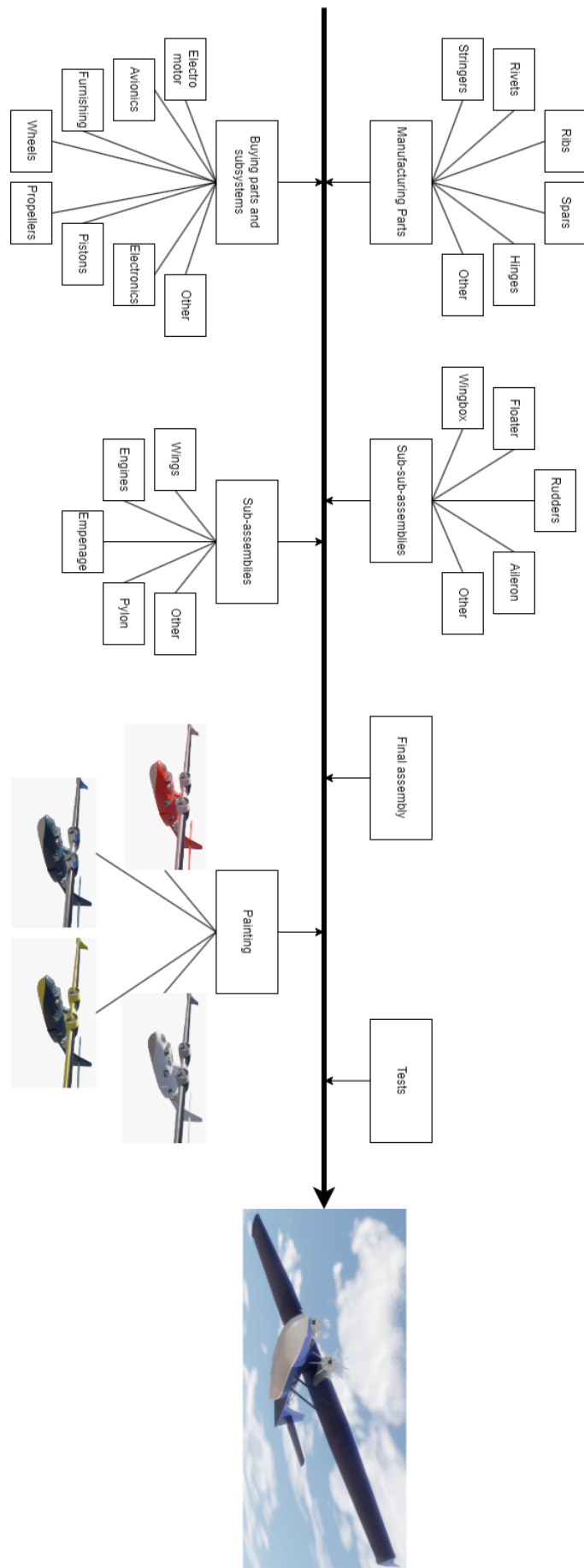


Figure 13.1: MAI plan of the aircraft

13.2. Project design & development logic

This section will talk about all the stuff that has to be done after the DSE project. The main structure of how the project should look after the DSE is shown in Figure 13.2. These are the main guidelines as in the baseline and midterm review, but they will be worked out more [1, 2]. The detailed design phase and the manufacturing of parts will most likely be the most time-consuming part of the aircraft development.

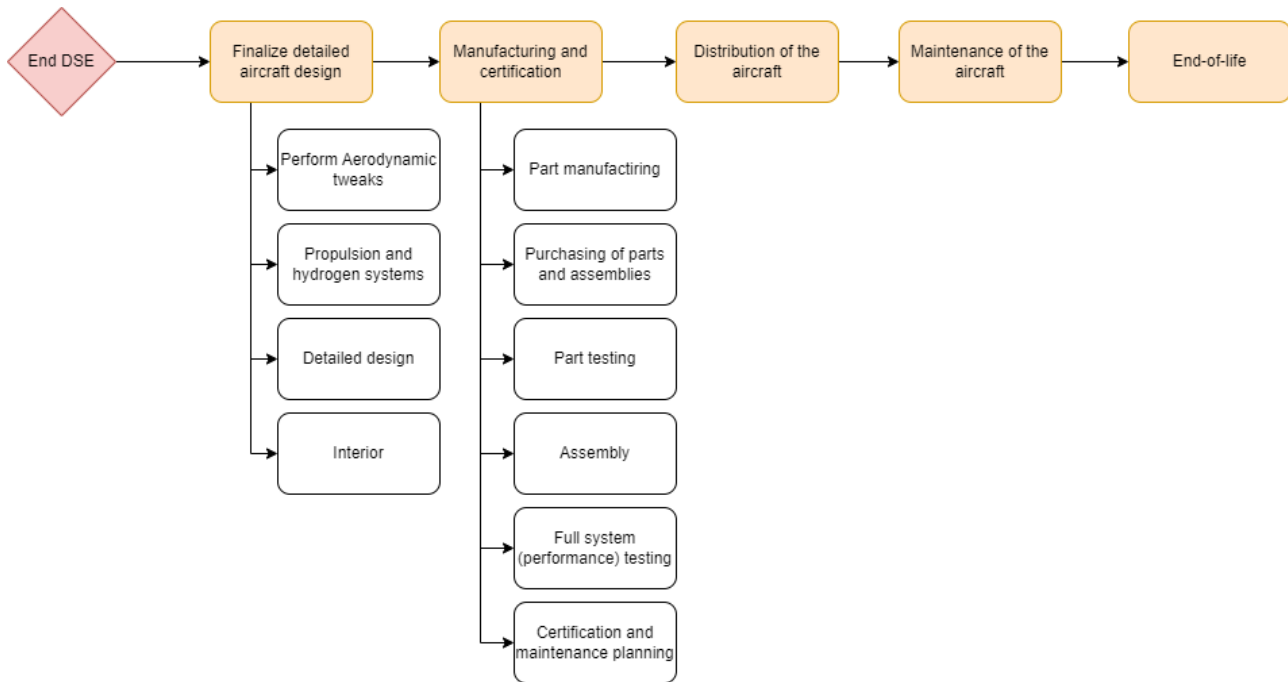


Figure 13.2: Future project & development logic diagram

13.2.1. Finalize detailed aircraft design

Perform aerodynamics tweaks

Within the DSE the preliminary aerodynamic characteristics of the aircraft are estimated. In order to prepare the aircraft for flight and optimize performance, tests should be done to validate the aircraft. This can be done by using CFD and wind tunnel tests.

Propulsion and hydrogen systems

The aircraft propulsion system will be preliminary at the end of the DSE. More research has to be done into the electric motors and their performance. The motor that is now being used in the design is not yet on the market. The performance might change compared to their initial numbers. This also has to be done for the fuel cells. The exact performance of the fuel cells might change during the design process. This can affect for example the fuel consumption of the system and it can affect the range of the aircraft.

The cooling of the engines also has to be researched and designed more in-depth. The system is very dependent on the motors and fuel cells. Also, the sizing method is an estimate of what is needed to cool the engines.

Besides the fuel cells the hydrogen system also has to be worked out further. This can be said for both the hydrogen tanks and the piping between the tanks and fuel cells. The tanks also need a thermal system such that the tanks will not overheat and increase the pressure.

The propellers designed in this DSE are just designed for aerodynamic and noise performance. The structure of the propellers has to be researched, in order to see if they are viable and will not break when used. Thus the propeller design can change in the future in order that they are structurally safe and still have sufficient performance related to noise and power.

Detailed design

Within the DSE the detailed design phase will not be completed. Thus this has to be done in order to finish the aircraft and make it flight ready.

To make it flight ready the aircraft should go more in-depth into the final structural design. The main structure design for the wingbox and fuselage will be done within the DSE. Yet the hull part has to be done following the DSE and assembly connections have to be designed and chosen. Another thing that also has to be done is tubing and electronics in the DSE. This also applies to the mechanical systems within the aircraft.

Interior

For the interior, some conceptual designs are made. This has to be further worked out in order to make sure that everything is up to the required safety standards. The interior will most likely be modular in order to fulfil the customers' needs.

13.2.2. Manufacturing and certification

During the design phase, it is important to already look at the manufacturing of the design. The part manufacturing will have limitations on the design of each part and assembly. When the designing is done, the production of the aircraft can commence.

Part manufacturing

The first thing that has to be done in the production phase is to create the base parts of the sub-assemblies and assemblies of the aircraft.

The parts initially designed might not be viable in real life due to the machinery. To fix this you have to get either specialized tooling or redesign certain parts. When all the designed parts can be produced with the available machinery, the production of the parts can start.

Purchasing of parts and sub assemblies

Not all parts and sub-assemblies will be produced in-house, so some of the production process has to be outsourced. This is because some things are too complicated or too expensive to produce if done in-house. This can be for example said for avionics, computers and sensor systems.

Part testing

If the aircraft follows a process-focused production, more tests have to be done in between each part created. The goal is to find defects in the materials of the created parts. If there is a pattern starting in a certain part of the production, the manufacturing process should be reconsidered. Another method of fixing this is to redesign that certain part in order to reduce the failure rate in the production process.

Assembly

When all parts are created and bought, each sub-assembly is completed. The final assembly can commence and create the final product. If a certain part or sub-assembly is outsourced or produced somewhere else it is important to account for transportation.

Full system (performance) testing

When the entire aircraft is produced, the full aircraft has to be validated. The functionality of each subsystem should be tested. If all the sub-systems work as intended, the final aircraft can be tested and checked if it will behave as intended.

Certification and maintenance planning

Before the aircraft can be distributed an aircraft maintenance manual has to be produced. This is for the customers and mechanics, and it shall show how parts can be inspected and replaced. It shall give the names of each component in the aircraft. This is in case the customer needs to replace a part.

For the aircraft to be flight worthy it needs to be certified by external and representative aviation agencies. The aircraft shall have to comply with regulations, like CS23. If it does not comply the aircraft will be redesigned in order to make it comply with the regulations.

13.2.3. Distribution of the aircraft

If the latter is done and approved the aircraft will be ready for distribution. The consumers can choose to either fetch the aircraft or have it delivered to their door. If the consumer goes to get the aircraft themselves it can be completely assembled. If the aircraft has to be delivered remotely and it is impossible for the aircraft to fly to,

it has to be sent in parts. Then the customer has to finish the assembly of the aircraft on sight. Thus the aircraft will be assembled in only sub-assemblies

13.2.4. Maintenance of the aircraft

During the lifetime of the aircraft, it will have to perform maintenance. The inspection methods used are visual and Non-destructive testing. If a part is damaged, repairs or part replacements have to be performed. If not possible the parts have to go to the end-of-life process. [1]

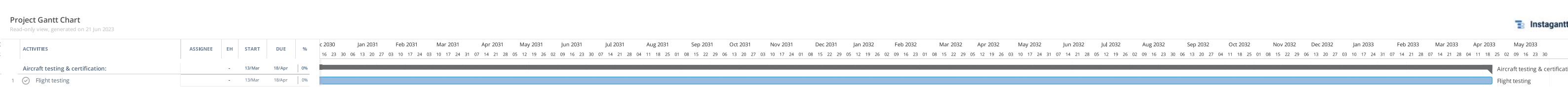
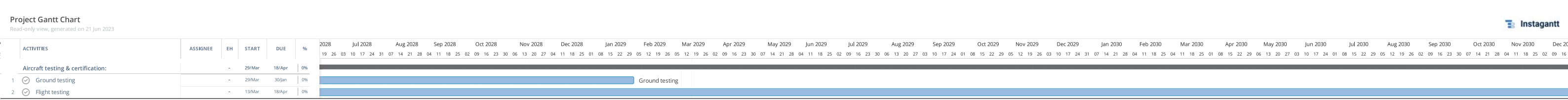
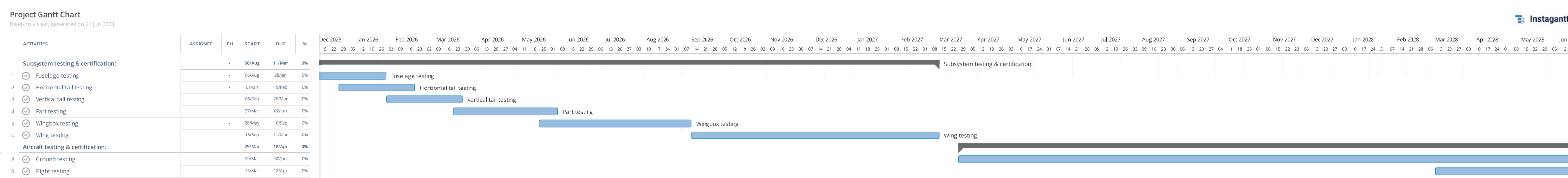
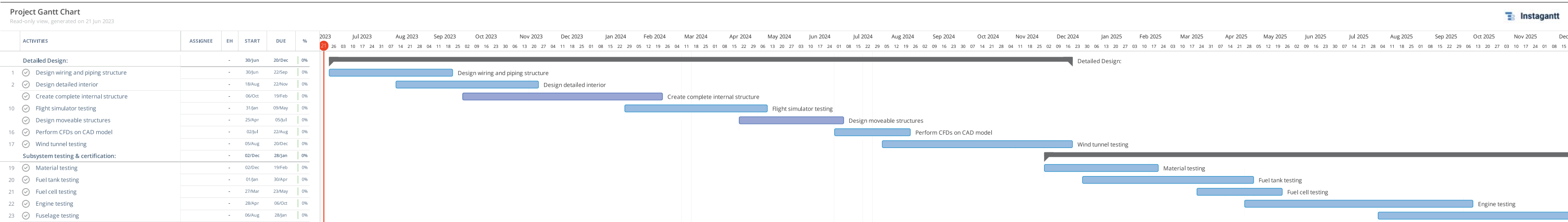
13.2.5. End-of-life

If the owner of the aircraft does not have a use for the aircraft anymore, the aircraft can be resold to a new owner. If this is the case it can be used as intended and it can follow its normal maintenance schedule.

If the aircraft is written off. The aircraft can be scraped for parts. They can be sold or even extracted and then recycled. Finally, if the parts can not be recycled they can maybe be burned for energy. The worst-case scenario is that some parts end up at an airplane scrapyards. [1]

13.3. Gantt chart

The post-DSE Gantt chart is shown in Figure 13.3. The detailed design phase, construction, assembly and certification/testing are shown and planned.



Conclusions & Recommendations

The goal of this report was to present a redesign of the PBY Catalina with state-of-the-art technology and emission-free operations into a luxury flying yacht experience. Caty was designed to minimise operational emissions and designed such that the production and end-of-life solutions would be emissions free. The aircraft should be usable for multiple day luxury chartering for the ultra-wealthy or island hopping scenic flights for tourists. These trips are likely to span multiple days and involve various activities, with flights serving as transportation between each activity. The design of the Caty is tailored for luxurious cruising with unparalleled views of the outside world. The water landing capability of the Caty, will pioneer a new market where private aviation is merged with adventurous activities. Each coastal town and island becomes accessible with the Caty, resulting in seamless travels between the passengers' destinations, with no need for further transport. The required range was set at 500 km with the emissions free operation in mind. In order to ensure the best user experience, requirements were set on the noise inside the aircraft, as well as near the ground to have as little impact on its surroundings.

Different types of propulsion systems were considered such as hydrogen, battery, sustainable aviation fuel, and hybrid configurations of these propulsion systems. Extensive analysis to the TRL, risks, emissions, cost and more led to a trade-off where hydrogen fuel cell propulsion was chosen for its low weight and cost, while having a high sustainability. Aerodynamic analysis resulted in a new wing profile for the main wing which improved the lift over drag, resulting in a larger range. The addition of wingtips improved the aerodynamic efficiency further while maintaining the feel of the PBY Catalina. A new propeller design aimed to reduce the noise level with respect to the PBY Catalina. Due to a substantial weight decrease, less power required greatly reduced the noise. To further improve the noise levels, a 9 bladed design rotating at slower speeds was chosen which further reduced noise. The propellers are powered by electric motors which are powered by hydrogen fuel cells. Currently, the cooling of fuel cells is considered a large challenge for the feasibility of hydrogen aircraft. Due to the low efficiency of fuel cells a large amount of heat has to be dissipated by the propulsion system. This heat has to be exhausted to the air. Another limitation of hydrogen propulsion are the low temperature of fuel cells. A RAM inlet is implemented to increase the air mass flow since the radiator inflow speed has to be limited to reduce drag. The intake and radiator is placed on top of and below the wing surface connected to the nacelle of the motor and fuel cells such that it retains the look of the PBY Catalina. The hydrogen is stored inside the rectangular part of the wing where one tank is positioned inside the leading edge on both sides. The other tanks are positioned behind the front spar of the wing box. The high energy density of hydrogen greatly reduced the fuel with respect to the PBY Catalina.

The design will use a mix of two different materials: aluminium and PEEK-carbon fibre composite. These materials are both completely recyclable, which decreases the environmental impact of the aircraft. Most of the structures will be made of the PEEK-carbon fibre composite, as it is lighter and stronger than the current composites used in the aviation industry. In addition to it being lighter, it can be assembled using rivetless bonding. This also reduces the total weight and increases aerodynamic efficiency.

Structural analysis was performed to have a detailed weight estimation of the OEM of the aircraft. The structural analysis increased the level of fidelity of the new design by calculating the actual structure required. The weight was reduced significantly after iterations which also required less powerful engines, resulting in further weight reduction. The aircraft's stability and controllability characteristics were analysed and adjusted for safe and comfortable operations. The change in the overall layout of the Caty was very little compared to the PBY Catalina which ensured the authentic look was kept. The interior of the Caty was designed with private jet

standards to appeal to the intended market of luxury chartering.

14.1. Recommendations

Throughout the course of this project, certain challenges with hydrogen aircraft have remained unresolved. The cooling system of fuel cells can be considered the largest obstacle since heat dissipation is difficult for relatively low temperatures. The implementation of ram intakes for the radiators improves air mass flow, increasing cooling capacity. The newly designed radiator and RAM intake should be fully integrated into a nacelle with the motor and fuel cells as the original design was proven not be sufficient.

Further research can explore the option of more hydrogen tanks inside the wingbox. A margin in the stability of the aircraft can enable the implementation of hydrogen tanks inside the wing. Structurally, the wing can be reinforced to account for the marginal weight increase. The potential increase in range by adding hydrogen tanks is significant, greatly increasing the use case of Caty. Due to time constraints, this was however not possible during this project.

Besides adding more hydrogen tanks, the addition of solar panels on the wing top surface greatly improves the usability and potential market as well. When the aircraft is landed on water or other remote places, electricity is consumed by interior lights, air conditioning and other equipment. This power would currently draw hydrogen fuel cells, reducing the range slowly. This causes the Caty to have a limited time on water, impacting the user experience. The implementation of solar panels on wing surfaces is still new for aircraft. However, sailing yachts such as the Imoca 60¹ have implemented solar panels on surfaces which are subject to impact regularly. Such a robust system can be integrated in the wing surface in further research to improve the user experience.

14.2. Final Note

To conclude, an elaborate initial design was performed proving the feasibility of a luxury hydrogen-powered aircraft during this project. The goal to design an aircraft with the spirit of the PBY Catalina was achieved while complying with sustainability and technological goals. The research into current fuel cell technology resulted in engineering solutions for the currently large challenges preventing hydrogen aviation to be mass adopted. By conducting further research, it is possible to refine and enhance this concept, ultimately leading to the development of a detailed design.

¹<https://www.solbian.eu/en/blog/the-solar-installation-onboard-imoca-60-malizia-n269> (Accessed on 20/06/2023)

References

- [1] Brian de Vrind, Nick Felten, Ties Harland et al. *Restomod Catalina Midterm Review*. Tech. rep. Delft University of Technology, May 2023.
- [2] J. van Bemmelen et al. *Restomod Catalina Baseline Review*. Tech. rep. Delft University of Technology, May 2023.
- [3] Easa. “European Aviation Safety Agency Certification Specifications for Normal, Utility, Aerobatic, and Commuter Category Aeroplanes | CS-23”. In: (2012).
- [4] Viking Air. *Twin Otter Series 400 Brochure*. 2008.
- [5] Dornier Seawings. “Seastar, World’s most advanced Amphibious Aircraft”. In: (2023).
- [6] J. Roskam. *Airplane Design Part V*. 2nd ed. Lawrence, Kansas, United States of America: Design, Analysis and Research Corporation, 1989.
- [7] G.L.M. Vonhoff. “Conceptual Design of Hydrogen Fuel Cell Aircraft”. Master thesis. Delft University of Technology, 2021.
- [8] Prof. dr. D.G. Simons and Prof. dr. ir. M. Snellen. *Course AE4431 Aircraft Noise and Emissions*. Tech. rep. Delft University of Technology, 2022.
- [9] G.J.J. Ruijgrok. *Elements of aviation acoustics*. Delft University Press, 1993.
- [10] A. Scoccimarro. *Preliminary Design Methods for the Thermal Management of Fuel Cell Powered Aero-engines*. (Accessed on 06/20/2023). Apr. 2023.
- [11] D. Koulovi. *HEAT RELEASE OF FUEL CELL POWERED AIRCRAFT*. http://gpps.global/wp-content/uploads/2021/02/GPPS-TC-2020_HT_99.pdf. (Accessed on 06/20/2023). Sept. 2020.
- [12] Y. A. Cengel and A. J. Ghajar. *Heat and Mass transfer*. 2015.
- [13] T. U. H. S. G. Manik et al. *The experimental study of the coolant flow rate of an ethylene glycol-mixed water to the heat transfer rate on the radiator*. <https://iopscience.iop.org/article/10.1088/1757-899X/505/1/012063/pdf>. (Accessed on 06/21/2023). 2019.
- [14] European Union Aviation Safety Agency. *MT-Propeller Entwicklung GmbH*. EASA, 2021.
- [15] M. Clarke et al. “Aerodynamic Optimization of Wing-Mounted Propeller Configurations for Distributed Electric Propulsion Architectures”. In: (2021). DOI: 10.2514/6.2021-2471.
- [16] L. Zhang et al. “Optimization and analysis of winglet configuration for solar aircraft”. In: *Chinese Journal of Aeronautics* 33.12 (2020), pp. 3238–3252.
- [17] S. F. Hoerner. *Fluid-dynamic drag*. 2th ed. Washington, D.C.: Hoerner, 1965.
- [18] Russell c. Hibbeler. *Mechanics of Materials*. 10th ed. Massachusetts, USA: Pearson, 2017.
- [19] T.H.G. Megson. *Aircraft structures for engineering students*. Pearson, 2012.
- [20] F. Oliveiro. *Systems Engineering and Aerospace Design*. 2023.
- [21] J. Roskam. *Airplane Design Part VI*. 8th ed. Lawrence, Kansas, United States of America: Design, Analysis and Research Corporation, 2022.
- [22] Consolidated Aircraft. *PBY-5A Handbook Maintenance Instructions*. 1951.
- [23] M. Sadraey. *Aircraft design : a systems engineering approach*. Hoboken, New Jersey, United States of America: Design, Analysis and Research Corporation, 2012.
- [24] J. Roskam. *Airplane Design Part II*. 2nd ed. Lawrence, Kansas, United States of America: Design, Analysis and Research Corporation, 1997.
- [25] E. Torenbeek. *Synthesis of subsonic aircraft design*. Delft University Press, 1976.